



universität  
wien

# DISSERTATION / DOCTORAL THESIS

Titel der Dissertation / Title of the Doctoral Thesis

„Confinement of therapeutic agents into mesoporous silica nanoparticles for oral delivery applications“

verfasst von / submitted by

Estelle Juère

angestrebter akademischer Grad / in partial fulfilment of the requirements for the degree of  
Doktorin der Naturwissenschaften (Dr. rer. nat.)

Wien, 2020 / Vienna, 2020

Studienkennzahl lt. Studienblatt /  
degree programme code as it appears on the student rec-  
ord sheet:

UA 796 605 419

Dissertationsgebiet lt. Studienblatt /  
field of study as it appears on the student record sheet:

Chemie

Betreut von / Supervisor:

Univ. Prof. Dr. rer. nat. Freddy Kleitz



## Abstract

---

Among the different drug administration pathways, the oral route remains the most preferable one for the patients, although quite challenging from a pharmaceutical point of view. The integrity of the pill has to be preserved up to the drug absorption site *i.e.*, in the intestine. It implies that the drug has to be stable in an acidic environment, soluble in near neutral pH and lastly, permeable through the intestinal epithelial barrier. Needless to mention that it is rarely the case as currently most of the drugs accepted for oral dosage are blocked because of their limited oral bioavailability. Promising approaches to maximize the chances to reach the systemic circulation could be found in the encapsulation of therapeutic agents into porous materials and in the design of pH-responsive formulations. A variety of porous materials are interesting for drug delivery but one kind is particularly worthy of investigation: mesoporous silica nanoparticles (MSNs). In this thesis, two types were investigated in particular: MCM-48-type nanoparticles and dendritic-type nanoparticles (DMSNs). Several therapeutic agents were incorporated in the pores of these MSNs: resveratrol, omeprazole and insulin which are all interesting models suffering from low solubility, low permeability or susceptible to acidic or enzymatic decomposition. Tableting these drug-loaded MSNs with succinylated  $\beta$ -lactoglobulin has prevented the release and therefore the degradation of drugs at acidic pH and has promoted their elution in near neutral pH. *In vitro* cytotoxic assays have been conducted using HT-29, Caco-2 and HCEC cell lines to get deeper insights into the biocompatibility of the various MSNs designed, and the mediation of the *in vitro* metabolic activity of the cells upon sustained release and enhanced drug permeation.



# Zusammenfassung

---

Unter den verschiedenen Wegen der Arzneimittelverabreichung bleibt der orale Weg für die Patienten der beliebteste auch wenn er aus pharmazeutischer Sicht recht herausfordernd ist. Die Pille muss nämlich bis zur Arzneimittelabsorptionsstelle d.h. im Darm intakt bleiben. Das Medikament sollte in einer sauren Umgebung stabil sein, bei einem nahezu neutralen pH-Wert löslich und schließlich durch die Darmepithelbarriere aufgenommen werden. Dieses Anforderungsprofil wird bei oraler Aufnahme von vielen Medikamenten wegen der limitierten biologischen Verfügbarkeit selten erfüllt. Um die Aufnahme zu verbessern ist die Einschließung von Therapeutika in poröse Materialien und die Verwendung von pH-abhängigen Systemen eine vielversprechende Strategie. Es gibt viele verschiedene poröse Materialien, die sich für die Wirkstofftransport eignen aber ein Typ ist besonders interessant: Mesoporöse Silica-Nanopartikel (MSNs). In dieser Dissertation wurden zwei Typen davon untersucht: MCM-48-Nanopartikel und DMSNs (dendritische Nanopartikel). Mehrere therapeutische Wirkstoffe, insbesondere Resveratrol, Omeprazol und Insulin, wurden in die Poren von MSNs geladen. Sie alle sind gute Beispiele für Medikamente mit geringer Löslichkeit, geringer Permeabilität oder die Anfälligkeit für saure und enzymatische Zersetzung. Die Herstellung von Tabletten bestehend aus mit Arzneimitteln beladenen MSNs und succinylierten  $\beta$ -Lactoglobulin hat es ermöglicht, dass die Freisetzung und damit der Abbau bei saurem pH unterbunden und die Elution bei nahezu neutralem pH-Wert gefördert wird. *In vitro*-Zytotoxizitätstests wurden mit HT-29-, Caco-2- und HCEC-Zelllinien durchgeführt um die Biokompatibilität der verschiedenen entwickelten MSNs sicher zu stellen. Weiters wurde die *in vitro* Stoffwechselaktivität der Zellen bei der fortlaufenden Freisetzung und bei höheren Wirkstoffkonzentrationen getestet.



## List of abbreviations

---

ADME	Absorption distribution metabolism excretion
BCS	Biopharmaceutical classification system
CP	Cross polarization
CPG	Controlled porous glass
CTAB	Cetyl trimethylammonium bromide
CTAC	Cetyl trimethylammonium chloride
DLS	Dynamic light scattering
DMSN	Dendritic mesoporous silica nanoparticles
DMSO	Dimethyl sulfoxide
EDL	Electric double layer
FA	Folic acid
FDA	Food and drug administration
FFA	Flufenamic acid
FID	Free induction decay
FITC	Fluorescein isothiocyanate
FTIR	Fourier transformed infrared spectroscopy
GIT	Gastro-intestinal tract
HCEC	Human colon epithelial cells
HMDS	Hexamethyldisilazane
IEP	Isoelectric point
i.v.	Intravenous
MAS	Magic angle spinning
MCF	Mesocellular foam
MSNs	Mesoporous silica nanoparticles
MW	Molecular weight
NMR	Nuclear magnetic resonance
OMS	Ordered mesoporous silica
PEG	Polyethylene glycol
PEI	Polyethylene imine
PSD	Pore size distribution
PXRD	Powder X-ray diffraction
QA	Quaternary ammonium
RES	Reticuloendothelial system
RT	Room temperature
SDA	Structure-directing agent
SEM	Scanning electron microscopy
SGF	Simulated gastric fluid
SIF	Simulated intestinal fluid
TEA	Triethanolamine
TEM	Transmission electron microscopy
TEOS	Tetraethyl orthosilicate
TG-DSC	Thermogravimetry-Differential scanning calorimetry
TMS	Trimethylsilyl
USP	United States Pharmacopeia
UV-Vis	Ultra-violet-visible spectrometry
ZP	Zeta potential





# Table of Content

---

<b>ABSTRACT</b> .....	<b>I</b>
<b>ZUSAMMENFASSUNG</b> .....	<b>III</b>
<b>LIST OF ABBREVIATIONS</b> .....	<b>V</b>
<b>TABLE OF CONTENT</b> .....	<b>VII</b>
<b>ACKNOWLEDGEMENT</b> .....	<b>IX</b>
<b>CHAPTER 1 – INTRODUCTION</b> .....	<b>1</b>
I.    ORAL DRUG DELIVERY.....	1
II.   THERAPEUTIC AGENTS.....	2
III.  NANOCARRIERS AND CONFINEMENT OF THERAPEUTIC AGENTS.....	3
IV.   SCOPE OF THE THESIS.....	4
<b>CHAPTER 2 – STATE-OF-THE-ART</b> .....	<b>7</b>
I.    MESOPOROUS SILICA NANOPARTICLES.....	7
I.1. <i>General overview</i> .....	7
I.2. <i>Principle of synthesis I: from micelles to OMS</i> .....	8
I.3. <i>Principle of synthesis II: from OMS to nanoparticles</i> .....	9
I.3.a.  pH of the reaction.....	9
I.3.b.  Particle size control and aggregation issues.....	10
I.3.c.  Biphasic approach.....	11
I.4. <i>Principle of functionalization</i> .....	12
II.   ENCAPSULATION AND RELEASE OF THERAPEUTIC AGENTS.....	14
II.1. <i>Method of drug encapsulation</i> .....	14
II.1.a.  Solvent diffusion.....	14
II.1.b.  Incipient wetness impregnation.....	15
II.1.c.  Melt loading.....	15
II.1.d.  Supercritical fluid.....	16
II.2. <i>Physico-chemical properties of encapsulated drugs</i> .....	17
II.2.a.  Drug / surface interaction.....	17
II.2.b.  Amorphization and polymorphism.....	19
II.2.c.  Stability of the confined drug.....	21
II.3. <i>Release performance</i> .....	23
II.3.a.  Influence of the silica surface.....	23
II.3.b.  Influence of the pore size.....	24
III.   MESOPOROUS SILICA NANOPARTICLES IN THE ORAL ROUTE.....	27
III.1. <i>Barriers of the GIT – overview</i> .....	27
III.1.a.  The gastric and intestinal milieu.....	27
III.1.b.  The mucosal barrier.....	28
III.1.c.  The epithelium barrier.....	28
III.2. <i>Toxicological considerations</i> .....	29
III.2.a.  In vitro.....	30
III.2.b.  In vivo.....	32
III.3. <i>pH responsive formulation</i> .....	34
III.3.a.  Proteins.....	34
III.3.b.  Lipids.....	35
III.3.c.  Polysaccharides.....	36
IV.   SUMMARY.....	39
<b>CHAPTER 3 – EXPERIMENTAL TECHNIQUES</b> .....	<b>41</b>
I.    GAS PHYSISORPTION.....	41
II.   ELECTRON MICROSCOPY.....	43
III.  DYNAMIC LIGHT SCATTERING.....	44
IV.   ZETA POTENTIAL.....	45

V.	POWDER X-RAY DIFFRACTION ANALYSIS .....	45
VI.	THERMOGRAVIMETRY AND DIFFERENTIAL SCANNING CALORIMETRY .....	46
VII.	SOLID-STATE NUCLEAR MAGNETIC RESONANCE SPECTROSCOPY .....	47
VIII.	ULTRAVIOLET-VISIBLE SPECTROSCOPY .....	48
<b>CHAPTER 4 – RESULTS.....</b>		<b>51</b>
I.	RESVERATROL-ENCAPSULATED MESOPOROUS SILICA NANOPARTICLES.....	51
II.	PROTEIN-SILICA NANOPARTICLE FORMULATION FOR ORAL OMEPRAZOLE DELIVERY .....	73
III.	CHARGE EFFECTS ON THE SILICA-NANOPARTICLE FORMULATION .....	95
IV.	ORAL INSULIN DOSAGE .....	115
<b>CHAPTER 5 – CONCLUSION .....</b>		<b>141</b>
I.	SUMMARY OF KEY RESULTS.....	141
II.	PERSPECTIVES.....	142
III.	CONCLUDING REMARKS .....	143
<b>REFERENCES .....</b>		<b>145</b>





# Acknowledgement

---

I have been able to bring this thesis to the final point thanks to the help and support of many people to which I wish to express my gratitude here.

Because this would not have been possible in the first place without him, I would like to thank my advisor, Prof. Freddy Kleitz, for his trust, his support, his advice, the freedom I had in organizing my work and realizing my ideas. I achieved exactly what I wanted to achieve and this is thanks to him. The second person I am thinking of when writing this part is Dr. Romain Caillard. It was a pleasure to collaborate with him, despite the distance, he has always been available to answer my questions, to advice and encourage me. Someone who also helped me a lot is Dr. Giorgia Del Favero. Thanks to her, I learned so many new things, she shared the passion she has for her field and made me like it. I really enjoyed working with her in these past few months. I am thankful to Dr. Amirali Popat for having warmly welcomed me into his group in Australia. I also learned valuable techniques while working with him which set me up for my whole thesis. I would like to acknowledge Prof. Doris Marko for welcoming me into her laboratories and participating in the scientific discussions around my projects.

I am grateful to Prof. Christian Becker and Prof. Jessica Rosenholm for agreeing to evaluate my thesis. I hope you will appreciate it and I am looking forward to presenting my work and will answer your questions during my defense.

I would like to acknowledge especially Anna Fabisikova. Her help and her ,can do' attitude were inspirational to me and pushed my research forward. For the same reasons, I would like to mention Eva Attakpah, she has supported my projects with the cellular studies and gave me numerous advices based on her solid experience. I am genuinely thankful to Christian Rentenberger, Hanspeter Kählig and Alexander Roller for their help and assistance with TEM, Solid-state NMR and PXRD, respectively.

Now, I would like to dedicate the following to my amazing colleagues and friends: those who supported my ,bad temper' on a daily basis: Tatiana Priamushko, Dr. Remy Guillet-Nicolas, Matthew Doyle, Cornelia von Baeckmann, Mariam Hohagen, Dr. Siegfried Fürtauer, Patrick Guggenberger and Alexander Roller.

Enfin, à mes parents Brigitte et Marc, ma soeur Charlène, ma nièce Syann: merci, simplement merci d'être présent, constamment, de me soutenir, souvent, dans mes aventures, mes choix. Merci d'avoir su trouver les mots lorsque le moral n'y était plus, merci de m'avoir récupérée à la petite cuillère, parfois. Votre force est la mienne et c'est elle qui me permet de surpasser mes limites. Je suis si fière de vous et je vous aime profondément.

Finally, and this is for real now, I would like to express my unconditional love to the unique two boys of my life, my race bike and Guizmo, my cat, I am so proud of you both!







# Chapter 1 – Introduction

---

## I. Oral drug delivery

In medicine, a drug can be administered through several biological pathways: either enteral, which refers to an absorption through the gastro-intestinal tract (GIT) *i.e.*, oral delivery, or parenteral, which refers to anything that does not go through the GIT *i.e.*, the intravenous (i.v.) but also the transdermal or the inhalational routes. Although, the oral route cannot completely replace the i.v. injection in the case of an emergency situation or when caring for a patient with irritated GIT for example, it needs to be further developed to provide therapeutic alternatives for cancer, diabetes or immune treatments. Very recently, the scientific community witnessed a breakthrough in the oral delivery of insulin. Abramson *et al.* developed a so-called self-orienting millimeter-scale applicator for pain-free application of insulin directly into the gastric mucosa with a plasma concentration comparable to those of subcutaneous administration.<sup>1</sup> Moreover, several clinical studies have shown that, in addition to increased patient compliance and decreased adverse effects, the oral pathway was as effective as the i.v. chemotherapy one.<sup>2,3</sup> Besides, oral chemotherapy could represent a cost-benefit since less medical care is needed which balances the higher cost associated with the formulation of drugs.<sup>4</sup> Contrary to i.v. injections where 100 % of the drug is available in the blood circulation, the bioavailability of orally administered drugs *i.e.*, the percentage of drug in the bloodstream, remains the greatest challenge of oral drug delivery. From a pharmacological point of view, the journey of a drug within the organism is described by four stages: the absorption, distribution, metabolism and excretion (ADME). The bioavailability or biodisponibility highly depends on the absorption. Indeed, among the physiological factors at play, the acidic conditions in the stomach, the pH of the GIT ranging from *ca.* 5.0 - 7.4, the presence of enzymes and the composition of the intestinal barrier greatly affect the exposure of the targeted tissues to the active drugs.<sup>5,6</sup> The ability of the drugs to successfully pass these successive barriers can be predicted from the chemical structure of a drug molecule since from one molecule to another, the intrinsic physico-chemical properties vary a lot and this may affect the ADME stages.

## II. Therapeutic agents

Depending on their chemical structure, therapeutic agents exhibit very different physico-chemical properties. For example, the hydrophilic/hydrophobic character of a molecule, characterized by  $\log P$ ,  $P$  being the partition of the drug concentration between a water/octanol biphasic system, has a major effect on the solubility and by extension on the permeability of the drug since only the solubilized portion of the administered drug would be absorbed.<sup>7</sup> In fact, there is a sort of paradox between solubility and permeability of a given drug in which a certain lipophilicity is needed for a molecule to be transported through the intestinal barrier but it is this exact lipophilicity that reduces the ability of a molecule to be solvated in an aqueous solution. Also, the molecular weight (MW) of potential drug candidates is believed to be rather low *i.e.*, below 500. Smaller compounds are more likely to be transported through aqueous pores, to navigate paracellularly across the epithelial cells and to reduce the risk of hepatic clearance.<sup>8</sup> It does not necessarily mean that higher MW compounds do not bear a chance against their small competitors: interest towards upper MW candidates has increased over time in pharmaceutical companies such as Merck or Pfizer and even acceptable bioavailability of compounds with MW above 500 have been reported.<sup>9</sup> Therefore, it might not be the molecular weight *per se* that influences the permeation properties of a drug but rather what can intuitively be correlated with it, namely, the molecular flexibility, the polar surface area, the hydrogen bonds, the rotatable bond counts and the aromatic proportion.<sup>10,11</sup> Back in 1997, Lipinski *et al.* proposed the so-called „rule of 5“ in which he stated that 90 % of the orally administered drugs analyzed fell into three out of the following categories:  $MW \leq 500$ ,  $\log P \leq 5$ , number of H-donor  $\leq 5$ , number of H-acceptor  $\leq 10$ .<sup>12</sup> Later on, the polar surface area ( $\leq 140 \text{ \AA}^2$ ) and number of rotatable bonds ( $\leq 10$ ) were also incorporated.<sup>13</sup>

Without a doubt, the close examination of these physico-chemical properties indicates the design of drug molecules to be potentially more efficient even though direct relationships between the chemical structure and the activity of the drug *in vivo* in terms of interaction with receptors, efflux proteins, metabolizing enzymes, cellular membranes are still far from being trivial. Nevertheless, as reported by Meanwell and coworkers, owing to a deeper understanding of chemical structure-biological activity correlation, the source of drug failure is no longer only a matter of poor bioavailability but concomitant commercial, formulation and toxicity reasons also come into consideration.<sup>14</sup> It can be well understood

that high throughput screening methods have generated a larger amount of potential drugs with a higher degree of molecular complexity which make their formulations more challenging. Unfortunately, this has become a major hurdle for pharmaceutical companies at the moment since the marketability of these potential candidates is plagued by a lack of effective formulations.<sup>15</sup> This can be seen as no less of an opportunity to engage in the development of efficient formulations that could overcome the limitations faced by the majority of the newly/previously discovered drugs which all belong to the class II, III and IV of the Biopharmaceutical classification system (BCS): poorly soluble and highly permeable (class II), highly soluble and poorly permeable (class III), or poorly soluble and permeable (class IV).<sup>16</sup>

### III. Nanocarriers and confinement of therapeutic agents

With the emergence of nanocarriers, strategies to overcome biopharmaceutical limitations associated to the therapeutic agents have become wider. Figure 1 illustrates the variety of nanocarriers that can be explored for drug delivery applications.<sup>17</sup> Whether they are polymeric solid dispersions, liposomes or nanostructured materials (*e.g.* inorganic nanoparticles), the common point is that they provide a nanosized space in which drugs are confined. Not

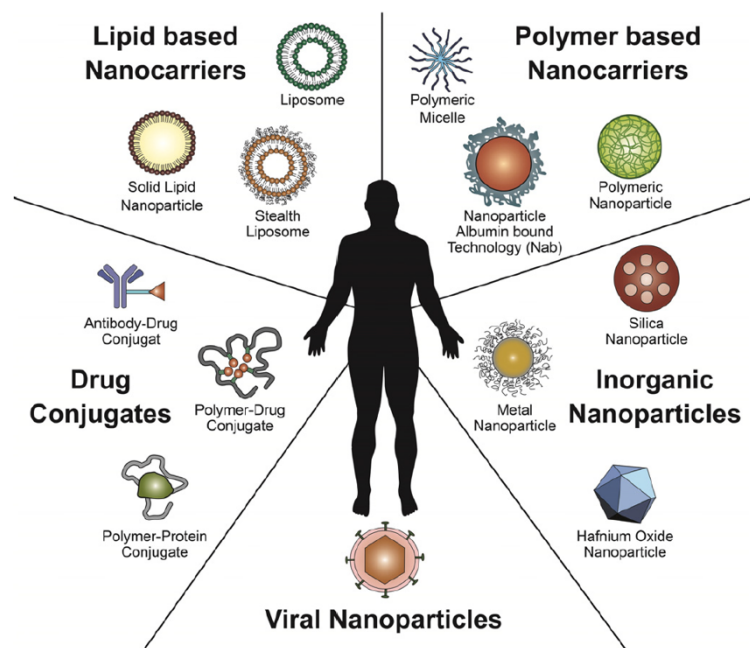


Figure 1: Schematic representation of the variety of nanocarriers under investigation for their ability to carry drugs through the body.<sup>17</sup> Copyright © Elsevier.

only does the confinement of drugs offers a protection against acidic or enzymatic aggressions through the GIT, it is also associated with the “amorphization phenomenon” which refers to the change of the solid state from crystalline to amorphous when the molecules are trapped in pores of a critical size, typically below 20 nm.<sup>18</sup> This phenomenon is of great pharmaceutical relevance as the physico-chemical properties of nanoconfined

drugs differ from their crystalline analogues.<sup>19</sup> The solubility of amorphous species would be enhanced, so this strategy could contribute to solve the first issue of oral delivery *i.e.*, the low solubility of some therapeutic agents. The next issue is the drug permeability; nevertheless, increasing the soluble portion of the administered drug will increase the chances to permeate through the intestinal barrier.

The development of nanocarriers has been an expanding area of research over recent years. For example, liposomes were the first ones to receive the Food and Drug Administration (FDA) approval with the Doxil® technology in 1995.<sup>20</sup> Taking into account that they were discovered back in 1961 by A. D. Bangham, it says a lot on the timeline associated with the process from the research to the marketability phase. A lot of criteria have to be met in order for the nanocarriers to be viable in the area of drug delivery: biocompatibility, stability throughout the GIT, high loading capacity of small/large molecules and ease of synthesis. Mesoporous silica nanoparticles (MSNs) seem to meet all these prerequisites and are therefore promising candidates.

#### IV. Scope of the thesis

The general aims of the thesis are:

- To demonstrate the usefulness of pore confinement effects on therapeutic agents in overcoming solubility, premature drug degradation or release in the GIT and by extension permeability issues
- To develop a versatile pH-responsive formulation for oral delivery that can be used to deliver gastro-sensitive drugs
- To develop a nanocarrier-based formulation for the oral delivery of insulin as an alternative to existing technologies

To accomplish these goals, first, resveratrol, a broad-spectrum nutraceutical whose promising anticancer, cardioprotective, anti-inflammatory and antioxidant activities are being hampered by its poor solubility, was first selected as a representative of the BCS class II. It was encapsulated into MCM-48-type MSNs with particle sizes ranging from 90 to 300 nm and pore sizes of either 3.5 or 7 nm. The solubility and release of resveratrol alone or encapsulated in the different kinds of MSNs were compared. The results indicated that the

encapsulation of the drug in the nanopores clearly increased the release of the drug in aqueous solution. In addition, the particle size of the nanocarriers could also influence the saturated solubility of the hydrophobic drug to some extent. However, the 7 nm pores failed in enhancing the solubility of resveratrol. The most promising combination *i.e.*, the smallest particle size of 90 nm and the smallest pore size of 3.5 nm was then selected for further tests on the permeability across Caco-2 cells and the anti-inflammatory activity. The results of this work were published in the journal *Molecular Pharmaceutics* in 2017 and are presented in the Chapter 4 – part I of this thesis.

Following this first study, an oral delivery formulation was developed by tableting a pH-responsive protein *i.e.*, succinylated  $\beta$ -lactoglobulin with MCM-48- and dendritic-type MSNs (DMSNs). To test the efficacy of such tablets, omeprazole was chosen and incorporated into the porous network of the MSNs. Omeprazole is a proton-pump inhibitor classified as the most transformative drug of the past 25 years, yet highly prone to gastric degradation. It is a good example of drugs needing to be formulated to avoid premature release and degradation in the stomach. Since using this formulation strategy the external surface of the MSNs remains free, methyl groups have been anchored and yielded a hydrophobic surface which could potentially influence the drug/surface interactions, the physical state of the drug and the release rate. In addition, possible cytotoxicity effects and metabolic cell dysfunctions of the drug, the MSNs and the drug-confined MSNs were screened using different intestinal cell lines (HT-29, Caco-2 and HCEC cells). The incorporation of omeprazole-confined MSNs into a pH-responsive formulation was performed and the pH-controlled release of omeprazole was demonstrated. The results have been submitted to the journal *European Journal of Pharmaceutics and Biopharmaceutics* in 2019 and are presented in the Chapter 4 – part II of this thesis.

Resveratrol-encapsulated MCM-48-type MSNs were also formulated with succinylated  $\beta$ -lactoglobulin to afford pH-responsive oral tablets. Pure, methyl- and amino-functionalized MCM-48-type MSNs were compared in terms of physical state of confined resveratrol and release in acidic and near neutral pH. Besides, a particular behavior of amino-functionalized MSNs in the presence of succinylated  $\beta$ -lactoglobulin was evidenced for the release of resveratrol and omeprazole at acidic pH. The results are presented as a manuscript in the Chapter 4 – part III of this thesis.

## Chapter 1 - Introduction

Lastly, a study was conducted to specifically answer the demand for oral insulin dosage. DMSNs were synthesized with various pore sizes, large enough to accommodate insulin and combined with succinylated  $\beta$ -lactoglobulin. A thiol functionality was grafted on the surface as a potential mucoadhesive permeation enhancer. The effect of pore sizes, surface functionalities and formulation strategies on the release of insulin in acidic and near neutral pH were systematically compared. *In vitro* assays based on the insulin starvation of the non-tumorigenic human colon epithelial cells (HCEC) initially cultured with insulin supplement have demonstrated the efficacy of the insulin-confined DMSNs in sustaining the metabolic activity of the cells in absence of insulin supplement. Finally, confocal fluorescent microscopy images have been recorded to demonstrate the role of DMSNs in the transcellular transport of confined-insulin. The results have been accepted for publication in the journal *Chemistry – A European Journal* in 2020 and are presented in the Chapter 4 – part IV of this thesis

## Chapter 2 – State-of-the-art

---

### I. Mesoporous silica nanoparticles

#### I.1. General overview

By definition, MSNs are materials with (1) a defined particle morphology *e.g.*, spheres, rods or other shapes tunable from 30 to 500 nm, and (2) a porous network *i.e.*, pores of size in the mesopore domain (ranging from 2 to 50 nm). Two families of MSNs have been used in this thesis: MCM-48-type and dendritic-type nanoparticles, their structures are illustrated in Figure 2.

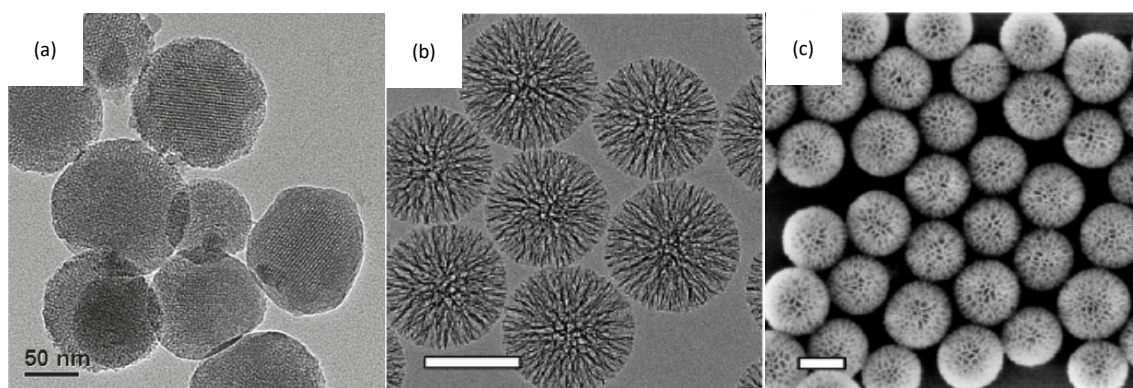


Figure 2: Transmission Electron Microscopy images of MCM-48-type nanoparticles (a) and DMSNs (scalebar 100 nm) (b); Scanning Electron Microscopy image of DMSNs (scalebar 100 nm) (c).<sup>33,24</sup> Copyright © 2014 American Chemical Society.

The ordered mesoporous silica (OMS) materials named MCM-41 were discovered by scientists from Mobil in 1992.<sup>21</sup> Bulk MCM-48 materials were first obtained through surfactant-assisted-synthesis and later on, their synthesis was adapted to produce MCM-48-type nanoparticles.<sup>22</sup> They consist in a 3D-ordered network of interconnected cylindrical-like pores which mesostructure commensurate with the  $Ia\bar{3}d$  cubic symmetry. The walls *i.e.*, the space between the pores, are constituted of amorphous silica.<sup>23</sup> DMSNs have been introduced as a more recent development in the work of Shen *et al.*<sup>24</sup> Their porous structure is center-radial and like the organic dendrimers, several porous shells of various nature can be grown. Typically, MCM-48-type MSNs and DMSNs have a high surface area, around 800 - 1000 m<sup>2</sup> g<sup>-1</sup>, and a high pore volume, > 1 cm<sup>3</sup> g<sup>-1</sup>, in common. However, their porous structures differ greatly; MCM-48-type MSNs have a narrow pore size distribution

(PSD) centered at around 3 nm whereas DMSNs have larger pores tunable from 6 to 20 nm and wider PSD. On the other hand, DMSNs have a very monodisperse particle size distribution with sizes of 70 – 80 nm. MCM-48-based nanoparticles are usually bigger, 150 nm, even though their synthesis has been revisited recently to tailor their particle size from 50 to 500 nm.<sup>25</sup>

## 1.2. Principle of synthesis I: from micelles to OMS

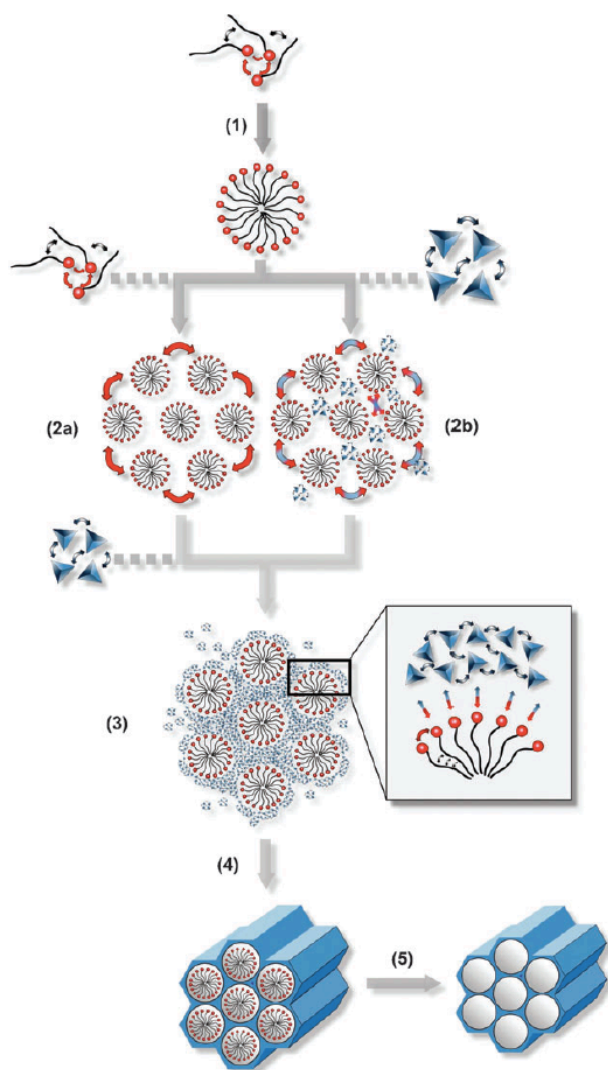


Figure 3: Mechanism of formation of OMS through cooperative self-assembly of SDA with the silica precursors. (1) Formation of the micelles in the SDA solution, (2) formation of the mesophases (2a) by increasing the SDA concentration or (2b) by adding the silica precursors, (3) interaction of the silica source with head-groups of the SDA, (4) polycondensation and formation of the mesostructured composite and (5) removal of the template.<sup>27</sup> Copyright © 2011 The Royal Society of Chemistry.

The mechanism of synthesis of OMS relies on the cooperative self-assembly mechanism between a structure-directing agent (SDA) and inorganic silica precursors in an aqueous solution, as illustrated in Figure 3. The deposition of inorganic silica precursors on isotropic micelles of the SDA leads to the formation of the mesostructure phase.<sup>26,27</sup> The micelles are key components in the formation of porous materials as they induce the final porosity of the materials. For example, cationic surfactants are used in the synthesis of MCM-48-type MSNs and DMSNs *i.e.*, cetyl trimethylammonium halogenides (CTAB,  $C_{16}H_{33}N(CH_3)_3Br$  and CTAC,  $C_{16}H_{33}N(CH_3)_3Cl$ , respectively). Once a certain critical micellar concentration is reached, micelles are formed in aqueous solution: due to their amphiphilic character, the cationic hydrophilic heads of the SDA are exposed to water while the hydrophobic tails interact together to reduce their contact with water. Consequently, the ionic interactions



of these exposed cationic heads with the anionic silicate species will lead to the formation of the silica network through sol-gel approach. Indeed, once the silica source *i.e.*, tetraethylorthosilicate (TEOS,  $\text{Si}(\text{OCH}_2\text{CH}_3)_4$ ) is added to the aqueous solution, the hydrolysis of TEOS under basic catalysis (NaOH,  $\text{NH}_4\text{OH}$  or triethanolamine, TEA) generate  $\text{SiO}^-$  species which interact with the cationic heads of the micelles as depicted in Figure 4.<sup>28</sup> The condensation of silicate species into siloxane bridges *i.e.*,  $\text{Si-O-Si}$ , in interaction with the micellar aggregates produces the hybrid mesophase. Being produced in rather mild conditions at low temperature *i.e.*, from room temperature (RT) to 80 °C, this mesophase is rather soft at first but is further consolidated upon aging and drying at higher temperature *i.e.*, 100 °C. Finally, after calcination at 500 °C, the organic moieties are eliminated and the porosity liberated.

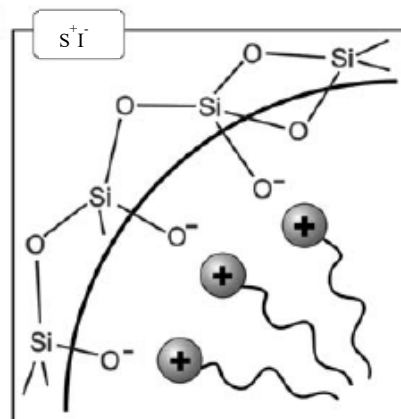


Figure 4: Illustration of the ionic interaction taking place between the SDA (S) and the silicate species (I).<sup>28</sup> Copyright © 2006 Wiley-VCH Verlag GmbH & Co. KGaA, Weinheim.

### I.3. Principle of synthesis II: from OMS to nanoparticles

The obtention of MSNs results from the combination of the cooperative self-assembly mechanism as described above and the Stöber-based synthesis. Non-porous silica spheres have been synthesized in the micron size domain in the late 60's, notably in the work of Stöber *et al.*<sup>29</sup> Silica spheres were successfully obtained through the hydrolysis and condensation of TEOS in an alcoholic mixture containing ammonia as a base catalyst. It was only in 1997, 5 years after the breakthrough of OMS bulk materials, that the adaptation of the Stöber protocol has permitted to release the first synthesis of MCM-41 microspheres exhibiting a particle size ranging from 400 to 1100 nm.<sup>30</sup>

#### I.3.a. pH of the reaction

Key factors that control the nucleation and growth of nanoparticles of a certain size and shape have been identified. As shown in Figure 5, the charge properties and the condensation rate of silica are pH-dependant.<sup>31</sup> Silica has an isoelectric point (IEP) around 2, which implies that at  $\text{pH} < \text{IEP}$ , positively charged species predominate and silica condensation rate is at its lowest. Contrastingly, in the pH range  $\text{IEP} < \text{pH} < 7$ , the concentration

of negatively charged species increases to reach  $\text{pH} > 7$ , where only negative species are present. However, beyond  $\text{pH} 10$  silicate species dissolve and consequently the condensation rate decreases. In this case, conditions of supersaturation are not met and nucleation and growth are not initiated. Nevertheless, in the MSNs-based synthesis, cationic surfactants are present and their strong interactions with anionic silicate species create a highly stable nuclei from which

the nanoparticle growth can start. Thus, the synthesis of MSNs is made in the  $\text{pH}$  range  $10 < \text{pH} < 12$ . In the early work of Stöber *et al.*, the increased concentration of ammonia leads to the formation of bigger colloidal spheres. Tuning the  $\text{pH}$  in this specific region is a way to (1) produce nanoparticles and (2) control their sizes. However, the smaller the size of the nanoparticles, the higher are the chances of aggregation, since by interacting with each other, they try to reduce their surface tension.

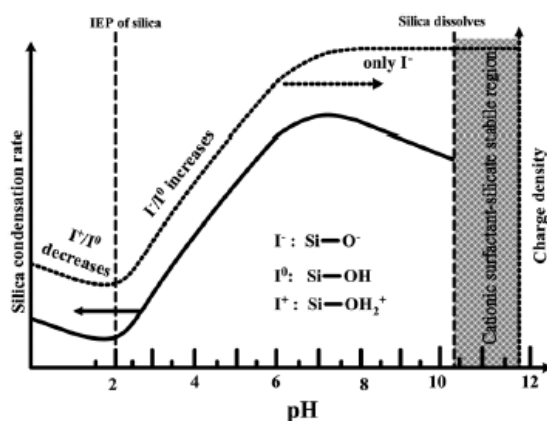


Figure 5: Influence of the  $\text{pH}$  on the condensation rate of silica (plain line) and the charge density (dot line).<sup>31</sup> Copyright © 2013 The Royal Society of Chemistry.

### I.3.b. Particle size control and aggregation issues

One way to circumvent this issue is through the use of co-surfactant as particle growth inhibitor and steric stabilizer. Suzuki *et al.* opted for this strategy and added the co-polymer block Pluronic F127 (EO<sub>106</sub>-PO<sub>70</sub>-EO<sub>106</sub>) to the reaction. As a result, the mesophase formed is wrapped by the co-polymer and the condensation of silanol groups is quenched as shown in Figure 6.<sup>31,32</sup> Later on, Kim *et al.* applied this principle to the synthesis of MCM-48-type MSNs and showed that increased concentration of F127 leads to smaller particle sizes *i.e.*,

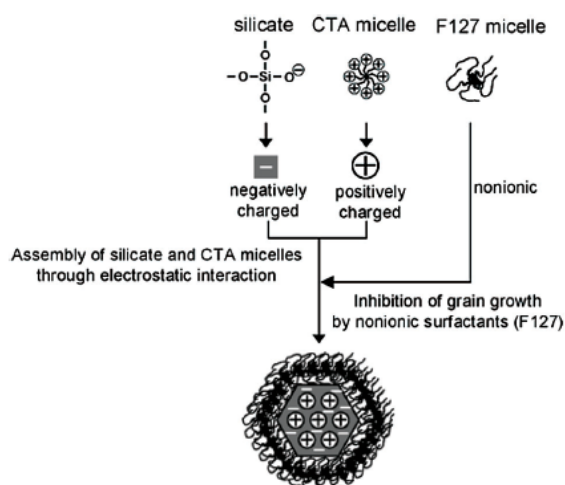


Figure 6: Schematic representation of the role of F127 in the synthesis of MSNs.<sup>31</sup> Copyright © 2013 The Royal Society of Chemistry.

around 70 nm, and *vice-versa*.<sup>33</sup> A principle that was further investigated by Bouchoucha *et al.* and permitted to generate 50 nm MCM-48-type nanoparticles.<sup>25</sup> Other compounds such as TEA have been employed as a base catalyst just as NaOH or NH<sub>4</sub>OH and for their ability to reduce the growth and aggregation through complexation of the silicates and nanoparticles.<sup>34</sup>

### I.3.c. Biphasic approach

The biphasic approach, elaborated by Shen *et al.* in 2014, is at the origin of the synthesis of DMSNs.<sup>24</sup> The water phase contains CTAC and TEA, while the oil phase comprises TEOS and a hydrophobic organic solvent, cyclohexane or cyclohexane for instance. In this inhomogeneous reaction, the interface of the two phases allows a fine control of the cooperative assembly between the cationic surfactant and the silica species, as illustrated in Figure 7. The formation of this type of silica nanoparticles is, up to now, not understood in detail as it involves many complex processes but various explanations have been proposed. As suggested, the special organization of the hydrophobic chain of CTAC at the interface allows the organic solvent to break into the water phase under mechanical stirring. Meanwhile, TEOS is being hydrolyzed and condensed at the interface thus forming hemimicelles with CTAC. Under continuous stirring, these as-formed seeds are very dynamic and can further reach the interface, assemble and grow bigger.<sup>35</sup>

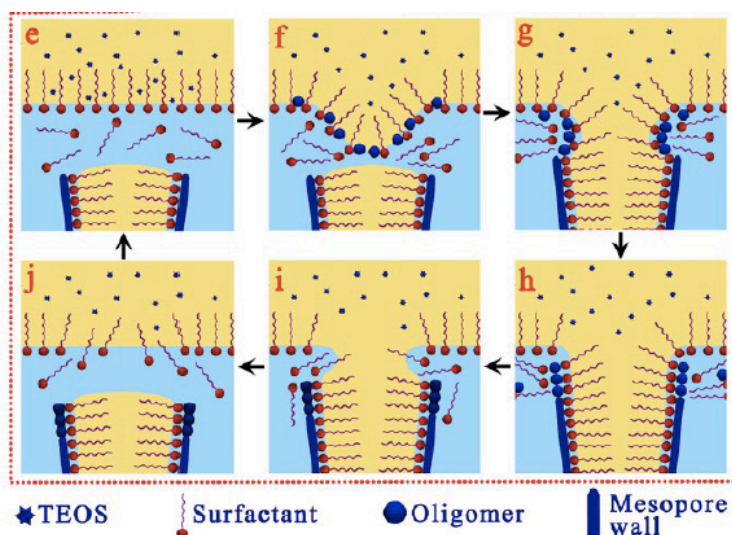


Figure 7: Schematic representation of the postulated mechanism of the formation of DMSNs.<sup>24</sup> Copyright © 2014 American Chemical Society.

Several other syntheses of dendritic-like MSNs have been established with similar mechanism and fine control of the morphology, pore and particle size has been shown as being

rather straightforward in the DMSNs-based synthesis.<sup>36</sup> For example, Dang *et al.* reported the effects of the concentration of the SDA (CTAB) and the stirring speed on the particle morphology, as illustrated in Figure 8, the temperature and the time of the reaction were also varied.<sup>37</sup> Wang *et al.* also emphasized the importance of the time reaction since disappearance of the dendritic structure upon increasing the reaction time from 0.3, 1, 2 to 5 h was witnessed (one-pot synthesis).<sup>38</sup> In another biphasic approach, Xiong *et al.* used cetyltrimethylammonium tylosate as a SDA and TEOS as the only constituent of the oil phase; they obtained what they called “stellate” MSNs.<sup>39</sup> In a one pot set-up, Meka *et al.* reported a vesicle supra-assembly approach to synthesize hollow DMSNs for protein delivery through the mediation of a second silica source made of an amine organosilane.<sup>40</sup>

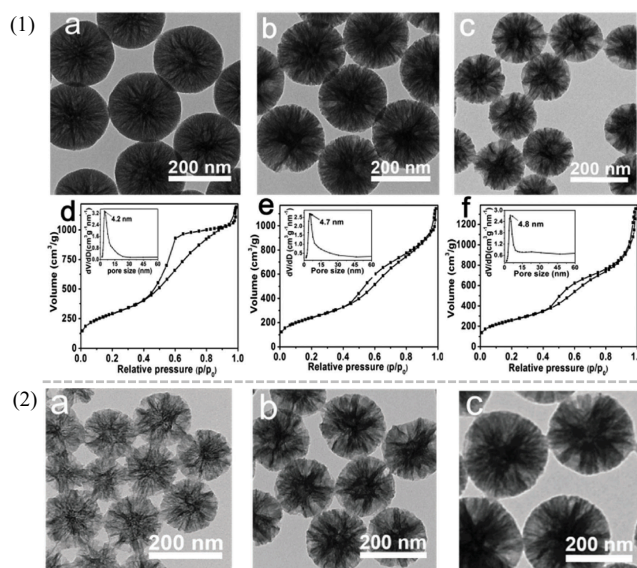


Figure 8: (1) Effect of the stirring rate: 500 (a and d), 300 (b and e) and 100 rpm (c and f); (2) effect of the CTAB concentration: 0.95 (a), 1.3 (b) and 1.9  $\text{mg ml}^{-1}$  (c) on the structure, porosity and particle size as evidenced by the TEM images and the  $\text{N}_2$  isotherms and PSD.<sup>37</sup> Copyright © 2017 The Royal Society of Chemistry.

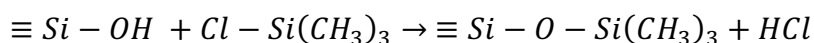
Whether it is the OMS bulk materials, the MCM-48- or the DMSNs-based synthesis, once the organic surfactants have been either calcined or extracted, silanol groups are exposed at the surface of the materials and can be further functionalized.

#### I.4. Principle of functionalization

In addition to their native properties *i.e.*, porosity, robustness, thermal stability, MSNs can be functionalized to fulfill the requirement of specific applications. Functional groups such as amine, thiol, phosphonate, carboxylic acid, can be covalently anchored at the

surface of MSNs through post-synthesis grafting (Figure 9a) or co-condensation method (Figure 9b). Silanization *i.e.*, reaction of simple organic silanes with the reactive free single ( $\equiv SiOH$ ) or geminal ( $= Si(OH)_2$ ) silanol groups takes place.<sup>28</sup> These groups will change the physico-chemical properties of the MSNs. For example,  $NH_2$  groups will shift the IEP to higher pH compared to the native silica or polyethylene glycol (PEG) will ensure a long colloidal stability of the MSNs in aqueous solution.<sup>41</sup> Alternatively, in order to drastically change the polarity of the surface, the silanol groups can be capped using methylsilanes *i.e.*, methyltrichlorosilane (Eq. 1) or hexamethyldisilazane (HMDS) (Eq. 2) as follow:

Eq. 1:



Eq. 2:



These are typical post-synthetic grafting reactions. When the functional groups are introduced *in situ* through co-condensation of TEOS and the organosilanes directly, they are located in the pore walls of the MSNs and distributed more homogeneously (Figure 9b). However, many disadvantages derive from this method: the materials cannot be calcined, otherwise the organosilanes will be combusted with the surfactants.<sup>27, 28</sup> Instead, surfactants can be extracted under reflux conditions, though the complete elimination can

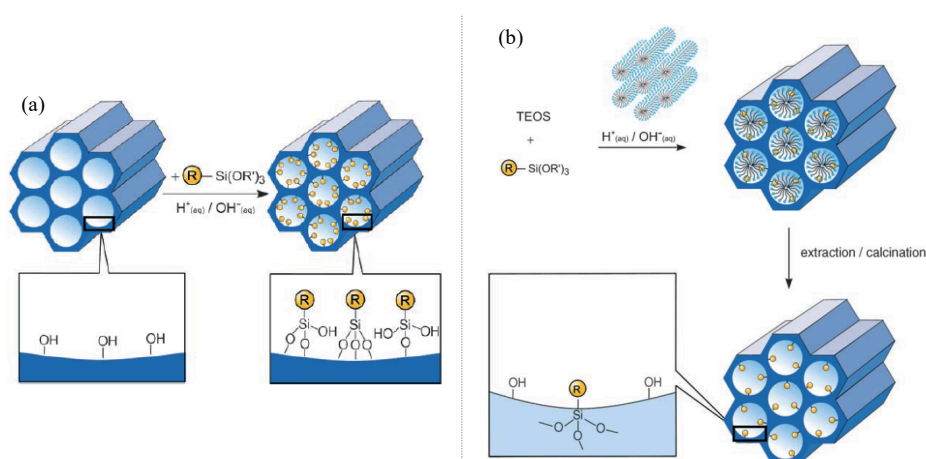


Figure 9: Schematic representation of the functionalization of OMS with different organosilanes  $(R'O)_3Si-R$  through post-synthesis grafting (a) or co-condensation (b).<sup>28</sup> Copyright © 2006 Wiley-VCH Verlag GmbH & Co. KGaA, Weinheim.

not be absolutely guaranteed and residues of CTAB or CTAC beyond toxic threshold can be an issue.<sup>42</sup> The organo-functionalization by co-condensation or post-synthetic grafting has opened the door to various coupling strategies.<sup>43</sup> Conjugation of functionalized or pure MSNs with biomacromolecules to specifically address the challenges of the oral delivery routes are further described and discussed in the section III.3. of this chapter.

## II. Encapsulation and release of therapeutic agents

Encapsulation of drugs is an inspiring area of development since the physico-chemical properties of the drugs, taken alone or confined into a nanosized space, differ greatly. Methods to introduce a therapeutic agent into pores of several nanometers have been set up and are reviewed in this section as well as the impact on the drug properties and release.

### II.1. Method of drug encapsulation

In order to diffuse homogeneously into the porous structure of any kind of nanocarriers, the drugs have to be solubilized or liquefied. They are either physically trapped in the pores through solvent diffusion, melting techniques or covalently anchored on the surface. Because the latter is outside the scope of this thesis, further details will not be discussed here but interesting work can be found elsewhere.<sup>44</sup>

#### II.1.a. Solvent diffusion

Undeniably, solvent diffusion is a widely used technique and it has several variations. Typically, the molecules are dissolved in a solvent prior to the addition of the MSNs. Under low speed stirring or shaking, the liquid progressively wet the surface through capillarity allowing the occurrence of non-covalent H-bonding and Van der Waals interactions between the silica surface and drug molecules.

##### 1.a.i. Nature of the solvent

The choice of the solvent must be appropriate. In this regard, two prerequisites have to be fulfilled: it should dissolve the drug up to high concentration and it should be easily removed from the MSNs. The latter case can be done by evaporation, centrifugation (followed by a drying step) or lyophilisation. It can be problematic in case of high boiling point solvent *i.e.*, dimethyl sulfoxide (DMSO) or dimethylformamide (DMF): respectively 189 °C and 153 °C at atmospheric pressure. Residues of solvent would stay trapped in the pores

and knowing the cytotoxicity of DMSO above certain concentrations, it would clearly limit the biological applicability of drug-loaded MSNs. Furthermore, the drug should be stable upon solvent removal *i.e.*, the temperature has to be carefully set which goes along with a judicious choice of the solvent.

#### 1.a.ii. Drug concentration

The choice of the concentration of the drug mainly depends on the technique of solvent removal. With the solvent evaporation technique, whether it is using rotary evaporation or not, the initial mass of drug added will be entirely integrated in the final product. A 20-30 % drug loading seems reasonable as it was done by Jambhrunkar *et al.* with the loading of curcumin from a methanol solution, or griseofulvin from a dichloromethane solution.<sup>45,46</sup> On the other hand, upon centrifugation, the amount of drug not adsorbed will be eliminated with the supernatant, thus increasing the uncertainty of drug loading. In this case, concentrated drug solutions are prepared in order to shift the equilibrium and maximize drug adsorption. Using this method, relatively low loading of doxorubicin, a well-known anticancer agent, are reported, 1.7 % from Meng *et al.*<sup>47</sup>, 4.8 % from Zhang *et al.*<sup>48</sup> and 8 % from Bouchoucha *et al.*<sup>49</sup>

#### II.1.b. Incipient wetness impregnation

A variant of the solvent diffusion technique can be found in the incipient wetness impregnation. In this case, the volume of solution is equal to the volume of the pores. Therefore, a small volume of a concentrated drug solution is dropped on the materials and upon active mixing with a spatula, a paste is formed and the drug diffuses through the porous network of the materials.

#### II.1.c. Melt loading

The melt loading technique relies on the same capillarity action as the previous ones, except that the mixture materials/drug is heated above the melting point of the drug under continuous stirring. The drug-loaded materials are obtained upon cooling to RT. No solvent is needed to dissolve the organic molecules which can represent an advantage for poorly soluble drugs and also suppress the drying step. However, it could potentially impair the therapeutic activity of the molecule upon induction of conformational changes. With this technique, it should be ensured that the host and the guest are thermally stable at the melt impregnation temperature.

## II.1.d. Supercritical fluid

Finally, it is worth mentioning the possibility of drug loading with supercritical CO<sub>2</sub> fluid. Instead of being dissolved in an organic solvent, a compressed high volatile fluid is used at temperature and pressure above the critical point of CO<sub>2</sub> (304.25 K and 7.39 MPa respectively).<sup>50</sup> Generally, the solubility of drugs in supercritical fluid is higher which is advantageous. However, although in comparison with other techniques, some steps are not needed anymore, it requires access to special high-pressure equipment.

To conclude, Figure 10 provides an overview of the most common techniques described above and the consequences they can have on the distribution of the drug throughout the porous network.<sup>51</sup> Mellaerts *et al.* revealed that the most appropriate method for loading itraconazole into the pores of SBA-15 is the incipient wetness method since a homogeneous distribution of the drug in the micropores and the mesopores was observed. In contrast, the melt technique failed in the penetration of itraconazole inside the pores due to the high viscosity of the molten state. As illustrated, homogeneous spreading of ibuprofen through the porous network of SBA-15 was reported even using the melt technique, ibuprofen being less viscous in its molten state.

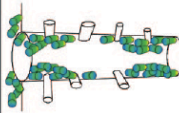

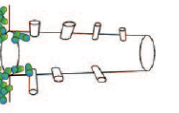
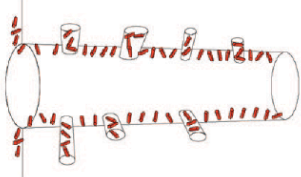
	Solvent	Incipient wetness	Melt
Itraconazole			
Ibuprofen			

Figure 10: Schematic representation of the influence of the chemical structure and the encapsulation techniques on the localization of itraconazole or ibuprofen in the pores of SBA-15 materials.<sup>51</sup> Copyright © 2008 American Chemical Society.



## II.2. Physico-chemical properties of encapsulated drugs

Regardless of the technique of encapsulation used, once the drugs are confined in a nano-sized domain, their physical state, mobility and stability can be modulated using materials with different porous and surface characteristics.

### II.2.a. Drug / surface interaction

As they are physically adsorbed, drugs are in close contact with the pore surface of the silica materials, thus depending on the chemistry of the surface *i.e.*, pure or functionalized surface, weaker/stronger interactions will be encountered.

#### 2.a.i. Pure silica surface

Silanol groups exposed at the surface of pure materials have a bivalent role: the oxygen ( $\equiv Si - OH$ ) can act as a donor atom and the terminal hydrogen ( $\equiv Si - OH$ ) as an acceptor atom. It is not impossible that silanol groups in close proximity can interact together. As demonstrated by Delle Piane *et al.*, the drugs themselves direct their interactions with the surface; while aspirin formed four H-bonding with silanol groups (three from the carboxylic group and one from the ester carbonyl), ibuprofen, being more apolar, interacts only through its carboxylic group.<sup>52</sup> Besides polarity, the rigidity of the molecules comes also into play to tackle well established theories on the strength and length of H-bonding. As pointed out by Gignone *et al.* with the example of the anti-fungal drug clotrimazole, weaker bonds such as  $Si-OH \cdots Cl$  and  $Si-OH \cdots \pi$  predominated over the stronger and shorter  $Si-OH \cdots N$ , in the case of the weakly hydroxylated surface of MSU-H-type OMS.<sup>53</sup> This latter case naturally brings into the question of the impact of the degree of hydroxylation of the surface *i.e.*, the density of silanol groups, on the adsorption of the drugs.

#### 2.a.ii. Apolar surface

The best way to get insight into the impact of the silanol groups on the adsorption of a drug is to eliminate the silanol groups from the equation. This has been done in the work of Mäkilä *et al.*, in which a comparison of the behaviour of ibuprofen in contact with a highly polar or highly apolar surface is reported.<sup>54</sup> As described previously, ibuprofen engaged its carboxylic group into H-bonding with the polar surface, as evidenced by the decrease in the Fourier Transformed Infrared Spectroscopy (FTIR) signal of  $\nu (Si-OH)$ . Another interesting behaviour has been elucidated using  $^1H$  Nuclear Magnetic Resonance

(NMR). A considerable difference in the chemical shift of the hydroxyl resonance peaks of ibuprofen has been pertinently noticed *i.e.*, from  $\delta = 9.4$  ppm to  $\delta = 12.3$  ppm in the case of polar and apolar surfaces respectively, and correlated with an environment dependency effect. In other terms, ibuprofen would rather bond with itself through intermolecular interactions than with an inhospitable environment, whereas H-bonding of the monomer ibuprofen with a polar surface is prioritized over intermolecular arrangement. Therefore, terminal protons of hydroxyl groups have a completely different environment which impacted on the NMR signals. Consequently, the loading capacity of apolar surface is somewhat lower as discussed by Andersson *et al.* For example 20 wt % of ibuprofen was successfully introduced in a fully hydroxylated silica surface vs 5 wt % for a silica surface calcined at 1173 K in which the remaining free silanol groups have likely condensed.<sup>55</sup>

#### 2.a.iii. Organofunctionalized silica surface

Upon functionalization of silica materials, the silanol groups react with the organosilanes and are replaced. It is an interesting approach to modulate electrostatic attraction between the drug and the functional groups of the materials. Towards this particular objective,  $NH_2$  groups have been extensively investigated. For example, a pertinent comparison of the mobility of aspirin loaded in either pure or amino-functionalized silica MSNs was published by Datt *et al.*<sup>56</sup> Therein, stronger interactions of aspirin with the amino-functionalized MSNs reduced the motion of the drug whereas the reverse effect was observed for pure MSNs.

Ballas *et al.* also employed amino-functionalized MCM-41 and SBA-15 materials to load the biphosphonate drug alendronate, active against bone diseases, from a pH 4.8 aqueous solution.<sup>57</sup> At this pH, there is an electrostatic attraction between positively charged amine groups  $NH_3^+$  and negatively charged phosphonate groups  $HPO_3^-$  resulting in a 3 times higher loading capacity for the amino-functionalized materials in comparison to the pure starting materials. Not only did they report a functionalization effect, they also found a pore size effect on the loading capacity of the materials. Indeed, 37 % of drug was successfully confined in the amino-functionalized MCM-41 materials vs 22 % in the larger pores of amino-functionalized SBA-15 materials. Special attention has been dedicated to the impact of the pore size of the materials on the physico-chemical properties of the confined drug and will be expounded upon in the next section.

## II.2.b. Amorphization and polymorphism

As already briefly introduced, the confinement of therapeutic agents into pores of a certain size  $d^*$  can be accompanied by a change in the physical state of the drug from crystalline to amorphous on the basis of the thermodynamic model proposed in the Gibbs-Thomson equation (Eq. 3):

Eq. 3:

$$d^* = \frac{4 \cdot \sigma_{cl} \cdot T_m^\infty}{[(T_m^\infty - T) \cdot \Delta H_m \cdot \rho_c]}$$

Where,  $\sigma_{cl}$  is the surface energy between crystal and melt,  $\Delta H_m$  the heat of melting,  $T_m^\infty$  the melting temperature of the bulk crystal and  $\rho_c$  the density of the bulk crystal.<sup>58</sup> Thus, by extrapolation, depending on the thermodynamic characteristics of a given drug, this critical pore size will change. Nevertheless, it is now commonly accepted that drugs confined in pores having  $d^* \leq 20 \times \text{molecular size}$  are prone to amorphization.<sup>54</sup> Numerous proofs of this idea can be found in the literature but one particularly established direct correlation between pore size, drug loading and physical state. Because fluorinated compounds have broken into the pharmaceutical development, Nartowski *et al.* followed the behaviour of flufenamic acid (FFA) confined in 3.2, 7.1 and 29 nm pores (MCM-41, SBA-15 and MCF materials respectively) using <sup>19</sup>F NMR.<sup>59</sup> For a clearer overview, their findings are compiled in Figure 11. The melt method was used in order to precisely incorporate various ratios of FFA. As demonstrated in this study, in the small pores, the drug never arranges in a crystalline phase whereas in the 29 nm pores, the crystalline phase is formed. Moreover, the first FFA molecules adsorbed are highly mobile and this, regardless of the pore size. A liquid-like state was also elucidated in the pioneering work of Azaïs *et al.*<sup>60</sup> Here, the pore size difference between the materials investigated was narrowed down and the nucleation of a crystalline phase of ibuprofen was already observed in the 11.6 nm pores as evidenced by <sup>13</sup>C Cross-Polarization (CP) NMR experiments. Besides, the cohabitation of a crystalline and a glassy state was also reported in the 11.6 nm pores. The encapsulation of drug in mesopores aims at the suppression of the crystallization or at the

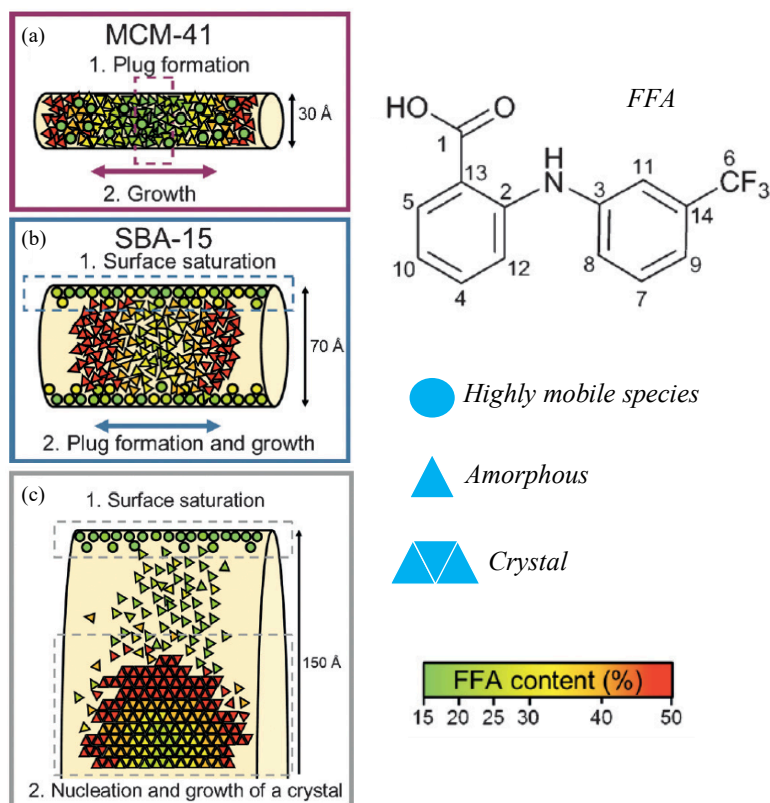


Figure 11: Influence of the loading and the pore size on the mechanism of formation of the amorphous or crystalline state of FFA in the pores of MCM-41 (a), SBA-15 (b) or MCF materials (c).<sup>59</sup> Copyright © 2016 Wiley-VCH Verlag GmbH & Co. KGaA, Weinheim.

nucleation of rare polymorph species which are both relevant for the pharmaceutical industry. A polymorph refers to the many different internal crystalline forms that one chemical structure can adopt in terms of packing and conformational arrangements. As a result, the physico-chemical properties change, such as melting temperature, solubility or dissolution rate to name a few.<sup>61</sup> Although, the use of larger pores could lead to crystallization, it could still be beneficial if the drug crystallize in a rare polymorph otherwise hardly obtained. In this regard, a recent report by Nartowski *et al.* highlights the crystallization and stabilization of the polymorphs of indomethacin upon confinement in the 30 and 55 nm pores of mesocellular foam materials (MCF) and controlled pore glass (CPG) materials, respectively. Indomethacin was introduced using the melt loading and depending on the pore size of the materials, the quantity of drug loaded and post-loading treatments, different physical state were obtained *i.e.*, amorphous, mixture of polymorphs, polymorph V or the most stable  $\gamma$ -phase, as illustrated in Figure 12.<sup>62</sup> Following up on this work, the authors more recently published the encapsulation of tolbutamide through melt loading in MCM-41 materials with 3.2 nm pores. The crystallization of the drug is

successfully inhibited up to 30 % loading, whereas at higher loading, the form V has been identified using powder X-Ray Diffraction (PXRD), Differential Scanning Calorimetry (DSC) and solid-state NMR data.<sup>63</sup> The amorphous and the polymorphous state are metastable however since the contribution of the pore surface compensates the energetic cost, the return to equilibrium *via* crystallization to a more stable phase is inhibited. Stabilizing both phases is one thing but their stability over a certain period of time needs to be considered and has been recently pointed out in the literature as discussed in the following part.

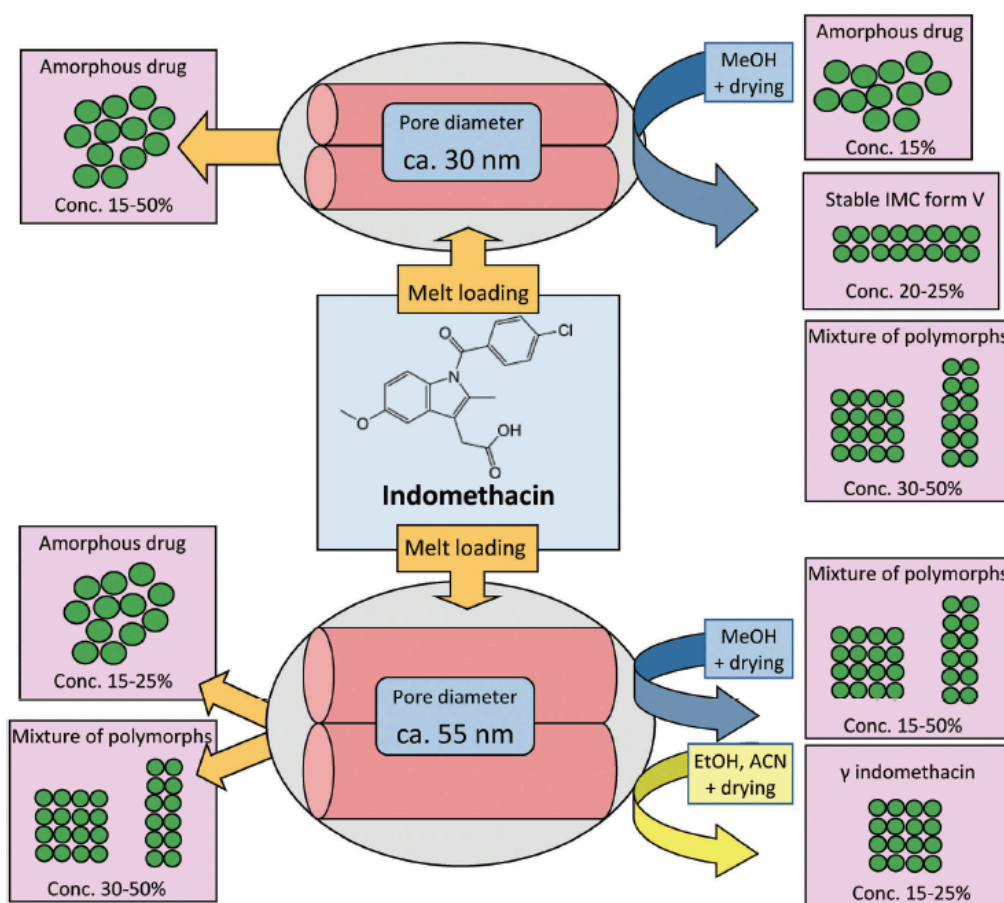


Figure 12: Schematic representation of the possible amorphous and crystalline transformations occurring during melt loading encapsulation of indomethacin into MCF and CPG materials.<sup>62</sup> Published by the PCCP Owner Societies.

### II.2.c. Stability of the confined drug

Since these metastable physical states are associated with defined physico-chemical properties, any physical state changes upon recrystallization would impair the solubility and the permeability of the drugs. In this regard as well, the loading can be the driving force for the precipitation of drugs. Indeed, it has been suggested by Wei *et al.* that 28 % loading of hesperidin remained amorphous after 6 months storage as evidenced by the powder

PXRD pattern presented in Figure 13. In contrast, the materials with a cargo of 60 % showed an endothermic peak in the DSC profile and diffraction peaks in the PXRD pattern after 6 months storage which were assigned to the precipitation of non-confined hesperidin on the external surface of the materials due to overloading.<sup>64</sup> An interesting differentiation was made on the loading of ezetimibe into 5 nm or 30 nm pores: after 5 months storage the drug confined in the 30 nm recrystallized but the one confined in the 5 nm did not, as evidenced by the absence of long range order in the PXRD pattern.<sup>65</sup> The effect of nanoconfinement was also demonstrated in the work of Ambrogi *et al.* When subjected to stressed conditions, 40 °C and 75 % of moisture, the encapsulated carbamazepine stayed amorphous while the growth of the polymorph III increased by 15-35 % in the case of the free drug.<sup>66</sup>

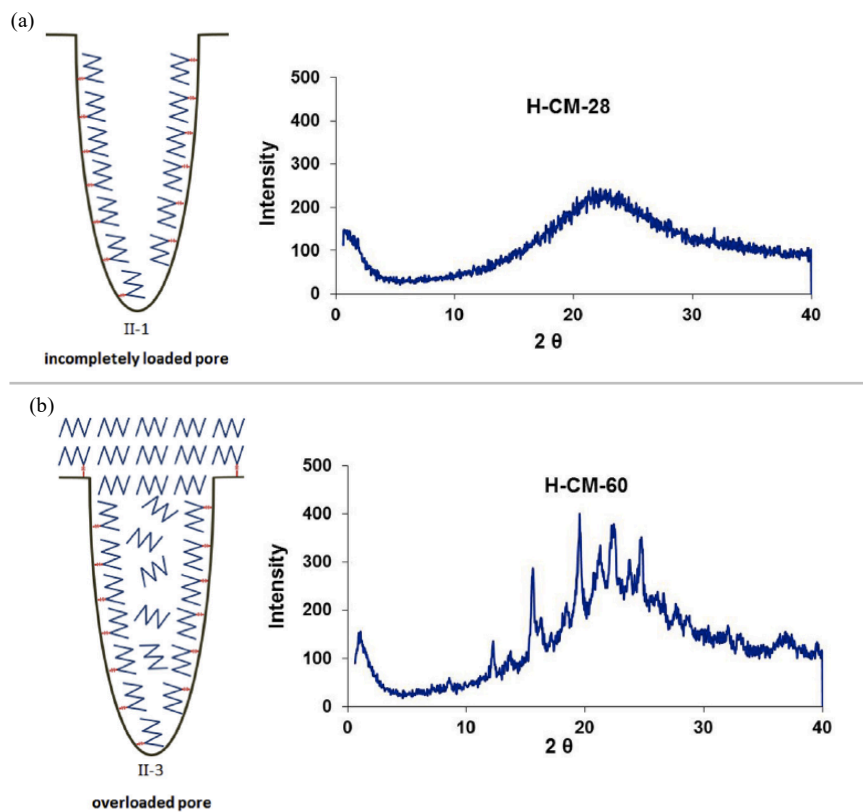


Figure 13: Schematic illustration of 28% (a) or 60% (b) of hesperidin loaded in Aeroperl 300 materials and the associated PXRD diffractograms recorded after 6 months storage at RT.<sup>64</sup> Copyright © 2016 Elsevier B. V.

### II.3. Release performance

The fact that upon encapsulation and nanoconfinement, properties of drugs can be tuned is really an asset for further pharmaceutical developments, however, all these achievements are irrelevant if the payload cannot be released in aqueous solutions.

#### II.3.a. Influence of the silica surface

##### 3.a.i. Pure surface

On the one hand, the release of drugs from pure silica materials might be associated to a burst release *i.e.*, the confined drug is often released very quickly in a short lapse of time. For example, after only 15 min in acidic media, 88 or 95 % of ibuprofen was released from SBA-15 and MCM-41 materials respectively. In comparison, only 16 % of ibuprofen crystals were dissolved.<sup>67</sup> Even though, the silanol groups and the drug interact together, the H-bonding has a short lifetime when the materials are poured in an aqueous solution owing notably to the wettability properties of the polar surface of pure silica materials. It is also likely that high mobility or liquid-like states are two factors that will immediately increase the elution of the confined molecules. On the other hand however, this might be of an advantage for highly hydrophobic drugs since owing to the amorphization phenomenon, the solubility or release might be several times higher than the free crystals. For example, Jambhrunkar *et al.*, revealed that after 72 h, 28 % of curcumin which is highly hydrophobic (aqueous solubility of 3  $\mu\text{g ml}^{-1}$ ), was released from MCM-41 nanoparticles whereas only 9 % of the free drug was dissolved.<sup>68</sup>

##### 3.a.ii. Functionalized surface

In contrast, when electrostatic attractions between the drug and the functionalized surface are involved, the elution occurs generally in a sustained manner. For example, it took 4 h for aspirin to almost completely diffuse out of MCM-41 materials, whereas 50 - 60 % was released from the amino-functionalized counterpart.<sup>56</sup> Similarly, a diffusion controlled mechanism was implemented through silylation of MCM-41 materials with HMDS silane. Indeed, the methyl groups grafted at the surface reduced the wettability of the materials and resulted in a progressive release of ibuprofen over a period of 10 h as opposed to the burst release observed using pure MCM-41 materials.<sup>69</sup> Jambhrunkar *et al.* compared the release of griseofulvin, a rather hydrophobic drug (aqueous solubility of 20  $\mu\text{g ml}^{-1}$ ), from pure MCM-41 and methyl-functionalized MCM-41 materials. After 24 h at pH

7.4, the quantity of drug eluted followed the ascending order: 20, 50 or 80 % for MCM-41-CH<sub>3</sub>, pure drug and MCM-41 materials. While the low performance of MCM-41-CH<sub>3</sub> is attributed to poor wettability of both hydrophobic drug and carrier, MCM-41 materials are believed to offer good wetting properties and confinement effects resulting in a higher release of the cargo.<sup>70</sup> Similarly, in the work of Ballas *et al.*, the elution of alendronate from amino-functionalized MCM-41 or SBA-15 materials was slower in comparison to their pure counterparts. Moreover, it seems that the mechanism of elution was somewhat different: for the smaller pores and larger surface area *i.e.*, MCM-41 materials, it was assumed that a surface-dependent phenomenon with a first-order-kinetic was at play while for the larger pores and smaller surface area *i.e.*, SBA-15 materials, a diffusion behaviour with a zero-order kinetic or linear model fitted better.<sup>57</sup>

From these results, two strategies can be extracted:

- For highly soluble drugs (BCS Class I and III): sustaining the drug release upon electrostatic interaction with the surface might be the path to take.
- For poorly soluble drugs (BCS Class II and IV): the amorphization effect allows the increased release of these drugs in aqueous media in comparison to the free drug crystals.

### II.3.b. Influence of the pore size

The influence of the pore size is still a major debate in the field of drug delivery and numerous studies have been published in recent years. An early work has been published by Horcajada *et al.* on the adsorption/desorption of ibuprofen. MCM-41 materials with pore size ranging from 2.5 to 3.6 nm have been successfully synthesized using SDA of different carbonyl chain lengths *i.e.*, 8, 12, 16 carbon atoms. Their finding showed that with 3.6 nm pores, the release rate was 24 mg h<sup>-1</sup> whereas with the 2.5 nm pores, it decreased to 5 mg h<sup>-1</sup>. They concluded that smaller pores caused a denser packing of the adsorbed ibuprofen which could reduce the velocity of the media in the pore channels and hence the desorption of the drug.<sup>71</sup> Although, it is a striking example demonstrating how the pore size can regulate the drug desorption, the pore sizes compared were very close and one might wonder if this trend is transposable to bigger pore size of 6-10 nm for instance. Part of the answer was made available in the work of Ukmur *et al.* From their perspective, the reason behind the effect of pore size on the release rate of the confined drug could be



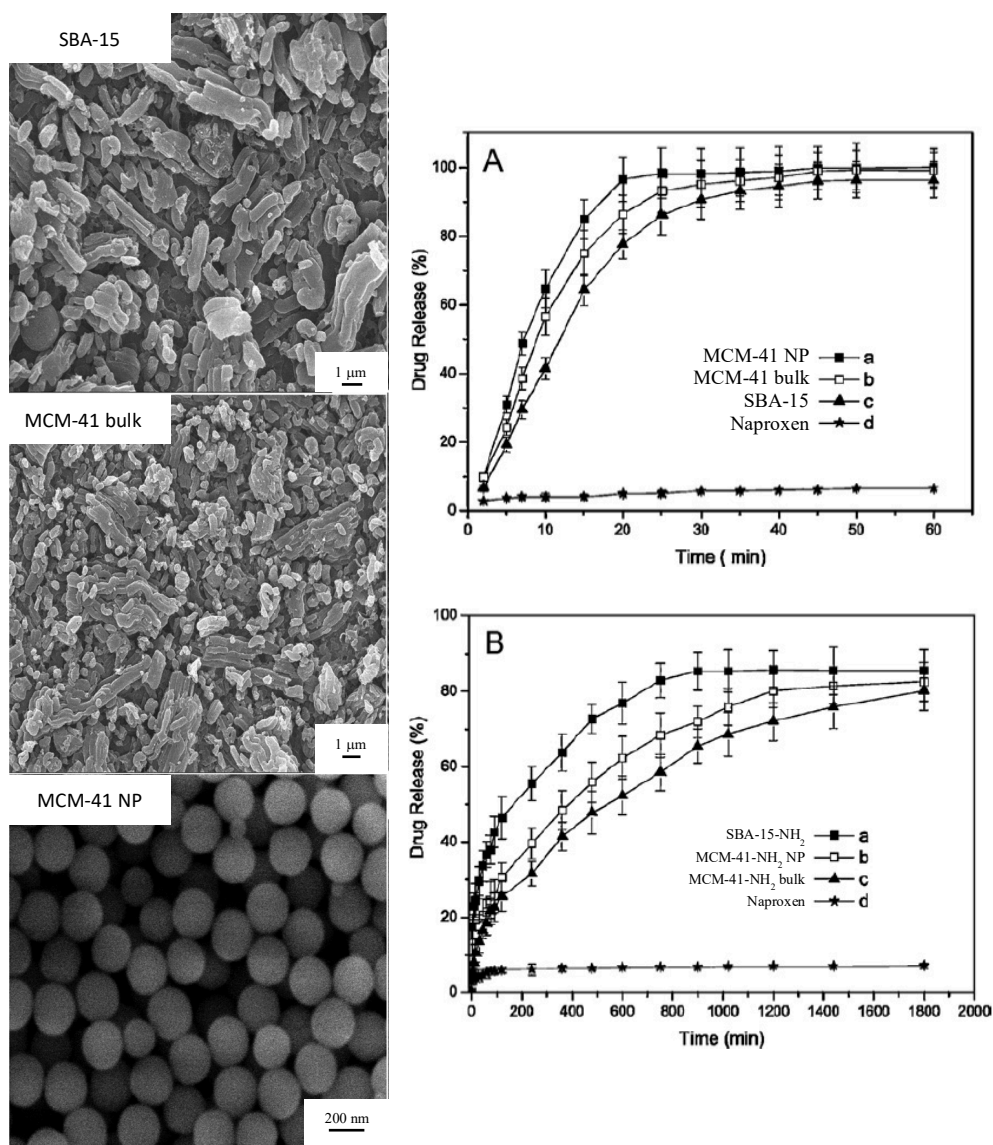


Figure 14: Scanning Electron Microscopy images of the different materials used for the loading of naproxen and release profile at simulated intestinal fluid (pH 6.8) from the pure (a) and the amino-functionalized matrices (b).<sup>73</sup> Copyright © 2013 Elsevier B. V.

the strength of the drug-surface attraction which influences the local fluxes in the porous network.<sup>72</sup> The pertinent example from Guo *et al.* would help in drawing clearer insights. They systematically studied the release of naproxen from pure and amino-functionalized MCM-41 and SBA-15 materials and the results are presented in Figure 14.<sup>73</sup> Concerning the pure materials, the elution was extremely fast, in 60 min all the drug was dissolved in the media. It was observed that the rate was lower with the larger pores accounting for the presence of a higher crystalline fraction of naproxen. In comparison, no matter which pore size was used, all the amino-functionalized materials slowed down the drug dissolution considerably *i.e.*, after 10 h, 60 or 80 % release was quantified for MCM-41-NH<sub>2</sub> or SBA-15-NH<sub>2</sub> respectively. Since among the amino-functionalized materials, no diffraction

peaks were observed in the diffractogram, it can be assumed that, here, the attraction between the carboxylic group of the drug and the amine functions of the materials regulated the diffusion. The interaction of the drug with the surface is stronger in the smaller pores of MCM-41-NH<sub>2</sub> and the flow is slower, therefore the delivery time is longer. The release from the MCM-41 nanoparticles was, in the two cases, faster than the bulk analogue, as a consequence of shorter pore channels in nanosized particles. The release performances were also discussed by Izquierdo-Barba *et al.* in terms of size of the molecules adsorbed using ibuprofen (length 11 Å, width 5 Å) and erythromycin (length 11 Å, width 16 Å) as representatives of small and large size molecules respectively.<sup>74</sup> They used spherical MCM-48-type nanoparticles with pore size of 3.6 nm and large pore materials having also a cubic porous structure with pore size of 5.7 nm. In both cases, the release was much faster from the larger pore materials than the smaller ones *i.e.*, after 24 h 70 and 100 % of the drug was eluted from the small and large pores respectively. However, due to stronger interactions with the silanol groups, the release of erythromycin was slower than ibuprofen *i.e.*, 30 and 70 % eluted, after 24 h, from small and large pores materials respectively. Again, a different story is revealed when a functionality is added. Indeed, a really low release was obtained upon anchoring hydrophobic carbon chains on the large pore materials *i.e.*, only 10 % release after 24 h.

These are examples showing how the release of a drug from OMS or MSNs can be regulated mainly upon pore size and surface functionality. However, for oral delivery, due to the hostile GIT environment, a gating mechanism based on biomacromolecules for instance is required in order to transport the drug to the intestine.

### III. Mesoporous silica nanoparticles in the oral route

#### III.1. Barriers of the GIT – overview

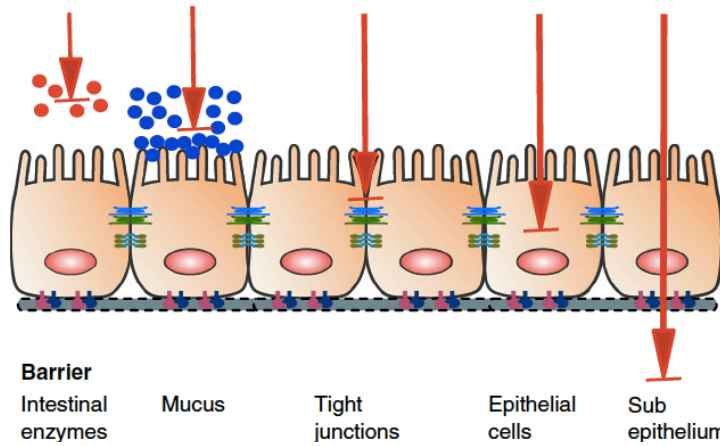


Figure 15: Schematic representation of the barriers of the GIT.<sup>75</sup> © 2016 The Authors. Published by Elsevier B. V.

In order to realize the challenges that the MSNs will have to face in the oral delivery route, a brief overview of the composition of the GIT is presented. The GIT *i.e.*, the stomach, the small intestine (duodenum, jejunum, ileum) and the colon, has two main functions: it processes the food and it defends the organs from pathogens. Several barriers

in the GIT may hinder the transport of drugs or nanoparticles to the intestine and further to the systemic circulation: the gastric and intestinal digestive environment, the mucus and the epithelium, as represented in Figure 15.<sup>75</sup>

#### III.1.a. The gastric and intestinal milieu

The stomacal fluid, having a pH of 1-3, is composed of a complex mixture of acid (HCl), salt (NaCl, KCl) and enzymes (amylase, pepsin, gastric and lingual lipase). The intestinal fluid has a near neutral pH and also contains enzymes such as proteases (trypsin, chymotrypsin), lipases or amylases. Already at this early stage of the oral administration, any organic substances or inorganic materials could be degraded; particularly, proteins might be inactivated through proteolysis. Conventional formulation such as enteric coatings are used to pass this first chemical barrier. Interestingly, a recent study, presented in Figure 16, highlighted the

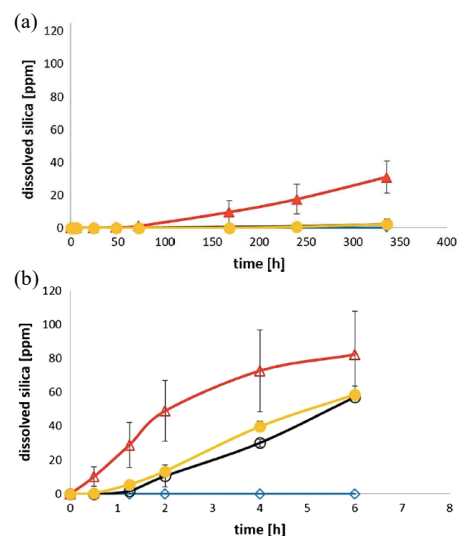


Figure 16: Dissolution kinetics of silica particles in SGF up to 15 days (a) and in SIF up to 6 h (b); Non-porous (blue diamond) and MSNs of 80 nm (black), 200 nm (red) and 1500 nm (yellow).<sup>76</sup> Copyright © 2016, Springer Science Business Media New York.

resistance of MSNs exposed to simulated gastric fluid (SGF) (pH 1.6, 34.2 mM NaCl, 0.08 mM sodium taurochlorate, 0.02 mM lecithine, 0.1 g l<sup>-1</sup> pepsin and 2.2 M HCl) over a period of 15 days. In contrast, progressive dissolution was noted in simulated intestinal fluid (SIF).<sup>76</sup>

### III.1.b. The mucosal barrier

The mucus is a viscous hydrogel secreted by the goblet cells which cover the epithelium. It is divided into an outer loose layer and an inner, strongly adherent firm layer which are mainly composed of large glycoproteins, the mucins, structured in stacked, parallel sheets. These layers, of varying thicknesses *e.g.*, 30-300 µm in the stomach, 150-400 µm in the small intestine and 30-280 µm in the colon, would physically hinder the passage of nanoparticles.<sup>77</sup> Thus, a cut-off of 100-200 nm is stated; smaller nanoparticles have been shown to penetrate more efficiently through the mucus layers. Besides, since the mucus is negatively charged, neutral or negatively charged MSNs are supposed to perform better as electrostatic interactions would be minimized.<sup>78</sup>

### III.1.c. The epithelium barrier

The intestinal epithelium is composed mainly of absorptive enterocytes. Dendritic immune cells, microfold M-cells, goblet cells and enteroendocrine cells are less abundant. After having successfully passed through the mucus, the MSNs or the therapeutic agents would have to cross epithelial cells using either transcellular absorption or paracellular absorption.

#### 1.c.i. Paracellular transport

The paracellular transport *i.e.*, passage between the cells, refers to the modulation of the proteins that form the tight junctions *i.e.*, the claudins and the occludins. Originally, the tight junctions regulate the flux of ions, water and small molecules but different permeation enhancers such as chitosan, thiolated polymers or fatty acids, have been shown to induce reversible leaks which enabled the passage of bigger molecules.<sup>77,79</sup> Although this approach is interesting, it has several limitations: (1) high concentrations of these permeation enhancers might be toxic for the epithelial cells and (2) the surface area that represents the tight junctions is highly negligible as compared to the overall epithelial surface area.

1.c.ii. Transcellular transport

Owing to the high surface area of the intestinal epithelium, the transcellular transport, or transport through the cells, is most likely the mechanism at play for the permeation of nanoparticles across the epithelium. The process of engulfment of nanoparticles or macromolecules upon forming a membrane-bound vesicle is known under the general term, endocytosis, which can be divided into two sub-categories: phagocytosis *i.e.*, cell eating large particles, and pinocytosis, cell drinking fluid. While phagocytosis is operated only by macrophages, dendritic or M-cells, pinocytosis is not cell-specific and is further divided into four main endocytosis pathways as depicted in Figure 17.<sup>80</sup>

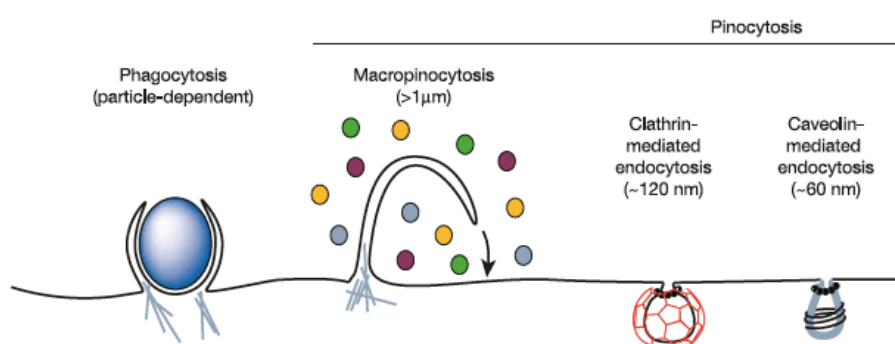


Figure 17: Mechanism of cell endocytosis.<sup>80</sup> Copyright © 2003, Springer Nature.

Briefly, macropinocytosis is similar to phagocytosis as the formation of an endocytic vesicle derives from the binding of protusions to the membrane.<sup>81</sup> Then, two types of carriers mediate the endocytosis:

- the clathrin-mediated endocytosis: receptor-ligand specific interactions.
- the caveolae-mediated endocytosis: non-specific interactions.

In addition, clathrin and caveolae-independent endocytosis exist but they remain poorly understood. Nanoparticles are mainly transported with the clathrin-mediated endocytosis although depending on their surface charge, hydrophilicity and size, different mechanisms can be adopted.<sup>80</sup>

III.2. Toxicological considerations

Because MSNs have been actively pursued as drug delivery systems, testing their biocompatibility *in vitro* is a crucial initial step that should lead to more advanced *in vivo* studies.

Growing attention has been devoted towards these materials which has diversified their chemical composition or their physical characteristics, thus systematic *in vitro* cytotoxic tests are performed on a large variety of cell lines using different colorimetric assays based on tetrazolium dyes MTT, WST or resazurin AlamarBlue, for example. However, in comparison, investigations on the behavior of MSNs *in vivo* are less conducted and this might compromise or at best delay their clinical translation.

### III.2.a. In vitro

#### 2.a.i. Effect of the size of the nanoparticles

One of the structural features of the MSNs that is suspected to play a major part in the interaction with the cellular environment is the size of the nanoparticles. For example, in a study conducted by Vallhov *et al.*, cell viability, uptake and immune regulations of dendritic human cells seemed to be less affected by the presence of the 270 nm MSNs than the 2.5  $\mu\text{m}$  particles.<sup>82</sup> Among nanosized particles, Mou *et al.* confirmed that smaller nanoparticles *i.e.*, 30 or 50 nm, were internalized in HeLa cells more than the 110 or 170 nm MSNs, and at the concentration of 100  $\mu\text{g ml}^{-1}$ , none of the MSNs provoked cell damage.<sup>83</sup> In the work of Bouchoucha *et al.*, phosphonate functionalized MCM-48-type MSNs of 45 and 150 nm particle size, were tested for their cytotoxic behavior against M21 (melanoma cells) and HT1080 (fibroblastic sarcoma) cells. Innocuousness of both sizes of MSNs was shown, up to 72 h, with concentrations up to 250  $\mu\text{g ml}^{-1}$ .<sup>25</sup> The phosphonate groups might increase the biocompatibility of the MSNs, as contradictory study, reported by Zhang *et al.*, showed that the 80 nm pure silica nanoparticles adhered more to the cells and therefore reduced both the cell viability and proliferation more than the 500 nm ones.<sup>84</sup> Recently, Chou *et al.* published a study on the size- and charge-dependent cytotoxicity of MSNs against macrophages and lung epithelial cells which contradicted earlier studies.<sup>85</sup> They concluded that only larger (> 100 nm) and positively charged MSNs generated a cytotoxic effect owing to a higher cellular uptake of the larger MSNs as can be observed in Figure 18.

#### 2.a.ii. Effect of the surface functionalities

Not only can the functionalities anchored at the surface of the MSNs be implemented to control the release through tailored interactions with the drug, they can also modulate the biocompatibility or cell uptake, notably by changing the charges of the MSNs. Starting

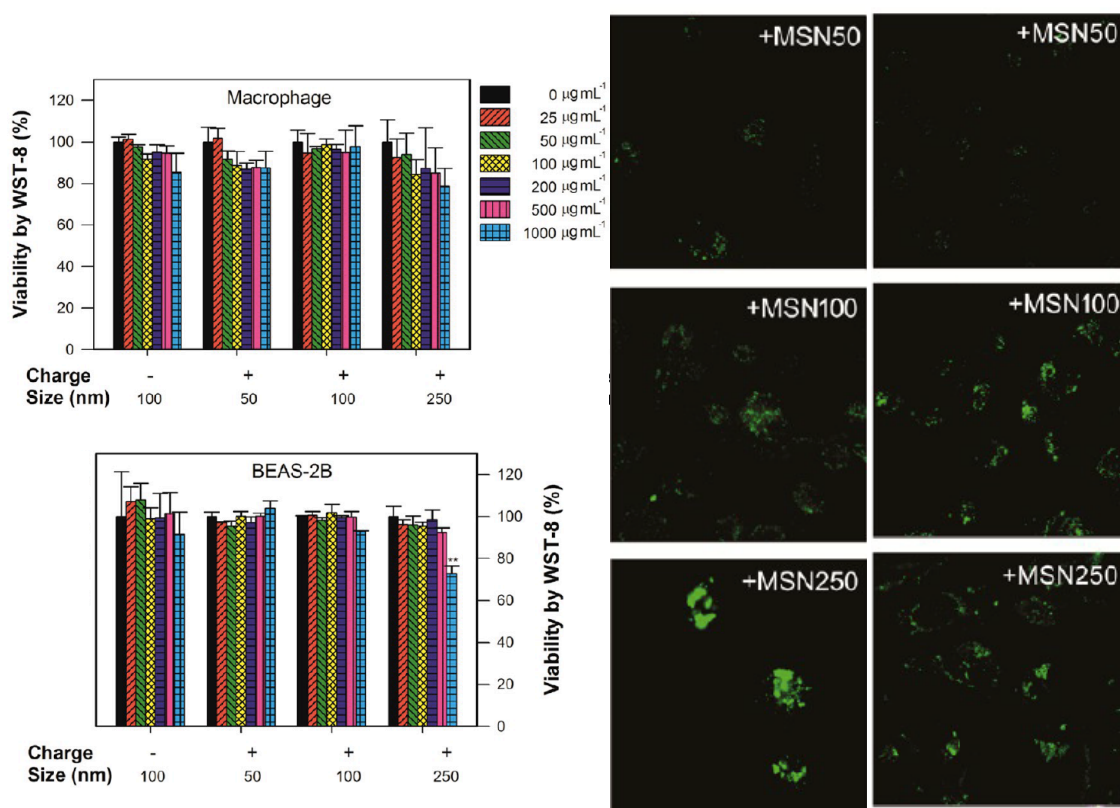


Figure 18: (a) Cell viability of the macrophages and the lung epithelial cells (BEAS-2B) exposed to MSNs of different sizes, charges and concentrations for 24h and (b) Confocal microscopy observation of the cellular distribution of the different FITC-labeled MSNs.<sup>85</sup> Copyright © 2017, American Chemical Society.

from simple functionalization *i.e.*, grafting of amine (MSN-NH<sub>2</sub>) or carboxylic groups (MSN-COOH), Braun *et al.* concluded that the cytotoxicity followed the order MSN-COOH < MSN < MSN-NH<sub>2</sub> implying that positively charged MSNs lead to higher cell death than the negatively charged ones. Nonetheless, all types of MSNs were shown to be biocompatible up to a concentration of 100  $\mu\text{g mL}^{-1}$ .<sup>86</sup> According to a pioneering study conducted by Slowing *et al.*, lower doses of positively charged MSNs were needed to obtain 50 % uptake by HeLa cancer cells. Besides, while negatively charged MSNs could escape the endosomes within 6 h, the positively charged ones remained trapped, which could result in higher cell damage.<sup>87</sup> Interestingly, the mechanism of engulfment varied from functionalities to functionalities, the MSNs with a folate group being internalized *via* the folic acid (FA) receptors expressed on the HeLa cells for example. Cytocompatibilities of several functionalities *i.e.*, PEG, polyethyleneimine (PEI) or FA (alone or combined), grafted on MSNs were tested on Caco-2 cells in a recent study conducted by Desai *et al.*<sup>88</sup> None of the MSNs, pure or functionalized, showed alarming cytotoxicity at concentrations lower than 50  $\mu\text{g mL}^{-1}$ . However, at 100  $\mu\text{g mL}^{-1}$ , all functionalized MSNs were more cytotoxic than the pure MSNs, as

shown in Figure 19. This can be correlated to the ability of the PEG-PEI or FA-PEG-PEI groups to penetrate the cellular intestinal membrane more efficiently and these groups ultimately helped in delivering the drug intracellularly.

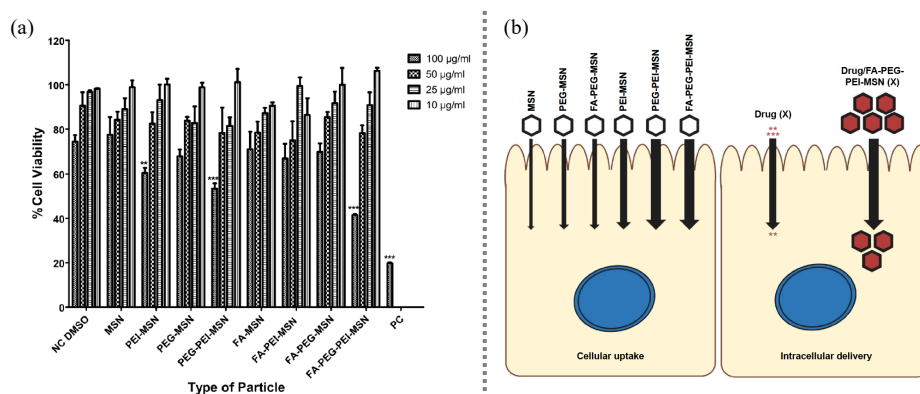


Figure 19: Viability of Caco-2 cells measured by WST-1 assay after 48h incubation with the different MSNs in the concentration range 10 - 100  $\mu\text{g ml}^{-1}$  (a) and Schematic representation of the uptake of the different MSNs by the intestinal cells (derived from fluorescent confocal images) and the consequences on the intracellular drug delivery.<sup>88</sup> Copyright © 2016 Desai *et al.* This work is published and licensed by Dove Medical Press Limited.

Even though, several results agreed on the therapeutic dose of 100  $\mu\text{g ml}^{-1}$ , contradictory findings regarding the effect of the size, charge and functionalities of the MSNs are often encountered. In fact, many other features have been suspected to modulate the cytotoxicity such as the particle morphology, the pore size and order of the porous structure.<sup>89</sup> One strategy to overcome toxicity limitations resides in the adsorption of proteins present in the serum. A study reported by Liu *et al.* showed that in the absence of proteins *i.e.*, serum-free media, the bare MSNs strongly adhered to the cell membrane and further caused cell damage. Contrary, in serum-containing media, the formation of the protein corona around the nanoparticles shields the direct contact of the MSNs with the cells and consequently reduced the cytotoxicity.<sup>90,91,92</sup> Although *in vitro* assays are usually used to predict *in vivo* behavior of drugs or MSNs, it has to be kept in mind that what seems to be safe *in vitro* is not necessarily *in vivo* and *vice et versa*.

### III.2.b. In vivo

Regardless of the mode of administration, once the MSNs reach the systemic circulation, they are distributed among the different tissues in proportion to the organ blood flow rates; they need to (1) reach their therapeutic target and (2) be excreted efficiently. According to the literature, as their particle size exceed the 5.5 nm threshold of the renal



clearance, they are likely to be taken up by the liver and the spleen through the reticulo-endothelial system (RES). Acute or chronic toxicity in these tissues can be generated from possible accumulation and absence of degradation.<sup>93</sup> Here again, the physico-chemical properties of the MSNs govern their biodistribution and clearance *in vivo*.<sup>94</sup> Recently, Dogra *et al.* implemented an imaging and mathematical model to elucidate the biodistribution of PEG-modified MSNs having various particle sizes and additional functionalities: PEI, Quaternary ammonium silane (QA) or Trimethylsilyl (TMS), as illustrated in Figure 20.<sup>95</sup> From their findings, smaller particles had enhanced systemic bioavailability. Besides, the TMS (neutral charge) and QA (positive charge) functions were particularly interesting for their low hepatic and splenic accumulation. Notably, TMS-MSNs had higher circulation times and would be beneficial for tumor targeting for instance. These findings

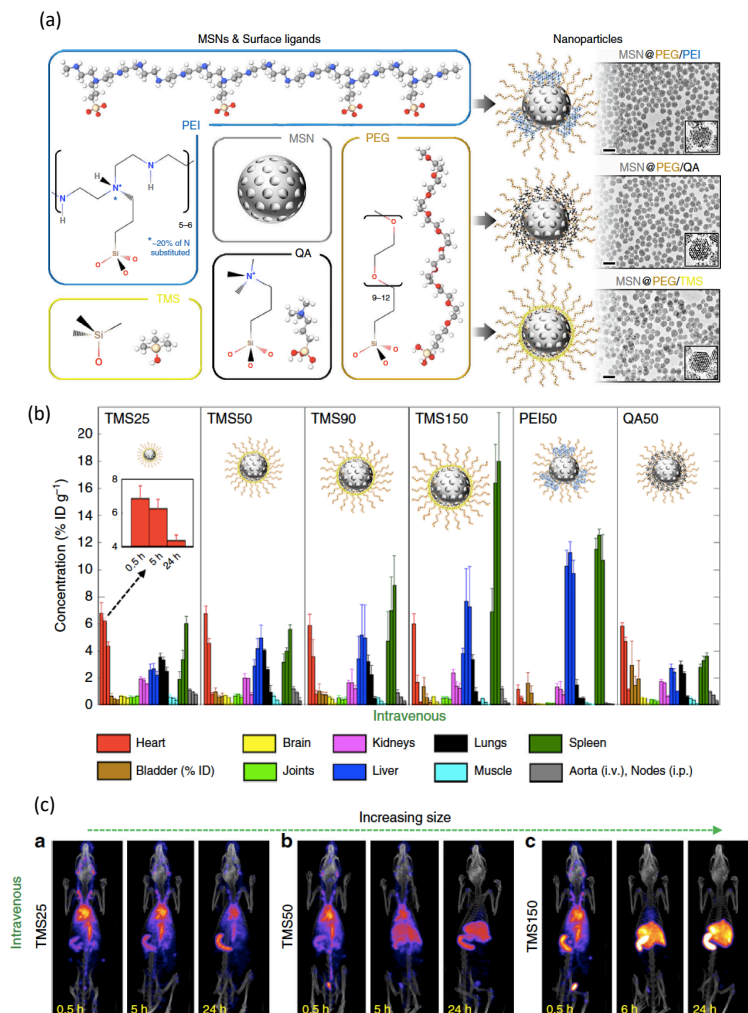


Figure 20: (a) Functionalities and schematic representation of the resulting MSNs used with respective TEM images; (b) Body quantitative biodistribution of MSNs following i.v. injection; (c) SPECT/CT images showing the spatio-temporal evolution of TMS-MSNs of various sizes after i.v. injection in rats.<sup>95</sup> Copyright © 2018, Springer Nature.

are of great relevance to support the progression of silica materials towards clinical trials. In this regard, the first-in-human trial has been granted by the FDA to Wiesner and co-workers for position emission tomography (PET) and optical imaging of silica nanoparticles of 5 melanoma patients. A rapid excretion was observed mainly operated by the kidneys and clearance half-time lower than the liposomes were reported.<sup>96</sup>

### III.3. pH responsive formulation

To reach the systemic circulation, the therapeutic agents have to be available in the intestine, where concomitant solubility and permeability would determine the efficacy of the administrated dose. To do so, the drug needs to be protected in the stomach and be released in the intestine upon exposure to external stimuli which include enzyme and pH.

#### III.3.a. Proteins

##### 3.a.i. $\beta$ -lactoglobulin

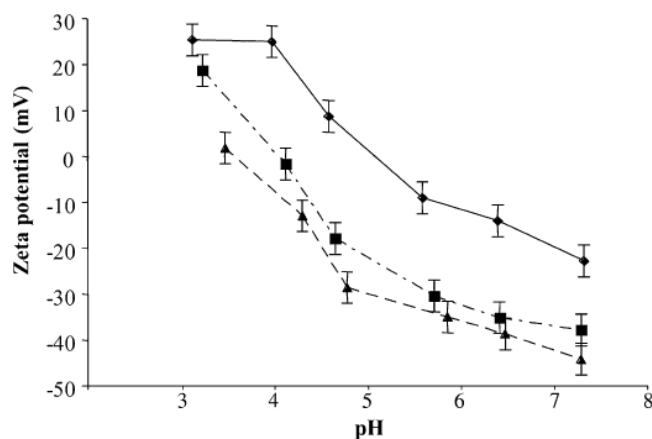


Figure 21: Zeta potential of  $\beta$ -lactoglobulin over the pH range 3 - 8 as a function of the succinylation degree (diamond 0%, square 50%, triangle 100%).<sup>97</sup> Copyright © 2010 Elsevier Ltd.

$\beta$ -lactoglobulin is a low cost whey protein dotted with several positive lysine groups which can be modified to negative carboxyl groups upon succinylation. Owing to this simple chemical modification, Caillard *et al.* have revealed a major decrease in the solubility of succinylated  $\beta$ -lactoglobulin in acidic pH and increased swelling properties at pH higher than 4.5, as a result of the change in charge density or zeta potential (ZP), as shown in Figure 21.<sup>97</sup>

In addition to low cytotoxicity, the dissolution of riboflavin was low at SGF, even in the presence of pepsin, and within 1h at SIF, the totality of the vitamin was dissolved. These results clearly highlighted the potential of this protein as an oral functional excipient. Guillet-Nicolas *et al.* took advantage of the pH-gating effect of this protein and conjugated it with MSNs to obtain a system with enhanced colloidal stability, low cytotoxicity and pH-triggered delivery of ibuprofen.<sup>98</sup> The succinylated  $\beta$ -

lactoglobulin was covalently coupled to the amine groups already grafted on the surface of MCM-48-type nanoparticles *via* the intermediate of 1-ethyl-3-(3-dimethylaminopropyl)carbodiimide hydrochloride, better known as EDC coupling agent. The release of ibuprofen from non-conjugated MSNs reached 40 and 70 % within 8 h at pH 1.2 and 7.4, respectively. However, upon conjugation with the protein, the release stayed really low until 24 h at pH 1.2, never reaching even 10 %, while attaining a plateau at approximately 60 % after 8 h at pH 7.4. The conjugated system was proven cytocompatible up to 500  $\mu\text{g ml}^{-1}$  using HEK 293 human kidney cells.

### 3.a.ii. Soy protein isolates

Caillard *et al.* also reported the great potential of succinylated soy protein isolates as excipient for oral transport to the small intestine.<sup>99</sup> Similarly to  $\beta$ -lactoglobulin, proteins isolated from soy bean are naturally occurring food component that can be degraded by digestive enzymes making them advantageous cheap materials. Here again, upon succinylation, the charge density decreased from 4.5 to 3.5, which in turn decreased the solubility at pH below 4.5, and increased it at pH higher than 4.5. As a consequence, the release of both highly and poorly soluble model molecules from the soy protein tablet was delayed in SGF and accelerated in SIF. Popat *et al.* also adopted the conjugation of amino-functionalized MCM-48-type nanoparticles with succinylated soy protein isolates with the aim to protect the pro-drug sulfasalazine from acidic and enzymatic degradation.<sup>100</sup> The resulting gating system successfully suppressed the release at SGF in the presence of the digestive enzyme pepsin and allowed a sustained delivery at SIF in the presence of pancreatin. Furthermore, being a pro-drug, 95 % of sulfasalazine was metabolized in the simulated bacterial media which contained the enzyme azo-reductase. More recently, the same strategy was adopted by Nguyen *et al.* for the release of prednisolone in the colon.  $\epsilon$ -polylysine was covalently bound to the amine groups *via* EDC to afford pH-responsive MCM-48-type MSNs.<sup>101</sup>

### III.3.b. Lipids

In the past decades, lipids have been extensively used in the field of drug delivery, given their capability to micellize into liposome vesicles and to permeate through the looklike lipidic bilayer of the cellular membranes. However, they suffer from low stability and low drug loading capacity. These disadvantages have been tackled through their combination

with MSNs, which act as a robust reservoir of a high drug loading capacity. In addition, the coating of a layer of lipids on the external surface of MSNs has improved the biocompatibility of the inorganic materials resulting in a winning situation. To obtain such hybrid materials, Mudakavi *et al.* separately synthesized MCM-41 spheres and liposomes made of the phospholipid DPPC : cholesterol in a 70:30 ratio.<sup>102</sup> Once mixed together, the liposomes fusion caused their deposition around the MCM-41-type nanoparticles with a shell thickness of approximately 5 nm. The polar surface of the MSNs can definitely be a source of multiple interactions with the hydrophilic head of the phospholipids. The as-synthesized lipid-coated MCM-41 nanoparticles were further filled with the antibiotic ciprofloxacin, and the *in vitro* release and bacterial activity against *Salmonella* were tested. Because of the increased solubility of ciprofloxacin in acid, almost 70 % of the cargo was eluted after 2 h at pH 2.5 (Figure 22). Yet, the bacteria was located in the small intestine where the pH is more neutral, the release at pH 7.4 was almost plateaued at 30 % after 2 h. Although, this might not be the best suited system to refrain the delivery of the drug in acidic pH, the improved biocompatibility and intravacuolar targeting permitted the antibiotic dose administrated *in vivo* to the mice to be lowered. Other combinations of phospholipids and MSNs showed a decrease in log *P* and a remarkably enhanced permeability across Caco-2 monolayer owing to the presence of phospholipid and an improved dissolution rate due to the amorphization effect occurring in the nanopores of OMS.<sup>103</sup>

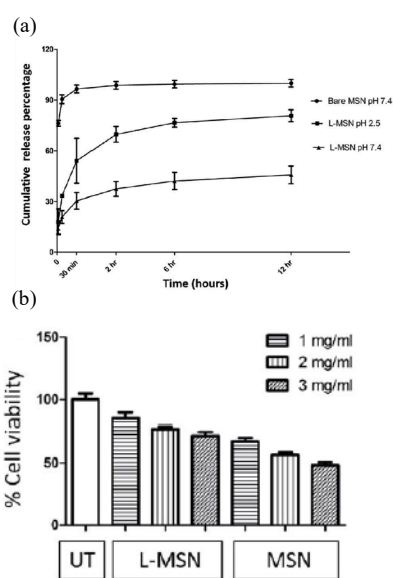


Figure 22: Release of ciprofloxacin from bare or lipid-coated MSNs (L-MSN) at pH 2.5 and 7.4; (b) Viability of RAW 264.7 cells treated with different concentrations of MSNs or L-MSN compared to untreated cells.<sup>102</sup> Reproduced with permission from The Royal Society of Chemistry.

### III.3.c. Polysaccharides

Polysaccharides have also been associated to MSNs and their ability to regulate the drug release was recently investigated. For example, Sun *et al* coated chitosan on MSNs.<sup>104</sup> In an acidic aqueous solution, positively charged amine groups of chitosan and the negatively charged silica surface self-assembled through electrostatic attraction. While a burst release of the poorly soluble drug, carvediol, was clearly observed for non-coated MSNs,

the release from the chitosan-coated MSNs was rather progressive over a period of 24h, even though 40 % was dissolved after 2h at SGF. Interestingly, after intragastric administration, the uncoated MSNs showed around 2-fold increased  $C_{max}$  and  $AUC_{0-48h}$  in comparison to the commercial formulation of carvediol. However, lower bioavailability was encountered for the chitosan-coated MSNs due to extensive metabolization of the drug *in vivo*. Also using layer-by-layer self-assembly, Hu *et al.* combined MSNs with two natural macromolecules of opposite charges at pH 5, chitosan and acacia.<sup>105</sup> A comparison of the coated MSNs with a commercial tablet showed similar release performances of felodipine. The pH-responsiveness of this combination might not be adequate for oral delivery as swelling of the coating was reported at pH 1.2. Diversely, Popat *et al.* covalently attached chitosan to the phosphonate groups grafted on the surface of MCM-41-type MSNs. MCM-41 nanoparticles were functionalized with 3-trihydroxysilylpropyl methylphosphonate prior to the activation of the terminal phosphonate groups with EDC, which was further substituted by chitosan. After the loading of ibuprofen, the release in different pH was tested and the ability of chitosan to refrain/allow the release at pH 5/pH 7.4 was confirmed.<sup>106</sup>

Aiming at the oral delivery of insulin, Sun *et al.* grafted MSNs with a pH sensitive shell made of dextran-maleic acid (Dex-Ma) and further modified the materials with a glucose-sensitive compound *i.e.*, 3-amidophenylboronic acid (APBA) as depicted in Figure 23a.<sup>107</sup> The results showed that the release of insulin from this formulation stagnated at around 20% at pH 1.2 and 7.4 over a period of 25 h. However, in the presence of 5 mg ml<sup>-1</sup> of glucose, 80 % of insulin was made available over a period of 5 h. Finally, the hypoglycemic effect of different formulations was tested on diabetic rats and the results showed outstanding performances of the Dex-Ma coated MSNs in comparison to the free insulin. Indeed, after subcutaneous administration of Dex-Ma MSNs, the blood glucose decreased by 40 % in 30 min and the level stayed stable until 7 h as opposed to the free insulin which only permitted to lower it by 20 % after 1.5 h and increased back to 100 % until 7 h. The Figure 23c shows the interaction of the coated MSNs with the intestinal villi of the diabetic rats.

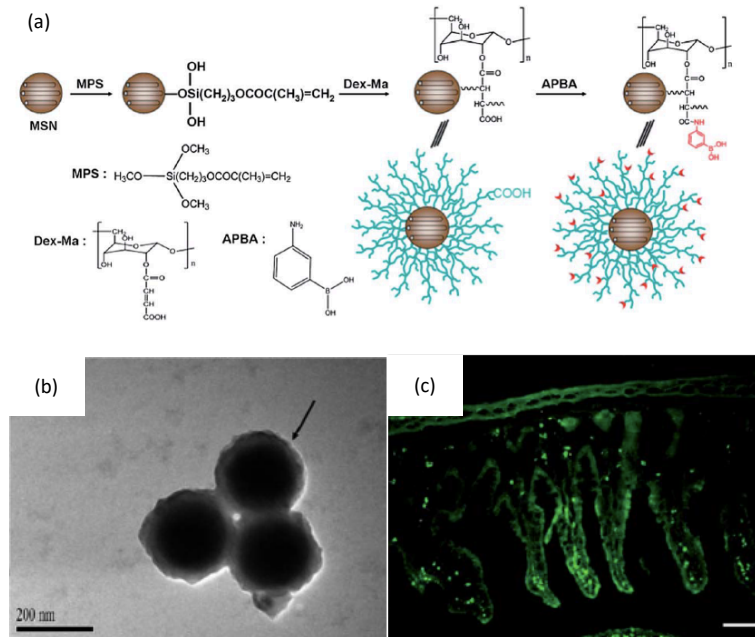


Figure 23: (a) Scheme of the functionalization of MSNs to afford pH- and glucose-sensitive shell; (b) TEM image of the coated MSNs; (c) Confocal microscopy image of the intestinal villi of rats invaded by FITC-coupled-insulin loaded into MSNs.<sup>107</sup> Reprinted with permission from The Royal Society of Chemistry.

Using porous silicon materials (PSi), Shresta *et al.* designed an oral insulin delivery platform with chitosan modified either with L-cysteine or oligoarginine groups. Although the release of insulin in SGF was effectively refrained, only 40 % was eluted at SIF over a period of 6 h. Besides, as shown in the Figure 24, the proposed system failed in reaching subcutaneous pharmacokinetic levels.<sup>108</sup>

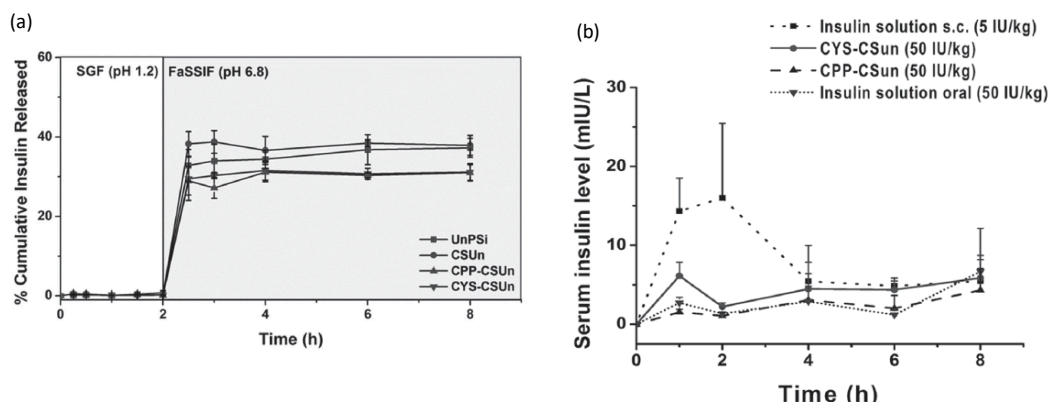


Figure 24: (a) In vitro release of insulin from unmodified PSi (UnPSi), unmodified-chitosan-grafted PSi (CSUn), oligoarginine modified chitosan PSi (CPP-CSUn) and cysteine modified chitosan PSi (CYS-CSUn); (b) Concentration of insulin in the serum of type 1 diabetic rats following sub-cutaneous administration, oral insulin solution, CPP-CSUn or CYS-CSUn.<sup>108</sup> Copyright © 2016, Wiley-VCH Verlag GmbH & Co. KGaA, Weinheim.

#### IV. Summary

- The principle of synthesis and functionalisation of OMS and MSNs as well as their resulting porous features have been presented. Unlike OMS or MCM-48-type MSNs whose synthesis mechanisms are well established, the formation of DMSNs is still debated and literature is furnished with multitudes of synthesis. Nevertheless, owing to their tunable pore sizes and narrow particle size distribution, DMSNs have paved the way to protein delivery nanocarriers (Chapter 2 – Part I. Mesoporous silica nanoparticles).
- Apart from the encapsulation method and the amount of drug loaded, the pore size and the functionalities of the nanocarriers hosting the drug influence the drug/surface interaction, the degree of amorphization and by extension the release of the drug in aqueous solution. Smaller pore size correlates generally with lower release rate due to restricted diffusion as compared to larger pore sizes (> 7nm) (Chapter 2 – Part II. Encapsulation and release of therapeutic agents).
- The challenge of oral delivery resides in bridging over the GIT barriers while satisfying toxicity safety thresholds *in vitro/ in vivo*. To address this issue, the design of pH responsive nanocarriers for oral delivery has been expanding but there is still room for deeper understanding on the nanocarriers, the loading/release of the therapeutic agents and the effect of the nanocarriers on biological processes (Chapter 2 – Part III. Mesoporous silica nanoparticles in the oral delivery route).





## Chapter 3 – Experimental techniques

### I. Gas physisorption

The physical adsorption of gas/adsorptive at cryogenic temperature, typically  $N_2$  at  $-196$  °C ( $77.4$  K), onto an adsorbent is a powerful technique widely used to characterize mesoporous silica materials in terms of specific surface area, PSD and the micropore and/or mesopore volumes. Such structural features are extracted from the adsorption isotherms which represent the volume of  $N_2$  molecules adsorbed as a function of the relative pressure  $P/P_0$ ,  $P_0$  being the saturated vapor pressure of the adsorptive. These isotherms are constructed point-by-point as follows: calibrated doses of  $N_2$  are admitted to a measurement cell containing the adsorbent at constant cryogenic temperature of  $-196$  °C. While

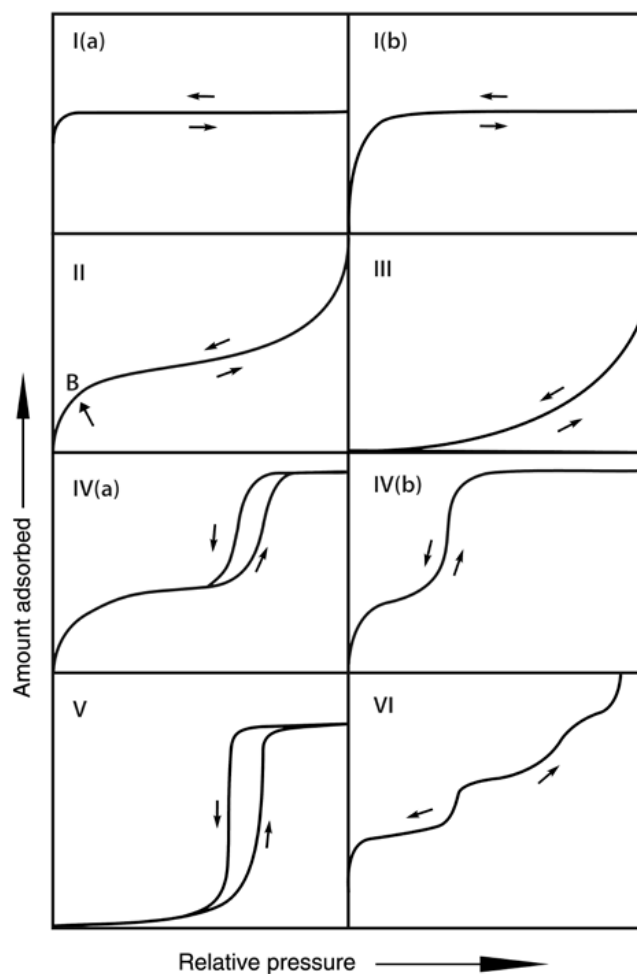


Figure 25: Classification of the different isotherms obtained from physisorption analysis.<sup>109</sup>

the gas comes into contact with the solid through weak Van der Waals and intermolecular repulsion forces, adsorption occurs until equilibrium is reached and the amount of gas adsorbed can be back calculated from the pressure variation in the cell after the administration of the successive doses i.e., the adsorbed gas does not account for the pressure anymore.<sup>109</sup> As depicted in Figure 25, various type of isotherms can be obtained, depending on the pore characteristics and chemical nature of the adsorbent. According to the IUPAC classification, type Ia and Ib refer to ultramicroporous (pore width below 1 nm) and supermicroporous (pore width between 1 and 2.5 nm) materials, respectively, while type II and III correspond to either non porous or

macroporous materials. In this thesis, only mesoporous materials have been synthesized which are represented by the type IV and V isotherms, the later only occurring for weak adsorbate/adsorbent interactions. The type VI is encountered in the case of multi-layer adsorption on highly uniform non-porous surface. As it can be seen, the type IV is further sub-categorized in type IVa or type IVb, depending on the presence/absence of an hysteresis. A common characteristic of type IVa and b is the steep increase of volume adsorbed at  $P/P_0 > 0.2$ . This originates from the fact that in mesopores, once a multilayer of  $N_2$  molecules have been adsorbed on the surface (situation B, Figure 26), the gas condenses to a liquid-like state (situation C). The first order transition occurs at relative pressures below the saturation pressure of the adsorptive due to the shift of the confined fluid in the nanopores.<sup>110</sup> Once the pores are filled, a plateau in the volume adsorbed is attained (situation D) if no other larger pores are present and if the external surface of the materials is negligible as compared to the one present in the pores. Then, the desorption process commences. Either the desorption will happen reversibly and the type IV(b) is observed, as it is the case for MCM-41 and MCM-48. Or a hysteresis appears due to a delay in the capillary condensation (situation E), as is the case in some DMSNs and more generally in SBA-15 type materials (OMS with a 2D hexagonal network of mesopores of 7-8 nm). This

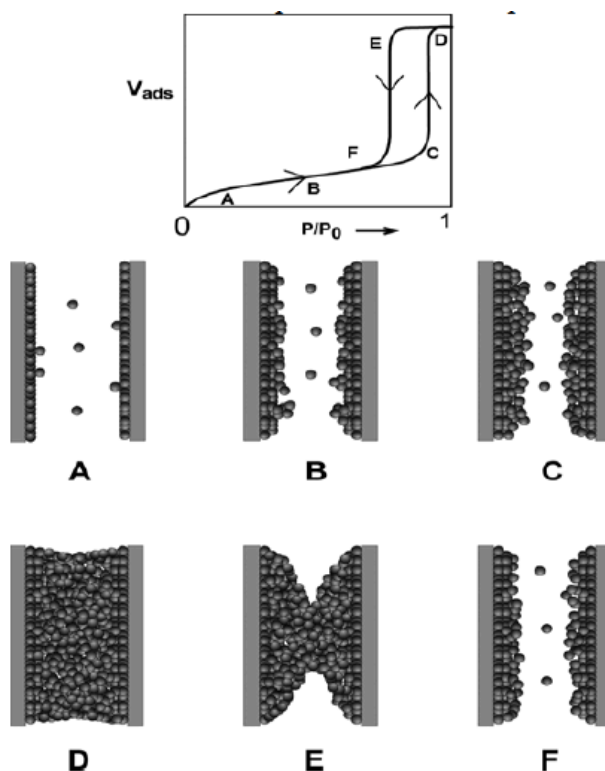


Figure 26: Type IV(a) isotherm with the schematic representation of the different steps of gas adsorption in a single mesopore: multilayer formation, pore condensation and hysteresis.<sup>110</sup>

phenomenon is influenced by the pore size, the type of adsorptive and the temperature. Typically, for materials exhibiting a pore size in the range 2 – 4 nm, the physisorption of N<sub>2</sub> at 77 K will not reveal hysteresis loop whereas for materials with pore size higher than 4 nm, hysteresis loops will be displayed with the same measurement condition.<sup>111</sup>

## II. Electron microscopy

In general, electron microscopy techniques such as Scanning or Transmission Electron Microscopy (SEM or TEM) allow the visualization of object in the nanometer range. In TEM, an electron beam is generated and passes through a set of condenser, objective and projection electromagnetic lenses to align the electrons on the optical trajectory. The electron beam bombard the sample and only the transmitted electrons constitute the signal resulting from the interaction electron/sample which is finally projected on a fluorescent screen. A representation of the device and the interaction of the electron with the matter is shown in Figure 27. Since it is a projection of the object, the sample has to be very thin, in order for the electrons to travel through it. Otherwise, SEM is more adapted for thicker samples. In SEM, the electron beam scan the surface of the sample and

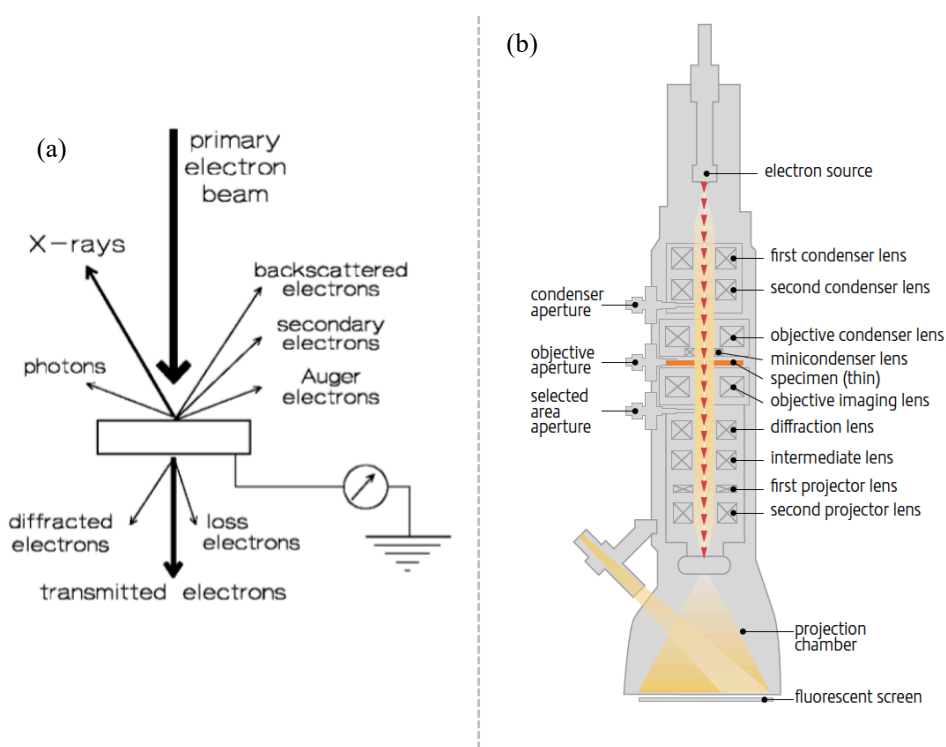


Figure 27: Overview of the interaction of electron with the sample (a) and the TEM device (b).<sup>113</sup>

contrary to TEM, only the backscattered and secondary electrons resulting from the interaction electron/sample are collected and form the image of the sample.<sup>112,113</sup>

In this thesis, TEM has been used to characterize the different MSNs synthesized in terms of morphology, size, porosity, polydispersity of the nanoparticles. Images of drug particles and drug-loaded MSNs have been recorded using SEM to evidence the encapsulation success.

### III. Dynamic light scattering

Dynamic Light Scattering (DLS) is a useful tool for measuring the hydrodynamic diameters of particles in suspension in the size range 1-10000 nm and for detecting the agglomerations in solution. When nanoparticles are dispersed in a liquid, they isotropically move due to the bombardment of the solvent molecules, as it is defined by Brownian motion. The velocity of this motion, defined as the translational diffusion coefficient noted  $D$ , allows the retrieval of the hydrodynamic diameter of the nanoparticles thanks to the Stokes-Einstein equation given below:

Eq. 4:

$$d(H) = \frac{kT}{3\pi\eta D}$$

Where  $d(H)$  is the hydrodynamic diameter of the sample,  $k$  the Boltzmann constant,  $T$  the temperature and  $\eta$  the viscosity. As it can be understood from the Eq. 4, the Brownian motion mainly depends on the size of the nanoparticles, faster motion being observed for smaller nanoparticles.

During a measurement, an incident beam generated by a laser passes through a cuvette containing the suspension which will scatter the light in all directions but only the backscattered light is detected at 173°. The fluctuation of the intensity of the scattered light over time is measured and translated into a correlation function. Finally, the size distributions are derived from this correlation function using several algorithms. Following similar principles, the zeta potential or the surface charge of the nanoparticles in suspension of varying pH can be determined.

In this thesis, DLS has been used to obtain information on the size of the pure or functionalized MSNs in aqueous solution and the quality of the colloidal suspension.

#### IV. Zeta potential

ZP refers to the electrokinetic potential at the slipping plane of particles in solution. In a

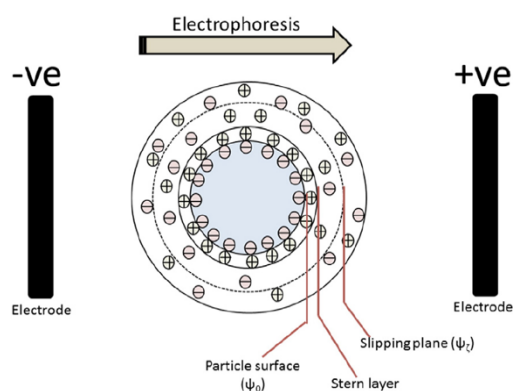


Figure 28: Schematic representation of the EDL adsorbed on a negatively charged particle during electrophoresis.<sup>114</sup> © 2016, Elsevier B. V.

dispersant of a certain pH, ions accumulate at the surface of the particles and create an electric double layer (EDL) made of a Stern and a diffuse layer. When submitted to an electric field, the particles move towards the opposite electrodes with the slipping plane being the interface particles/dispersant. Practically, the electrophoretic mobility of the particles is determined through the shift of frequency between the scattered and the reference beam.<sup>114</sup>

In this thesis, the ZP measurements permitted to gain information on the surface charges of the MSNs, before and after amine-, methyl- and thiol-functionalization. A titrator coupled to the DLS instrumentation was used to precisely control the pH over the range 3 - 7.4.

#### V. Powder X-ray diffraction analysis

PXRD is powerful technique to precisely characterize the order at low angle and crystallinity, structure properties and phase composition of powder samples at wide angles.

First, monochromatic X-Rays are generated through the collision of an accelerated electron beam with a metal target i.e., copper in most cases ( $\text{Cu K}\alpha$ ), which releases excess energy as X-rays during the transition of electrons from an outer orbital to the  $1s$  orbital. These X-rays are then diffracted by the atoms of the materials, atoms that are organized in different plans as defined by the Miller indices  $hkl$ . Only reflections satisfying the Bragg law (Eq. 5) constitute the diffractogram since the diffracted X-Ray beams are in phase and interfere constructively.

Eq. 5:

$$n\lambda = 2 d_{hkl} \sin \theta$$

Where  $n$  is the number of diffraction,  $\lambda$  is the wavelength of the incident X-Ray beam,  $d$  is the reflecting interplanar spacing and  $\theta$  is the incident Bragg angle. Therefore, the resulting diffractogram displays the intensity of all the reflection peaks, if any, as a function of the Bragg angle. As it can be deduced from the Eq. 5, wider  $2\theta$  corresponds to smaller interplanar distance as is the case for crystalline structure. In the particular case of OMS, rather than the atomic order, it is the periodic arrangement of the pores that determine the reflections in the diffractogram. As the distance between pores is more important than in crystals, lower  $2\theta$  in the range  $0.5 - 8^\circ$  are investigated to characterize the pore network of OMS.

In this thesis, low-angle PXRD was conducted on MCM-48-type MSNs since the most intense reflections corresponding to the plans 211, 220, 420, 332 confirm the 3-D  $Ia\bar{3}d$  cubic structure. Because of the non-ordered porous network of DMSNs, no PXRD was recorded. Wide-angle PXRD was also used to obtain insights into the crystallinity of the therapeutic agents themselves and after confinement in the pore of different MSNs.

## VI. Thermogravimetry and differential scanning calorimetry

Thermogravimetry and differential scanning calorimetry (TG-DSC) are coupled techniques that measure the mass loss of a sample upon heating while simultaneously recording the thermic processes occurring during possible physical state transitions. As the temperature ranges typically from 40 up to 1000 °C, the organic matter is decomposed whereas inorganic materials, such as silica, are stable under such thermal treatments. Therefore, quantification of organic molecules adsorbed or grafted can be precisely determined and enthalpies of physical state transitions like fusion, crystallization or evaporation can be extracted.

In this thesis, TG-DSC has been particularly useful in calculating the amount of organosilanes grafted on the surface of MSNs or the amount of therapeutic agents loaded into the pore of MSNs. The differences in the DSC profiles of confined and non-confined drugs have also been encountered and discussed.

## VII. Solid-state Nuclear Magnetic Resonance spectroscopy

Solid-State NMR spectroscopy is used to determine the atomic chemical environment within solid materials. When submitted to an external magnetic field noted  $B_0$ , the nuclear spin  $I$  (with  $I \neq 0$ ) of an atom rotates around the axis of the magnetic field at the Larmor frequency. Due to the Zeeman effect, the  $2I + 1$  energy levels will be separated by  $\Delta E$  which depends on  $B_0$  according to the Eq. 6 given below:

Eq. 6:

$$\Delta E = \frac{\gamma h B_0}{2\pi} = \frac{\mu B_0}{I}$$

With  $\gamma$  the magnetogyric ratio which depends on the magnetic moment of the nucleus  $\mu$ ,  $h$  the Planck constant. In NMR spectroscopy, the transitions between these levels are observed and result from the excitation of the spin by second magnetic field  $B_1$  (RF impulsion), perpendicular to  $B_0$ . After the excitation, the return to equilibrium, characteristic of the spin population is transformed into a Free Induction Decay (FID) signal and processed by the Fourier transformation.

Due to the fast movement of molecules in a liquid, the isotropic chemical shift is observed. In a solid, the presence of additional anisotropic interactions such as the dipolar coupling and the chemical shift anisotropy results in broadening the resonance peaks. To minimize these interactions, the sample is rotated at high frequency (10 kHz) and at the Magic Angle Spinning (MAS)  $\theta = 54,7^\circ$  relative to the applied magnetic field. In addition, the transfer of polarization via the dipolar coupling from an abundant nucleus typically  $^1\text{H}$ , to a nucleus with a poor natural abundance such as  $^{13}\text{C}$  or  $^{29}\text{Si}$ , is commonly operated to increase the sensibility, this technique is named the cross-polarization (CP).

In this thesis, Solid-state NMR spectroscopy was used to confirm the functionalization of different organosilanes. When an organic molecule is chemically anchored at the surface of silica materials, characteristic resonance peaks appear in the  $^{13}\text{C}$  CP NMR spectrum and in the  $^{29}\text{Si}$  spectrum. For example, in the  $^{29}\text{Si}$  NMR spectrum,  $\text{Q}^n$  species represent the silicon atoms where  $n$  ( $1 < n < 4$ ) is the number of neighboring silicon atom and  $\text{M}^n$ ,  $\text{D}^n$  or  $\text{T}^n$  species refers to the Si-C bonds as illustrated in Figure 29.<sup>115</sup>

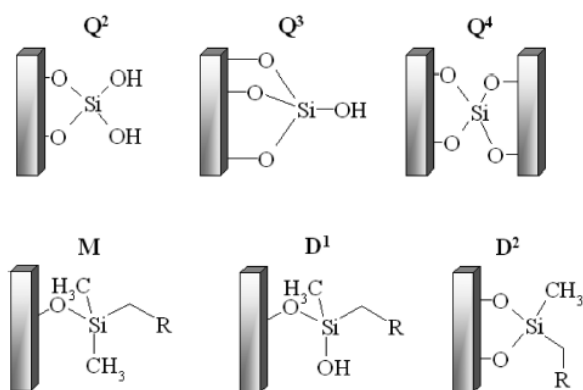


Figure 29: Schematic illustration of the different species observed in  $^{29}\text{Si}$  NMR spectra.<sup>115</sup>

### VIII. Ultraviolet-visible spectroscopy

The ultraviolet-visible (UV-Vis) spectroscopy is a technique widely used for the quality and quantitative analysis of molecules in solution. It relies on several electronic transitions from the ground to the excited state originating from the absorption of the light in the UV-Vis region (200 – 800 nm). The difference of intensity between the reference beam  $I_0$  and the transmitted beam  $I$  is measured and either the transmittance  $T = \frac{I}{I_0}$  or the absorbance  $A = -\log(T)$  are expressed as a function of the wavelength  $\lambda$ . Since according to the Beer-Lambert law, the absorbance is proportional to the number of molecules in solution, the concentration can be retrieved as follow:

Eq. 7:

$$A = \varepsilon c x$$

With  $\varepsilon$  the molar absorption coefficient,  $c$  the concentration of the molecule, and  $x$  the length of the cuvette.

In this thesis, the UV-Vis spectroscopy has been used to quantify the therapeutic agents such as resveratrol or omeprazole in aqueous solution of various pH. Since this technique is not the most adequate one for insulin quantification, an ultra-high performance liquid chromatography setup coupled with a mass spectrometer (UHPLC-MS) was used.







## Chapter 4 – Results

---

### I. Resveratrol-encapsulated mesoporous silica nanoparticles

This work was accepted for publication in the journal *Molecular Pharmaceutics* on the 2<sup>nd</sup> November 2017.

As a first author, I have synthesized and characterized the 150 nm MCM-48-type MSNs in the laboratory of Prof. Freddy Kleitz at Université Laval (Québec, Canada). I have incorporated resveratrol in all the MSNs, characterized the resveratrol-encapsulated samples and carried out the release tests; this has been done in the laboratory of Dr. Amirali Papat at the University of Queensland (Brisbane, Australia). I have interpreted the data, created the figures, written the initial manuscript and corrected it according to the co-authors suggestions.

Dr. Justyna Florek synthesized the pore-swelled MCM-48-type MSNs and Dr. Meryem Bouchoucha synthesized and characterized the 90 and the 300 nm MCM-48-type MSNs. (Université Laval, Québec, Canada). Dr. Siddharth Jambhrunkar provided additional thermogravimetric analyses and solubility tests, helped me in the design of the solubility and release tests and Kuan Yau Wong performed the anti-inflammatory and the cellular membrane permeability tests under the guidance of Dr. Amirali Papat (The University of Queensland, Brisbane, Australia). Dr. Amirali Papat and Prof. Freddy Kleitz have both supervised my work and participated in editing the manuscript.



## In Vitro Dissolution, Cellular Membrane Permeability, and Anti-Inflammatory Response of Resveratrol-Encapsulated Mesoporous Silica Nanoparticles

Estelle Juère,<sup>†,‡</sup> Justyna Florek,<sup>†</sup> Meryem Bouchoucha,<sup>‡</sup> Siddharth Jambhrunkar,<sup>§,⊥</sup> Kuan Yau Wong,<sup>§,⊥</sup> Amiralı Papat,<sup>§,⊥</sup> and Freddy Kleitz<sup>\*,†,‡,⊥</sup>

<sup>†</sup>Department of Inorganic Chemistry – Functional Materials, Faculty of Chemistry, University of Vienna, Währinger Straße 42, 1090 Vienna, Austria

<sup>‡</sup>Department of Chemistry, Université Laval, Quebec City G1V 0A6, Canada

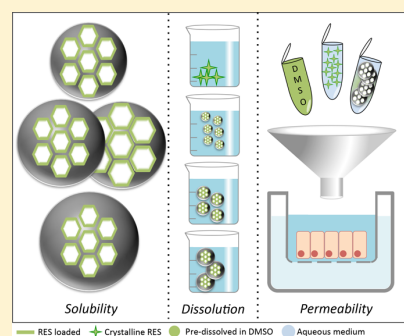
<sup>§</sup>School of Pharmacy, The University of Queensland, Brisbane QLD 4072, Australia

<sup>⊥</sup>Inflammatory Disease Biology and Therapeutics Group, Mater Research Institute – The University of Queensland, Translational Research Institute, Woolloongabba QLD 4102, Australia

### Supporting Information

**ABSTRACT:** Sizing drugs down to the submicron and nanometer scale using nanoparticles has been extensively used in pharmaceutical industries to overcome the poor aqueous solubility of potential therapeutic agents. Here, we report the encapsulation and release of resveratrol, a promising anti-inflammatory and anticancer nutraceutical, from the mesopores of MCM-48-type silica nanospheres of various particle sizes, i.e., 90, 150, and 300 nm. Furthermore, the influence of the carrier pore size on drug solubility was also evaluated (3.5 vs 7 nm). From our results, it is observed that the saturated solubility could depend not only on the pore size but also on the particle size of the nanocarriers. Moreover, with our resveratrol-mesoporous silica nanoparticles formulation, we have observed that the permeability of resveratrol encapsulated in MCM-48 nanoparticles (90 nm) can be enhanced compared to a resveratrol suspension when tested through the human colon carcinoma cell monolayer (Caco-2). Using an *in vitro* NF- $\kappa$ B assay, we showed that resveratrol encapsulation did not alter its bioactivity and, at lower concentration, i.e., 5  $\mu$ g mL<sup>-1</sup>, resveratrol encapsulation provided higher anti-inflammatory activity compared to both resveratrol suspension and solution. All combined, the reported results clearly highlight the potential of small size mesoporous silica nanoparticles as next generation nanocarriers for hydrophobic drugs and nutraceuticals.

**KEYWORDS:** oral drug delivery, mesoporous silica nanoparticles, resveratrol, solubility, Caco-2 monolayer, anti-inflammatory



## INTRODUCTION

Recent efforts have been oriented toward the oral administration of therapeutic agents rather than the invasive intravenous pathways due to ease of administration and improved patient compliance. However, more than 40% of new chemical entities coming out of high throughput screening often have poor solubility in aqueous environment, poor stability, and low bioavailability.<sup>1</sup> The journey of an orally delivered drug in our body starts with its absorption in the gastrointestinal tract (GIT) prior to its distribution to targeted tissues. At this early stage, many factors influence the drug performance, for instance, aqueous solubility throughout GIT, chemical stability in contact with enzymes present in the lumen, and drug permeability through the intestinal epithelial membrane.<sup>2–4</sup> Nanocarriers have somewhat tackled the problems of drug hydrophobicity, solubility, and crystallization. However, there are only few nanocarriers, which have surpassed the hurdles of taking formulation from laboratory to scale up

and technology transfer scale. For instance, hydrophobic molecules, such as curcumin,<sup>5</sup> griseofulvin,<sup>6,7</sup> resveratrol,<sup>8,9</sup> and telmisartan,<sup>10</sup> have tremendous therapeutic potential for many cancers, fungal, inflammatory, and cardiovascular diseases, however their pharmaceutical developments are still hampered by their limited oral bioavailability.<sup>11</sup> In particular, resveratrol, a nontoxic natural product found in grapes, peanuts, and red wine, is a good example of a promising broad-spectrum nutraceutical with various positive health effects (antioxidant, anti-inflammatory, and most importantly, anticancer activities), which is however hampered by poor solubility, low bioavailability, and poor pharmacokinetic properties.<sup>8,9,12</sup> Such drawbacks may be circumvented through the encapsulation of

**Received:** June 23, 2017

**Revised:** October 31, 2017

**Accepted:** November 2, 2017

**Published:** November 2, 2017

the drugs into smart nanomaterials capable to reduce both hydrophobicity and stability issues across the GIT. The solubility of a drug depends upon several factors, notably particle size of the compound where smaller drug particle size provides large surface area per volume leading to higher solubility.<sup>13,14</sup> Thus, one can expect that encapsulation of drugs into nanopores could provide a nanosized environment and keep the drug into amorphous state, which further positively affects the solubility.<sup>15,16</sup> Simultaneous effects of encapsulation include the decrease of the drug particle size from the bulk down to the nanometer range and the change of the solid state from crystalline to amorphous through the interaction with the surface of the nanopores. This phenomenon has been reported using polymer nanoparticles,<sup>17</sup> polymer nanocapsules,<sup>18</sup> liposomes,<sup>19,20</sup> silicon microparticles,<sup>21</sup> soy protein isolate,<sup>22</sup> and mesoporous silica nanoparticles (MSNs).<sup>23–28</sup> In particular, improving the aqueous solubility of a potential drug through the tuning of the physicochemical properties of the MSNs is of growing interest and this has been widely reported in terms of surface functionalization,<sup>25</sup> geometry, and order of the mesoporous network,<sup>29–31</sup> but scarcely in terms of particle size.<sup>32</sup> Yet, reducing the size of the nanoparticles has been the focus in the field over the past few years. Especially, since smaller particles are expected to cross the cellular membranes more efficiently than their bigger counterparts,<sup>33</sup> it would be relevant to improve both membrane permeation and solubility by simply reducing the size of the nanocarriers. Therefore, to explore further on this topic and gain better insights into particle and pore size effects on oral drug delivery, MSNs are materials of choice considering their biocompatibility, stability, loading capacity,<sup>34,35</sup> and the multitude of possibilities to adjust their physicochemical properties, i.e., size of the spheres, size of the pores,<sup>36</sup> their colloidal stability, and pH-responsiveness through various modes of functionalization.<sup>37–39</sup>

In the present contribution, we used MCM-48 MSNs with tailor-made particle sizes, i.e., 90, 150, and 300 nm, and with a pore size of 3.5 nm, to encapsulate 20% w/w of resveratrol used here as a model drug, and compare its solubility. As a control, we have also included in this study, silica nanoparticles with a larger pore size, i.e., 7 nm with a fixed particle size, i.e., 150 nm, to account for the pore size effect on the solubility of the drug. Dissolution rate of the free resveratrol was also compared to the encapsulated drug using the three particle sizes. To assess the repercussions of drug encapsulation on permeability, we have studied transportation of our optimized formulation across Caco-2 monolayer cells. Moreover, the biological stability and anti-inflammatory activity of resveratrol were also tested using lipopolysaccharide (LPS)-dependent NF- $\kappa$ B activation assay by measuring green fluorescent protein (GFP) expression using RAW 264.7 NF- $\kappa$ B reporter cells. Finally, cytotoxicity of the pristine MCM-48(90 nm) nanoparticles is also reported.

## ■ EXPERIMENTAL SECTION

**Chemicals and Reagents.** CTAB (cetyltrimethylammonium bromide, 99%), Pluronic F127 (EO<sub>106</sub>PO<sub>70</sub>EO<sub>106</sub>), TEOS (tetraethylorthosilicate, 99%), TWEEN20, and the dialysis cellulose tubing membrane were purchased from Sigma-Aldrich. TMB (1,3,5-trimethylbenzene, 99%) was obtained from Alfa-Aesar (USA). Trans-resveratrol (99%) was obtained from MegaResveratrol, USA.

**Synthesis of the MSNs.** MCM-48-type nanoparticles with controlled particle size were synthesized by adapting the procedure previously reported.<sup>40,41</sup> Briefly, 1.0 g of CTAB and

“*x*” g of Pluronic F127 (with *x* = 2, 4, or 8 g for MCM-48 with particle sizes of 300, 150, and 90 nm, respectively) were dissolved in 298 mL of NH<sub>4</sub>OH (2.8 wt %)/EtOH = 2.5:1 (v/v). Then, 3.6 g of TEOS was added and the solutions were vigorously stirred (1000 rpm) for 1 min. The mixtures were aged under static conditions at room temperature (RT) for 24 h and recovered by centrifugation (30 min, 10 000 rpm). Prior to the centrifugation of the 90 nm-particles synthesis medium, the volume of the obtained solution was doubled with EtOH. Afterward, all the white resulting solids were washed twice with 250 mL of water and dried in air at 60 °C overnight. Finally, the resulting products were calcined (550 °C, air, 5 h). The resulting materials are called MCM-48(90), MCM-48(150), and MCM-48(300); the number between the parentheses refers to the measured size of the particles.

Pore-swollen silica nanoparticles were prepared according to the procedure reported in the literature.<sup>42</sup> For this, noncalcined MCM-48(150) (0.8 g) were dispersed in 40 mL EtOH (100%) by shaking (15 min) and sonication (30 min). Simultaneously, a solution of 40 mL of H<sub>2</sub>O/TMB = 1:1 v/v was prepared using a vortex (1 min) and added to the suspension of noncalcined MSNs. The mixture was placed in an autoclave and kept for 2 days at 100 °C. The resulting powder was filtered, washed three times with water and once with EtOH, and dried at 100 °C for 24 h. Finally, the resulting product was calcined (550 °C, air, 5 h). This material is named MCM-48(PE-150).

**Encapsulation of Resveratrol into MSNs.** Resveratrol (25 mg) was loaded into MSNs using the rotary evaporation technique as previously reported.<sup>26</sup> Resveratrol was placed in a rotary evaporation flask and dissolved in methanol (10 mL) using sonic bath (RT, 5 min). Then, the MSNs (100 mg) were added to the solution and dispersed using sonic bath (RT, 5 min) in order to achieve a loading of 20% w/w. The solvent was slowly evaporated with a rotary evaporator at 40 °C until dried powder could be observed in the flask. The obtained solid was then dried under air overnight at 50 °C in an oven.

**Materials Characterization.** Powder X-ray diffraction (XRD) measurements were performed using a Siemens D5000 (reflection,  $\theta$ – $\theta$  configuration; Cu K $\alpha$ :  $\lambda$  = 1.541 Å; 40 kV; 30 mA; 1–8 or 10–40° 2 $\theta$ ; step size: 0.02 2 $\theta$ ; 0.02 s/step). The data were analyzed using the Jade software coupled with JCPDS and ICDD databases. For the transmission electron microscopy (TEM), the nanoparticles were dispersed in ethanol. This suspension (4  $\mu$ L) was deposited on a carbon-coated copper grid and images were taken in TEM (JEM-1230) at an accelerating voltage of 80 keV. High-resolution scanning electron microscopy images (HR-SEM) were taken with a Verios 460 (FEI) at a landing voltage of 1 kV in deceleration mode (stage bias voltage: 4 kV) (KAIST, Daejeon, Republic of Korea). The samples were mounted without metal coating. N<sub>2</sub> physisorption isotherms were measured at –196 °C (77 K) using an Autosorb-iQ<sub>2</sub> sorption analyzer (Quantachrome Instruments, Boynton Beach, FL, USA). Prior to the analysis, the pristine MSNs and the resveratrol-encapsulated MSNs were respectively outgassed 10 h at 200 °C or 20 h at 35 °C. The specific surface area ( $S_{\text{BET}}$ ) was determined using the Brunauer–Emmet–Teller (BET) equation in the relative pressure range 0.05–0.2. The total pore volume was determined at  $P/P_0 = 0.95$ . The pore size distributions (PSDs) were calculated with the nonlocal density functional theory (NLDFT) method considering the silica cylindrical pore model.<sup>43</sup> Dynamic light scattering (DLS) analyses were recorded on a Malvern DTS Nano Zetasizer 173° (equilibrium

time set at 3 min, 3 measurements for each sample). The samples were dispersed in water, shaken and sonicated prior to the analysis. Thermogravimetric analysis (TGA) was performed on a Mettler Toledo instrument under airflow of 20 mL min<sup>-1</sup> with a heating rate of 10 °C min<sup>-1</sup>, from 40 to 900 °C. The drug loading was assessed between the range of temperature of 150–650 °C.

**Drug Solubility and *in Vitro* Dissolution.** The solubility of resveratrol was determined using a procedure previously reported.<sup>26</sup> Excess amounts of free and encapsulated drug equivalent to ca. 2000 µg mL<sup>-1</sup> were dispersed in 1 mL of water. The resulting solution was stirred at 37 °C for 48 h. The supernatant was recovered by centrifugation prior to the determination of the concentration of resveratrol by UV–vis spectroscopy at  $\lambda = 305$  nm (Varian Cary 50 Bio). The data reported are average values obtained using different starting MSNs, i.e., from various batches of MSNs synthesis ( $n = 8$ ). The release of the encapsulated resveratrol was performed using the dialysis bag technique. Nanoparticle-encapsulated resveratrol equivalent to 20 mg of free drug was introduced inside the membrane (14 kDa molecular weight cutoff) with 5 mL of phosphate buffer saline (PBS) and subsequently immersed into 220 mL of 0.5% TWEEN20/PBS (v/v) at 37 °C with continuous stirring. At adequate period of time, 2 mL of solution was withdrawn and immediately replaced with the equivalent volume of 0.5% TWEEN20/PBS to maintain the initial volume. The removed samples were analyzed by UV–vis spectroscopy at  $\lambda = 305$  nm. As a control, the same experiment was conducted with 20 mg of free resveratrol. The data presented are average of triplicates.

**Cell Viability.** Analysis of cell viability was measured by flow cytometry. Typically, Caco-2 and RAW 264.7 cells (500 000) were seeded in a 12-well plate and treated with various concentrations, i.e., 10, 50, and 100 µg mL<sup>-1</sup> of MCM-48(90) for 24 h in Minimum Essential Media (MEM) and Dubelcco's Modified Eagle's Media (DMEM) supplemented with 10% fetal bovine serum, respectively. Then, the cells were trypsinised and harvested by centrifugation at 400 g for 5 min at RT. The supernatant was discarded and the cells were washed once with PBS and resuspended in 0.2% bovine serum albumin (BSA)/PBS. Cells were stained with 7-aminoactinomycin D (7-AAD) for 10 min and analyzed by Cytoflex flow cytometer (Beckman Coulter). Cells without MSNs were used as a control.

**Caco-2 Permeability Experiments.** Permeability of resveratrol was evaluated *in vitro* by using well-recognized Caco-2 cell monolayer assay. Caco-2 cells were seeded at a density of  $1 \times 10^5$  cells/well in 12-well cell culture inserts (1 µm pore diameter, 0.9 cm<sup>2</sup> area) (Corning Costar, NY) and were grown in supplemented DMEM + 1% PEST + 1% Glutamine for 10–14 days. Transepithelial electrical resistance (TEER) values were regularly measured using an electrode connected to an EVOM volt-ohmmeter (World Precision Instruments, USA). Only Caco-2 cell monolayers with initial TEER values higher than 600 Ω cm<sup>2</sup> were used for further experiments. The permeability studies were carried out by adding  $V = 0.5$  mL of various concentrations, i.e., 5, 10, and 20 µg mL<sup>-1</sup> of resveratrol suspended in Hank's Balanced Salt Solution (HBSS), MCM-48(90) loaded with RES and suspended in HBSS and resveratrol predissolved in a small quantity of DMSO and diluted in HBSS on the apical compartment of the insets. Blank medium (HBSS) and nanoparticles were used as controls. The basolateral compartment (receiver compartment) was filled out with 1.2 mL of

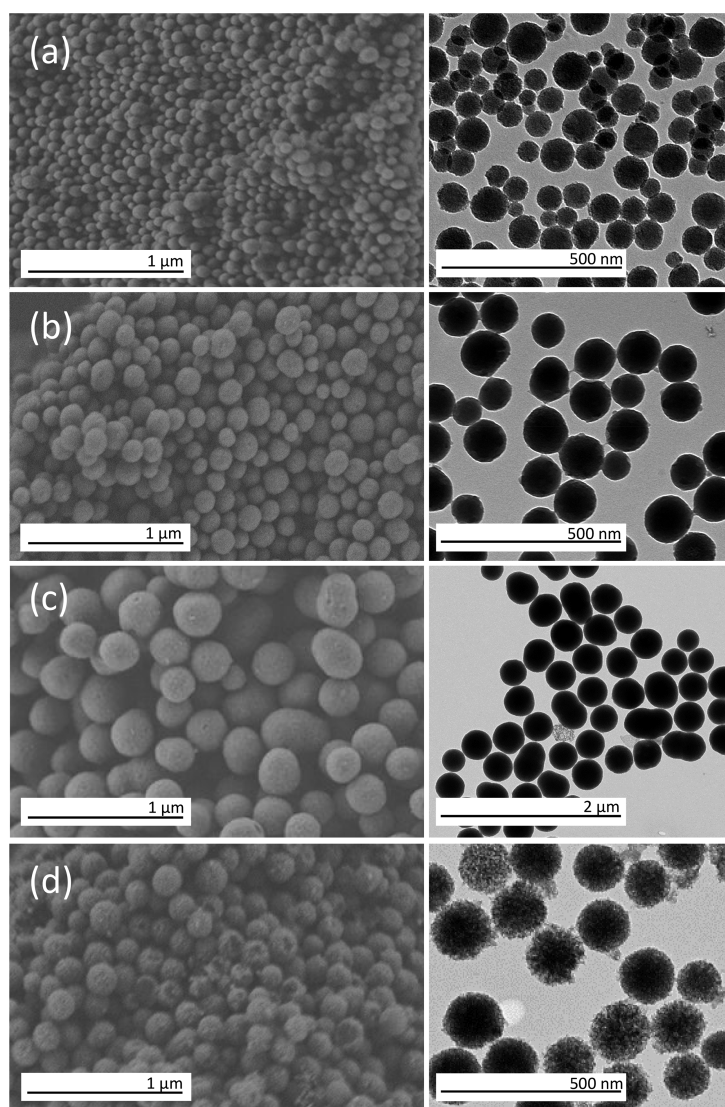
HBSS + 10 mM hydroxyethyl piperazineethanesulfonic acid (HEPES) + 1% BSA. After 2 h of incubation, samples were collected from the basolateral compartment and the amount of resveratrol present in the receiver compartment was determined by UV–vis spectroscopy.

***In Vitro* Anti-Inflammatory Assay.** According to previously reported methods,<sup>22</sup> RAW 264.7 cells transfected with a NF-κB reporter gene plasmid were seeded at 500 000 cells/well in 24-well plates in a fully humidified incubator containing 5% of CO<sub>2</sub> and 95% of air. To study the effect of resveratrol loaded in MCM-48(90) on inhibition of NF-κB, after overnight incubation, the cells were pretreated with a range of concentrations of resveratrol in DMSO, DMEM, and MCM-48(90) loaded with resveratrol, for 6 h and then 10 ng mL<sup>-1</sup> of LPS was added to activate NF-κB within the macrophages. After overnight incubation, cells were trypsinized, harvested, and GFP expression due to NF-κB activation assessed by flow cytometry using a CyAn ADP Analyzer (Beckman Coulter) and Flowjo 8.8.7v for analysis. To avoid any interferences due to the nanoparticles, independently of the drug, MCM-48(90) was included in this assay as a negative control with and without addition of LPS. We acknowledge that exposure to drug and/or the carriers may lead to some cell death. Therefore, while analyzing flow cytometry for each sample we have gated on the live cells using their forward and side scatter characteristics (standard practice in flow cytometry) and therefore only live cells were included in our analysis.

## RESULTS AND DISCUSSION

**Materials Characterization. Size and Surface of the MSNs.** Size of the nanoparticles is a key attribute when designing materials for oral drug delivery for human use because they have to cross the intestinal mucosal barrier.<sup>4,44</sup> Fine-tuning the size of MCM-48 particles was achieved *in situ* by adapting the amount of F127, a surfactant used in the synthesis to inhibit the growth of the MCM-48 particles.<sup>40</sup> More specifically, the more F127 is added, the less the particles could grow, therefore the mass of F127 surfactant used for the classical MCM-48 MSNs synthesis, being 4 g, is reduced down to 2 g for the bigger MCM-48 MSNs and increased up to 8 g for the smaller ones.<sup>41</sup> On the other hand, expansion of the pore size requires an additional step in the synthesis of MCM-48 nanoparticles. A traditional pore swelling agent, trimethylbenzene (TMB), was used to infiltrate the micelles of the noncalcined particles in a mixture EtOH/H<sub>2</sub>O at high temperature, i.e., 100 °C.<sup>42</sup> Indeed, it was reported that TMB can penetrate and interact with the alkyl chains of the surfactant, i.e., CTAB in our case, through hydrophobic interactions. In addition for this MCM-48-based synthesis, TMB may also interact to some extent with F127 (EO<sub>106</sub>PO<sub>70</sub>EO<sub>106</sub>), including with the EO groups of the block copolymer as these are expected to be dehydrated at the temperature of the synthesis, i.e., 100 °C.<sup>45</sup> Then, under the solvothermal conditions applied, it is assumed that silica precursors undergo redissolution and redeposition around the mesopores resulting in the increase of the pore size. The ability of the swelling agent to incorporate the core of the micelles relies on several factors, such as its molecular size and its solubility in the solvent used.<sup>46</sup>

The characterization of the particles using electron microscopy is therefore necessary to assess the success of these syntheses. HR-SEM images of the obtained MCM-48 nanoparticles are depicted in Figures 1 and S1. As it can be



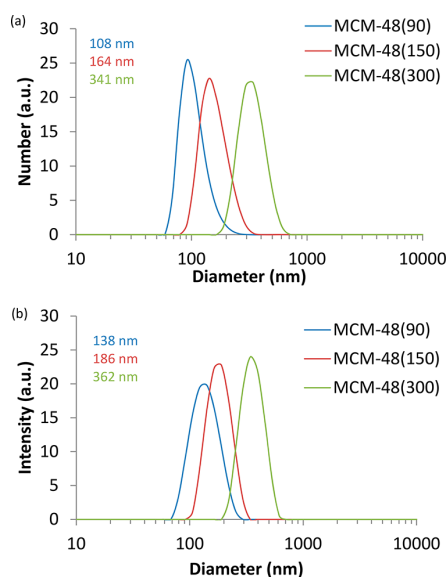
**Figure 1.** HR-SEM (left) and TEM (right) images of (a) MCM-48(90), (b) MCM-48(150), (c) MCM-48(300), and (d) MCM-48(PE-150).

seen, neither the variation of the particle size nor the expansion of the pore size have greatly affected the morphology of the nanoparticles since mostly spherical particles have been obtained which is expected with the MCM-48 based synthesis. Nevertheless, the surface of the pore-swelled nanoparticles seems to be rougher than the other nanoparticles synthesized. The TEM images presented in Figures 1 and S1 suggest that nonagglomerated particles with well-defined mesoporous network have been synthesized with sizes of about 90, 150, and 300 nm. However, both SEM and TEM images suggest that polydispersity increased upon decreasing the particle sizes from 150 to 90 nm. From the TEM images of MCM-48(PE-150) in Figures 1d and S1d, one can observe that the nanoparticles appeared somewhat less dense upon exposure to the electronic beam possibly because of the increase of the pore size. Furthermore, DLS has been used to evaluate the behavior of these nanoparticles in aqueous solution and the distributions of the hydrodynamic diameters are shown in Figure 2. As it can be seen, pure MSNs show narrow particle size distribution in

aqueous medium and absence of agglomeration owing to the low polydispersity index (PDI,  $0.02 < \text{PDI} < 0.08$ ) and the colloidal stability of the suspended MCM-48(90, 150, and 300) nanospheres. Also, the increase of the hydrodynamic diameter in number mode, i.e., 108, 164, and 341 nm for MCM-48(90), MCM-48(150), and MCM-48(300), is in accordance with the electron microscopy analyses. Although the size of the MCM-48(PE-150) particles is comparable to the classic MCM-48(150), 163 vs 164 nm in number mode, respectively, the diameter in intensity mode and the PDI increased, i.e., 186 vs 256 nm and 0.03 vs 0.174 for MCM-48(150) and MCM-48(PE-150), respectively (see Figure S2a,b).

**Mesoporous Network.** The three-dimensional (3-D) interconnected network of the MCM-48 nanospheres is frequently favored over the two-dimensional (2-D) hexagonal structure of MCM-41 silica owing to the superior diffusion of entities throughout the mesopores of MCM-48 materials.<sup>37,47</sup> Although smaller particles, such as MCM-48(90), exhibit restricted coherent scattering domain, a broad X-ray reflection, which can

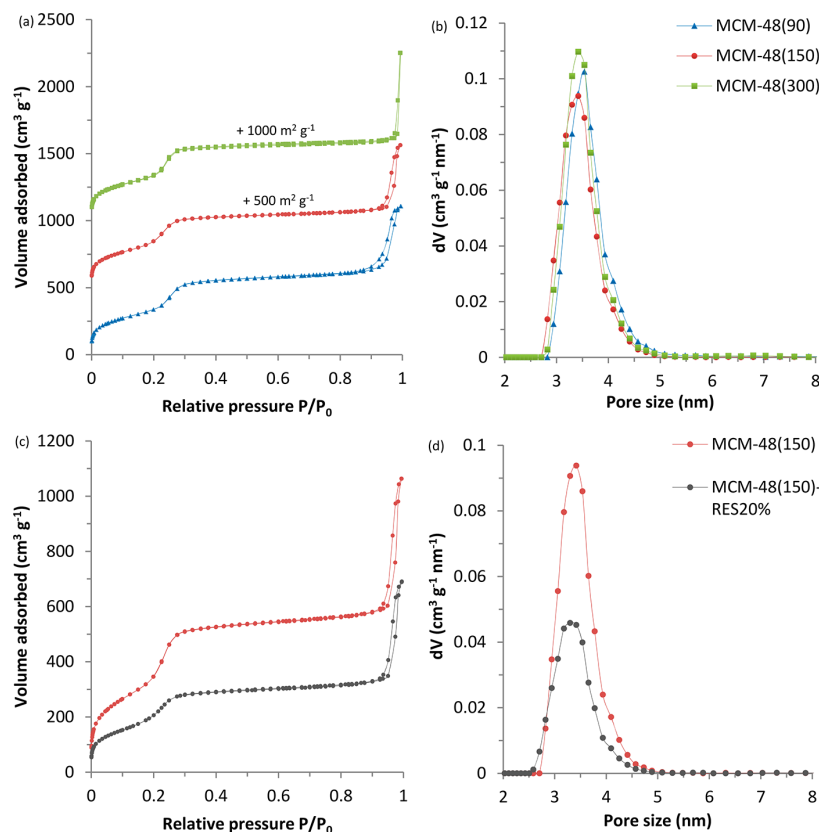




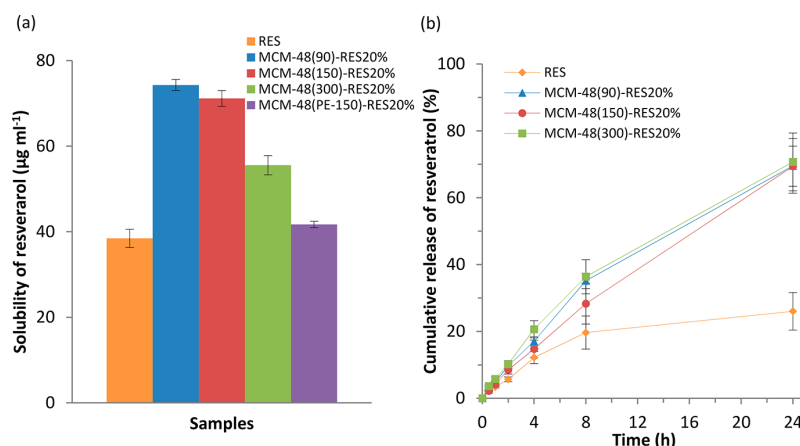
**Figure 2.** Hydrodynamic diameters of the pure MCM-48(90, 150 and 300) measured by dynamic light scattering, in number (a) and intensity mode (b).

still be attributed to the (211) plan of the 3-D cubic  $Ia3d$  structure, can be observed in the powder diffraction pattern shown in Figure S3a. On the other hand, higher degree of order has been obtained for the bigger nanoparticles, i.e., MCM-48(150) and MCM-48(300) with the appearance of well-resolved (211) and (220) reflections.<sup>41</sup>

The  $N_2$  sorption analysis reveals a type IV isotherm characteristic of the cylindrical mesopores of MCM-48-like nanoparticles, as it can be seen in the Figure 3a. Tailoring of the particle size through the adjustment of the particle growth inhibitor, pluronic F127, has affected neither the shape of the isotherms nor the physicochemical parameters, which are listed in Table S1. Nevertheless, an effect associated with the increasing particle size can be noticed in the interparticle region of the  $N_2$  isotherms, i.e., as of  $P/P_0 = 0.9$ , since higher volume of  $N_2$  is adsorbed from MCM-48(90), MCM-48(150) to MCM-48(300), due to higher void volume. Both MCM-48(90) and MCM-48(300) nanoparticles maintained high surface area, i.e., 1243 and 1241  $m^2 g^{-1}$  and high pore volume, i.e., 1.10 and 0.93  $cm^3 g^{-1}$ , respectively, which is very comparable to the regular MCM-48(150) material, i.e., 1285  $m^2 g^{-1}$  and 0.94  $cm^3 g^{-1}$ . In addition, the synthesis used the same structure-directing agent, i.e., CTAB, therefore the pore size remains constant for MCM-48(90), MCM-48(150), and MCM-48(300), being around 3.5 nm (see Figure 3b). Typically, the pore condensation step of  $N_2$  at  $-196^\circ C$  inside MCM-48 nanospheres with pore size around 3.5 nm occurs in



**Figure 3.**  $N_2$  physisorption isotherms measured at  $-196^\circ C$  of (a) MCM-48(90, 150, and 300), (c) MCM-48(150) and MCM-48(150)-RES20%, and (b) and (d) their respective pore size distributions obtained from the adsorption branch using the NLDFT method considering the (silica) cylindrical pore model.



**Figure 4.** (a) Solubility of resveratrol from the pure (RES) and the encapsulated samples (MCM-48(90, 150, 300, and PE-150)-RES20%) in water. (b) Cumulative release of resveratrol from the pure (RES) and the encapsulated samples (MCM-48(90, 150, and 300)-RES20%). Statistics: mean  $\pm$  SD ( $n = 8 \pm$  SD and  $n = 3 \pm$  SD for solubility and release data, respectively).

the relative pressure range 0.2–0.3 without hysteresis.<sup>48</sup> Increasing the pore size of the MCM-48 nanoparticles results in a shift of the pore condensation to the higher relative pressure range 0.6–0.9, as well as the occurrence of H1 hysteresis loop.<sup>49,50</sup> Thus, the physisorption isotherm and the respective pore size distribution of the pore-expanded MSNs, MCM-48(PE-150), presented in Figure S4, confirm the success of the pore swelling process, as pores of about 7 nm have been obtained. The increase of the pore diameter is accompanied by a decrease of the surface area down to  $851 \text{ m}^2 \text{ g}^{-1}$  and an increase of the pore volume to  $1.67 \text{ cm}^3 \text{ g}^{-1}$ . Besides, as it can be verified from the SEM and TEM images in Figures 1 and S1, respectively, quite monodisperse and nonagglomerated MCM-48(PE-150) nanoparticles were obtained and the mesoporous network was essentially preserved. In the following, the MCM-48(PE-150) sample will serve as a reference to illustrate the behavior of larger pore materials.

**Drug Loading and Confined Structure.** Encapsulation using the rotary evaporation technique is a common way to circumvent solubility issues through amorphization of the drug. Typically, the drug is first dissolved in a sufficient volume of organic solvent prior to the addition of the nanoparticles.<sup>51</sup> Once the solvent evaporates, adsorption of the drug on the surface of the pores occurs, which lowers the Gibbs free energy and yields in an amorphous drug/particle system.<sup>52</sup> Being restricted to a certain spatial environment, the amorphous drug is not prone to crystallization. On the other hand, increasing the size of the mesopores may promote mobility of the drug up to the point where recrystallization may happen.<sup>53</sup> Therefore, in the current study, 7 nm pore size will be compared to the smaller 3.5 nm pore size in terms of degree of crystallinity and saturated solubility of resveratrol. Apart from the size of the pores, drug loading is also suspected to play a role on the amorphous/crystalline character of the confined drug.<sup>11</sup> In this case, the solvent evaporation technique is a valuable technique since it allowed us to precisely control the amount of resveratrol introduced and to load equal quantity, i.e., 20% w/w, in the different MSNs. As it can be noticed from the mass loss profile obtained from the thermogravimetric analysis (TGA) (Figure S5 and Table S2), the experimental and the expected drug loadings are very close. This further affirms reliability and reproducibility of the rotary evaporation method.

As expected, the introduction of resveratrol did not affect the mesostructure of the MCM-48 nanoparticles, as highlighted by the XRD and the  $\text{N}_2$  physisorption analyses (Figures S3b and 3c).

As previously discussed, immobilization of drugs inside the pores tends to change the structure of the organic entity from crystalline to amorphous. This has been confirmed with the sample MCM-48(150)-RES20% since no reflections associated with the crystallized state of the molecule can be detected from the wide-angle powder XRD pattern in the Figure S3d. On the other hand, simple physical mixture of RES with MCM-48(150) does not provide conditions for the amorphization of the drug, as revealed by the presence of the peaks associated with the crystalline drug in Figure S3c. However, using larger pore MCM-48 nanoparticles, i.e., MCM-48(PE-150), it can be observed that few reflections attributed to resveratrol appeared at  $2\theta = 19.2, 22.3, \text{ and } 28.2^\circ$  in the diffraction pattern presented in the Figure S3d. Therefore, despite being nanosized, confined resveratrol inside the 7 nm pore MCM-48(PE-150) seems to preserve a higher fraction of crystallized drug than the 3.5 nm pores. The  $\text{N}_2$  physisorption isotherms and pore size distributions of MCM-48(150) and MCM-48(150)-RES20% are presented in Figure 3c,d. As it can be seen, the volume of  $\text{N}_2$  adsorbed and the specific BET surface area drastically decreased after the encapsulation, while the pore size of MCM-48(150)-RES20% is similar to that of the pristine MCM-48(150) sample, i.e., 3.3 vs 3.4 nm, respectively. Therefore, the decrease of the surface area and pore volume, along with the minor change in the interparticle region and pore size, may suggest that the confinement of resveratrol inside the nanopores of MCM-48 occurs likely as a monolayer in the internal surface of the MSNs.<sup>27,52</sup> Besides, the particle size distributions obtained from DLS analysis of all the RES-loaded MCM-48 nanoparticles, which are shown in Figure S2, reveal one single peak, further confirming the absence of agglomeration.

In addition, we have verified that, once encapsulated inside MCM-48 nanoparticles, resveratrol can remain as the biologically active *trans* isomer over a prolonged period of time. As a test, resveratrol was eluted in ethanol from a 10-month-old MCM-48(150)-RES20% sample and the resulting solution was analyzed by UV–vis spectroscopy. As shown in the Figure S6,

the maximum absorbance appeared at  $\lambda = 305$  nm for both the reference and the eluted resveratrol, demonstrating the chemical stability (vs isomerization) of the drug upon encapsulation and aging/storage. Furthermore, powder XRD data collected for the 10-month-old MCM-48(150)-RES20% sample confirmed that resveratrol remained amorphous for at least this period of time (see Figure S3e). Nevertheless, shelf life of the encapsulated drug is a critical aspect for these (nano)formulations which will need to be taken into account in a comprehensive and dedicated study.

**Drug Solubility and *in Vitro* Dissolution.** There are indications that *trans*-resveratrol could degrade upon light exposure and/or pH variations. In particular, it has been recently shown that almost 30% of the initial concentration could be degraded after 24 h at pH 7.4.<sup>54</sup> Thus, we have first performed preliminary stability tests under similar conditions and a degradation of about 10% was observed using UV–vis spectroscopy (data not shown). In our case, we aimed at comparing the encapsulated resveratrol to the free one, thus, regardless of the slight degradation, the differences observed will still be valid.

**Drug Solubility.** In this study, the saturated aqueous solubility of the free and encapsulated drug is compared. To do so, excess amounts of free and encapsulated resveratrol are soaked in water for 48 h at 37 °C followed by centrifugation to collect the supernatant, and the amount of solubilized resveratrol in the supernatant was determined using UV–vis spectroscopy. The solubility results expressed in  $\mu\text{g mL}^{-1}$  of the pure and encapsulated resveratrol inside MCM-48(90, 150, 300, and PE-150) are presented in Figure 4a. As it can be observed, regardless of the type of MCM-48 nanoparticles used, the solubility of encapsulated resveratrol is higher than that of the crystalline free drug. Indeed, the crystalline/amorphous character of the free/encapsulated resveratrol can explain this phenomenon. Furthermore, using a larger pore material, i.e., 7 nm MCM-48(PE-150)-RES20%, the solubility of resveratrol seems to be lower than with the smaller pore equivalent, i.e., 3.5 nm MCM-48(150)-RES20%, presumably because of the higher fraction of crystalline resveratrol present in MCM-48(PE-150)-RES20%, as discussed in the previous section. Regarding the particle size effect on the solubility, we observed a rather nonsignificant trend, i.e., smaller nanoparticles seem to increase more the aqueous solubility of resveratrol. The ratio of solubility of the encapsulated resveratrol to free resveratrol is 1.93, 1.85, and 1.44 for MCM-48(90)-RES20%, MCM-48(150)-RES20%, and MCM-48(300)-RES20%, respectively. Unlike the pore size effect on the solubility, which has been documented in the literature throughout the years, particle size effect has not been substantiated yet. Consequently, further studies will be needed in order to achieve clearer relationship between the aqueous solubility of an organic molecule and the size of the carriers used. Nevertheless, this observation is of valuable interest as smaller nanoparticles attract recently more attention in an attempt of cell uptake enhancement, for instance.<sup>33,41</sup>

Additionally as control experiments, we also recorded UV–vis spectra (see Figure S7 for details) of resveratrol solubilized in water over time, i.e., 0, 2, 24, and 48 h (under the exact same experimental conditions as described for the solubility tests in the Experimental Section). As it can be observed, the maximum absorbance remained at  $\lambda = 305$  nm, which shows that *trans*-resveratrol is stable under these conditions. Furthermore, the solubility does not fluctuate much between 0 and 48 h, being

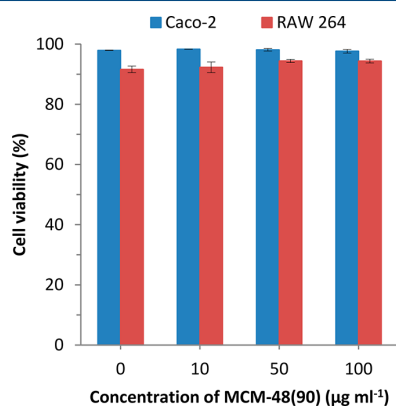
45.2 and 45.7  $\mu\text{g mL}^{-1}$ , respectively. Moreover, the powder XRD patterns of the drug, measured before and after the solubility test, i.e., “fresh” and recovered resveratrol, are very similar. In light of these observations, we assume that we are not in the presence of a solution-mediated phase transformation. Furthermore, the pH of the dissolution medium, i.e., water, was checked and only little variation was observed, with pH = 6.08 at  $t = 0$  h (directly after addition of RES) and pH = 6.15 at  $t = 48$  h.

***In Vitro* Dissolution.** Considering the screening of the different materials performed through the saturated solubility study, we decided to focus our kinetic release tests toward the different particle sizes of MCM-48 nanoparticles. Thus, the release of resveratrol in the dissolution medium (pH 7.4) under diluted conditions was performed using free and encapsulated resveratrol samples, RES, and MCM-48(90, 150, and 300)-RES20%. The results are compiled in Figure 4b. As it can be immediately seen, 26 vs 70% of release after 24 h were obtained from the free vs the encapsulated resveratrol. Thus, the fraction of resveratrol dissolved from the silica formulations is almost 3 fold higher compared to the free drug. On the other hand, contrary to the saturated solubility test, a comparable release percent was calculated for the three MCM-48 nanoparticles, i.e., 70, 69 and 71% for MCM-48(90)-RES20%, MCM-48(150)-RES20%, and MCM-48(300)-RES20%, respectively. Therefore, we suggest that the release of the drug from the nanoparticles could be diffusion controlled. Our hypothesis is that, under saturated conditions, the solubility of the drugs tends to rely on the size of the nanocarriers; in a restricted volume of solution, smaller particles MCM-48(90) would be presumably better dispersed than MCM-48(150) or MCM-48(300) so the saturated solubility of the drug out of the silica matrix might be enhanced. Differently, under diluted conditions, the release of resveratrol seems to be achieved regardless of the particle size of the carrier; since all the nanoparticles that we used are colloidally stable, dispersion is not a limiting factor anymore. Our experimental data have been fitted with the semiempirical power law that usually describes the drug release mechanism and the results are presented in Figure S8 and Table S3. As the  $R^2$  values implied, the model fits well with our experiment. For all the samples, the diffusional exponent  $n$  is comprised between 0.5 and 1, which for a nonswellable system corresponds to a non-Fickian or anomalous transport model.<sup>55</sup> It is reported that this mechanism may be due to structure change, temperature variations or saturation of the release media. Interestingly, as the size of the nanoparticles decreases from 300 to 90 nm, the  $n$  value increases and gets closer to 1 (i.e., 0.846, 0.916, and 0.944 for MCM-48(300)-RES20%, MCM-48(150)-RES20%, and MCM-48(90)-RES20%, respectively). It is known that for  $n > 1$ , a zero-order kinetic model drives the drug dissolution, independently of the concentration of the drug released. Our results correlate well with earlier reports in terms of quantity of resveratrol released, although our kinetic observations may differ.<sup>26</sup> These differences can originate from experimental conditions used for the dissolution studies as well as from the materials themselves. It is worth noting that higher release percent from the MSNs is still expected after 24 h whereas the equilibrium seems to be reached for the free resveratrol.

**Cell Studies.** For cellular uptake and transport, evidence suggest that small particles show better endocytosis compared to their larger counterparts.<sup>33</sup> Hence, accounting for the results obtained with the solubility and the *in vitro* dissolution

experiments, we have used MCM-48(90) loaded with 20% of resveratrol for our cell-based assays.

**Cell Viability.** As can be seen in Figure 5, various concentrations of MCM-48(90) were used to perform the *in vitro*



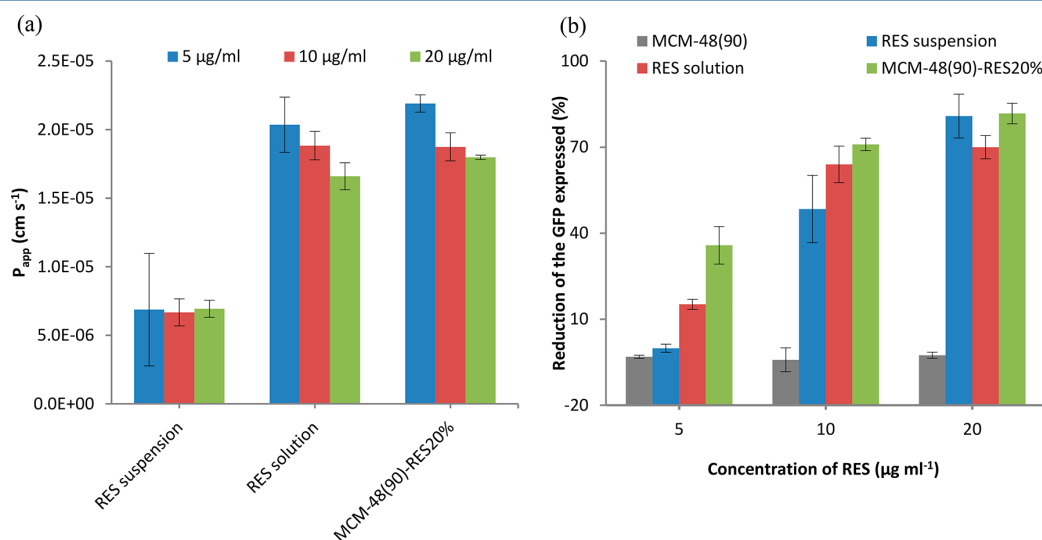
**Figure 5.** *In vitro* cytotoxicity of various concentrations of MCM-48(90) nanoparticles against Caco-2 and RAW 264 cells using flow cytometry. Statistics: mean  $\pm$  SD ( $n = 3 \pm$  SD).

*in vitro* cytotoxicity assays with Caco-2 and RAW 264.7 cells using flow cytometry. We observed no particular toxicity of the pristine silica nanoparticles on these two cell lines. Therefore, we can conclude that our results are not influenced by toxicity originating from our nanocarriers, which is consistent with previous reports with MSNs.<sup>41</sup>

**Caco-2 Permeability.** The apparent permeability coefficient ( $P_{app}$ ) index of a drug or nanoparticle correlates with the level of permeability *in vitro* and the level of absorption *in vivo*. Although according to the biopharmaceutics classification system (BCS), resveratrol is a class II drug with high permeability in solution, we wanted to test the effect of nanoencapsulation on its  $P_{app}$  value using Caco-2 monolayer as

a model. For nanoparticles, a bigger  $P_{app}$  value suggests better transport across the gastrointestinal barrier *in vivo*, however that is not the indication for complete absorption, as there are other factors such as solubility and stability at play. As shown in Figure 6a, encapsulation of resveratrol within small size silica particles enhanced its permeability more than 5 fold, compared to free resveratrol dispersed in HBSS, i.e., RES suspension. Interestingly, the permeation of resveratrol suspension seems to be independent of the concentration, i.e., same  $P_{app}$  values have been obtained for the three concentrations of resveratrol used (5, 10, and 20  $\mu\text{g mL}^{-1}$ ). Whereas, for MCM-48(90)-RES20% and RES solution, higher concentration of resveratrol decreased the  $P_{app}$  values. It is important to note that the  $P_{app}$  value for MCM-48(90) loaded with resveratrol was comparable to resveratrol predissolved in DMSO, i.e., RES solution, to mimic complete solubilization, further substantiating our solubility results. From Figure 6a, it is also evident that nanoencapsulation of resveratrol into our MSNs particles did not have any detrimental effects on its permeability and it is comparable to the drug solution.

**Anti-Inflammatory Assay.** The anti-inflammatory effect of resveratrol is due to down regulation of several pathways and cytokines such as NF- $\kappa$ B and IL-6.<sup>56,57</sup> We assessed the applicability of our small size MCM-48 particles on the down regulation of NF- $\kappa$ B on LPS-activated RAW 264.7 cells using flow cytometry. This test is also a high-throughput way to confirm the stability and bioactivity of resveratrol encapsulated into MCM-48 nanoparticles. As shown in Figure 6b, cells activated by LPS show extremely high mean fluorescence intensity (MFI) due to release of GFP. Cells pretreated with different concentrations of soluble resveratrol showed a concentration-dependent decrease in NF- $\kappa$ B. On the other hand, the resveratrol suspension showed inconsistent decrease in MFI suggesting that solubility of resveratrol is important for its biological activity. As hypothesized, resveratrol encapsulated in MCM-48(90) showed the highest decrease in MFI at lower concentrations (5  $\mu\text{g mL}^{-1}$  and 10  $\mu\text{g mL}^{-1}$ ) further attesting of the advantages of our formulation over resveratrol



**Figure 6.** (a) Apparent permeability ( $P_{app}$ ) of resveratrol suspension, solution (predissolved in DMSO), and MCM-48(90)-RES20% across Caco-2 monolayer. (b) *In vitro* assay measuring inhibition of the NF- $\kappa$ B activation by LPS using RAW 264.7 macrophages transfected with a NF- $\kappa$ B reporter plasmid. Statistics: mean  $\pm$  SD ( $n = 3 \pm$  SD and  $n = 5 \pm$  SD for  $P_{app}$  and NF- $\kappa$ B data, respectively).

suspension or RES predissolved in DMSO. On the other hand, at the higher concentration of  $20 \mu\text{g mL}^{-1}$ , the % GFP reduction has plateaued, causing no difference among the different samples. It is important to note that bare particles alone showed minimal interference with the fluorescence measurement confirming that the observed effect is due to the controlled release and improved solubility of resveratrol from the nanoformulation.

## CONCLUSION

The aim of this study was to draw the attention toward the effects of pore and particle size of the nanocarriers and their repercussions on the biological properties of a highly absorbed, yet scarcely bioavailable drug, such as resveratrol. In agreement with the literature, encapsulation of the hydrophobic drug inside nanopores has proven to enhance the solubility of the drug in comparison to the free crystalline equivalent. Not only that, we have also observed a certain trend regarding the effect of the particle size of the carriers. Nevertheless, additional studies including functionalization of the silica surface have to be carried out in order to clarify any hypothetical relationship. Then, as hypothesized, we have observed that the transportation of the encapsulated resveratrol, i.e., MCM-48(90)-RES20%, across the tight junctions of Caco-2 monolayer in aqueous solution was high compared to resveratrol in suspension. Thus, the combination of solubility, drug release, and transport enhancement greatly improves the physicochemical properties and bioactivity of resveratrol owing to its encapsulation into porous nanoparticles. Finally, considering the enhanced anti-inflammatory activity obtained with our nanoformulations, even at low concentration, our study demonstrates that it is possible to bypass the detrimental hydrophobicity and promote the therapeutic effect of resveratrol, and possibly other similar hydrophobic drugs. Our comprehensive investigations into the potential influence of particle structure on the biological activity of hydrophobic nutraceutical emphasize clearly the interest and applicability of MSNs as next generation nanocarriers for hydrophobic drugs and nutraceuticals.

## ASSOCIATED CONTENT

### Supporting Information

The Supporting Information is available free of charge on the ACS Publications website at DOI: [10.1021/acs.molpharmaceut.7b00529](https://doi.org/10.1021/acs.molpharmaceut.7b00529).

Additional HR-SEM and TEM images of the pure nanoparticles, DLS analyses of MCM-48(PE-150) and the encapsulated nanoparticles, powder XRD patterns, physicochemical parameters of all the pure nanoparticles, isotherms and NLDFT PSD of MCM-48(PE-150), TGA mass loss profiles of all the encapsulated samples with the corresponding loading and the linear regression of the dissolution experiment (PDF)

## AUTHOR INFORMATION

### Corresponding Author

\*[freddy.kleitz@univie.ac.at](mailto:freddy.kleitz@univie.ac.at)

### ORCID

Justyna Florek: [0000-0001-8891-2474](https://orcid.org/0000-0001-8891-2474)

Freddy Kleitz: [0000-0001-6769-4180](https://orcid.org/0000-0001-6769-4180)

## Notes

The authors declare no competing financial interest.

## ACKNOWLEDGMENTS

The authors are thankful to the Natural Sciences and Engineering Research Council of Canada (NSERC, grant number RGPIN-2014-05821) and the University of Vienna for financial support. We also thank The National Health and Medical Research Council's Project Grant 1107836 and Early Career Fellowship 1071796 (A. Popat) and the Fonds de Recherche Québécois Nature et Technologies (FRQNT, Quebec, Canada) as well as the UQ Summer Research Program (The University of Queensland, Brisbane, Australia) who also supported this project through scholarships (E. Juère). We wish to acknowledge Dr. Kyoungsoo Kim and Prof. Ryong Ryoo for providing high-resolution SEM images (KAIST and IBS, Daejeon, Republic of Korea), and Gabriel R. Reisinger for performing additional powder XRD studies (University of Vienna, Vienna, Austria). Finally, the authors thank Naisarg Pujara and Anand Meka for their valuable technical help in the laboratory (The University of Queensland, Brisbane, Australia).

## REFERENCES

- (1) Savjani, K. T.; Gajjar, A. K.; Savjani, J. K. Drug solubility: importance and enhancement techniques. *ISRN Pharm.* **2012**, *2012*, 1–11.
- (2) Lipinski, C. A. Drug-like properties and the causes of poor solubility and poor permeability. *J. Pharmacol. Toxicol. Methods* **2000**, *44*, 235–249.
- (3) Lipinski, C. A. Poor aqueous solubility – an industry wide problem in drug discovery. *Am. Pharm. Rev.* **2002**, *5*, 82–85.
- (4) Florek, J.; Caillard, R.; Kleitz, F. Evaluation of mesoporous silica nanoparticles for oral drug delivery – Current status and perspective of MSNs drug carriers. *Nanoscale* **2017**, *9*, 15252–15277.
- (5) Aggarwal, B. B.; Harikumar, K. B. Potential therapeutic effects of curcumin, the anti-inflammatory agent, against neurodegenerative, cardiovascular, pulmonary, metabolic, autoimmune and neoplastic diseases. *Int. J. Biochem. Cell Biol.* **2009**, *41*, 40–59.
- (6) Aggarwal, N.; Goindi, S. Preparation and evaluation of antifungal efficacy of griseofulvin loaded deformable membrane vesicles in optimized guinea pig model of Microsporum canis—Dermatophytosis. *Int. J. Pharm.* **2012**, *437*, 277–287.
- (7) Jambhrunkar, S.; Qu, Z.; Popat, A.; Karmakar, S.; Xu, C.; Yu, C. Modulating in vitro release and solubility of griseofulvin using functionalized mesoporous silica nanoparticles. *J. Colloid Interface Sci.* **2014**, *434*, 218–225.
- (8) Summerlin, N.; Soo, E.; Thakur, S.; Qu, Z.; Jambhrunkar, S.; Popat, A. Resveratrol nanoformulations: Challenges and opportunities. *Int. J. Pharm.* **2015**, *479*, 282–290.
- (9) Siddiqui, I. A.; Sanna, V.; Ahmad, N.; Sechi, M.; Mukhtar, H. Resveratrol nanoformulation for cancer prevention and therapy. *Ann. N. Y. Acad. Sci.* **2015**, *1348*, 20–31.
- (10) The ONTARGET Investigators Yusuf, S.; Teo, K. K.; Pogue, J.; Dyal, L.; Copland, I.; Schumacher, H.; Dagenais, G.; Sleight, P.; Anderson, C. Telmisartan, ramipril, or both in patients at high risk for vascular events. *N. Engl. J. Med.* **2008**, *358*, 1547–1559.
- (11) Williams, H. D.; Trevaskis, N. L.; Charman, S. A.; Shanker, R. M.; Charman, W. N.; Pouton, C. W.; Porter, C. J. H. Strategies to address low drug solubility in discovery and development. *Pharmacol. Rev.* **2013**, *65*, 315–499.
- (12) Cottart, C. H.; Nivet-Antoine, V.; Laguillier-Morizot, C.; Beaudeau, J. L. Resveratrol bioavailability and toxicity in humans. *Mol. Nutr. Food Res.* **2010**, *54*, 7–16.
- (13) Kaptay, G. On the size and shape dependence of the solubility of nano-particles in solutions. *Int. J. Pharm.* **2012**, *430*, 253–257.
- (14) Rabinow, B. E. Nanosuspensions in drug delivery. *Nat. Rev. Drug Discovery* **2004**, *3*, 785–796.

- (15) Kesisoglou, F.; Panmai, S.; Wu, Y. Nanosizing – Oral formulation development and biopharmaceutical evaluation. *Adv. Drug Delivery Rev.* **2007**, *59*, 631–644.
- (16) Jambhrunkar, S.; Yu, M.; Yang, J.; Zhang, J.; Shrotri, A.; Endo-Munoz, L.; Moreau, J.; Lu, G.; Yu, C. Stepwise pore size reduction of ordered nanoporous silica materials at angstrom precision. *J. Am. Chem. Soc.* **2013**, *135*, 8444–8447.
- (17) Wang, X. Q.; Zhang, Q. pH-sensitive polymeric nanoparticles to improve oral bioavailability of peptide/protein drugs and poorly water-soluble drugs. *Eur. J. Pharm. Biopharm.* **2012**, *82*, 219–229.
- (18) Wang, Y.; Yan, Y.; Cui, J.; Hosta-Rigau, L.; Heath, J. K.; Nice, E. C.; Caruso, F. Encapsulation of water-insoluble drugs in polymer capsules prepared using mesoporous silica templates for intracellular drug delivery. *Adv. Mater.* **2010**, *22*, 4293–4297.
- (19) Lu, X. Y.; Hu, S.; Jin, Y.; Qiu, L. Y. Application of liposome encapsulation technique to improve anti-carcinoma effect of resveratrol. *Drug Dev. Ind. Pharm.* **2012**, *38*, 314–322.
- (20) Soo, E.; Thakur, S.; Qu, Z.; Jambhrunkar, S.; Parekh, H. S.; Popat, A. Enhancing delivery and cytotoxicity of resveratrol through a dual nanoencapsulation approach. *J. Colloid Interface Sci.* **2016**, *462*, 368–374.
- (21) Salonen, J.; Laitinen, L.; Kaukonen, A. M.; Tuura, J.; Björkqvist, M.; Heikkilä, T.; Vähä-Heikkilä, K.; Hirvonen, J.; Lehto, V.-P. Mesoporous silicon microparticles for oral drug delivery: Loading and release of five model drugs. *J. Controlled Release* **2005**, *108*, 362–374.
- (22) Pujara, N.; Jambhrunkar, S.; Wong, K. Y.; McGuckin, M.; Popat, A. Enhanced colloidal stability, solubility and rapid dissolution of resveratrol by nanocomplexation with soy protein isolate. *J. Colloid Interface Sci.* **2017**, *488*, 303–308.
- (23) Zhu, W.; Wan, L.; Zhang, C.; Gao, Y.; Zheng, X.; Jiang, T.; Wang, S. Exploitation of 3D face-centered cubic mesoporous silica as a carrier for a poorly water soluble drug: Influence of pore size on release rate. *Mater. Sci. Eng., C* **2014**, *34*, 78–85.
- (24) Jambhrunkar, S.; Karmakar, S.; Popat, A.; Yu, M.; Yu, C. Mesoporous silica nanoparticles enhance the cytotoxicity of curcumin. *RSC Adv.* **2014**, *4*, 709–712.
- (25) Jambhrunkar, S.; Qu, Z.; Popat, A.; Yang, J.; Noonan, O.; Acauan, L.; Nor, Y. A.; Yu, C.; Karmakar, S. Effect of surface functionality of silica nanoparticles on cellular uptake and cytotoxicity. *Mol. Pharmaceutics* **2014**, *11*, 3642–3655.
- (26) Summerlin, N.; Qu, Z.; Pujara, N.; Sheng, Y.; Jambhrunkar, S.; McGuckin, M.; Popat, A. Colloidal mesoporous silica nanoparticles enhance the biological activity of resveratrol. *Colloids Surf., B* **2016**, *144*, 1–7.
- (27) Abbaraju, P. L.; Meka, A.; Jambhrunkar, S.; Zhang, J.; Xu, C.; Popat, A.; Yu, C. Floating tablets from mesoporous silica nanoparticles. *J. Mater. Chem. B* **2014**, *2*, 8298–8302.
- (28) Zhang, Y.; Wang, J.; Bai, X.; Jiang, T.; Zhang, Q.; Wang, S. Mesoporous Silica Nanoparticles for Increasing the Oral Bioavailability and Permeation of Poorly Water Soluble Drugs. *Mol. Pharmaceutics* **2012**, *9*, 505–513.
- (29) Andersson, J.; Rosenholm, J.; Areva, S.; Lindén, M. Influences of material characteristics on ibuprofen drug loading and release profiles from ordered micro- and mesoporous silica matrices. *Chem. Mater.* **2004**, *16*, 4160–4167.
- (30) Du, X.; Li, X.; Xiong, L.; Zhang, X.; Kleitz, F.; Qiao, S. Z. Mesoporous silica nanoparticles with organo-bridged silsesquioxane framework as innovative platforms for bioimaging and therapeutic agent delivery. *Biomaterials* **2016**, *91*, 90–127.
- (31) Li, Y.; Shi, J. Hollow-structured mesoporous materials: Chemical synthesis, functionalization and applications. *Adv. Mater.* **2014**, *26*, 3176–3205.
- (32) Hartono, S. B.; Hadisoewignyo, L.; Yang, Y.; Meka, A. K.; Antaresti, Y.; Yu, C. Amine functionalized cubic mesoporous silica nanoparticles as an oral delivery system for curcumin bioavailability enhancement. *Nanotechnology* **2016**, *27*, 505605–505611.
- (33) Lu, F.; Wu, S. H.; Hung, Y.; Mou, C. Y. Size effect on cell uptake in well-suspended, uniform mesoporous silica nanoparticles. *Small* **2009**, *5*, 1408–1413.
- (34) Tang, F.; Li, L.; Chen, D. Mesoporous silica nanoparticles: Synthesis, biocompatibility and drug delivery. *Adv. Mater.* **2012**, *24*, 1504–1534.
- (35) Bouchoucha, M.; Gaudreault, R. C.; Fortin, M. A.; Kleitz, F. Mesoporous silica nanoparticles: Selective surface functionalization for optimal relaxometric and drug loading performances. *Adv. Funct. Mater.* **2014**, *24*, 5911–5923.
- (36) Wu, S. H.; Mou, C. Y.; Lin, H. P. Synthesis of mesoporous silica nanoparticles. *Chem. Soc. Rev.* **2013**, *42*, 3862–3875.
- (37) Guillet-Nicolas, R.; Popat, A.; Bridot, J. L.; Monteith, G.; Qiao, S. Z.; Kleitz, F. pH-responsive nutraceutical-mesoporous silica nanoconjugates with enhanced colloidal stability. *Angew. Chem., Int. Ed.* **2013**, *52*, 2318–2322.
- (38) Popat, A.; Liu, J.; Lu, G. Q.; Qiao, S. Z. A pH-responsive drug delivery system based on chitosan coated mesoporous silica nanoparticles. *J. Mater. Chem.* **2012**, *22*, 11173–11178.
- (39) Argyo, C.; Weiss, V.; Bräuchle, C.; Bein, T. Multifunctional mesoporous silica nanoparticles as a universal platform for drug delivery. *Chem. Mater.* **2014**, *26*, 435–451.
- (40) Kim, T. W.; Chung, P. W.; Lin, V. S. Y. Facile Synthesis of monodisperse spherical MCM-48 mesoporous silica nanoparticles with controlled particle size. *Chem. Mater.* **2010**, *22*, 5093–5104.
- (41) Bouchoucha, M.; Côté, M. F.; C.-Gaudreault, R.; Fortin, M. A.; Kleitz, F. Size-controlled functionalized mesoporous silica nanoparticles for tunable drug release and enhanced anti-tumoral activity. *Chem. Mater.* **2016**, *28*, 4243–4258.
- (42) Kim, M. H.; Na, H. K.; Kim, Y. K.; Ryoo, S. R.; Cho, H. S.; Lee, K. E.; Jeon, H.; Ryoo, R.; Min, D. -H. Facile synthesis of monodispersed mesoporous silica nanoparticles with ultralarge pores and their application in gene delivery. *ACS Nano* **2011**, *5*, 3568–3576.
- (43) Kleitz, F.; Bérubé, F.; Guillet-Nicolas, R.; Yang, C. M.; Thommes, T. Probing adsorption, pore condensation, and hysteresis behavior of pure fluids in three-dimensional cubic mesoporous KIT-6 silica. *J. Phys. Chem. C* **2010**, *114*, 9344–9355.
- (44) Yun, Y.; Cho, Y. W.; Park, K. Nanoparticles for oral delivery: Targeted nanoparticles with peptidic ligands for oral protein delivery. *Adv. Drug Delivery Rev.* **2013**, *65*, 822–832.
- (45) Liu, J.; Yang, T.; Wang, D.; Lu, G. Q.; Zhao, D.; Qiao, S. Z. A facile soft-template synthesis of mesoporous polymeric and carbonaceous nanospheres. *Nat. Commun.* **2013**, *4*, 2798.
- (46) Mizutani, M.; Yamada, Y.; Nakamura, T.; Yano, K. Anomalous pore expansion of highly monodispersed mesoporous silica spheres and its application to the synthesis of porous ferromagnetic composite. *Chem. Mater.* **2008**, *20*, 4777–4782.
- (47) Popat, A.; Liu, J.; Hu, Q.; Kennedy, M.; Peters, B.; Lu, G. Q.; Qiao, S. Z. Adsorption and release of biocides with mesoporous silica nanoparticles. *Nanoscale* **2012**, *4*, 970–975.
- (48) Schumacher, K.; Ravikovitch, P. I.; Du Chesne, A.; Neimark, A. V.; Unger, K. K. Characterization of MCM-48 Materials. *Langmuir* **2000**, *16*, 4648–4654.
- (49) Ravikovitch, P. I.; Domhnaill, S. C.; Neimark, A. V.; Schüth, F.; Unger, K. K. Capillary Hysteresis in nanopores: Theoretical and experimental studies of nitrogen adsorption on MCM-41. *Langmuir* **1995**, *11*, 4765–4772.
- (50) Thommes, M.; Kaneko, K.; Neimark, A. V.; Olivier, J. P.; Rodriguez-Reinoso, F.; Rouquerol, J.; Sing, S. W. Physisorption of gases, with special reference to the evaluation of surface area and pore size distribution (IUPAC Technical Report). *Pure Appl. Chem.* **2015**, *87*, 1051–1069.
- (51) Leuner, C.; Dressman, J. Improving drug solubility for oral delivery using solid dispersions. *Eur. J. Pharm. Biopharm.* **2000**, *50*, 47–60.
- (52) Qian, K. K.; Bogner, R. H. Application of mesoporous silicon dioxide and silicate in oral amorphous drug delivery systems. *J. Pharm. Sci.* **2012**, *101*, 444–463.

(53) Miura, H.; Kanebako, M.; Shirai, H.; Nakao, H.; Inagi, T.; Terada, K. Stability of amorphous drug, 2-benzyl-5-(4-chlorophenyl)-6-[4-(methylthio)phenyl]-2H-pyridazin-3-one, in silica mesopores and measurement of its molecular mobility by solid-state  $^{13}\text{C}$  NMR spectroscopy. *Int. J. Pharm.* **2011**, *410*, 61–67.

(54) Zupančič, Š.; Lavrič, Z.; Kristl, J. Stability and solubility of trans-resveratrol are strongly influenced by pH and temperature. *Eur. J. Pharm. Biopharm.* **2015**, *93*, 196–204.

(55) Siepman, J.; Peppas, N. A. Mathematical modeling of controlled drug delivery. *Adv. Drug Delivery Rev.* **2001**, *48*, 137–138.

(56) Chávez, E.; Reyes-Gordillo, K.; Segovia, J.; Shibayama, M.; Tsutsumi, V.; Vergara, P.; Moreno, M. G.; Muriel, P. Resveratrol prevents fibrosis, NF- $\kappa$ B activation and TGF- $\beta$  increases induced by chronic  $\text{CCl}_4$  treatment in rats. *J. Appl. Toxicol.* **2008**, *28*, 35–43.

(57) Wung, B. S.; Hsu, M. C.; Wu, C. C.; Hsieh, C. W. Resveratrol suppresses IL-6-induced ICAM-1 gene expression in endothelial cells: Effects on the inhibition of STAT3 phosphorylation. *Life Sci.* **2005**, *78*, 389–397.





*In vitro* Dissolution, Cellular Membrane  
Permeability and Anti-Inflammatory Response of  
Resveratrol-Encapsulated Mesoporous Silica  
Nanoparticles

*Estelle Juère,<sup>†,‡</sup> Justyna Florek,<sup>†</sup> Meryem Bouchoucha,<sup>‡</sup> Siddharth Jambhrunkar,<sup>§,⊥</sup> Kuan Yau  
Wong,<sup>§,⊥</sup> Amirali Popat,<sup>§,⊥</sup> Freddy Kleitz<sup>†,‡\*</sup>*

<sup>†</sup> Department of Inorganic Chemistry – Functional Materials, Faculty of Chemistry,  
University of Vienna, Währinger Straße 42, 1090 Vienna, Austria

<sup>‡</sup> Department of Chemistry, Université Laval, Quebec city, Canada

<sup>§</sup> School of Pharmacy, The University of Queensland, Brisbane, Australia

<sup>⊥</sup> Inflammatory Disease Biology and Therapeutics Group, Mater Research Institute – The  
University of Queensland, Translational Research Institute, Woolloongabba, Australia

Supporting Information (SI), Juère *et al.*

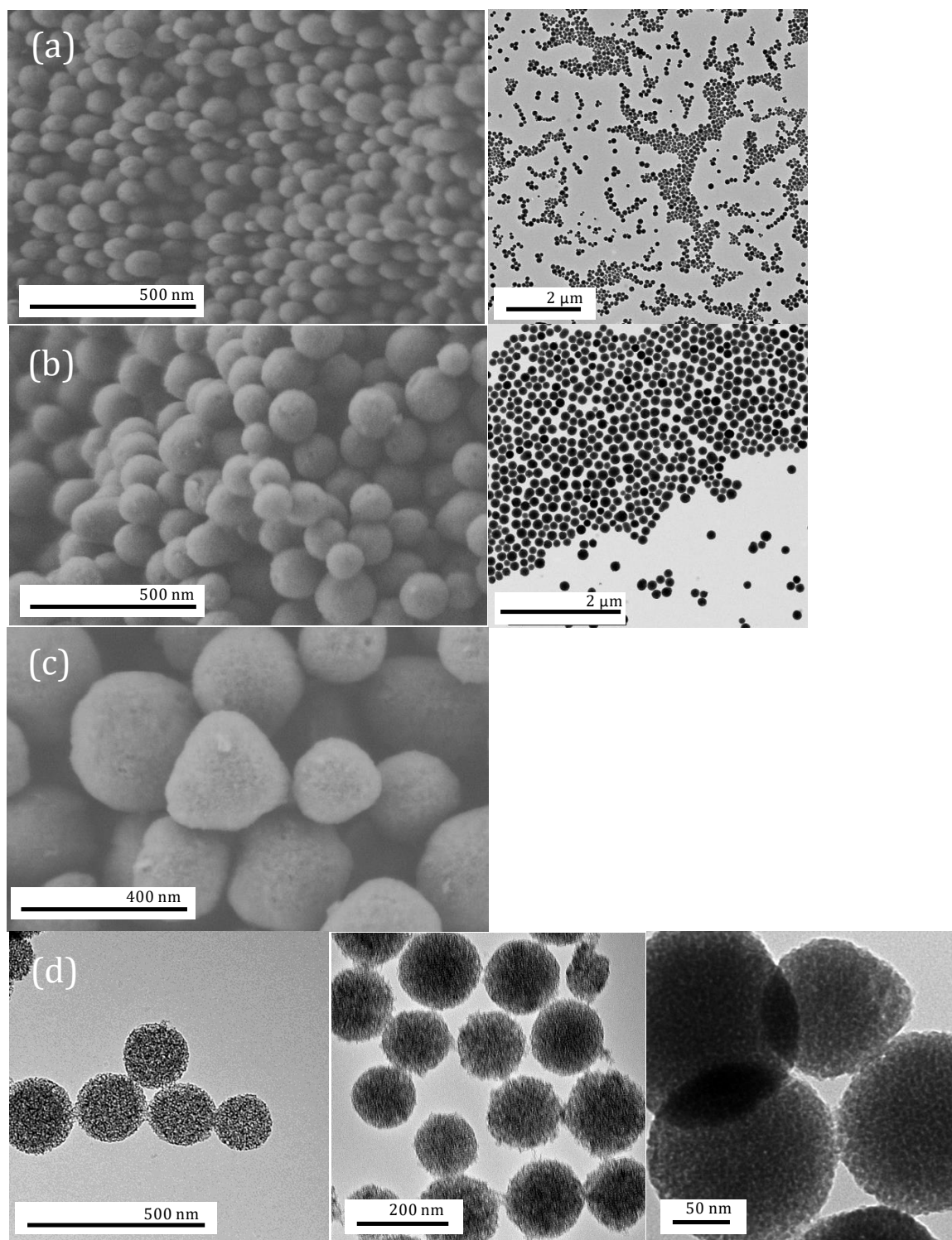


Figure S1: High resolution SEM (left) and TEM (right) images of MCM-48(90), MCM-48(150) and MCM-48(300) (a, b, c) and TEM images of MCM-48(PE-150) (d).

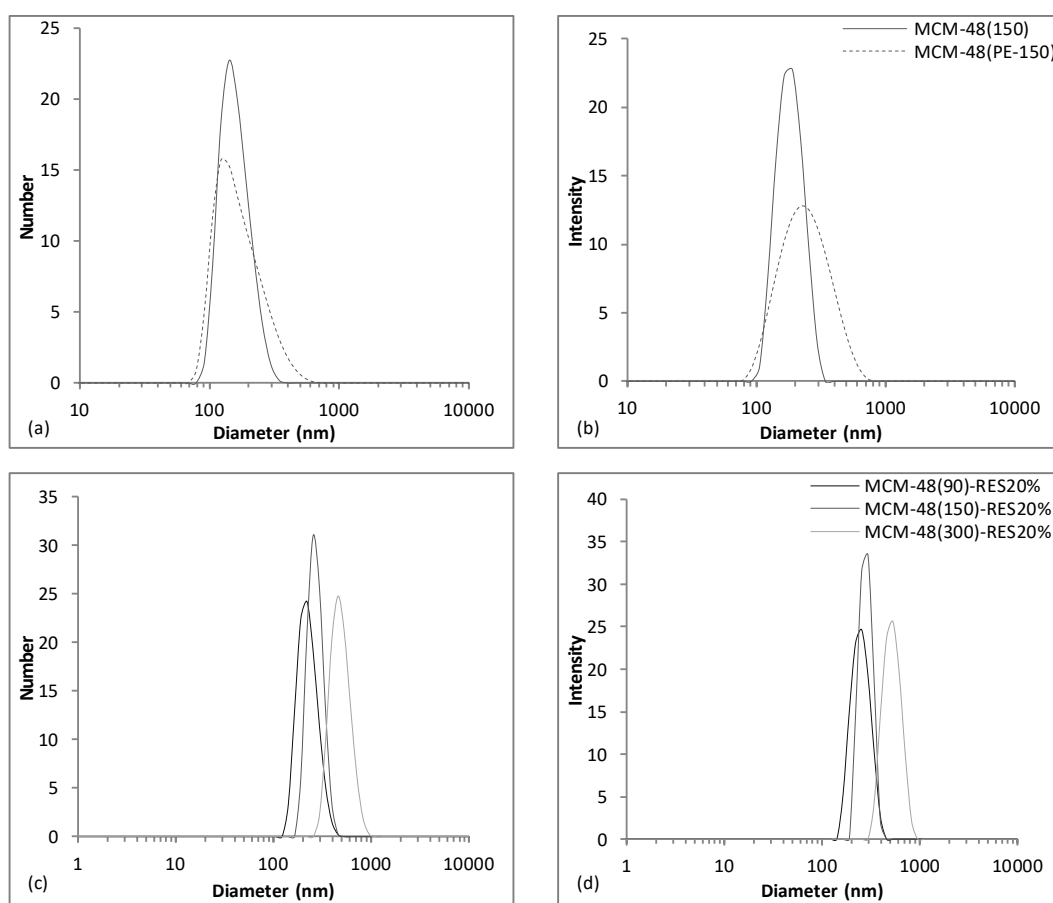
Supporting Information (SI), *Juère et al.*

Figure S2: Hydrodynamic diameters measured in number and intensity mode of (a, b) pure MCM-48(150 and PE-150) and (c, d) the encapsulated MCM-48(90, 150 and 300)-RES20%, as-indicated.

## Supporting Information (SI), Juère et al.

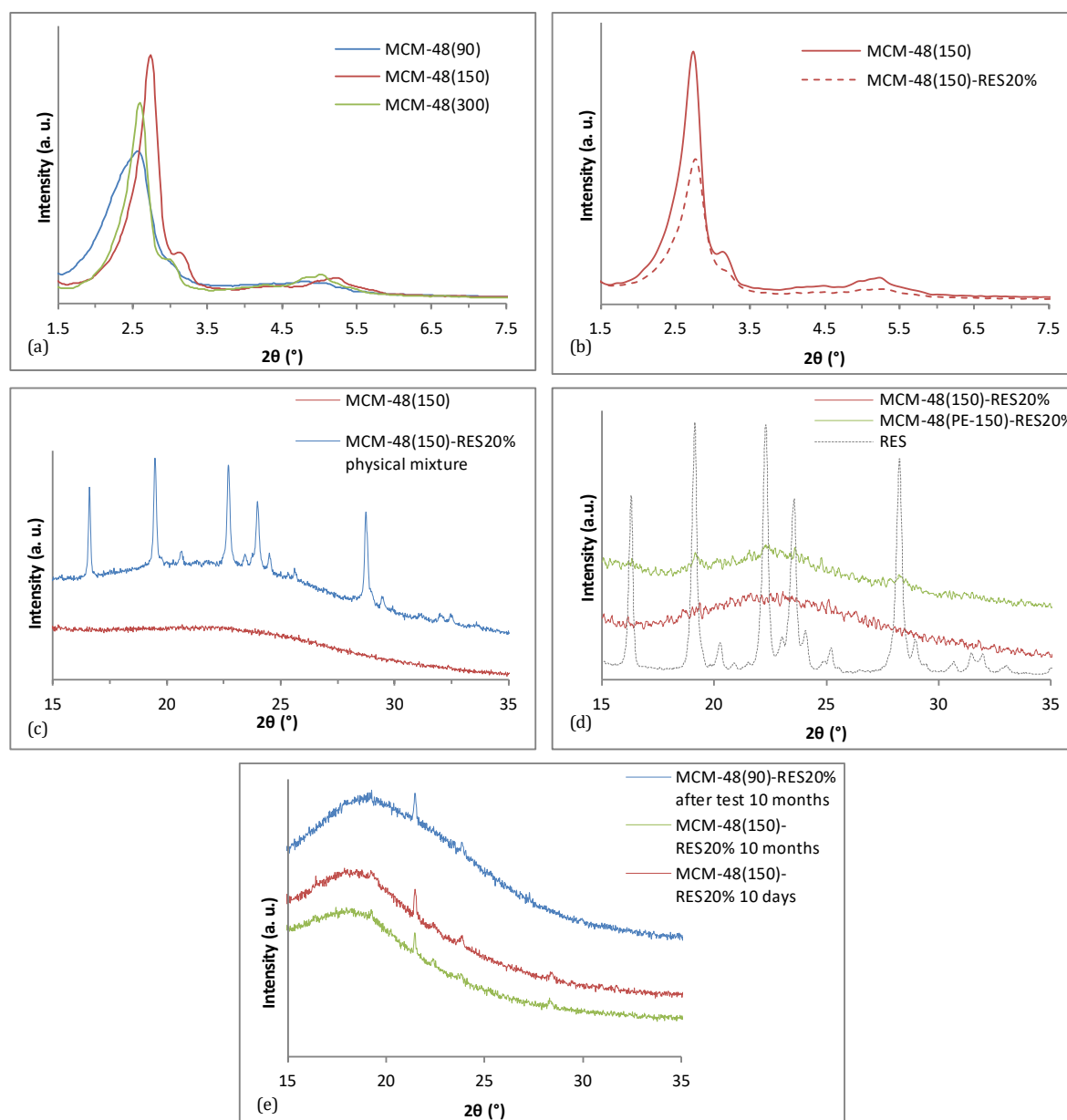
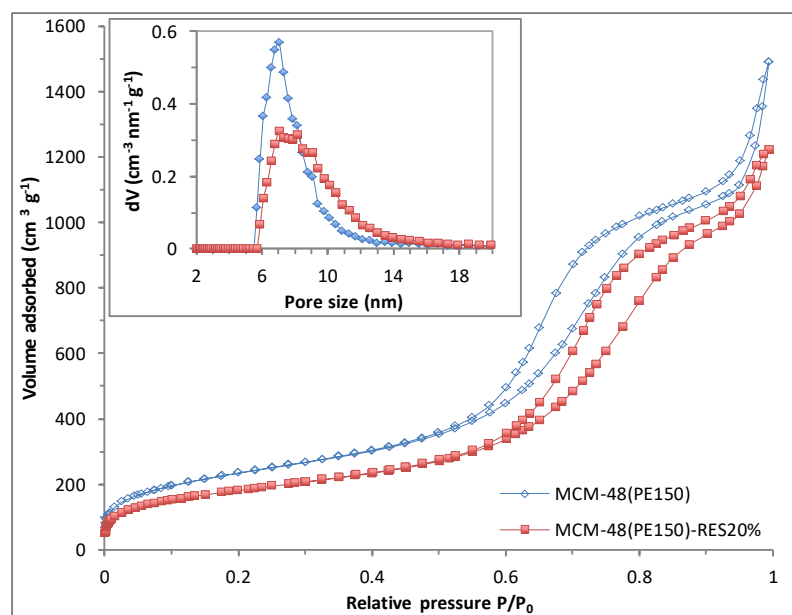


Figure S3: Low-angle X-ray diffractograms of pristine MCM-48 nanoparticles (a) and pristine MCM-48(150) sample and the resveratrol-encapsulated counterpart MCM-48(150)-RES20% (b); Wide-angle X-ray diffractograms of resveratrol mixed with MCM-48(150) and pristine MCM-48(150) (c), resveratrol encapsulated inside MCM-48(150) nanoparticles in comparison with free resveratrol (d), and resveratrol encapsulated inside MCM-48 nanoparticles for either 10 days or 10 months, as well as a recovered MCM-48(90)-RES20% sample after the *in vitro* dissolution studies, which has been aged 10 months as well (note that the sharp peaks observed here originate from the binder used for this specific XRD sample preparation) (e).

Supporting Information (SI), Juère *et al.*Table S1: Physicochemical parameters of the pristine and the encapsulated nanoparticles determined by N<sub>2</sub> physisorption analysis.

	Surface area (m <sup>2</sup> g <sup>-1</sup> )	Pore volume (cm <sup>3</sup> g <sup>-1</sup> )	Pore size (nm)
MCM-48(90)	1243	1.10	3.5
MCM-48(150)	1285	0.94	3.4
MCM-48(300)	1241	0.93	3.4
MCM-48(PE-150)	851	1.67	7.0
MCM-48(150)-RES20%	750	0.90	3.3
MCM-48(PE-150)-RES20%	664	1.58	7.0

Figure S4: N<sub>2</sub> physisorption isotherms measured at -196 °C of MCM-48(PE-150) and MCM-48(PE-150)-RES20%; inset: respective pore size distributions obtained from the adsorption branch using the NLDFT method considering a cylindrical pore model.

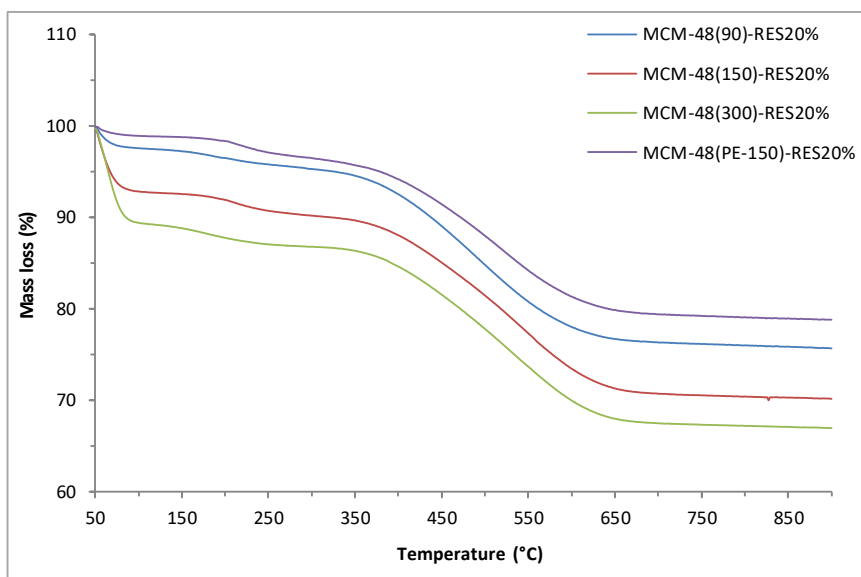
Supporting Information (SI), *Juère et al.*

Figure S5: TGA mass loss profiles of the encapsulated MCM-48(90, 150, 300 and PE-150) nanoparticles.

Table S2: Mass loss of resveratrol encapsulated inside the various MCM-48 nanoparticles determined from thermogravimetric analysis considering the temperature range 150-650 °C.

	Loading of resveratrol (%)
MCM-48(90)	20.5
MCM-48(150)	21.3
MCM-48(300)	20.8
MCM-48(PE-150)	18.9

Supporting Information (SI), *Juère et al.*

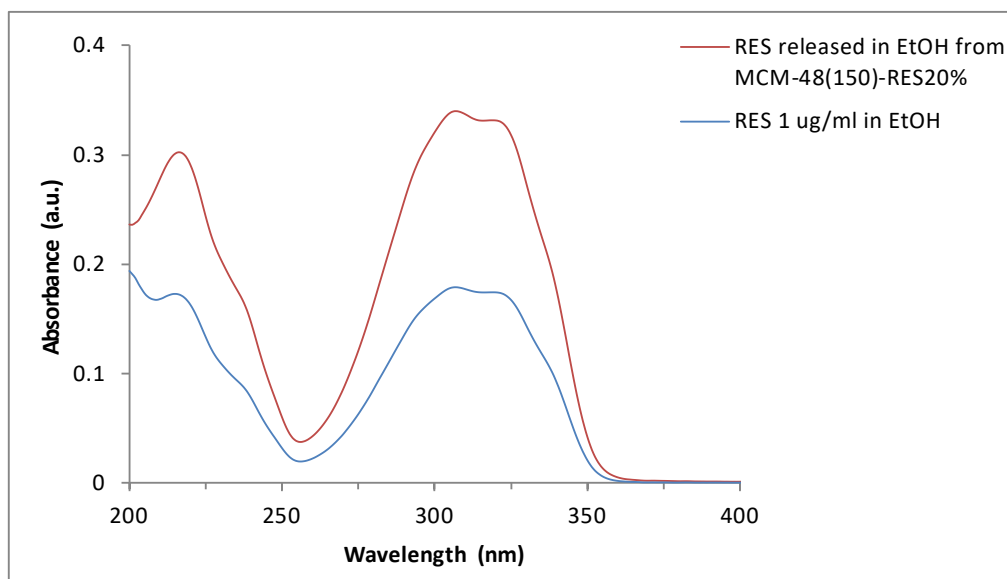


Figure S6: Qualitative comparison of the UV-Vis spectrum of resveratrol released in ethanol from a 10-month-old MCM-48(150)-RES20% sample (red) and free resveratrol in ethanol (blue).





## II. Protein-silica nanoparticle formulation for oral omeprazole delivery

This work has been accepted for publication in the journal *European Journal of Pharmaceutics and Biopharmaceutics* on 24<sup>th</sup> March 2020.

As a first author, I have synthesized, functionalized and characterized all the materials *i.e.*, the drug, the MSNs and the protein tablets, of this article in the laboratory of Prof. Freddy Kleitz at University of Vienna (Vienna, Austria). I have incorporated omeprazole in the MSNs, characterized the omeprazole-encapsulated samples and carried out the dissolution tests and the quantification of the released omeprazole. I did the cell cultures, cell staining and cytotoxicity assays with the help of Eva Attakpah (Department of Food Chemistry and Toxicology, University of Vienna). I have interpreted the data, created the figures, written the initial manuscript and corrected it according to the co-authors suggestions.

Dr. Giorgia Del Favero has trained me with the cell cultures, helped me in designing the experiments and interpreting the results. She has supervised my work with all cell assays and participated in the design of the figures and the corrections of the manuscript (Department of Food Chemistry and Toxicology, University of Vienna). Florence Masse has supported me, during her internship, in the realization of the preliminary work: encapsulation of omeprazole in the MSNs, quantification method developments and tableting succinylated  $\beta$ -lactoglobulin with the MSNs (Université Laval, Québec, Canada). Prof. Doris Marko has contributed to the scientific discussions and to the correction of the manuscript (Department of Food Chemistry and Toxicology, University of Vienna). Dr. Amirali Popat contributed to increase the yield of the DMSNs synthesis and corrected the manuscript (The University of Queensland, Brisbane, Australia). Dr. Romain Caillard has supplied the succinylated  $\beta$ -lactoglobulin proteins which he produces in his company Aventus Innovations (Lévis, Canada). Dr. Romain Caillard and Prof. Freddy Kleitz have continuously supported my work, contributed to the interpretation of the data and the improvement of the manuscript.





Contents lists available at ScienceDirect

European Journal of Pharmaceutics and Biopharmaceutics

journal homepage: <http://ees.elsevier.com>

## Gastro-protective protein-silica nanoparticles formulation for oral drug delivery: *In vitro* release, cytotoxicity and mitochondrial activity

Estelle Juère<sup>a</sup>, Giorgia Del Favero<sup>b</sup>, Florence Masse<sup>c</sup>, Doris Marko<sup>b</sup>, Amirali Popat<sup>d,e</sup>, Justyna Florek<sup>a</sup>, Romain Caillard<sup>f</sup>, Freddy Kleitz<sup>a</sup>

<sup>a</sup> Department of Inorganic Chemistry – Functional Materials, Faculty of Chemistry, University of Vienna, 1090 Vienna, Austria

<sup>b</sup> Department of Food Chemistry and Toxicology, Faculty of Chemistry, University of Vienna, 1090 Vienna, Austria

<sup>c</sup> Department of Chemistry, Université Laval, Quebec City, G1V 0A6 QC, Canada

<sup>d</sup> School of Pharmacy, The University of Queensland, Woolloongabba, QLD 4102, Australia

<sup>e</sup> Mater Research Institute – The University of Queensland, Translational Research Institute, Woolloongabba, QLD 4102, Australia

<sup>f</sup> Aventus Innovations, Levis, G6W 0L9 QC, Canada

### ARTICLE INFO

#### Keywords

Mesoporous silica nanoparticles  
Omeprazole  
-Lactoglobulin  
mitochondrial Morphology effect  
Intestinal cells

### ABSTRACT

Our contribution aims to provide an efficient solution to one of the major challenges of oral delivery of gastro-sensitive drugs, namely preventing their premature release and degradation in the gastric fluid in order to maximize the absorption in the small intestine. Our results show that a pH-responsive protein, i.e., succinylated -lactoglobulin (BL), together with the key attributes of mesoporous silica nanoparticles (MSNs), can synergistically reduce the release of the gastro-sensitive drug, omeprazole (OMP), in acidic pH and enhance the dissolution in intestinal pH conditions. Two families of MSNs were synthesized, MCM-48-based and dendritic-type MSNs, and both materials were additionally functionalized with trimethylsilyl groups to produce a hydrophobic surface that can further modulate the interaction of the MSNs with the succinylated protein in the nanoformulation. The methyl-functionalization of the MSNs also impacted on the physical state of the confined OMP and consequently on its release in near neutral pH. Our cytotoxicity screening revealed no particular mitochondrial dysfunction originating from the MSNs. Moreover, upon progressive release of the drug confined into dendritic-type MSNs, the cytotoxicity against tumorigenic and non-tumorigenic cells (Caco-2 and HCEC) was significantly lower in comparison to the drug pre-dissolved in DMSO and this, up to 8 h.

### 1. Introduction

Because of the aggressive environment in the gastro-intestinal tract (GIT), the activity of drugs can be hindered due to poor stability, solubility, and permeability in the pH range 1.5–8 [1]. Yet, the drugs have to reach the small intestine (duodenum and jejunum) where the absorption occurs [2]. In the case of successful transport across the intestinal barrier through the transcellular or paracellular mechanism, they are still submitted to a first hepatic passage prior the distribution to specific tissues [1]. However, due to the lack of effective oral drug delivery platforms, the therapeutic potential of many drugs can not be fully exploited.

Omeprazole (OMP), a proton pump inhibitor widely used to inhibit the gastric secretion of  $H^+K^+$ -ATPase in the case of gastric ulcers, is a good model of gastro-sensitive drug. As a pro-drug, OMP is converted into its active form, sulphenamide, in an acidic environment provided by the active  $H^+K^+$ -ATPase, located in the membranes of the parietal

cells of the gastric mucosa [3]. One can actually consider that all conditions are met in the stomach for OMP to react, but the acidic degradation at low pH would kinetically unfavor its conversion by  $H^+K^+$ -ATPase resulting in poor drug bioavailability [4]. Thus, formulations are required in order to carry acid-sensitive drug like OMP through the GIT. Traditionally, enteric coated granules made of an assembly of excipients such as hydropropyl methyl cellulose (HPMC), methacrylic acid and ethyl acrylate are materials of choice for the development of oral formulation but their uses seem to affect the chemical stability of the drug which could also alter the bioavailability [5,6]. Novel approaches have been reported including the use of multi-layer films [7], hydrogels [8], polymeric nanoparticles [9] and liposomes [10] and also more natural and biocompatible materials have been investigated as pH-responsive tools, such as chitosan or alginate beads [11]. In this regard, proteins attract increasing attention as they are naturally occurring, biodegradable (i.e., by enzymes) and they also possess functional

E-mail addresses: [rc@aventusinnov.com](mailto:rc@aventusinnov.com) (R. Caillard); [freddy.kleitz@univie.ac.at](mailto:freddy.kleitz@univie.ac.at) (F. Kleitz)

<https://doi.org/10.1016/j.ejpb.2020.03.015>

Received 1 October 2019; Received in revised form 18 March 2020; Accepted 24 March 2020

Available online xxx

0939-6411/© 2020.

groups that can be further modified. For instance, via a simple succinylation reaction, studies have revealed the unprecedented emulsifying and gelation properties of  $\alpha$ -lactoglobulin, a low-cost whey protein [12]. Indeed, through this reaction, positive lysine amino groups are replaced by negatively charged carboxyl groups, resulting in lower solubility of the protein at acidic pH and a higher solubility at pH > 5. Nevertheless, the pH-responsiveness of these proteins solves only partially the challenge of oral drug delivery since once in the intestine, the drugs have to solubilize and permeate through the intestinal barrier which could be problematic for some drugs [13]. The confinement of molecules into porous nanoparticles has been recently discussed in the literature as a way to circumvent these limitations [14]. In this regard, mesoporous silica nanoparticles (MSNs) show interesting features: high porosity, tunable pore and particle size, and multitudes of possible functionalizations [15–17]. For example, MCM-48-based nanoparticles display a high surface area  $\sim 1000 \text{ m}^2 \text{ g}^{-1}$ , high pore volume  $\sim 1 \text{ cm}^3 \text{ g}^{-1}$  and a 3-D ordered porous network with a pore size of about 3 nm, which is sufficient to accommodate small drug like doxorubicin, ibuprofen or resveratrol [18–21]. However, nowadays, protein therapeutics are believed to possess advantages over small drug molecules in medical applications, therefore, material scientists have dedicated their work towards increasing the pore size of silica nanoparticles as the pores of typical MCM-41 or MCM-48 nanoparticles could indeed be too small to accommodate such macromolecules [22–25]. On the other hand, dendritic-type MSNs (DMSNs), having a center radial porous network with a surface area of  $\sim 700 \text{ m}^2 \text{ g}^{-1}$  and a pore volume of  $\sim 1 \text{ cm}^3 \text{ g}^{-1}$ , can have pores larger than 6 nm, which make them an interesting host for protein loading [26]. Though using only bare MSNs, drugs can diffuse rather quickly throughout the open porous network and be released prematurely.

Therefore, as a proof-of-concept, we report that drug-loaded mesoporous silica nanoparticles combined with succinylated  $\alpha$ -lactoglobulin (BL) offer a proficient alternative to existing formulation since this system (1) protects the drug throughout the GIT, (2) enhances solubility in the intestine through the confinement of the drug in the pores, and (3) permits anchoring other functionalities on the free surface of the MSNs to ultimately enhance the permeability or tune the drug release. Herein, OMP was used as a pharmaceutically interesting model of acid-sensitive drug that was encapsulated into pure or methylated MCM-48 MSNs and DMSNs, as representative materials for small and large pores, respectively. Then, the cytotoxicity and mitochondrial effects of such MSNs, being often fairly questioned in the literature, was tested on tumorigenic and non-tumorigenic intestinal cells [27–30]. Finally, the release of OMP from MSN-free or MSN-based  $\alpha$ -lactoglobulin tablets was compared at pH 1.2 and 7.4.

## 2. Experimental section

**Materials and reagents.** Cetyltrimethylammonium bromide (CTAB, 99%), Cetyltrimethylammonium chloride (CTAC, 25 wt% H<sub>2</sub>O), Pluronic F127 (EO<sub>20</sub>PO<sub>70</sub>EO<sub>20</sub>), Tetraethylorthosilicate, (TEOS, 99%), Hexamethyldisilazane (HMDS, 99%) and omeprazole were obtained from Sigma Aldrich. Triethanolamine (TEA, 98%) was purchased from Alfa Aesar (USA). 50% succinylated  $\alpha$ -lactoglobulin was provided by Aventus Innovation (Levis, QC, Canada). Materials for cell culture and cytotoxicity experiments were purchased from GIBCO Invitrogen (Karlruhe, Germany), Lonza Group Ltd (Basel, Switzerland), Sigma-Aldrich Chemie GmbH (Munich, Germany) and Sarstedt AG&Co (Nuembrecht, Germany).

**Synthesis of mesoporous silica nanoparticles (MSNs).** MCM-48-type nanoparticles were synthesized by adapting the procedure previously reported [31]. Briefly, 1 g of CTAB and 4 g of Pluronic F127 were dissolved in 298 ml of NH<sub>4</sub>OH (2.8 wt%)/EtOH = 2.5: 1 (v/v). Then, 3.6 g of TEOS was added and the solution was vigorously stirred (1000 rpm) for 1 min. The mixture was aged under static conditions at

room temperature for 24 h and recovered by centrifugation (20 min, 10000 rpm). Afterwards, the resulting white solid was washed twice with 250 ml of water and dried in air at 60 °C overnight. Finally, the resulting product was calcined (550 °C, air, 5 h).

Dendritic mesoporous silica nanoparticles were synthesized by adapting a procedure previously reported [32]. First, the aqueous solution was prepared: 8 ml of CTAC, 360 mg of TEA and 72 ml of H<sub>2</sub>O were mixed together for 1 h at 60 °C (stirring plate IKA, stirring rate 375 rpm). Then, the organic solution was prepared: 32 ml cyclohexane and 8 ml TEOS were mixed and subsequently added to the first solution. The solution was kept at 60 °C under the same stirring rate overnight. Prior to the centrifugation at 10000 rpm for 20 min, the organic phase was removed. After drying at 100 °C overnight, the as-made nanoparticles were extracted for 2 h with 100 ml of EtOH and 1 drop of HCl (37%). After drying the extracted nanoparticles at 100 °C overnight, they were calcined under air at 550 °C for 5 h.

**Functionalization of the MSNs with HMDS.** Briefly, 1 g of MCM-48 MSNs or DMSNs were suspended in 50 ml of anhydrous toluene for 2 h under continuous stirring and N<sub>2</sub> atmosphere. Then, 3 ml of HMDS was added and the solution was kept at 80 °C under continuous stirring overnight. Finally, the product was recovered by centrifugation (10000 rpm, 15 min), washed with toluene and EtOH and dried at 80 °C overnight. The resulting products are named MCM-48\* and DMSN\*.

**Encapsulation of the drug into MSNs.** OMP was loaded into pure MSNs, i.e., MCM-48 MSNs and DMSNs, and functionalized MSNs, i.e., MCM-48\* and DMSN\* using the rotary evaporation technique, as previously reported [33]. OMP (75 mg) was placed in a rotary evaporation flask and dissolved in acetone (30 ml) using an ultrasonic bath (RT, 5 min). Then, MSNs (300 mg) were added to the solution and dispersed using an ultrasonic bath (RT, 5 min). The solvent was slowly evaporated with a rotary evaporator at 35 °C until dried powder could be observed in the flask. The resulting products (MCM-48-OMP and MCM-48\*-OMP; DMSN-OMP and DMSN\*-OMP) correspond to a loading of 20 wt% of OMP, as measured by TGA. For comparison purpose, physical mixtures of pure MCM-48 MSNs and DMSNs were prepared by mixing with the spatula 20 mg of OMP with 80 mg of the respective silica materials. The resulting materials are named MCM-48-OMP-PM and DMSN-OMP-PM.

**Materials characterization.** Wide angle X-ray diffraction (WXR) measurements were performed using a Bruker D8 diffractometer (reflection, 2 configuration; Cu K : = 1.5406 Å; 40 kV; 40 mA; 10 40° 2 , step size: 0.02 2 ; 0.02 s/step). For the Transmission Electron Microscopy (TEM), the nanoparticles were dispersed in EtOH. This suspension (4 l) was deposited on a carbon-coated copper grid and images were taken in TEM (Philips CM200) at an accelerating voltage of 200 keV. N<sub>2</sub> physisorption isotherms were measured at 196 °C (77 K) using an Autosorb-iQ<sub>3</sub> sorption analyzer (Quantachrome Instruments, Boynton Beach, FL, USA). Prior to the analysis, the pristine MSNs were outgassed 10 h at 150 °C and the functionalized MSNs 12 h at 80 °C. The specific surface area (S<sub>BET</sub>) was determined using the Brunauer-Emmet-Teller (BET) equation in the relative pressure range 0.05–0.2 for DMSNs and pure MCM-48 MSNs, this range was adjusted to 0.05–0.1 for MCM-48\*. The total pore volume was determined at P/P<sub>0</sub> = 0.95. The pore size distributions (PSD) were calculated using the non-local density functional theory (NLDFT) method considering a model of silica with cylindrical pores. Dynamic light scattering (DLS) experiment were performed on a Malvern DTS Nano Zetasizer 173\* in order to measure the hydrodynamic diameter and the zeta potential of the different MSNs (equilibrium time set at 3 min, 3 measurements for each sample). The samples were dispersed in water, shaken and sonicated prior to the analysis. Thermogravimetric and Differential scanning calorimetry (DSC) analyses were performed on a Netsch instru-

ment (STA 449-F3 Jupiter) under an airflow of 20 ml min<sup>-1</sup> with a heating rate of 10 °C min<sup>-1</sup>, from 40 to 700 °C.

**Cell cultures.** Non tumorigenic human intestinal cells (HCEC) were kindly provided by Prof. Jerry W. Shay (UT Southwestern Medical Center, Dallas, TX, USA) and cultivated, as previously described, in DMEM supplemented with 2% medium 199 (10X), 2% cosmic calf serum, HEPES 20 mM, gentamycin (50 g ml<sup>-1</sup>), insulin-transferrin-selenium-G (10 g ml<sup>-1</sup>), recombinant human EGF (20 ng ml<sup>-1</sup>), hydrocortisone (1 g ml<sup>-1</sup>). Human colon adenocarcinoma cell line HT-29 were cultivated in DMEM supplemented with 10% fetal bovine serum (FBS) and 1% penicillin/streptomycin (P/S, 50 U ml<sup>-1</sup>) [34,35]. Human colon carcinoma cell line (Caco-2) were cultivated in DMEM with 10% FBS, 1% P/S, 1% sodium pyruvate and insulin-transferrin-selenium-G. All cells were incubated in a humidified incubator with 5% CO<sub>2</sub> at 37 °C.

**Cytotoxicity assays.** Cells were seeded (7500 cells/well) in black bottom Costar 96-well plates. Stock solutions of OMP, the drug-free MSNs, i.e., MCM-48 MSNs, MCM-48\*, DMSNs and DMSN\* and the drug-loaded DMSN-OMP were prepared by dissolving OMP 10 mg in 1 ml of DMSO or by dispersing 5 mg of the different MSNs into 5 ml of DMEM. A vortex (20 sec) and sonics (10 min) were applied once for the drug-loaded DMSNs-OMP and three times for the drug-free MSNs in order to bring the nanoparticles in suspension. The OMP solution and all the MSN suspensions were then diluted with DMEM to the desired concentrations, i.e., 10, 50 and 100 g ml<sup>-1</sup> for OMP and 40 to 400 g ml<sup>-1</sup> for the MSNs. A volume of 100 l of each of the solutions was first applied to the cells followed by the addition of 100 l of the respective cell culture media twice concentrated. The treated cells with OMP and the MSNs were incubated 24 h in the incubator (5% CO<sub>2</sub> at 37 °C). For each concentration and type of MSNs of each 96-wells plate, triplicates were made. The cytotoxicity was measured using Alamar Blue as follows.

**Alamar Blue (AB) assay.** AB assay was used following methods previously reported with slight modifications [36]. Briefly, a solution of 10% AB in DMEM (v/v) was prepared and 100 l of this solution was added to each well. The reaction was allowed for 40 min in the incubator, the fluorescence was measured at 530/560 nm (excitation/emission) using a Cytation 3 Imaging Multi Mode Reader (BioTek, Bad Friedrichshall, Germany). Cells incubated with OMP or the MSNs were compared to the respective control cells and the ratio treated over control was calculated in %. The suspensions of MSNs were incubated in the wells without cells, thus possible interferences between the dye and MSNs were excluded (data not shown). The data presented are the mean ± standard deviation of at least three independent experiments (cell preparations) made in triplicates. Statistical analysis was performed with OriginPro 9.55 (OriginLab) applying one-way ANOVA with Fisher test for pairwise comparison (threshold value  $p < 0.05$ ).

**Sulforhodamine B (SRB) assay.** SRB is a dye that bind to cellular protein under mild acidic conditions and permits to assess cell viability and proliferation. According to recently reported protocol, after the AB assay was performed, the cells were washed twice with PBS prior to their fixation with 50 l of a solution of trichloroacetic acid (50% in PBS, v/v) in each well [34]. After 1 h at 4 °C, the plates were washed twice with distilled water and dried at RT. Subsequently, the cells were washed twice with PBS and 50 l of the SRB solution (0.4% w/w diluted in 1% acetic acid) was added to each well. After 1 h at RT, the SRB solution was removed and the plates were washed twice with distilled water and dried at RT. The protein-bound dye was dissolved using 100 l of Tris-base (10 mM) and the absorbance was measured at = 570 nm using the plate reader. Here again, cells incubated with OMP or the MSNs were compared to the respective control cells and the ratio (treated over control) was calculated in %. The data presented are the mean ± standard deviation of at least three independent cell preparations made in triplicate. Statistical analysis was performed with

OriginPro 9.55 (OriginLab) applying one-way ANOVA with Fisher test for pairwise comparison (threshold value  $p < 0.05$ ).

**Mitochondria labelling.** After the AB assay, the cells were washed twice with PBS prior to their staining with Mitotracker Green (diluted 1:1000 with Live Cell Imaging solution). A volume of 100 l was added to each well and the cells were incubated 1 h, washed twice with LCI before imaging.

**Mitochondrial morphology analysis.** The analysis was made using the Mitochondrial Network Analysis (MiNA) tool available in the FIJI distribution of ImageJ [37]. As described, the images are first equally processed using unsharp masking (2 pixel radius), Enhance Local Contrast (CLAHE) and median filtering (2 pixel radius) to gain contrast and resolution. The images are then converted to binary and skeletonized prior to the analysis of the skeletons. For each 96-wells plate, images of the triplicates were recorded and further analyzed.

**Preparation of tablets with and without MSNs.** The tablets were directly compressed using a single punch press (PerkinElmer). MSN-free tablet is composed of 20 mg of OMP and 200 mg of BL. MSN-based tablets are composed of 100 mg of drug-loaded MSNs and 200 mg of BL. All tablets have a diameter of 13 mm and a thickness of 0.2 mm. Prior to the compression, the powders, i.e., BL with either the free drug or the drug-loaded MSNs were physically mixed together. The list of the tested formulations is presented in Table 1.

**Preparation of the in-vitro release media.** Both pH 1.2 and 7.4 media were prepared according to a previously reported procedure [38]. For the solution at pH 1.2, 2 g of NaCl, 7 ml of HCl (37%) and 1 l of distilled water were mixed. For the solution at pH 7.4, first 6.8 g of KH<sub>2</sub>PO<sub>4</sub> was dissolved in 250 ml of distilled water and then combined to 190 ml of NaOH 0.2 M and 400 ml of distilled water. The pH was adjusted using NaOH 0.2 M and the volume was completed to 1 l with distilled water.

**Drug solubility studies.** To ensure sink conditions, the solubility of OMP at pH 1.2 and pH 7.4 was determined using a procedure previously reported [19]. The amount of OMP, i.e., 10 mg ml<sup>-1</sup>, was dispersed in each medium. The resulting solution was stirred at 37 °C for 48 h. The supernatant was recovered by centrifugation (10,000 rpm, 5 min) prior to the determination of the concentration by UV Vis spectroscopy (OMP: = 284 nm at pH 1.2 and = 298 nm at pH 7.4). From an initial concentration of 10 mg ml<sup>-1</sup>, around 8.39 mg.ml<sup>-1</sup> were dissolved in pH 1.2 and only 0.33 mg ml<sup>-1</sup> in pH 7.4, so it is 25 times more soluble in acid than in neutral pH (Fig. S1).

**Dissolution studies.** Dissolution tests were performed using pH 1.2 and 7.4 with an initial concentration of OMP of 44 g ml<sup>-1</sup>. For each dissolution test, 450 ml of medium was introduced into a 500 ml erlenmeyer, subsequently placed inside an incubator set at 37 °C. Stirring at 300 rpm was allowed prior to the addition of the tablets. Each test was

**Table 1**  
List of the prepared tablets.

N°	Name	Composition
1	BL-OMP	20 mg OMP 200 mg BL
2	BL-MCM48-OMP	100 mg MSN-OMP
3	BL-MCM48*-OMP	
4	BL-DMSN-OMP	
5	BL-DMSN*-OMP	

performed as follows: the tablets were placed 2 h at pH 1.2, then the tablets were taken out and directly placed in 5 ml of PBS for few minutes to prepare the media at pH 7.4. Once transferred in pH 7.4, the test continued for the next 24 h. Aliquots of 1 ml were taken out at adequate period of time and replaced by 1 ml of the fresh medium to maintain the same volume. The concentration of OMP released in both media was quantified using UV Vis spectroscopy. All the tests were performed in triplicates. Statistical analysis was performed with OriginPro 9.55 (OriginLab) applying one-way ANOVA with Fisher test for pairwise comparison (threshold value  $p < 0.05$ ).

### 3. Results and discussion

#### 3.1. Materials characterization

##### 3.1.1. Pure and functionalized MSNs

The differences in the pore structures between both types of nanoparticles are undeniable from the TEM images presented in Fig. 1. On one hand, the highly ordered 3-D porous network of MCM-48-based nanoparticles presents an array of small pores, yet still well accessible from the external environment. In comparison, the large pores of the DMSNs present a flower-like organization. Indeed, in this latter case, two populations of pores can be distinguished: smaller pores in the centre and larger ones at the rim. Also, the MCM-48 nanoparticles are almost twice as big as the DMSNs, i.e., 150 and 80 nm, respectively.

The  $N_2$  physisorption isotherms measured at  $196^\circ\text{C}$  corroborate well these observations as it can be seen in Fig. 2. Indeed, typical type IVb isotherms associated with a pore condensation step in the relative pressure range 0.1–0.3 can be recognized and easily attributed to the cylindrical small mesopores of MCM-48 nanoparticles (Fig. 2a) [39]. After the post-synthesis grafting of the methylsilane, the porosity of the native MCM-48 nanoparticles is occupied and therefore the surface area, the pore volume and the pore size have decreased ( $S_{\text{BET}}$ : from 1140 to 966  $\text{m}^2 \text{g}^{-1}$ , pore volume: from 0.87 to 0.53  $\text{cm}^3 \text{g}^{-1}$  and pore size from 3.4 to 3.2 nm) as compiled in the Fig. 2a, 2c and the Table S1.

Since the pores of DMSNs are larger, the pore condensation occurs at higher relative pressure range, i.e., 0.6–0.9 with a sharp hysteresis loop, still an isotherm type IVa can be recognized (Fig. 2b) [39]. The volume of  $N_2$  adsorbed at lower pressure range might derive from the presence of smaller pores of about 3–4 nm, as visible in the pore size distribution profile of pure DMSNs presented in Fig. 2d. Indeed, two peaks, centered at 3.6 and 9.4 nm can be distinguished, which is in line with the above qualitative description of the TEM images (see Fig. 1). Interestingly, after the post-synthesis grafting of the methylsilane, the peak corresponding to the 3.6 nm pores disappeared whereas the main one at 9.4 nm remains almost identical to the pure materials. Therefore, it can be postulated that the majority of the methylsilane is preferentially located in smaller pores, as confirmed by the minor decrease in

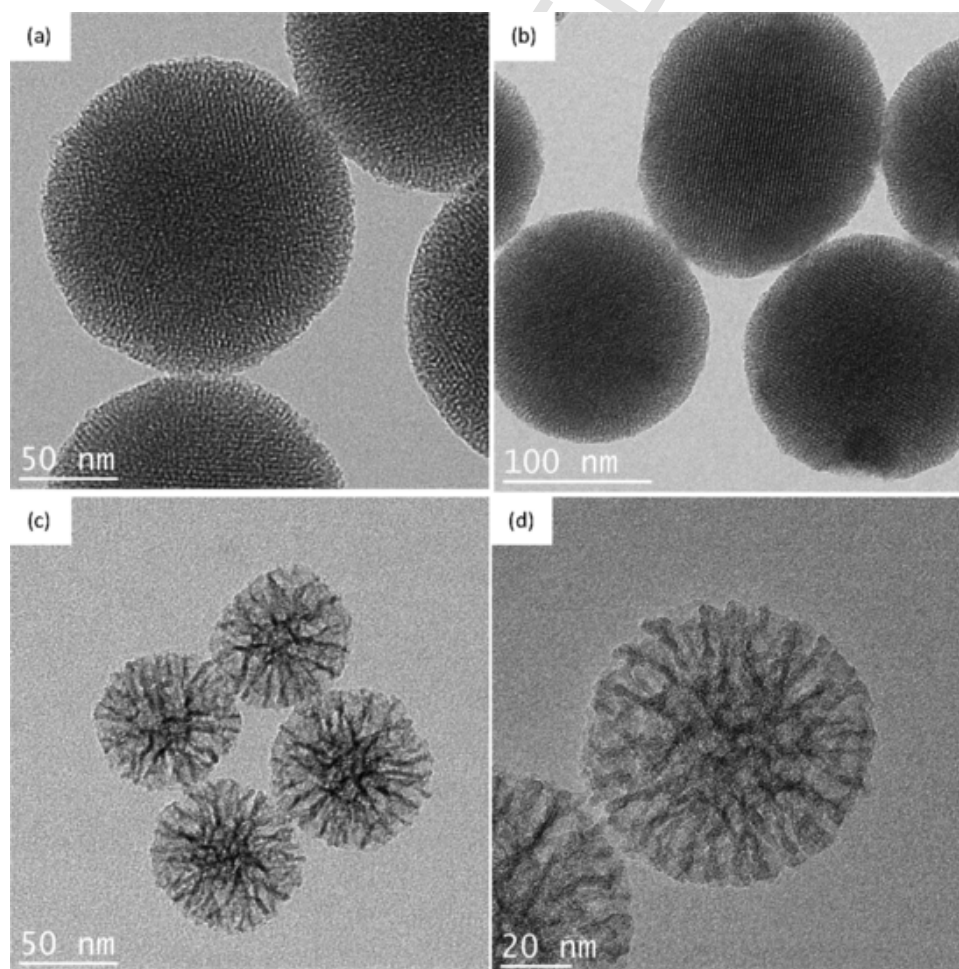


Fig. 1. TEM images of MCM-48 (a, b) and DMSN nanoparticles (c, d).

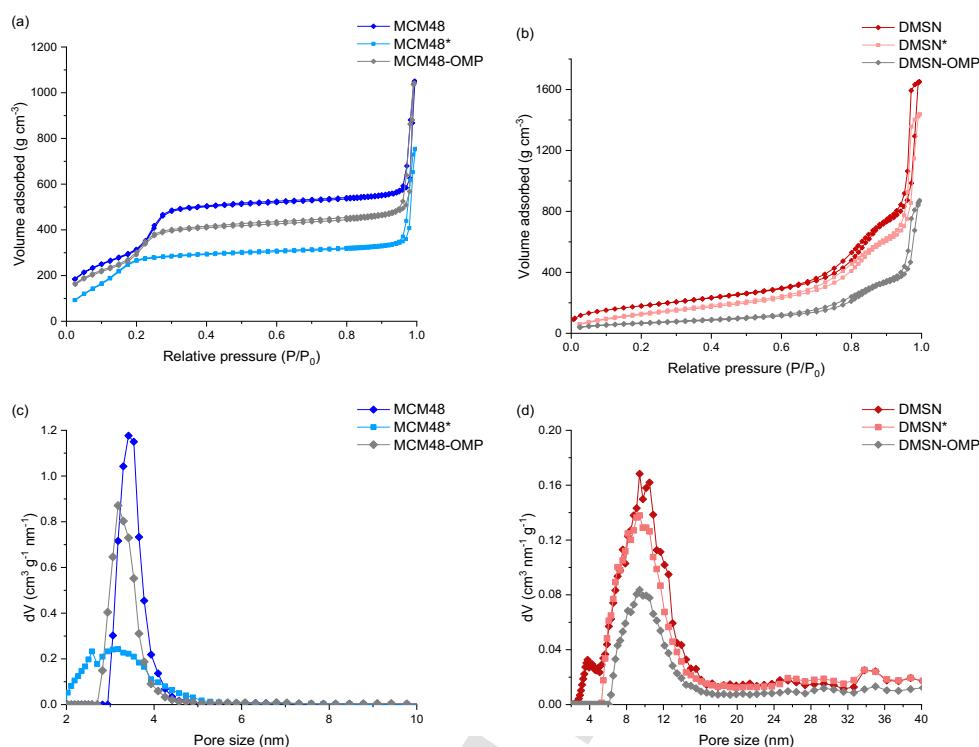


Fig. 2. (a, b) N<sub>2</sub> physisorption isotherms measured at 196 °C of the pure, methyl-functionalized MCM-48 MSNs and DMSNs and omeprazole-loaded MCM-48 MSNs and DMSNs; (c, d) The corresponding pore size distributions determined using the NLDFT method on the adsorption branch of cylindrical pore models.

pore volume and pore size, i.e., from 1.30 to 1.08 cm<sup>3</sup> g<sup>-1</sup> for the pore volume of native DMSNs and DMSN\*, respectively. The consistency of the grafting can be judged from the Table S1 and the Fig. S2c and d, since for both type of nanoparticles, similar methylsilane content has been achieved, i.e., 6.3 w% and 5.6 w% for MCM-48\* and DMSN\*, respectively (the DSC profile of the methyl-functionalized nanoparticles is available in the Fig. S2b). In addition, similar hydrodynamic diameters and zeta potentials of the methyl-grafted MSNs have been obtained as compared to the pure starting MSNs, as it can be seen in the Fig. S3. We observed that the hydrodynamic sizes of the methyl-grafted DMSNs and MCM-48 MSNs were slightly smaller than their pure counterparts owing to the hydrophobicity created by the methyl groups (Fig. S3a).

### 3.1.2. Drug-loaded MSNs

OMP was loaded into four different kinds of materials using the rotary evaporation technique aiming at a final loading of 20 w/w %. This technique was chosen for its reproducibility as we aim to compare the release profile using different formulations, equal amount of OMP has to be incorporated in the different MSNs. This was successfully achieved, as it can be seen in the mass loss profile obtained from TGA presented in the Fig. S2c, d and the Table S1, around 19 and 18% of OMP was incorporated into MCM-48 MSNs and MCM-48\*, respectively, and 20 and 18% in DMSNs and DMSN\*.

It is well documented that the process of drug encapsulation is often accompanied by the amorphization of the organic entity resulting in an amorphous drug confined in the pores of the particles [14,40–42]. From our results, hints in this direction can be found from the DSC analysis. As it can be observed in the Fig. S2a, the melting of OMP is characterized by a sharp endothermic peak at 160 °C followed by an exothermic combustion at 171 °C. This endothermic peak can only be found in the samples where OMP has been physically mixed with either

MCM-48 MSNs or DMSNs, i.e., MCM-48-OMP-PM or DMSN-OMP-PM, Fig. 3. The endothermic effect is not as pronounced in this case because only 20 w/w % of OMP was introduced. Therefore, it can be concluded that when OMP is confined inside the mesopores of both MCM-48 MSNs and DMSNs, it is in an amorphous or liquid-like state, so it does not melt, and it is burnt directly. Taking a closer look, one can actually realize that the samples with the grafted methyl groups, i.e., MCM-48\*-OMP and DMSN\*-OMP, have a very small shoulder at 148 °C: a small fraction of non-amorphous OMP might still be present. It is unlikely that this peak originates from the methylsilane as its combustion takes place at around 400 °C (see DSC analysis of methyl-functionalized nanoparticles, Fig. S2b). In order to confirm these observations, WXR D analyses were recorded on all the samples and the results are presented in the Fig. S4. OMP displays few diffraction peaks, which, after encapsulation into the different type of MSNs, are replaced by a wide amorphous halo. Nevertheless, few small diffraction peaks, e.g., at  $2\theta = 12.3^\circ$  and  $17.2^\circ$ , can be ascribed to the crystalline structure of OMP, in the case of MCM48\*-OMP and DMSN\*-OMP. The reason for that particular behavior might originate from the hydrophobic interactions between the aromatic rings of OMP and the methyl groups exposed at the surface of the MSNs which could limit the movement of OMP in close proximity to the surface.

Since the drug is confined in the mesopores of the materials, the porosity after the loading is noticeably reduced. In the case of pure MCM-48 nanoparticles, only a slight decrease in the pore size can be noticed from the PSD presented in the Fig. 2c, i.e., from 3.4 to 3.2 nm for MCM-48 and MCM-48-OMP, respectively. This is in line with our previous report, in which we showed that resveratrol might be adsorbed as a layer that covers the surface of the pores [19]. In the case of DMSNs, here once again, smaller pores seem to be occupied preferentially by OMP since the peak centered at 3.6 nm for the pure DMSNs

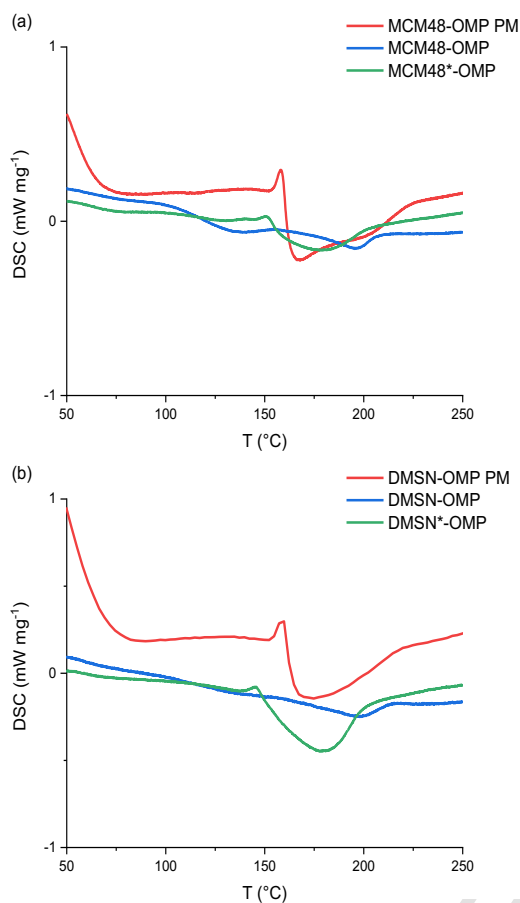


Fig. 3. DSC profiles of omeprazole physically mixed with either MCM-48 MSNs or DMSNs and confined omeprazole into pure and methyl-functionalized MCM-48 MSNs and DMSNs; (a) MCM-48 and (b) DMSN nanoparticles.

disappeared completely (see Fig. 2d). Nevertheless, OMP has also been adsorbed in the larger ones since the volume associated to the main peak centered at 9.2 nm decreased in comparison to pure DMSNs.

### 3.1.3. Qualitative characterization of the physical mixture

To gain more insights into the interaction of the protein and the nanoparticles, SEM images were recorded for the mixture of BL with MCM-48-OMP and MCM-48\*-OMP. As seen in the Figs. 4 and S5, the obvious differences in morphology and size of the three components, i.e., BL, OMP and drug-loaded MCM-48 nanoparticles, make their distinction easier. BL forms spherical microparticles of about 20  $\mu\text{m}$  (see Fig. S5a, b), OMP has a straight shape with a size not exceeding 1  $\mu\text{m}$  (see Fig. S5c, d) and finally, MCM-48 are spherical nanoparticles of about 150 nm. Therefore, attention can be drawn to the fact that, no crystal particles of OMP remained, as seen in the Fig. 4, which proves again the success of the encapsulation process. The presence of some amorphous OMP on the external surface of the MCM-48 particles (or any MSNs used) can occur, however, as the external surface area is significantly lower in comparison to the internal surface area, the largest amount of loaded OMP is most likely inside the mesopores. The main information that can be extracted from these images is that, when the silica nanoparticles are methylated, i.e., MCM-48\*-OMP, their density per microparticle of BL seems to be increased in comparison to MCM-48-OMP. This visual observation is in agreement with earlier re-

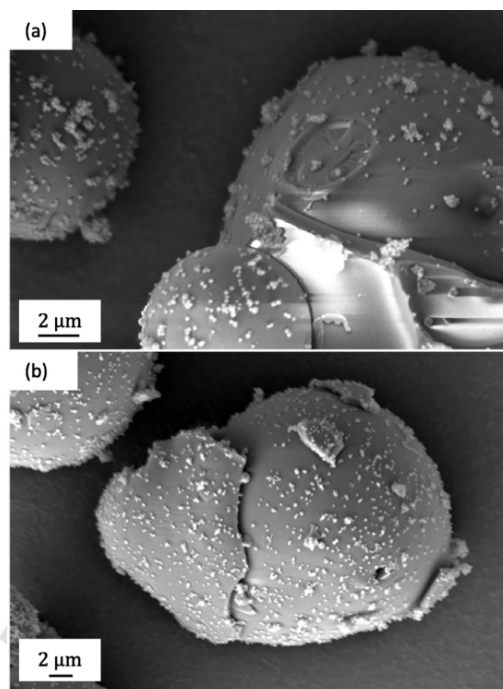


Fig. 4. SEM images of the mixtures (a) BL and MCM-48-OMP and (b) BL and MCM-48\*-OMP.

ports stating that BL is involved into hydrophobic interactions with lipids or polyphenols, for example [43,44].

## 3.2. Cytotoxicity studies

### 3.2.1. Omeprazole and drug-free MSN effects on HT-29 and Caco-2 cell lines

The two tests chosen to evaluate the toxicity of OMP and the drug-free MSNs on different cell lines are complementary. On one hand, the AB assay refers to the metabolic activity of cells as it is based on redox reactions. Resazurin, a non-fluorescent reagent, is taken up, reduced intracellularly by enzymes into resorufin, a fluorescent product, which returns back in the cell culture media where it can be quantified [45]. On the other hand, the SRB assay refers to the cellular growth as this dye binds to protein under mildly acidic conditions, typically TCA-fixed cells, and thus permits to quantify the cellular protein content which correlates with the cell density [46].

From our results, no peculiar cytotoxicity was encountered for HT-29 and Caco-2 cells, as shown in the Figs. 5 and S6. Nevertheless, higher concentration of OMP, i.e., 25 or 50  $\text{g ml}^{-1}$ , mediated a lower cell viability in HT-29 and Caco-2 cells. Regarding the MSNs, an interesting systematic trend can be extracted, i.e., methyl-functionalized nanoparticles seem generally to affect slightly more the HT-29 cells than the pure ones. The most significant decrease ( $*p < 0.05$ ) appears when comparing pure MCM-48 MSNs (around 110% cell viability) and DMSN\* (around 90% cell viability) (Fig. 5a). This observation is also valid for Caco-2 cells (Fig. 5b). Besides, Caco-2 cells appear to be more sensitive than the HT-29 cells. Unlike HT-29 cells, a concentration-dependant effect of the nanoparticles against Caco-2 cells seems to be drawn from the SRB assay (Fig. S6b). In order to get deeper insights into any metabolic activity dysfunctions after OMP and MSNs treatments, the mitochondria of the Caco-2 cells were stained and their morphologies were further analyzed.



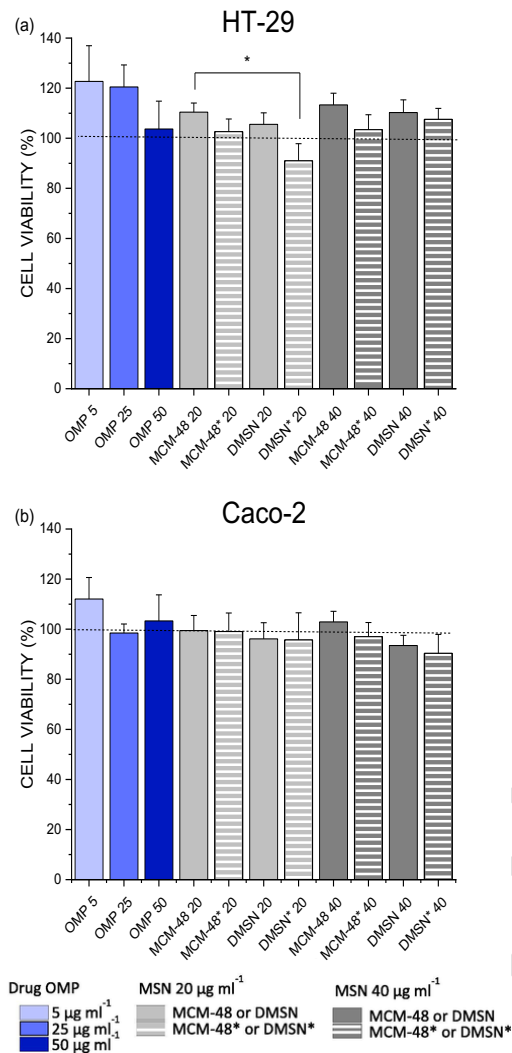


Fig. 5. Alamar Blue *in vitro* cytotoxicity assays of (a) HT-29 and (b) Caco-2 cells. Mean  $\pm$  SE (n = 3), \* $p$  < 0.05 express significant difference (one-way ANOVA and Fisher test).

### 3.2.2. Morphological characterization of the Caco-2 mitochondria

If not the most important constituent of cells, the mitochondria play undeniably a crucial role in the cellular activity as metabolic reactions, e.g., oxidative phosphorylation, Krebs cycle and cell apoptosis are conducted in this organelle [47]. Any dysfunctions or mutations will lead to severe diseases like diabetes, neurodegenerative disorders or mitochondrial myopathy, for example [48]. Their structure includes an array of membranes, well interconnected by tubular structures of varying length, i.e., the cristae junction or contact site, that separates the mitochondrial matrix from the external cellular environment. Mitochondria are dynamic systems that undergo fusion and fission to sustain DNA mitochondrial synthesis, cell cycle progression and metabolic regulation. Any alterations originating from physiological changes or pathological mutations would change the mitochondrial organization from branched to fragmented [49]. A parallel between abnormal inhibition of the mitochondrial fusion and fragmentation of the network was made and can lead to cell apoptosis [50].

In our studies, the mitochondria of control Caco-2 cells were compared to the cells treated with solvent control (DMSO), OMP 50  $\mu\text{g ml}^{-1}$  and 40  $\mu\text{g ml}^{-1}$  of pure DMSNs or DMSN\*, in terms of mean and maximum branch length, number of branches and junctions. The results, together with examples of the fluorescent images used, are compiled in Fig. 6. From a pure qualitative observation, some morphological differences in the fluorescent images between the treatment conditions could be observed. In control conditions, an articulate mitochondrial network could be clearly seen in Caco-2 cells. In cells incubated with OMP, a transition toward a more compact assembly of the organelles was visible. Differently, Caco-2 cells treated with pure DMSNs and DMSN\* resemble more the control cells with extended filaments of mitochondria. This observation, yet being only visual, is actually well aligned with the different parameters determined by image analysis. Indeed, it can be seen in Fig. 6 (f, g), that the mean and maximum branch length as well as the number of branches and junctions for DMSNs and DMSN\* are, in all cases, as high as the control cells, contrary to the OMP treatment, for which all these parameters show a trend toward decrease. Indeed, this observation is also in line with recent literature describing the mitochondria as targets of the proton pump inhibitor esomeprazole [51]. No significant differences have been observed between pure DMSNs and DMSN\*. In definitive, the informations extracted from the mitochondrial morphological assessment suggest that DMSO and OMP treatments could modify of the mitochondrial network, i.e., reduced branch length, number of branches and junctions, unlike the treatments with MSNs. Therefore, it is important to know that the use of MSNs might not cause any mitochondrial damages, at least at the concentrations investigated, which could lead to severe consequences as discussed above. To bring our toxicological profiling to the next step, a time-concentration-cell type dependent test has been designed.

### 3.2.3. Omeprazole, pure DMSNs and OMP-loaded DMSNs effects on HCEC and Caco-2 cells

Since our system is dedicated to oral drug delivery, the drug loaded MSNs being released in the intestinal region would be in contact with healthy cells like epithelial intestinal cells. Therefore, neither the model drug, the MSNs nor the combination of the two (drug loaded DMSN, DMSN-OMP) should harm these cells while permeating across the intestinal barrier. The AB and the SRB tests allowed us to monitor kinetically the viability of HCEC and Caco-2 cells after treatments of pure DMSNs at particle concentrations 100 and 200  $\mu\text{g ml}^{-1}$ , OMP at concentrations 25 and 50  $\mu\text{g ml}^{-1}$  and the drug-loaded DMSNs with equivalent concentration of OMP, i.e., 25 and 50  $\mu\text{g ml}^{-1}$ . The results are compiled in Fig. 7.

Considering the AB assay first, whether it is 100 or 200  $\mu\text{g ml}^{-1}$ , pure DMSNs show no cytotoxicity against both Caco-2 and HCEC cell lines, i.e., approximately 100% of cell viability was recorded at all time periods. Interestingly, after 30 min, OMP confined in DMSNs seems to be less cytotoxic than pure OMP, this effect is indeed particularly visible with the non-tumorigenic HCEC cells (\*\* $p$  < 0.001). For example, after 30 min, the viability of HCEC cells treated with 50  $\mu\text{g ml}^{-1}$  of OMP is around 80% whereas it is 100% for DMSN-OMP at equivalent concentration of OMP. This 20% difference between OMP and DMSN-OMP can be observed until 8 h. However, after 24 h of treatment, the viability decreases to 75 or 66% for HCEC cells exposed to DMSN-OMP with either 25 or 50  $\mu\text{g ml}^{-1}$  of OMP, respectively. This cytotoxicity might originate from the fact that DMSNs are taken up by the cells and carry higher concentration of OMP intracellularly, the cells are exposed to the maximum concentration of OMP leading to higher toxicity (cf. Fig. 8) [52]. It is worth mentioning that the Caco-2 cells seem to be slightly more resistant to the drug than the HCEC, e.g., at 8 h the Caco-2 viability after OMP treatment is 92 vs 81% for the HCEC; a similar behavior was already described in the response of HCEC and HT-29

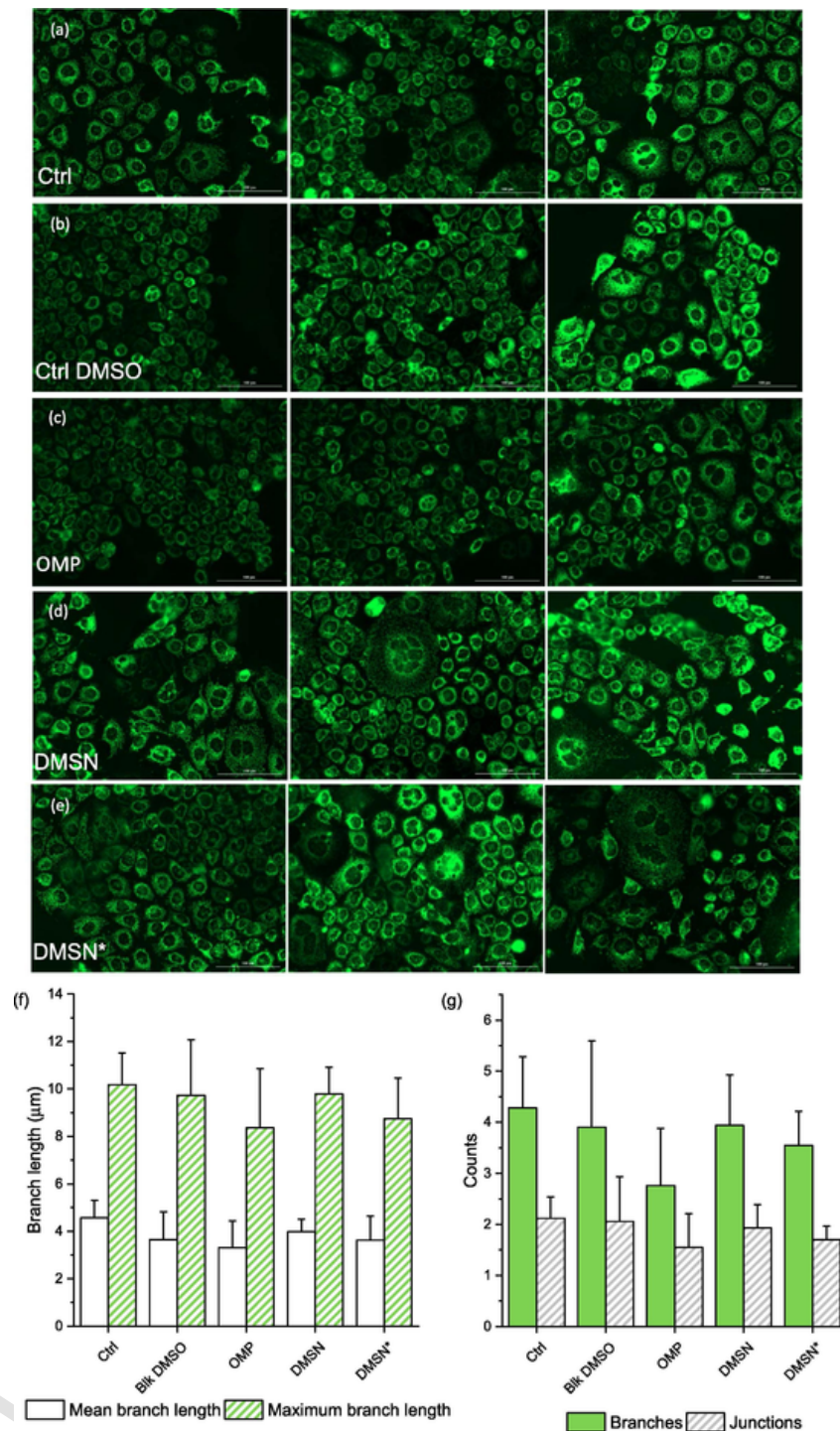
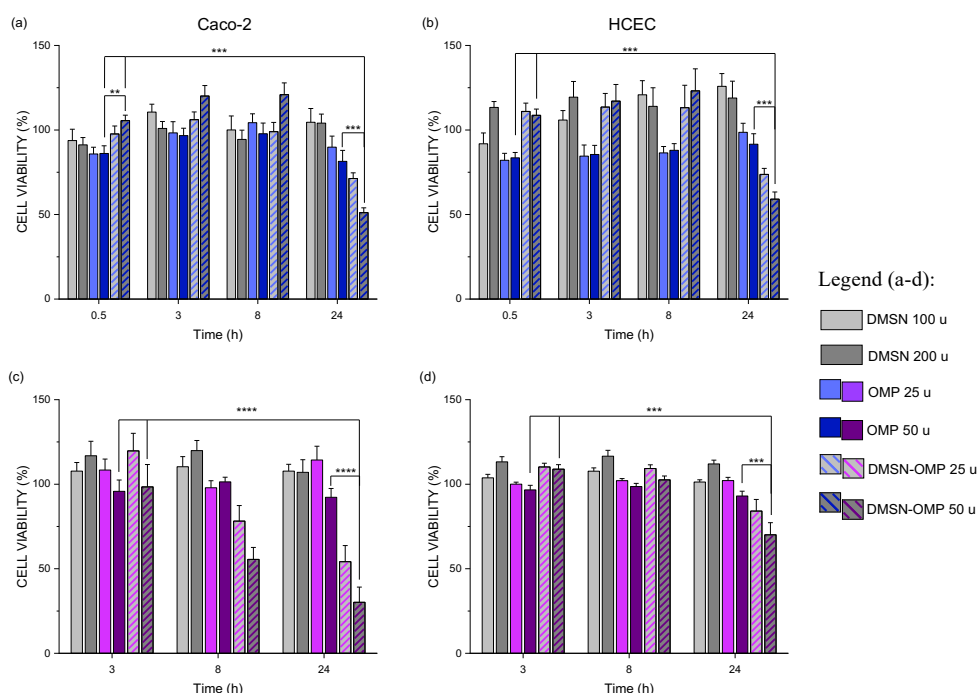


Fig. 6. (a-e) Selected fluorescent images of Caco-2 cells of (a) control, (b) DMSO control, (c) OMP pre-dissolved in DMSO and diluted with DMEM to the concentration  $50 \text{ g ml}^{-1}$ , (d, e) pure DMSN and DMSN\* suspended in DMEM at the concentration  $40 \text{ g ml}^{-1}$ ; Morphological parameters such as (f) the mean and maximum branch length of a network mitochondria and (g) the number of branches and junctions obtained using a MiNA toolset run on ImageJ. Mean  $\pm$  SE (n = 3).

to food-contaminant mycotoxins and it is probably to be expected for tumorigenic and non-tumorigenic cells [34]. Finally, the SRB test of the HCEC shows 100% cell growth up to 8 h and a significant difference is observed between DMSN-OMP and free OMP (concentration

equivalent to  $50 \text{ g ml}^{-1}$ ) after 24 h incubation correlating well the AB assay. For the Caco-2 cells, the same conclusion can be drawn with higher significant gap.



**Fig. 7.** *In vitro* cytotoxicity assays of (a, b) Alamar Blue of Caco-2 (left) and HCEC cells (right) and (c, d) SRB of Caco-2 (left) and HCEC cells (right). Mean  $\pm$  SD ( $n = 4$ ). \*\* $p < 0.01$ , \*\*\* $p < 0.001$  and \*\*\*\* $p < 0.0001$  express significant difference (one-way ANOVA and Fisher test).

This is an unprecedented proof of the advantages that MSNs represent: (1) upon progressive release of the drug, cytotoxicity thresholds stay uncrossed in the period of the absorption, in other words, the cells are not exposed to the full concentration at once, and (2) no DMSO is required; consequently in both cases, less cytotoxic effects are generated. Nevertheless, from our results, long-term exposure, i.e., 24 h, of the cells to drug-loaded MSNs provoked a higher degree of cytotoxicity. For further development in the oral delivery of MSNs, it might be an issue as clearance kinetic processes are, as of now, not yet fully understood, especially *in vivo*.

### 3.3. Drug release/dissolution experiments

To begin with, as it can be noticed in the Fig. 8, the release of OMP in pH 1.2 from the DMSN-based tablet is 3 times lower than from BL-OMP, i.e., after 2 h only around 10% of OMP is released from BL-DMSN-OMP whereas around 30% is released from BL-OMP. Therefore, owing to the addition of MSNs in the formulation, the resulting tablets could satisfy the USP requirements which state that 10% is the upper limit for the release of drugs in gastric environment [53]. Then, at pH 7.4, the release of OMP from BL-DMSN-OMP tablet was, up to 8 h, higher than BL-OMP (Fig. 8b) and finally reached a plateau at 24 h. For MSNs-based tablets, the release rate depended on the functionalization of the nanoparticles. Indeed, the release was lower in the case of methylated DMSNs, i.e., 55% for BL-DMSN\*-OMP after 8 h against almost 80% for BL-DMSN-OMP (see Fig. S7c and e). Few hypotheses can be generated to explain such results: (1) the fraction of crystalline OMP remaining in the methylated MSNs, as discussed above, is not solubilized and decreases the release, and (2) due to hydrophobic interactions, the density of methylated MSNs per microparticle of BL, as shown by SEM images presented in Fig. 4, is higher than pure MSNs, therefore, at acidic pH, when BL forms a gel, the nanoparticles are more individually embedded in this gel in comparison to pure nanoparticles, which might be present rather as a group of nanoparticles in the

gel. Apart from the functionalization effect, there seems to be a non-significant pore size effect since the release from BL-DMSN-OMP is only slightly higher than BL-MCM48-OMP (see Fig. S7), i.e., 76 and 65% after 4 h at pH 7.4, which can be due to higher diffusion of OMP in the larger pores of DMSNs. However, a reverse trend was obtained for methylated MSNs, i.e., 46 and 38% of release was measured for BL-MCM48\*-OMP and BL-DMSN\*-OMP, respectively. In this case, it might not be a matter of diffusion but rather due to the fraction of crystalline OMP remaining in these two methylated cases.

### 4. Conclusion

In this study, we investigated the cytotoxicity of two families of MSNs, MCM-48 MSNs and dendritic-type MSNs, either pure or functionalized with methyl groups, against HT-29 and Caco-2 cells. Although, no cytotoxicity was revealed for OMP and the pure MSNs, the methyl-functionalized MSNs, MCM-48\* and DMSN\*, systematically mediated higher cell mortality. The mitochondrial morphology of the Caco-2 cells seemed to be less affected by the presence of the pure DMSNs than the methyl-functionalized DMSNs which is agreement with the latter observation. Nevertheless, when treated with OMP, the mean and maximum branch lengths and the number of branches and junctions of the mitochondria were always lower than all the other treatments which might indicate a slightly lower tolerance against the compound of interest. Furthermore, the design of a time-concentration-cell type dependant test permitted to observe a pertinent effect of the progressive release of OMP upon confinement inside DMSNs. While both HCEC and Caco-2 cells showed toxicity to OMP treatment after 30 min, this effect was abolished for OMP encapsulated inside DMSNs up to 8 h. Finally, the smart addition of BL in the formulation of MSN permitted to satisfy the USP requirements which state that 10% is the upper limit for the release of drugs in gastric environment. After the gastric step, the elution of OMP at near neutral pH from the DMSNs was higher than the MSN-free formulation owing to the nanopore confinement effects. Taken all together, our results present solid foundations

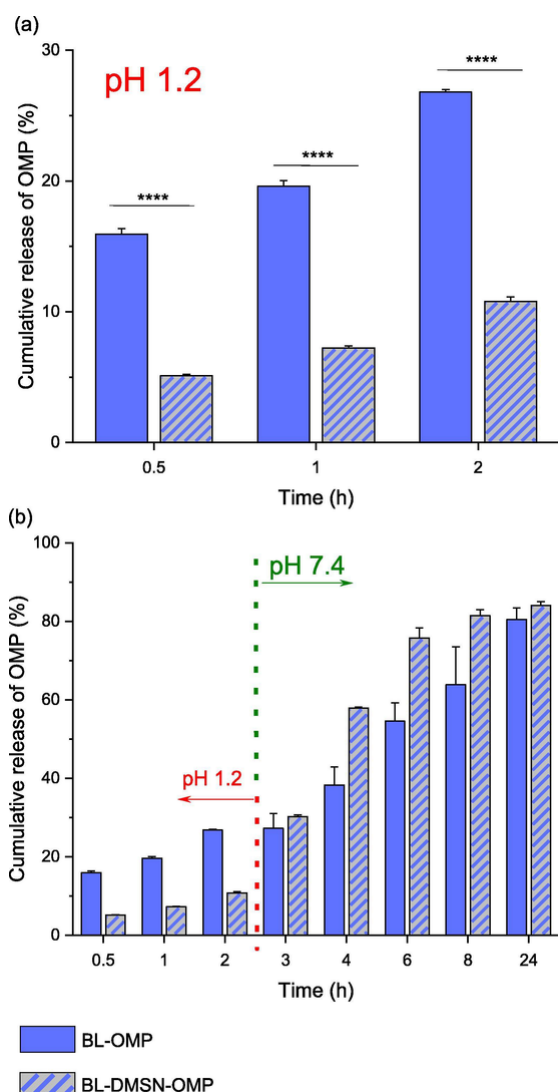


Fig. 8. *In vitro* release comparison of BL tablets of omeprazole vs BL tablets of omeprazole confined into pure DMSN in pH 1.2 (2 h) followed by pH 7.4 at 37 °C. Mean  $\pm$  SE. \*\*\*\* $p$  < 0.0001 express significant difference (one-way ANOVA, Fisher test).

on which we would rely on for further *in-depth in vitro/in vivo* studies.

#### Acknowledgements

The authors are thankful to the University of Vienna for the funding support and to the Core Facility Multimodal Imaging of the Faculty of Chemistry (Member of the VLSI) for the technical support. Authors acknowledge NHMRC Career Development Fellowship to Dr. Amirali Popat and Funding from School of Pharmacy, The University of Queensland.

#### Appendix A. Supplementary material

Supplementary data to this article can be found online at <https://doi.org/10.1016/j.ejpb.2020.03.015>.

#### References

- [1] M N Martinez, G L Amidon, *J. Clin. Pharmacol.* 42 (2002) 620–643.
- [2] J M DeSesso, C F Jacobson, *Food Chem. Toxicol.* 39 (2001) 209–228.
- [3] L Olbe, E Carlsson, P Lindberg, *Nat. Rev. 2* (2003) 132–139.
- [4] G Sachs, *Pharmacotherapy* 23 (2003) 685–735.
- [5] A G Davidson, A McCallum, *Drug Dev. Ind. Pharm.* 22 (2013) 1173–1185.
- [6] A Stroyer, J W McGinity, C S Leopold, *J. Pharm. Sci.* 95 (2006) 1343–1353.
- [7] W He, L F Fan, Q Du, B Xiang, C L Li, M Bai, Y Z Chang, D Y Cao, *Chem. Pharm. Bull.* 57 (2009) 122–128.
- [8] K E McNeel, N Siraj, I Negulescu, I M Warner, *Talanta* 177 (2018) 66–73.
- [9] E R Bendas, A A Abdelbary, *Int. J. Pharm.* 468 (2014) 97–104.
- [10] J Parmentier, G Hofhaus, S Thomas, L C Cuesta, F Gropp, R Schröder, K Hartmann, G Fricker, *J. Pharm. Sci.* 103 (2014) 3985–3993.
- [11] M George, T E Abraham, *J. Control. Release* 114 (2006) 1–14.
- [12] R Caillard, Y Boutin, M Subirade, *Int. Dairy J.* 21 (2011) 27–33.
- [13] A K Meka, L J Jenkins, M Dávalos-Salas, N Pujara, K Y Wong, T Kumeria, J M Mariadason, A Popat, *Pharmaceutics* 10 (2018) 283–299.
- [14] E Juère, F Kleitz, *Micropor. Mesopor. Mater.* 270 (2018) 109–119.
- [15] C von Baeckmann, R Guillet-Nicolas, D Renfer, H Kählig, F Kleitz, *ACS Omega* 3 (2018) 17496–17510.
- [16] J Florek, R Caillard, F Kleitz, *Nanoscale* 9 (2017) 15252–15277.
- [17] K Möller, T Bein, *Chem. Mater.* 29 (2017) 371–388.
- [18] R Guillet-Nicolas, A Popat, J L Bridot, G Monteith, S Q Qiao, F Kleitz, *Angew. Chem. Int. Ed.* 52 (2013) 2318–2322.
- [19] E Juère, J Florek, M Bouchoucha, S Jambhrunkar, K Y Wong, A Popat, F Kleitz, *Mol. Pharm.* 14 (2017) 4431–4441.
- [20] M Bouchoucha, R C Gaudreault, M A Fortin, F Kleitz, *Adv. Funct. Mater.* 24 (2014) 5911–5923.
- [21] M Bouchoucha, M F Côté, R C Gaudreault, M A Fortin, F Kleitz, *Chem. Mater.* 28 (2016) 4243–4258.
- [22] M Yu, Z Gu, T Ottewill, C Yu, *J. Mater. Chem. B* 5 (2017) 3241–3252.
- [23] M Hartmann, *Chem. Mater.* 17 (2005) 4577–4593.
- [24] Z Zhou, M Hartmann, *Chem. Soc. Rev.* 42 (2013) 3894–3912.
- [25] NŽ Knežević, J O Durand, *Nanoscale* 7 (2015) 2199–2209.
- [26] D Shen, J Xiang, X Li, L Zhou, R Zhang, W Li, L Chen, R Wang, F Zhang, D Zhao, *NANO Lett.* 14 (2014) 923–932.
- [27] K Braun, C M Stürzel, J Biskupek, U Kaiser, F Kirchhoff, M Lindén, *Toxicol. In Vitro* 52 (2018) 214–221.
- [28] T Asefa, Z Tao, *Chem. Res. Toxicol.* 25 (2012) 2265–2284.
- [29] H Gehrke, A Frühmesser, J Pelka, M Esselen, L L Hecht, H Blank, H P Schuchmann, D Gerthsen, C Marquardt, S Diabaté, C Weiss, D Marko, *Nanotoxicology* 7 (2012) 274–293.
- [30] H C Winkler, M Suter, H Naegeli, *J. Nanobiotechnol.* 14 (2016) 44.
- [31] T-W Kim, P-W Chung, V S-Y Lin, *Chem. Mater.* 22 (2010) 5093–5104.
- [32] C Lei, C Xu, A Nouwens, C Yu, *J. Mater. Chem. B* 4 (2016) 4975–4979.
- [33] N Summerlin, Z Qu, N Pujara, Y Sheng, S Jambhrunkar, M McGuckin, A Popat, *Colloid Surface B* 144 (2016) 1–7.
- [34] G del Favero, R Zaharescu, D Marko, *Arch. Toxicol.* 92 (2018) 3535–3547.
- [35] V Khare, K Dammann, M Asboth, A Krnjic, M Jambrich, C Gasche, *Inflamm. Bowel Dis.* 21 (2015) 287–296.
- [36] L Woelflingseder, G del Favero, T Blažević, E H Heiss, M Haider, B Warth, G Adam, D Marko, *Toxicol. Letters* 299 (2018) 104–117.
- [37] A J Valente, L A Maddalena, E L Robb, F Moradi, J A Stuart, *Acta Histochem.* 119 (2017) 315–326.
- [38] R Caillard, M Subirade, *Int. J. Pharm.* 437 (2012) 130–136.
- [39] M Thommes, K Kaneko, A V Neimark, J P Olivier, F Rodriguez-Reinoso, J Rouquerol, K S W Sing, *Pure Appl. Chem.* 87 (2015) 1051–1069.
- [40] K K Qian, R H Bogner, *J. Pharm. Sci.* 101 (2012) 444–463.
- [41] K Letchmanan, S-C Shen, W Kiong Ng, R B H Tan, *Colloids Surf. B* 155 (2017) 560–568.
- [42] A Maleki, H Kettiger, A Schoubben, J M Rosenholm, V Ambrogio, M Hamidi, *J. Control. Release* 262 (2017) 329–347.
- [43] T Lefèvre, M Subirade, *Int. J. Food Sci. Technol.* 34 (1999) 419–428.
- [44] L Jakobek, *Food Chem.* 175 (2015) 556–567.
- [45] S N Rampersad, *Sensors* 12 (2012) 12347–12360.
- [46] P Skehan, R Storeng, D Scudiero, A Monks, J McMahon, H Vistica, J T Warren, H Bokesch, S Kenney, M R Boyd, *J. Natl Cancer Inst.* 82 (1990) 1107–1112.
- [47] J R Friedman, J Nunnari, *Nature* 505 (2014) 335–343.
- [48] J Nunnari, A Suomalainen, *Cell* 148 (2012) 1145–1159.
- [49] M Karbowski, R J Youle, *Cell Death Differ.* 10 (2003) 870–880.
- [50] G Benard, N Bellance, D James, P Parrone, H Fernandez, T Letellier, R Rossignol, *J. Cell Science* 120 (2006) 838–848.
- [51] M L Marino, S Fais, M Djavaheri-Mergny, A Villa, S Meschini, F Lozupone, G Venturi, P Della Mina, S Patingire, L Rivoltini, P Codogno, A De Milito, *Cell Death Dis.* 1 (2010) e87.
- [52] E Juère, R Caillard, D Marko, G Del Favero, F Kleitz, *Chem. Eur. J.* (2020), doi:10.1002/chem.202000773.
- [53] USP <724> Drug release, Delayed-release articles General drug release standard.

## Electronic Supplementary Material

Gastro-protective protein-silica nanoparticles formulation for oral drug delivery: *in vitro* release, cytotoxicity and mitochondrial activity

Estelle Juère,<sup>1</sup> Giorgia Del Favero,<sup>2</sup> Florence Masse,<sup>3</sup> Doris Marko,<sup>2</sup> Amirali Popat,<sup>4,5</sup>  
Justyna Florek,<sup>1</sup> Romain Caillard,<sup>6\*</sup> Freddy Kleitz<sup>1\*</sup>

<sup>1</sup> Department of Inorganic Chemistry – Functional Materials, Faculty of Chemistry, University of Vienna, 1090 Vienna, Austria

<sup>2</sup> Department of Food Chemistry and Toxicology, Faculty of Chemistry, University of Vienna, 1090 Vienna, Austria

<sup>3</sup> Department of Chemistry, Université Laval, Quebec City, Canada

<sup>4</sup> School of Pharmacy, The University of Queensland, Brisbane, Australia

<sup>5</sup> Mater Research Institute –The University of Queensland, Translational Research Institute, Woolloongabba, Australia

<sup>6</sup> Aventus Innovations, Levis, Canada

E-mail : [rc@aventusinnov.com](mailto:rc@aventusinnov.com) - [freddy.kleitz@univie.ac.at](mailto:freddy.kleitz@univie.ac.at)

## Electronic Supplementary Material

Table S1: Physico-chemical parameters of the pure, functionalized materials obtained from the N<sub>2</sub> physisorption analysis and mass loss of methylsilane and omeprazole determined by thermogravimetric analysis considering the temperature range 100-700 °C (see TGA profiles in the Figure S2).

		<b>S<sub>BET</sub></b>	<b>V<sub>p</sub></b>	<b>Pore size</b>	<b>TGA</b>	
		<i>m<sup>2</sup> g<sup>-1</sup></i>	<i>cm<sup>3</sup> g<sup>-1</sup></i>	<i>nm</i>	Material %	OMP %
MCM-48	Pure	1140	0.87	3.4	-	19.4
	* (CH <sub>3</sub> )	966	0.53	3.2	6.3	24.3
DMSNs	Pure	654	1.30	9.4	-	20.0
	* (CH <sub>3</sub> )	485	1.08	9.3	5.6	23.7

## Electronic Supplementary Material

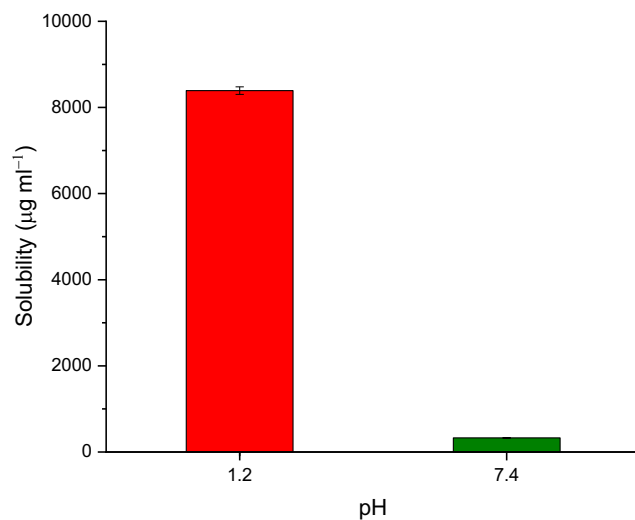


Figure S1: Solubility of omeprazole at pH 1.2 and 7.4 from a saturated solution ( $10 \text{ mg ml}^{-1}$ ) measured after 48 h.

## Electronic Supplementary Material

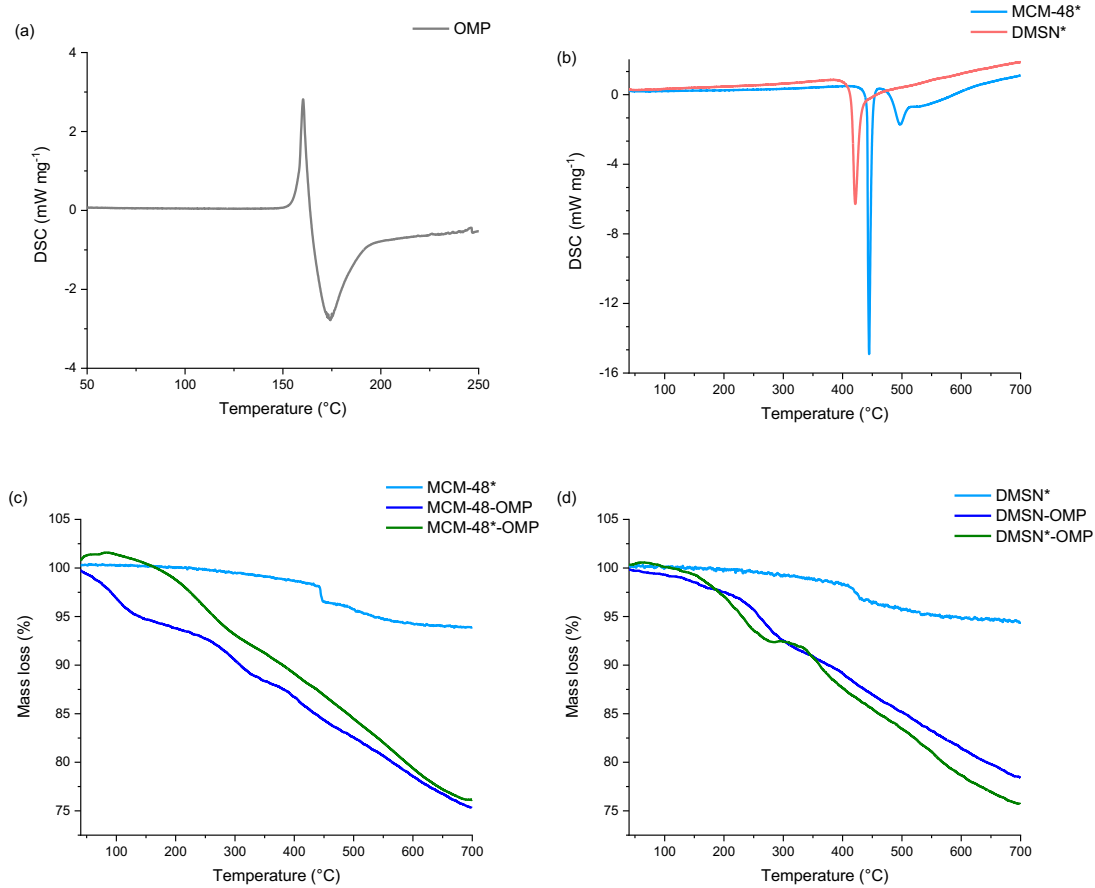


Figure S2: DSC profiles of (a) omeprazole and (b) methyl-functionalized MCM-48 MSNs and DMSNs; Mass loss profiles of the functionalized and drug loaded MCM-48 (c) and DMSN nanoparticles(d).



## Electronic Supplementary Material

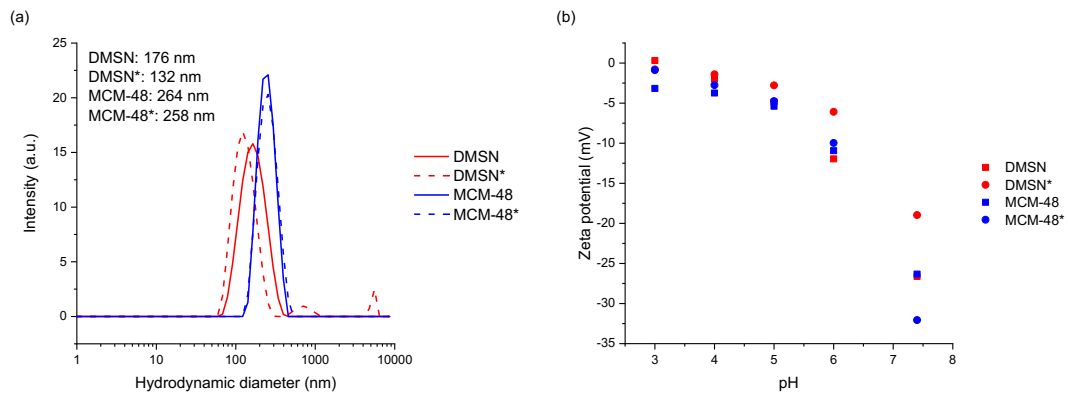


Figure S3: Hydrodynamic diameters of the pure and methyl-grafted DMSNs and MCM-48-type MSNs (a) and zeta potential values obtained in the pH range 3 – 7.4 by DLS (b).

## Electronic Supplementary Material

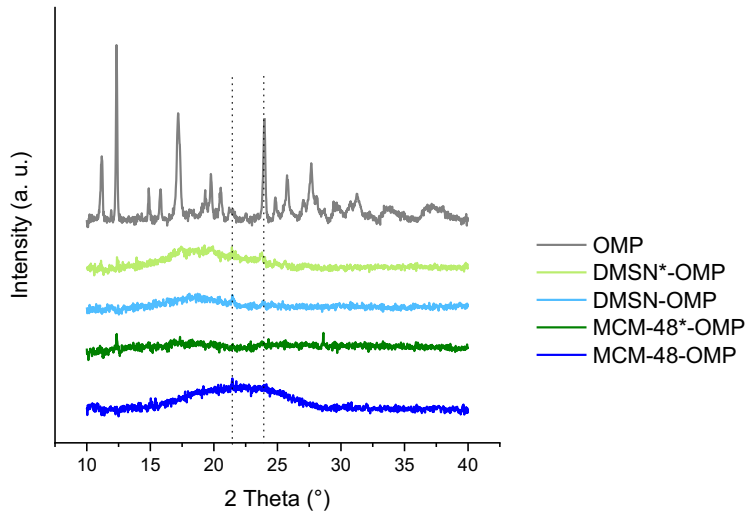


Figure S4: Wide angle XRD of pure omeprazole and omeprazole encapsulated inside the different pure and functionalized nanoparticles.

## Electronic Supplementary Material

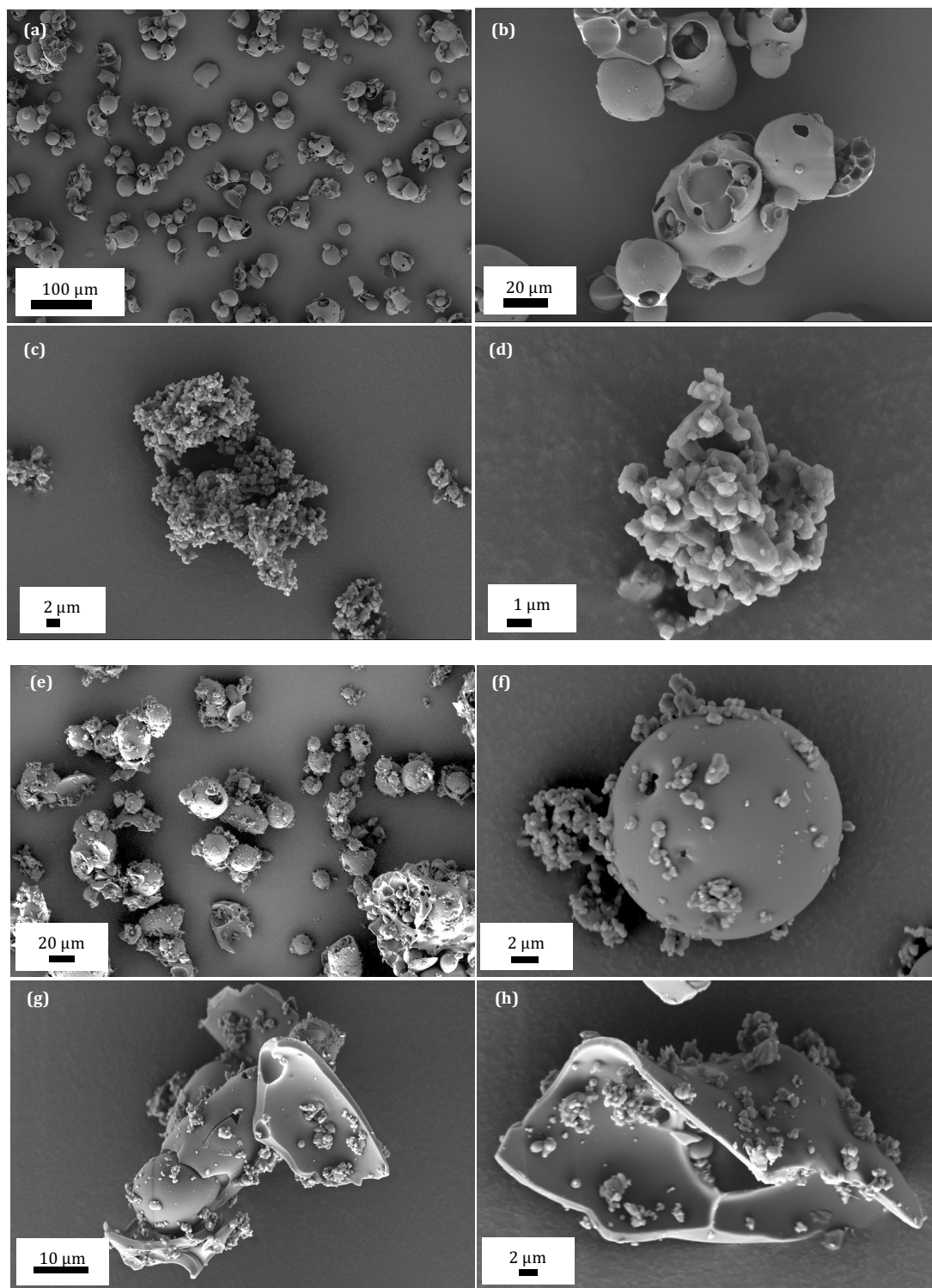


Figure S5: SEM images of (a, b) BL, (c, d) omeprazole (e-h) BL and omeprazole mixed together.

## Electronic Supplementary Material

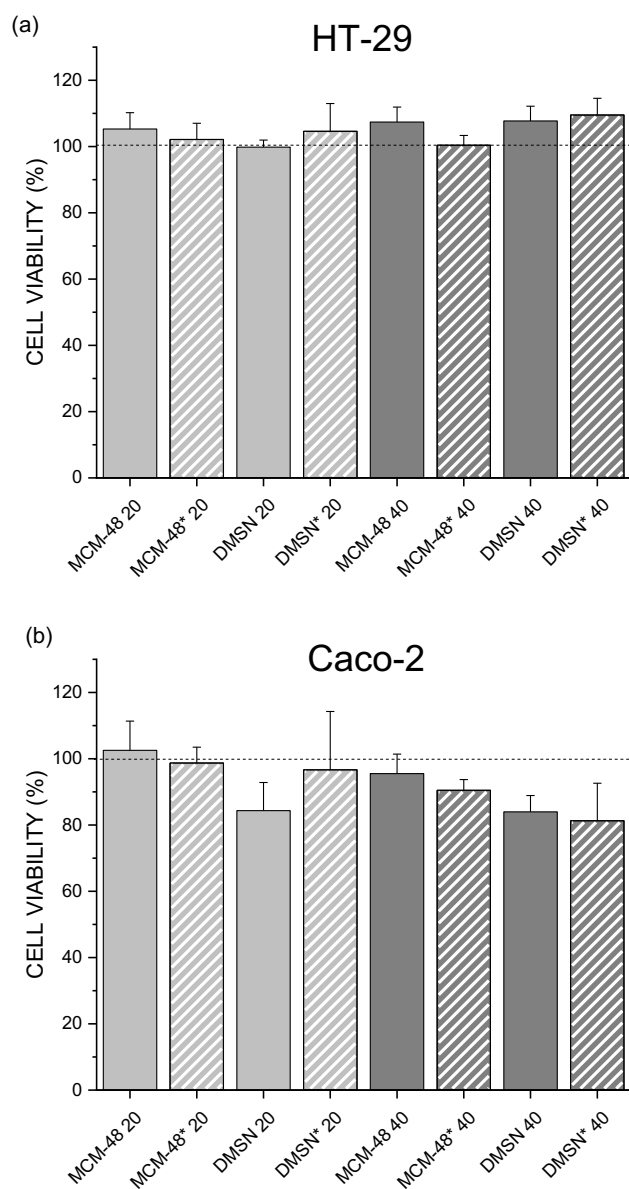


Figure S6: *In vitro* SRB assay of (a) HT-29 and (b) Caco-2 cells treated with pure and methyl-functionalized MCM-48 and DMSN nanoparticles. Mean  $\pm$  SE ( $n \geq 3$ ).

# Electronic Supplementary Material

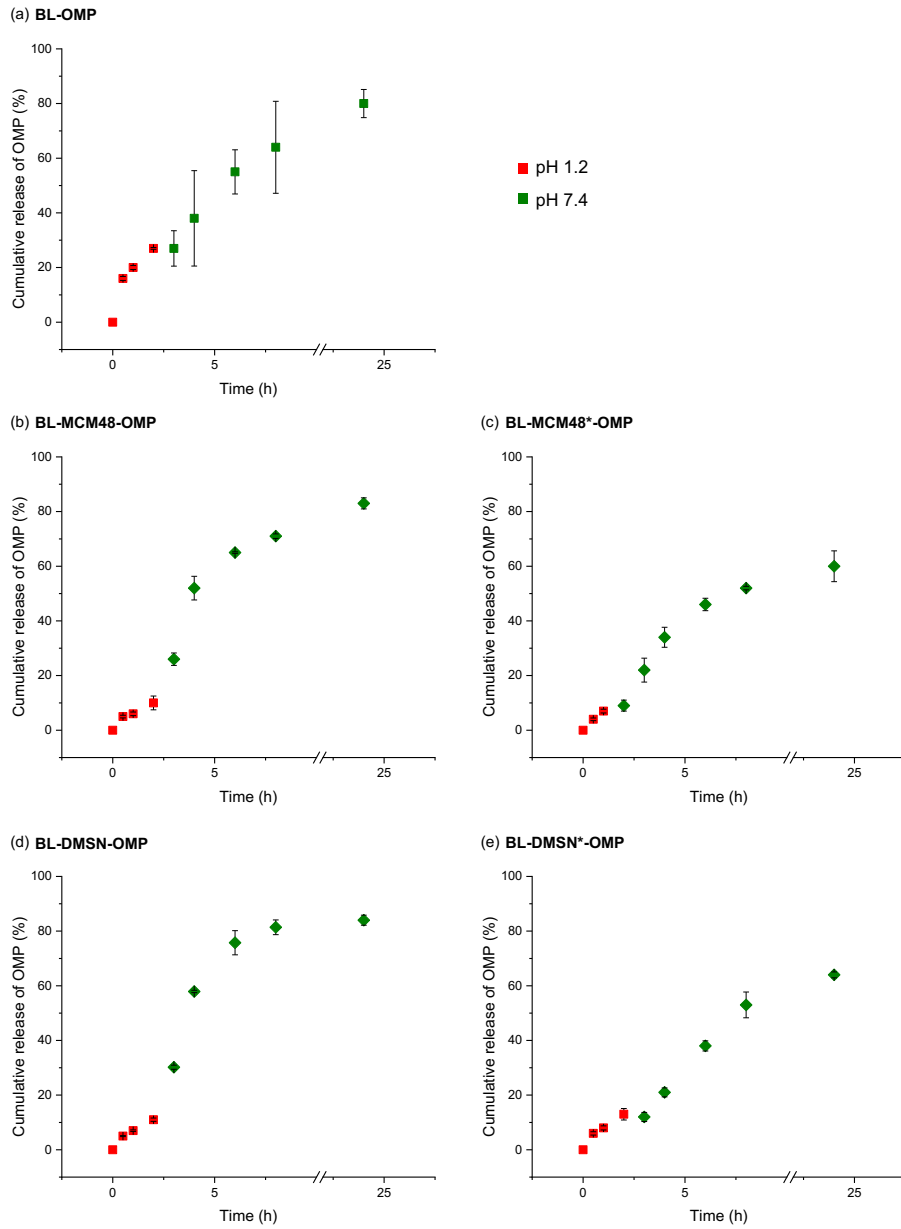


Figure S7: *In vitro* release of (a) BL-OMP, (b) BL-MCM-48-OMP, (c) BL-MCM-48\*-OMP, (d) BL-DMSN-OMP and (e) BL-DMSN\*-OMP, 2h at pH 1.2 followed by pH 7.4. Mean ± SE.



### III. Charge effects on the silica-nanoparticle formulation

This work has been submitted to the journal *Microporous Mesoporous Materials* on 20<sup>th</sup> April 2020.

In this study, I have synthesized, functionalized and characterized all the materials in the laboratory of Prof. Freddy Kleitz at the University of Vienna (Vienna, Austria). I have incorporated the drugs in the MSNs, characterized the drug-encapsulated samples and carried out the dissolution tests and the quantification of the released drugs. I have interpreted the data, created the figures and written the initial manuscript.

Dr. Romain Caillard and Prof. Freddy Kleitz have continuously supported my work, contributed to the interpretation of the data and the improvement of the manuscript.





Pore confinement and surface charge effects in protein-mesoporous silica nanoparticles formulation for oral drug delivery

Estelle Juère,<sup>1</sup> Romain Caillard,<sup>2</sup> Freddy Kleitz<sup>1\*</sup>

<sup>1</sup> *Department of Inorganic Chemistry – Functional Materials, Faculty of Chemistry, University of Vienna, 1090 Vienna, Austria*

<sup>2</sup> *Aventus Innovations, Levis, G6W 0L9 QC, Canada*

**Keywords:** Mesoporous silica nanoparticles; drug confinement; nanopores; surface charge; succinylated beta-lactoglobulin; pH-responsive protein tablets

**Highlights**

- MCM-48-type MSNs provide a nanosized environment altering the drug physical state
- Drug physical state depends on the functionalization of MCM-48-type nanoparticles
- pH-responsive lactoseric protein refrains drug release in simulated gastric fluid
- MCM-48-type MSNs enhance drug release in simulated intestinal fluid
- Repulsion of positively charged drug, MSN and BL provokes premature tablet collapse

**Abstract**

The recent pharmaceutical interest toward confinement effects on the physical state, solubility and release of drugs has paved the way to new material designs for drug delivery. Deeper understanding on how the pore size or the additional functionalities of the nanocarriers can influence the bioavailability of the cargo is nonetheless needed to explore further the potential of nanocarriers in this area. Through the combination of pure or amino-functionalized MCM-48-type mesoporous silica nanoparticles (MSNs) and succinylated beta-lactoglobulin as a protein excipient, we developed versatile tablets for the oral delivery of resveratrol and omeprazole. pH-

gating properties of the protein excipient refrained resveratrol from elution in simulated gastric fluid and owing to effective nanopore confinement, increased release in simulated intestinal conditions was successfully achieved. Specific effects of positively charged MCM-48-type nanoparticles on the stability of the protein tablets were encountered and appeared to be drug dependent.

### **Introduction**

The demand for performant formulations has increased with the idea of replacing intravenous injections by oral drug delivery as alternative treatments to major diseases of our time, e.g., cancer, neurodegenerative diseases or diabetes. Yet, challenges remain because of the limited bioavailability of drugs transiting through the gastro-intestinal tract (GIT) originating from acidic or enzymatic degradation, poor solubility in intestinal fluid and limited permeability across the epithelium barrier.[1] Two model drugs can be given as representative examples: resveratrol, a naturally occurring polyphenol, is hampered by poor aqueous solubility and chemical instability, and omeprazole, a gastric ulcers inhibitor highly prone to decomposition in the gastric fluid.[2,3] Without proper formulation, these two molecules show limited oral bioavailability which reduces drastically their therapeutic efficacy. Existing marketed formulations are manufactured with pH-responsive enteric coatings that refrain/suppress the release of the drug in the stomach and upon dissolution of the capsule at near neutral pH, the drug is released in the intestine. While these coatings ensure protection of the drug against acidic decomposition, solubility and permeability issues remain.[4] With the recent development of nanocarriers, modulation of the physicochemical properties of the drugs through their confinement within nanopores (pore size < 100 nm) has emerged as one promising pathway to increase the solubility and permeability of drugs *via* a change in the physical state from crystalline to amorphous.[5–7] Additional features of MSNs such as their particle morphology, their particle size and their functionalities, are also suspected to play a role in the cellular uptake of the nanoparticles.[8] For example, smaller MSNs are suspected to permeate more easily through the membrane, although contradictory reports

## Chapter 4 – Results

can be found in the literature.[9,10] On the other hand, the transcellular transport of MSNs carrying the drug can be modulated upon functionalization with a variety of chemical groups, e.g., thiol, methyl, amine, polyethylene imine, polyethylene glycol.[8–12] As suggested in the literature, the presence of these functions affects the charge of the resulting MSNs and thus the release of drugs in aqueous solution.[13,14] However, the impact of the functionality/charge of MSNs on the stability of pH-responsive tablet has been, as far as we know, rarely explored and is of great importance for further pharmaceutical developments.[15]

In a recent report, we demonstrated that the encapsulation into the pores of pure MCM-48-type MSNs increased the saturated solubility and the *in vitro* release of resveratrol in aqueous solution as compared to the non-encapsulated resveratrol.[16] Herein, we pursue our efforts toward the oral delivery of sensitive (model) drugs and, to this aim, resveratrol- or omeprazole-encapsulated MCM-48-type MSNs were tableted with a protein excipient, succinylated  $\beta$ -lactoglobulin (BL) to afford pH-responsive tablets. Unlike previously reported work where BL was conjugated to the MSN surface [17], in this contribution the external surface of MCM-48-type MSNs is free, allowing also methyl or amine groups to be anchored through post-synthesis grafting to yield hydrophobic or positively charged surfaces, respectively. In this study, we especially compare the physical state of resveratrol (RES) confined in differently functionalized MSNs, and the *in vitro* release of this drug from BL-based tablets in simulated gastric and intestinal fluids. Moreover, we evidence the charge effects of the pure or functionalized MCM-48-type MSNs and the drugs, *i.e.*, resveratrol and omeprazole, on the stability of the BL tablet at the acidic stage.

### Experimental section

*Materials and reagents.* Cetyltrimethylammonium bromide (CTAB, 99%), Pluronic F127 (EO<sub>106</sub>PO<sub>70</sub>EO<sub>106</sub>), tetraethylorthosilicate, (TEOS, 99%), 3-aminopropyltriethoxy silane (APTS, 99%), hexamethyldisilazane (HMDS, 99%) and omeprazole were purchased from Sigma Aldrich. 50 % succinylated  $\beta$ -lactoglobulin was supplied by Aventus Innovations (Levis, QC, Canada). Trans-resveratrol (99%) was obtained from MegaResveratrol (USA).

## Chapter 4 – Results

*Synthesis of mesoporous silica nanoparticles (MSNs).* MCM-48-type nanoparticles were synthesized by adapting a procedure previously reported.[18] Briefly, 1 g of CTAB and 4 g of Pluronic F127 were dissolved in 298 ml of  $\text{NH}_4\text{OH}$  (2.8 wt %)/EtOH = 2.5: 1 (v/v). Then, 3.6 g of TEOS was added and the solution was vigorously stirred (1000 rpm) for 1 min. The mixture was aged under static conditions at room temperature for 24 h and recovered by centrifugation (20 min, 10000 rpm). Afterwards, the resulting white solid was washed twice with 250 ml of water and dried in air at 60 °C overnight. Finally, the resulting product was calcined (550 °C, air, 5 h) to afford pure MCM-48 MSNs, noted MCM-48.

*Functionalization of the MSNs with APTS or HMDS.* Briefly, 1 g of MCM-48 MSNs were suspended in 50 ml of anhydrous toluene for 2 h under continuous stirring and  $\text{N}_2$  atmosphere. Then, either 1 ml of APTS or 3 ml of HMDS was added and the solution was kept at 80 °C under continuous stirring overnight. Finally, the products were recovered by centrifugation (10000 rpm, 15 min), washed with toluene and EtOH and dried at 80 °C overnight. The resulting products are named MCM-48-N or MCM-48\* for the functionalization with APTS and HMDS, respectively.

*Encapsulation of resveratrol.* Resveratrol (75 mg) was placed in a rotary evaporation flask and dissolved in ethanol (30 ml) using an ultrasonic bath (RT, 5 min). Then, 300 mg of either MCM-48, MCM-48-N or MCM-48\* MSNs were added to the solution and further dispersed in an ultrasonic bath (room temperature (RT), 5 min). The solvent was slowly evaporated with a rotary evaporator (Buchi rotary evaporator, Interface I-100) at 35 °C until dried powder could be observed in the flask. Then, the resulting products were dried at 50 °C overnight in an oven. Similar method was used for the encapsulation of omeprazole in MCM-48-N except that omeprazole was dissolved in acetone (30 ml). The loaded MSNs are labeled as follows: MCM-48-RES, MCM-48-N-RES, MCM-48-N-OMP and MCM-48\*-RES.

## Chapter 4 – Results

*Materials characterization.* Powder X-ray diffraction (PXRD) measurements were performed using a PANalytical Empyrean diffractometer (Malvern PANalytical, UK) in reflection geometry (Bragg–Brentano HD) using Cu  $K\alpha_{1+2}$  radiation operated at a voltage of 45 kV, a tube current of 40 mA, with a fixed divergence slit of 0.05 mm. The measurements were performed in a continuous mode with a step size  $2\theta$  of  $0.01313^\circ$  and a time per step of 198.645 s. For the transmission electron microscopy (TEM) images, a suspension of the MSNs (4  $\mu$ l) was deposited on a carbon-coated copper grid and images were taken with a Philips CM200 at an accelerating voltage of 200 keV.  $N_2$  physisorption isotherms were measured at  $-196^\circ\text{C}$  (77 K) using an Autosorb-iQ<sub>3</sub> sorption analyzer (Quantachrome Instruments, Boynton Beach, FL, USA). Prior to the analysis, the pristine MSNs were outgassed 10 h at  $150^\circ\text{C}$ , the functionalized MSNs 12 h at  $80^\circ\text{C}$  and the drug loaded MSNs 20 h at  $35^\circ\text{C}$ . The specific surface area ( $S_{\text{BET}}$ ) was determined using the Brunauer-Emmett-Teller (BET) equation in the relative pressure range 0.05-0.2 for the pure MCM-48 MSNs, this range was adjusted to 0.05-0.1 for MCM48-N and MCM-48\*. The total pore volume was determined at  $P/P_0 = 0.95$ . The pore size distributions were calculated using the non-local density functional theory (NLDFT) method considering a model of silica with cylindrical pores. Dynamic light scattering (DLS) experiments were performed on a Malvern DTS Nano Zetasizer 173° in order to measure the size and the zeta potential of the different MSNs (equilibrium time set at 3 min, 3 measurements for each sample). The samples were dispersed in water, shaken and sonicated prior to the analysis. The zeta potentials were measured over the pH range 3 – 7.4 using a titrator coupled to the Malvern DTS Nano Zetasizer. Thermogravimetric analyses (TGA) were performed with a Netzsch instrument (STA 449-F3 Jupiter) under an airflow of  $20\text{ ml min}^{-1}$  with a heating rate of  $10^\circ\text{C min}^{-1}$ , from  $40$  to  $700^\circ\text{C}$ . Solid-state NMR spectroscopy analyses of the functionalized MSNs were performed on a Bruker AVANCE NEO 500 wide bore system (Bruker BioSpin, Rheinstetten, Germany) using a 4 mm triple resonance magic angle spinning (MAS) probe.

The resonance frequency for  $^{13}\text{C}$  was 125.78 MHz and 99.38 MHz for  $^{29}\text{Si}$ , and the MAS rotor spinning was set to 14 kHz for  $^{13}\text{C}$  and 8 kHz for  $^{29}\text{Si}$ . Cross-polarization (CP) experiments were

## Chapter 4 – Results

achieved by a ramped contact pulse with a contact time of 2 ms for  $^{13}\text{C}$ . During acquisition,  $^1\text{H}$  was high power decoupled using SPINAL with 64 phase permutations. The chemical shifts for  $^{13}\text{C}$  are reported in ppm and are referenced external to adamantane by setting the low field signal to 38.48 ppm and to 4,4-dimethyl-4-silapentane-1-sulfonic acid for  $^{13}\text{C}$  and  $^{29}\text{Si}$  respectively.

*Preparation of tablets with and without MSNs.* The tablets were directly compressed using a single punch press (PerkinElmer). MSNs-free tablet is composed of 20 mg of RES and 200 mg of BL. MSNs-based tablets are composed of 100 mg of drug-loaded MSNs and 200 mg of BL. Prior to the compression, the powders, *i.e.*, BL with either the free drug or the drug-loaded MSNs, were physically mixed together. The tablets of resveratrol are named BL-RES, BL-MCM-48-RES, BL-MCM-48-N-RES, BL-MCM-48\*-RES and a tablet of omeprazole was used for comparison purpose and is labeled BL-MCM-48-N-OMP.

*Dissolution studies.* Dissolution tests were performed using pH 1.2 and 7.4 with an initial concentration of resveratrol or omeprazole of  $44\ \mu\text{g ml}^{-1}$ . It should be noted that with this initial concentration, the sink conditions are only respected in the case of omeprazole as its aqueous solubility is around  $300\ \mu\text{g ml}^{-1}$ , resveratrol having an aqueous solubility around  $30\ \mu\text{g ml}^{-1}$ . The solution at pH 1.2 was prepared using 2 g of NaCl, 7 ml of HCl (37 %) and 1 l of distilled water. For the solution at pH 7.4, 6.8 g of  $\text{KH}_2\text{PO}_4$  was dissolved in 250 ml of distilled water and then 190 ml of NaOH 0.2 M and 400 ml of distilled water were added. The pH was adjusted using NaOH 0.2 M and the volume was completed to 1 l with distilled water. For each dissolution test, 450 ml of medium was introduced into a 500 ml Erlenmeyer, subsequently placed inside an incubator set at 37 °C. Stirring at 300 rpm was allowed prior to the addition of the tablets. Each test was performed as follows: the tablets were placed 2 h at pH 1.2, then the tablets were taken out and directly placed in 5 ml of phosphate buffer saline (PBS) for few minutes to prepare the media at pH 7.4. Once transferred in pH 7.4, the test continued for the next 24 h. Aliquots of 1 ml were taken out at adequate period of time and replaced by 1 ml of the fresh medium to maintain the same

volume. The concentration of drugs released in both media was quantified using UV-Vis spectroscopy (Onda Spectrometer; RES:  $\lambda = 305$  nm; OMP:  $\lambda = 284$  nm at pH 1.2 and  $\lambda = 298$  nm at pH 7.4). All the tests were performed in triplicates.

## Results and discussions

### Characterization of the starting MSNs.

MCM-48-type MSNs have a well-defined spherical particle morphology as confirmed with the TEM images depicted in Figure 1a. The cross-sectional electron density profile presented in Figure 1b shows two steep losses of intensity which correspond to the absorption of the electrons by the MSNs. Within this region, *i.e.*, where the nanoparticles are located, several peaks of increased intensity can be distinguished and are assigned to the pores of the MSNs, *i.e.*, where the electrons

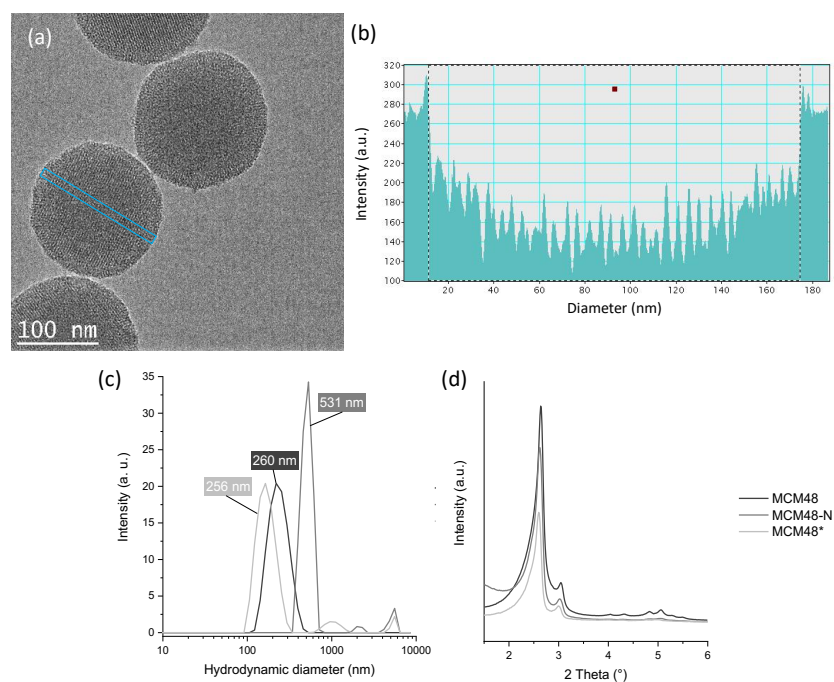


Figure 1: (a) TEM image of the pure MCM-48-type MSNs; (b) Electron density profile associated to the cross-section indicated in blue in the TEM image; (c) Hydrodynamic diameters of the different MSNs in water measured by DLS; (d) Low-angle PXRD measurements of MCM-48-, MCM-48-N- and MCM-48\*-type MSNs.

## Chapter 4 – Results

Table 1: Physicochemical parameters of the pure, functionalized, and drug-loaded MCM-48-type MSNs. Obtained from <sup>a</sup> physisorption analysis and <sup>b</sup> TGA.

	S <sub>BET</sub> <sup>a</sup> m <sup>2</sup> g <sup>-1</sup>	V <sub>p</sub> <sup>a</sup> cm <sup>3</sup> g <sup>-1</sup>	Pore size <sup>a</sup> nm	Mass loss <sup>b</sup> %
MCM-48	1140	0.87	3.4	-
MCM-48*	966	0.53	3.2	5
MCM-48-N	784	0.41	2.9	12
MCM-48-RES	645	0.51	3.4	22
MCM-48*-RES	683	0.46	3.2	27
MCM-48-N-RES	46	0.12	-	29
MCM-48-N-OMP	73	0.12	-	29

passed through without being absorbed. A particle size of approximately 160 nm can be determined through TEM but when dispersed in water, the diameter of the MSNs increases owing to the hydration sphere formed in aqueous colloidal suspension, as shown in Figure 1c. The pure and the methyl-functionalized MSNs have a hydrodynamic diameter around 260 nm in water and form a stable colloidal suspension. However, bigger agglomerates at around 530 nm are detected in the suspension of MCM-48-N and affect the aqueous colloidal stability. This originates from the electrostatic attraction between positive amine and free silanol groups remaining at the surface of MSNs. With the use of PXRD, the ordered porous network of these MSNs belonging to the cubic  $Ia\bar{3}d$  symmetry could be confirmed. As it can be seen in Figure 1d, the reflections of the (211) and (220) planes are well resolved whether the MSNs have been functionalized or not, however, the higher order reflections are only distinguished for the native MCM-48 MSNs. Following the functionalization of the pure MCM-48-type MSNs, typical decreases of the pore size, pore volume and specific surface area were observed in comparison to the native MCM-48-type MSNs, as seen in Table 1. TGA revealed higher mass loss when amine groups are attached to the materials surface than for methyl groups, with calculated values of 12 and 5 wt%, respectively. Consequently, the decrease of porosity is more important in the case of MCM-48-N than for MCM-48\*. The chemical structure of the anchored groups might support this observation as APTS silane has propyl chains which are longer than single methyl groups of HMDS silane. The carbons from



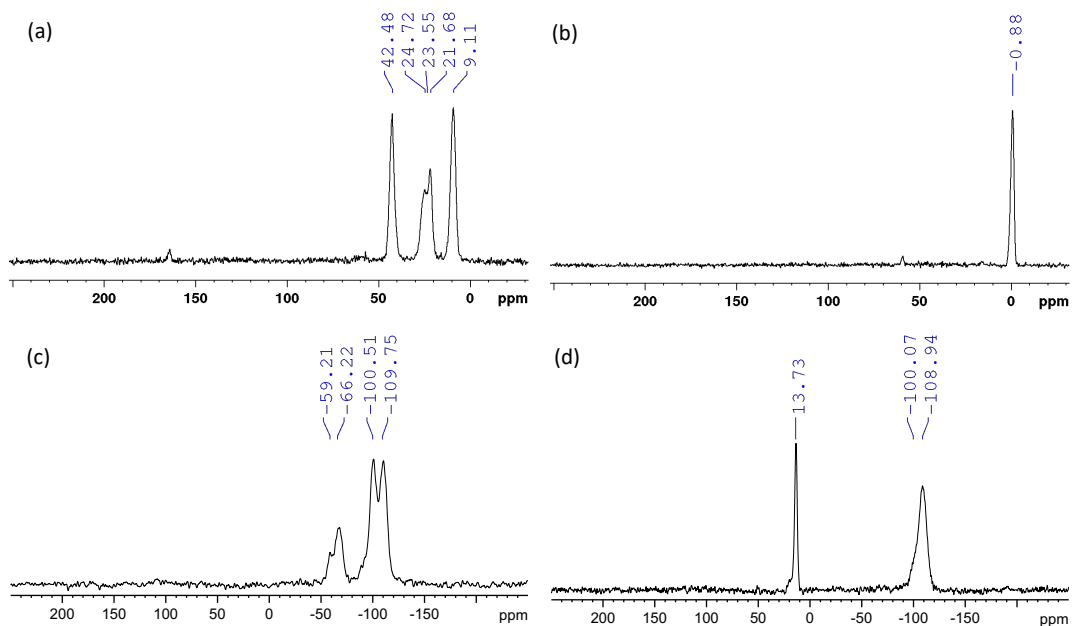


Figure 2:  $^{13}\text{C}$  CP (top) and  $^{29}\text{Si}$  direct observation (bottom) solid-state MAS NMR spectra of MCM-48-N (a, c) and MCM-48\*-type MSNs (b, d).

the propyl chains of APTS and the methyl groups of HMDS were detected through solid-state CP/MAS NMR spectroscopy at chemical shifts of 9, 23 and 42 ppm for APTS and 0.9 ppm for HMDS, as viewed in Figure 2a-b. In case of the grafting of MSNs with APTS, resonance peaks of T<sup>2</sup> (=  $\text{Si}(\text{OEt})((\text{CH}_2)_3\text{NH}_2)$ ) and T<sup>3</sup> species ( $\equiv \text{Si}((\text{CH}_2)_3\text{NH}_2)$ ) appeared in the  $^{29}\text{Si}$  MAS NMR spectra (Figure 2c) at chemical shifts of -59 ppm and -66 ppm, respectively. For HMDS, M species, *i.e.*,  $-\text{Si}(\text{CH}_3)_3$ , can be recognized at -14 ppm (Figure 2d).[19]

#### Characterizations of the drug-loaded MSNs.

Upon loading of resveratrol, the decrease of porosity seemed to depend on the nature of the surface (see Figure 3). For example, loading of resveratrol in MCM-48-N has resulted in almost complete filling of the pores, as visible by the N<sub>2</sub> adsorption-desorption isotherms and the respective pore size distributions presented in Figure 3b. Differently, the porosity of MCM-48\* was the least affected by the drug loading as only a slight shift in the volume of N<sub>2</sub> adsorbed was

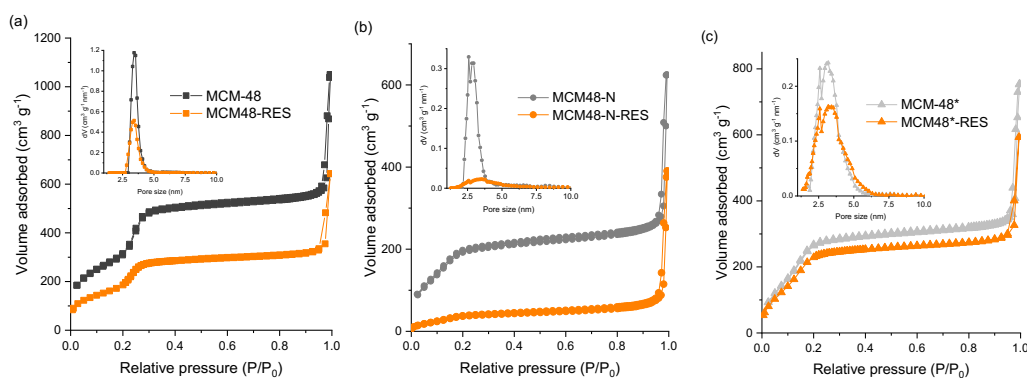


Figure 3:  $N_2$  adsorption-desorption isotherms measured at 77 K with the corresponding pore size distributions of the starting and the drug-loaded (a) MCM-48, (b) MCM-48-N and (c) MCM-48\*.

determined as shown in Figure 3c. The pores of MCM-48-RES are also still well accessible, which is in line with our previous report (Figure 3a).[16]

To get insights into the physical state of resveratrol-confined MSNs, DSC analyses were recorded. As seen in Figure 4a, the melting temperature of crystalline resveratrol is characterized by an endothermic peak appearing at approximately 275 °C. This peak was found only when resveratrol was encapsulated into methyl-functionalized MSNs, *i.e.*, MCM-48\*-RES, while none of the pure MCM-48- or amine-functionalized MSNs displayed this endothermic process. Thus, it can be suggested that a crystalline fraction remains in MCM-48\*-RES and that the amorphization phenomenon, generally occurring in a restricted space is, to a certain extent, reduced by “unfavorable” chemical interactions, hydrophobic interactions in the present case. Despite the presence of the amine groups, MCM-48-N seemed to behave as pure silica MSNs in this context, whether it is for resveratrol or omeprazole, as no endothermic peaks were revealed in the DSC analysis of MCM-48-N-RES or MCM-48-N-OMP (Figure 4c). The mass loss profiles of the drug-loaded MCM-48-type MSNs are presented in Figure 4b and 3d and the drug loading was calculated in the temperature range 100-700 °C.

*In vitro* dissolution comparison.

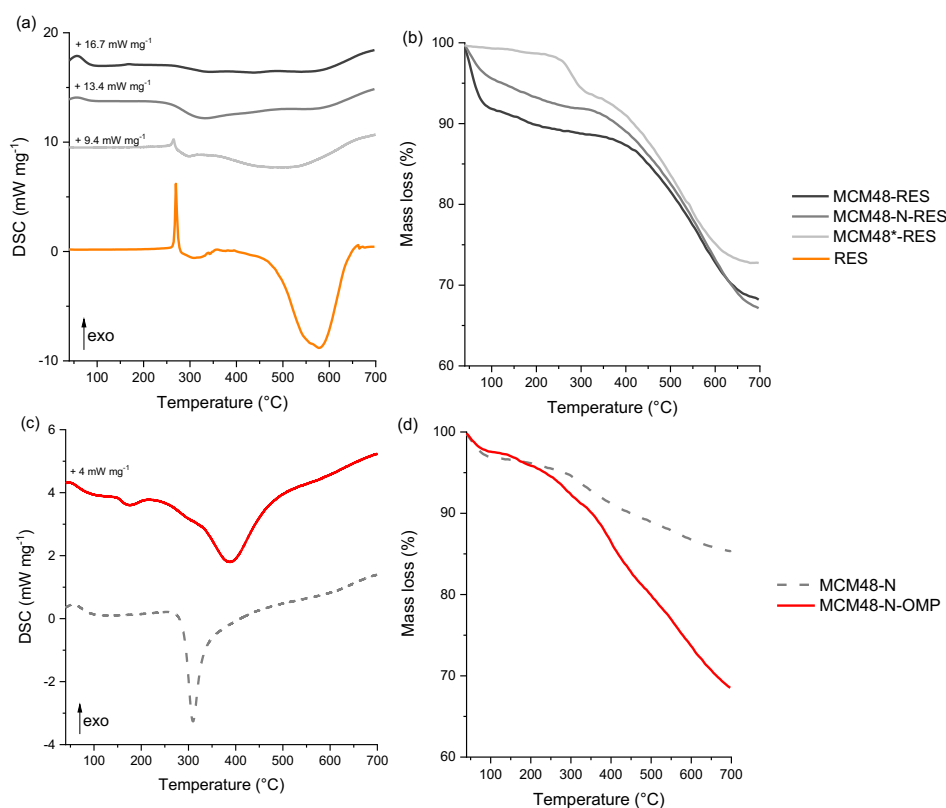


Figure 4: DSC profiles with the corresponding mass loss profiles generated by TGA (a, b, respectively) of resveratrol-loaded MCM-48-type MSNs, and (c, d) the starting MCM-48-N and omeprazole-encapsulated MCM-48-N-type MSNs.

In order to correlate these differences in the physical state of the confined resveratrol with its dissolution in aqueous media, drug release tests were conducted, and the results are presented in Figure 5. Based on the literature, a burst drug release from pure MSNs is expected; a modulation of the release rate can be achieved through the functionalization of the MSNs but essentially, for oral solid dosage of resveratrol and omeprazole, a pH-gating system is necessary.[20] Therefore, after loading of resveratrol in MCM-48-, MCM-48\*- and MCM-48-N-type MSNs, the resulting products were tableted with BL. A complete study on the encapsulation and release of omeprazole is available elsewhere, and here omeprazole was loaded in MCM-48-N-type MSNs for comparison purpose only.[21] As seen in Figure 5a, in the first 2 h at pH 1.2, the release of resveratrol from all the tablets was considerably low, *i.e.*, < 10 %, which permitted to ensure that the majority of the cargo stayed in the tablets. After the transfer to simulated intestinal pH, the tablets eroded and as

## Chapter 4 – Results

seen in the dissolution profile, resveratrol started to be eluted. While in the beginning, the cumulative release was comparable between all formulations, albeit a release rate a bit higher is observed for BL-MCM-48\*-RES, more pronounced differences appeared clearly after 8 h. The release of resveratrol from the MSNs free tablet, *i.e.*, BL-RES, was around 20 % at 8 h. Contrastingly, around 45 % of resveratrol was eluted from BL-MCM-48-RES at 8 h, more than twice the release of resveratrol from BL-RES, and it continued to increase up to 70 % after 24 h. Hence, among these 3 tablets, the one based on pure (non-functionalized) MCM-48-type MSNs was the most performant one as the dissolution of resveratrol at simulated intestinal pH was increased 3-fold in comparison to BL-RES, supporting the interest of the addition of the MSNs in the formulation.[22] Moreover, these results correlated well with the DSC analyses showing a

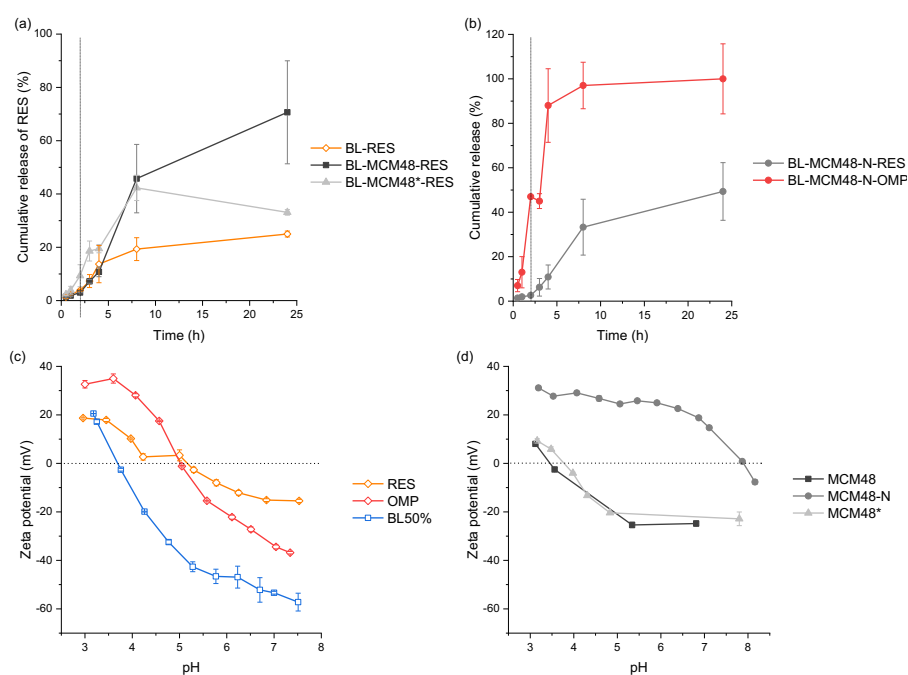


Figure 5: Release of the drugs from BL tablets of (a) the pure MCM-48- and methyl-functionalized-MCM-48-type MSNs and (b) the amino-functionalized MCM-48-type MSNs after 2 h in pH 1.2 followed by pH 7.4 until 24 h (the dotted line indicates the change in pH zone); Zeta potential profiles of (a) the drugs and BL (noted BL50%, *i.e.*, succinylated protein) and (b) the MCM-48-type MSNs measured by DLS.

## Chapter 4 – Results

remaining crystalline fraction in MCM-48\*-RES that is suspected to decrease the release of the drug in aqueous media. Using amino-functionalized MSNs, not only does the release profile differ, the stability of the tablets at pH 1.2 reached also some limitations depending on the drug used, *i.e.*, resveratrol or omeprazole. On one hand, refrained elution of resveratrol (< 5 %) from BL-MCM-48-N-RES in the acidic stage was consistent with the performances of the other tablets, *i.e.*, BL-RES, BL-MCM-48\*-RES and BL-MCM-48-RES; these results are also well in line with our previous study, in which we have successfully evidenced the ability of pure or methyl-functionalized MCM-48-based tablets to avoid the acidic release of omeprazole (< 10 %).[22] On the other hand, the MCM-48-N-based tablet failed in reducing the release of omeprazole in acidic medium, as around 50 % was already dissolved after 2 h at pH 1.2. Our hypothesis is that a high repulsion of positively charged drug-loaded MSNs and BL caused the undesired premature erosion of the BL-MCM-48-N-OMP tablet.

### *Charge effect investigations.*

To confirm the above-mentioned assumption, zeta potentials of the different components were recorded over the pH range 3-7.4 and the results are presented in Figure 5 (c, d). Owing to the functionalization with amine groups, MCM-48-N-type MSNs show a positive charge around + 30 mV at pH 3 and an isoelectric point (IEP) of 8, whereas pure MCM-48 and MCM-48\* had an overall charge of around + 10 mV at this pH and an IEP of 3.5 and 3.7, respectively. As for BL, the charge flipped from +20 mV at pH 3 to lower than – 40 mV at a pH above 5, thus the IEP is around 4 which is in line with previous report.[23] Although, zeta potential measurements are dedicated to colloids, recently their uses have been extended to the elucidation of the pKa and the ionization behavior of natural and synthetic polymers in solutions of varying pH. [24,25] With similar objectives, we have correlated zeta potential profiles of omeprazole and resveratrol, as depicted in Figure 5c, with pKa values in order to predict ionization behavior/charges of these two drugs in solution.

## Chapter 4 – Results

Theoretically, omeprazole can accept one proton on the N atom of the benzimidazole ring ( $pK_{a1} = -0.21$ ) and a second one on the N atom of the pyridine group ( $pK_{a2} = 3.98$ ) which means that below  $pH \sim 4$ , omeprazole is ionized and should have a positive charge (see Figure 6a). This is in good agreement with the zeta potential profile since omeprazole has a positive charge of +33 mV at pH 3 and remains positive until  $pH \sim 5$ . As the pH increases toward basic pH, a negative charge is observed, *i.e.*,  $\sim -40$  mV, which corresponds to the deprotonation of the N atom of the benzimidazole ring ( $pK_{a3} = 8.7$ ).[26]

In the case of resveratrol, it acts rather as a weak acid: its ionization is driven by three steps, *i.e.*,  $pK_{a1} = 8.8$ ,  $pK_{a2} = 9.8$  and  $pK_{a3} = 11.4$  (Figure 6b).[27] At  $pH < pK_{a1}$ , the unionized form predominates which contradicts slightly the zeta potential profile. Indeed, at pH 3, resveratrol has a positive charge of about +20 mV and a negative charge appears at  $pH > 5.5$ . The reason can be that due to their hydrophobicity/poor aqueous solubility ( $\log P > 0$ ), resveratrol and omeprazole are likely to form particles/aggregates in an aqueous solution under saturated condition, therefore their theoretical ionization behavior might differ from their zeta potential profiles. From both theoretical ionization behavior and experimental zeta potential analyses, omeprazole has a higher positive charge at acidic pH than resveratrol, therefore this could lead to pronounced repulsions and premature erosion of BL-MCM-48-N-OMP at the acidic stage. This behavior was not encountered for BL-MCM-48-N-RES due to lower charge effects of resveratrol. It might also be explained by the formation of a resveratrol-BL complex stabilized by hydrophobic interactions:

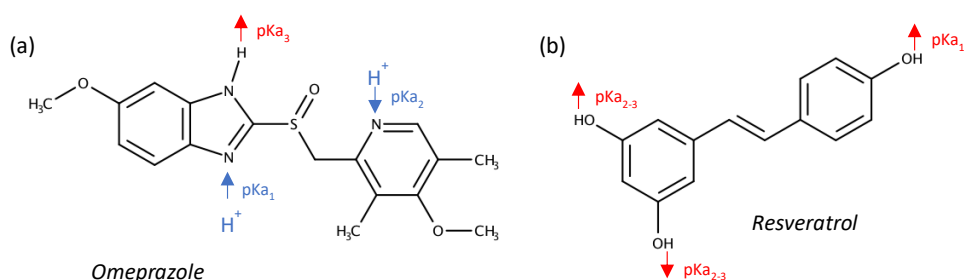


Figure 6: Chemical structure and theoretical protonation/deprotonation of (a) omeprazole and (b) resveratrol.

## Chapter 4 – Results

upon succinylation, the protein unfolding occurs and tends to expose the hydrophobic cavity of the protein which is composed notably of tryptophan residues implicated in the interactions with resveratrol.[28–30] Therefore, despite the overall positive charge, these interactions would indeed contribute to consolidate the tablet. It has to be highlighted that the influence of charged drugs on the overall zeta potential of nanoparticles/nanocarriers has only been investigated for liposomes, and the consequence that this may have on the stability of the final formulation has rarely been reported in the literature.[31–33]

### Conclusion

Through the use of a versatile oral delivery platform based on the combination of a pH-sensitive protein and drug-loaded MSNs, several useful findings have been generated. The functionalities anchored at the surface of MCM-48-type MSNs, *i.e.*, amine or methyl groups, affected the porosity of the resulting drug-loaded MSNs, the physical state of the confined drug and the release of resveratrol in aqueous media. We revealed the undesired effect of additional positive charges originating from the protonation of omeprazole on the stability of the omeprazole-amine-based tablet, *i.e.*, BL-MCM-48-N-OMP, at the acidic stage (SGF). Differently, the protonation of resveratrol at acidic pH being unfavorable, the reduced positive charge along with hydrophobic interactions with BL prevented the premature erosion of the resveratrol-amine-based tablet, *i.e.*, BL-MCM-48-N-RES. Since pure-MCM-48- and methyl-functionalized MCM-48-type MSNs have lower zeta potentials at acidic pH than amine-functionalized MCM-48, the resulting BL-MCM-48-RES, BL-MCM-48\*-RES and BL-MCM-48\*-OMP[21] tablets were highly stable at pH 1.2. Within this contribution, new insights into the synergistic effects of a pH-responsive protein,  $\beta$ -lactoglobulin, and MSNs pave the way toward efficient oral (nano)formulation of therapeutic agents. We point out that the ionization behavior of drugs has to be taken into consideration when designing platform for oral delivery and we believe that this work also provides foundations for the delivery of more complex entities such as proteins, enzymes or siRNA.

### Acknowledgement

The authors (E. J., F. K.) are thankful to the University of Vienna (Austria) for the funding support. The authors would like to acknowledge the NMR center of the Faculty of Chemistry, University of Vienna, for the solid-state NMR measurement. We are grateful to Dr. Christian Rentenberger (Physics of Nanostructured materials, Faculty of Physics, University of Vienna) for his technical assistance with the TEM measurements.

### Author contributions

E. J. conducted the experiments, analyzed the data and wrote the initial manuscript. R. C. contributed to the interpretation of the data and edited the manuscript. F.K. being the principal investigator of this work, contributed to the interpretation of the data and to the design and revision of the manuscript.

### References

- [1] M. W. Tibbitt, J. E. Dahlman, R. Langer, *J. Am. Chem. Soc.* 138 (2016) 704–717.
- [2] N. Summerlin, E. Soo, S. Thakur, Z. Qu, S. Jambhrunkar, A. Papat, *Int. J. Pharm.* 479 (2015) 282–290.
- [3] J. Roberts, M.L. McNaughtan, J. MacLachlan, C. Hunter, O. Pahl, *Rapid Commun. Mass Spectrom.* 32 (2018) 929–941.
- [4] N.D. Machado, M.A. Fernández, D.D. Díaz, *Chempluschem* 84 (2019) 951–973.
- [5] E. Juère, F. Kleitz, *Microporous Mesoporous Mater.* 270 (2018) 109–119.
- [6] A.H. Ibrahim, J.H. Smått, N.P. Govardhanam, H.M. Ibrahim, H.R. Ismael, M.I. Afouna, A.M. Samy, J.M. Rosenholm, *Eur. J. Pharm. Sci.* 142 (2020) 105103.
- [7] K.P. Nartowski, D. Malhotra, L.E. Hawarden, J. Sibik, D. Iuga, J.A. Zeitler, L. Fábíán, Y.Z. Khimyak, *Angew. Chemie* 128 (2016) 9050–9054.
- [8] D. Desai, N. Prabhakar, V. Mamaeva, D.Ş. Karaman, I.A.K. Lähdeniemi, C. Sahlgren, J.M. Rosenholm, D.M. Toivola, *Int. J. Nanomedicine* 11 (2016) 299–313.



## Chapter 4 – Results

- [9] P. Dogra, N.L. Adolphi, Z. Wang, Y.S. Lin, K.S. Butler, P.N. Durfee, J.G. Croissant, A. Nouredine, E.N. Coker, E.L. Bearer, V. Cristini, C.J. Brinker, *Nat. Commun.* 9 (2018) 1–14.
- [10] J. Florek, R. Caillard, F. Kleitz, *Nanoscale* 9 (2017) 15252–15277.
- [11] S. Behzadi, V. Serpooshan, W. Tao, M.A. Hamaly, M.Y. Alkawareek, E.C. Dreaden, D. Brown, A.M. Alkilany, O.C. Farokhzad, M. Mahmoudi, *Chem. Soc. Rev.* 46 (2017) 4218–4244.
- [12] C.T.H. Nguyen, R.I. Webb, L.K. Lambert, E. Strounina, E.C. Lee, M.O. Parat, M.A. McGuckin, A. Popat, P.J. Cabot, B.P. Ross, *ACS Appl. Mater. Interfaces* 9 (2017) 9470–9483.
- [13] A. Datt, I. El-Maazawi, S. C. Larsen, *J. Phys. Chem. C* 116 (2012) 18358–18366.
- [14] F. Balas, M. Manzano, P. Horcajada, M. Vallet-Regí, *J. Am. Chem. Soc.* 128 (2006) 8116–8117.
- [15] A. Popat, S. Jambhrunkar, J. Zhang, J. Yang, H. Zhang, A. Meka, C. Yu, *Chem. Commun.* 50 (2014) 5547–5550.
- [16] E. Juère, J. Florek, M. Bouchoucha, S. Jambhrunkar, K.Y. Wong, A. Popat, F. Kleitz, *Mol. Pharm.* 14 (2017) 4431–4441.
- [17] R. Guillet-Nicolas, A. Popat, J.-L. Bridot, G. Monteith, S.Z. Qiao, F. Kleitz, *Angew. Chemie* 125 (2013) 2374–2378.
- [18] T.W. Kim, P.W. Chung, V.S.Y. Lin, *Chem. Mater.* 22 (2010) 5093–5104.
- [19] P. Shinde, S. Sen Gupta, B. Singh, V. Polshettiwar, B.L.V. Prasad, *J. Mater. Chem. A* 5 (2017) 14914–14921.
- [20] S. Jambhrunkar, Z. Qu, A. Popat, S. Karmakar, C. Xu, C. Yu, *J. Colloid Interface Sci.* 434 (2014) 218–225.
- [21] E. Juère, G. Del Favero, F. Masse, D. Marko, A. Popat, J. Florek, R. Caillard, F. Kleitz, *Eur. J. Pharm. Biopharm.* (2020) DOI:10.1016/j.ejpb.2020.03.015.
- [22] E. Juère, R. Caillard, D. Marko, G. Del Favero, F. Kleitz, *Chem. – A Eur. J.* 26 (2020) DOI:10.1002/chem.202000773.
- [23] R. Caillard, Y. Boutin, M. Subirade, *Int. Dairy J.* 21 (2011) 27–33.
- [24] S. Bhattacharjee, *J. Control. Release* 235 (2016) 337–351.
- [25] J.A.C. Barbosa, M.S.E. Abdelsadig, B.R. Conway, H.A. Merchant, *Int. J. Pharm.* X 1 (2019)

## Chapter 4 – Results

100024.

- [26] A. Brändström, N.-Å. Bergman, I. Grundevik, S. Johansson, L. Tekenbergs-Hjelte, K. Ohlson, *Acta Chem. Scand.* 43 (1989) 569–576.
- [27] J.M. López-Nicolás, F. García-Carmona, *J. Agric. Food Chem.* 56 (2008) 7600–7605.
- [28] R. Caillard, M. Subirade, *Int. J. Pharm.* 437 (2012) 130–136.
- [29] Y. Hemar, M. Gerbeaud, C.M. Oliver, M.A. Augustin, *Int. J. Food Sci. Technol.* 46 (2011) 2137–2144.
- [30] E. Ghorbani Gorji, E. Rocchi, G. Schleining, D. Bender-Bojalil, P.G. Furtmüller, L. Piazza, J.J. Iturri, J.L. Toca-Herrera, *J. Food Eng.* 167 (2015) 217–225.
- [31] C. Matos, B. de Castro, P. Gameiro, J. L. F. C. Lima, S. Reis, *Langmuir* 20 (2003) 369–377.
- [32] D.G. Fatouros, S.G. Antimisiaris, *J. Colloid Interface Sci.* 251 (2002) 271–277.
- [33] Z. Wu, Y. Jiang, T. Kim, K. Lee, *J. Control. Release* 119 (2007) 215–221.





#### IV. Oral insulin dosage

This work was accepted for publication in the journal *Chemistry – A European Journal* on the 14<sup>th</sup> February 2020.

As a first author, I have synthesized, functionalized and characterized all the materials in the laboratory of Prof. Freddy Kleitz at University of Vienna (Vienna, Austria). I have incorporated insulin in the DMSNs, characterized the resulting insulin-confined DMSNs samples and carried out the release tests. I did the cell cultures and the metabolic activity assays (Department of Food Chemistry and Toxicology, University of Vienna). Eva Attakpah assisted me with the live cell imaging experiments and recorded some of the confocal images. Anna Fabisikova has developed the analytical method using the UHPLC-MS system and has analysed all the samples collected during the release tests and the insulin-FITC samples (Mass Spectrometry Centre, University of Vienna). Alexander Roller has provided the PXRD analyses. I have created the figures, written the initial manuscript and corrected it according to the co-authors suggestions.

Dr. Giorgia Del Favero has contributed to the design of the cell assays, to the live cell imaging with the confocal microscope and to the interpretation of the results. She has supervised my work with all cell assays and corrected the manuscript (Department of Food Chemistry and Toxicology, University of Vienna). Prof. Doris Marko has further supervised the cellular studies.

Dr. Romain Caillard and Prof. Freddy Kleitz have continuously supported my work, contributed to the interpretation of the data and the improvement of the manuscript.



## Medicinal Chemistry

# Smart Protein-Based Formulation of Dendritic Mesoporous Silica Nanoparticles: Toward Oral Delivery of Insulin

Estelle Juère,<sup>[a]</sup> Romain Caillard,<sup>[b]</sup> Doris Marko,<sup>[c]</sup> Giorgia Del Favero,<sup>[c]</sup> and Freddy Kleitz\*<sup>[a]</sup>

**Abstract:** Oral insulin administration still represents a paramount quest that almost a century of continuous research attempts did not suffice to fulfill. Before pre-clinical development, oral insulin products have first to be optimized in terms of encapsulation efficiency, protection against proteolysis, and intestinal permeation ability. With the use of dendritic mesoporous silica nanoparticles (DMSNs) as an insulin host and together with a protein-based excipient, succinylated  $\beta$ -lactoglobulin (BL), pH-responsive tablets permitted the shielding of insulin from early release/degradation in the stomach and mediated insulin permeation across the intestinal cellular membrane. Following an original in vitro cellular assay based on insulin starvation, direct cellular fluorescent visualization has evidenced how DMSNs could ensure the intestinal cellular transport of insulin.

major drawbacks would be eliminated by oral administration of insulin, it remains an issue that the pharmaceutical industry is still challenged to tackle. The reason is that the oral bioavailability is far from reaching subcutaneous injection levels, in which 100% of the injected dose is immediately disposable in the blood. Because of its high molecular weight, insulin is scarcely bioavailable, the susceptibility to gastric and intestinal proteolysis is high and the permeability across the intestinal barrier, low. Hopefully, owing to the recent development of *smart* drug (nano)carriers, the impact of these parameters on the resulting oral bioavailability can be downgraded. For instance, very recently, a self-orienting millimeter-applicator has been developed to inject insulin through the gastric mucosa and plasma concentration comparable to subcutaneous or intragastric injection has been reported for the very first time.<sup>[3]</sup> Even though this represents a major breakthrough, potential chronic side effects such as mucosa perforation or body response to a foreign millimeter-sized device have to be envisaged. Differently, owing to their nanometer-scale size, mesoporous silica nanoparticles (MSNs) can simultaneously penetrate the cellular epithelial membrane safely while carrying their protected cargoes.<sup>[4]</sup> More specifically, dendritic (i.e., dendrimer-like) MSNs (DMSNs) offer customizable pores in the range 6–20 nm, large enough to host insulin, and almost monodispersed particle size distribution in the range 50–100 nm, which is small enough to navigate through the epithelial intestinal barrier.<sup>[5]</sup>


Herein, we report the successful nanoconfinement of insulin into the dendritic mesopores of DMSNs as a promising way to significantly reduce the release/degradation in the stomach (pH 1.2) and enhance the transport of insulin towards the intestine (pH 7.4).<sup>[6]</sup> DMSNs of various pore sizes have been designed and a thiol-functionality was anchored on the free silica surface as a potential permeation and mucoadhesion enhancer.<sup>[7]</sup> Highly reproducible loadings of insulin were achieved through electrostatic attraction between the oppositely charged insulin and DMSNs. The insulin-confined DMSNs were then tableted with a pH-responsive whey protein, namely succinylated  $\beta$ -lactoglobulin (BL). The combination of DMSNs and BL is essential to synergistically refrain the degradation at pH 1.2 and enhance both the release at pH 7.4 and the cellular transport of insulin. Fluorescent images provided evidence to support the hypothesis that DMSNs are nanoparticles of choice to overcome the permeation limitations faced by most peptides and especially insulin. Finally, mechanistic insights into the modulation of the in vitro metabolic activity of human epithelial colon cells (HCEC) through the mediation of DMSNs

By 2045, the proportion of diabetic patients is expected to increase by 51% worldwide and yet, the only marketed treatment available is through subcutaneous injection of insulin on a daily basis.<sup>[1]</sup> For both Type 1 and 2 diabetes, the production of insulin by the  $\beta$ -cells of pancreatic islets is either relatively absent due to autoimmune reaction (Type 1) or inappropriate to cover high blood glucose concentration due to the development of insulin resistance by the body (Type 2). Hence, patients face hyperglycemia, with the symptoms associated to it, and their threatened life relies on insulin delivery from external sources. On top of the discomfort felt during needle injections, complications like skin infections can occur.<sup>[2]</sup> While these

[a] E. Juère, Prof. Dr. F. Kleitz  
Department of Inorganic Chemistry—Functional Materials  
Faculty of Chemistry, University of Vienna  
Währinger Straße 42, 1090 Vienna (Austria)  
E-mail: freddy.kleitz@univie.ac.at

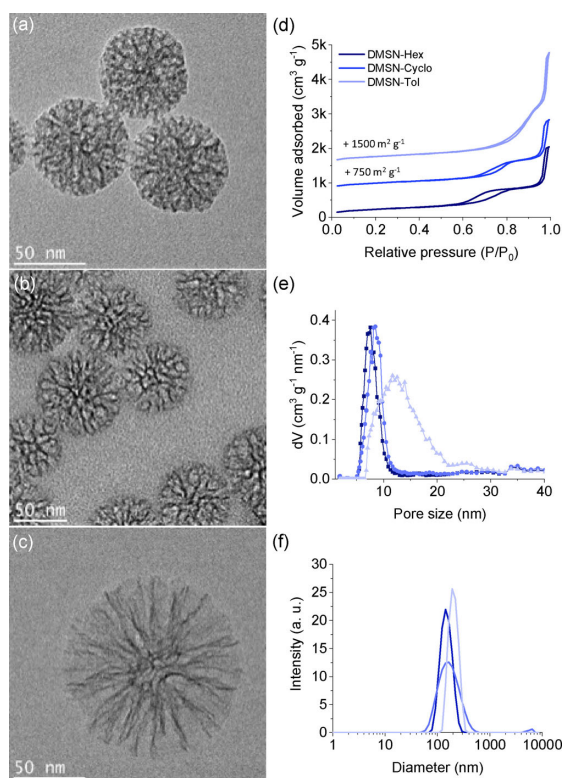
[b] Dr. R. Caillard  
Aventus Innovations, 4820 rue de la Pascaline, Suite 230  
G6W 0L9 Levis (QC) (Canada)

[c] Prof. Dr. D. Marko, Dr. G. Del Favero  
Department of Food Chemistry and Toxicology  
Faculty of Chemistry, University of Vienna  
Währinger Straße 38–40, 1090 Vienna (Austria)

 Supporting information and the ORCID identification number(s) for the author(s) of this article can be found under:  
<https://doi.org/10.1002/chem.202000773>. It contains experimental sections, detailed description of the synthesis and characterization of the materials, release tests, and live cell images.

have been gained using an insulin-containing/deprived experimental setup.

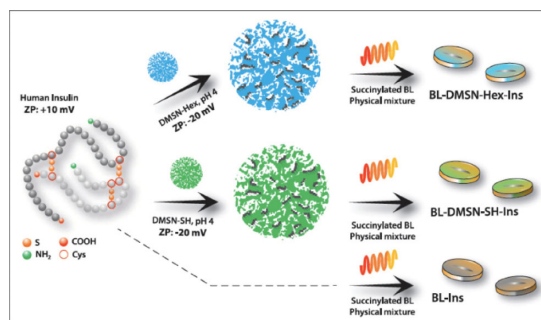
The formation of DMSNs takes place at the interface of the organic/aqueous phases during the synthesis. DMSNs of various pore sizes have been obtained upon changing the nature of the organic phase. As the organic solvent is suggested to be located in between the alkyl chains of the CTAC surfactant, it can be well understood that from a linear solvent (hexane) to a cyclic one (cyclohexane) and further to an aromatic ring (toluene), the in situ generated steric hindrance differs greatly, which in turn permitted to precisely control the swelling of the pores at the nanometer scale.  $N_2$  isotherms supported this hypothesis since from hexane to toluene, the condensation step in the isotherms shifted to higher relative pressure upon increase of the pore size (Figure 1d–e, Table S1, Supporting Information). This evolution of the pore structure and the increased particle size from DMSN-Hex to DMSN-Tol is also well visible in the transmission electron microscopy (TEM) images (Figure 1a–c). In addition, upon functionalization with thiol groups, the porosity of the resulting DMSN-SH was reduced as compared to the starting DMSN-Hex but the particle size did not change (see Figure S1).



**Figure 1.** (a–c) TEM images of the DMSNs synthesized with either hexane (DMSN-Hex), cyclohexane (DMSN-Cyclo) or toluene (DMSN-Tol); (d, e) Isotherms and respective pore size distributions obtained from  $N_2$  physisorption analyses ( $-196^\circ\text{C}$ ); (f) Particle size distribution of the DMSNs obtained from dynamic light scattering (DLS) measurements.

Considering the size of insulin and the pore sizes of the DMSNs, both smaller and larger pore size platforms, i.e., DMSN-Hex and DMSN-Tol, respectively, were selected (Figure S2a). The optimal pH of the loading was set to 4 as both parts, i.e., insulin and the different DMSNs, have opposite charges at this specific pH (Figure S2b). As a result, the favorable electrostatic attraction between the positively charged insulin and negatively charged DMSNs<sup>[8]</sup> permitted to successfully incorporate about 20 wt% of insulin into DMSN-Hex, DMSN-Tol and DMSN-SH (Figures S3 and S4). Furthermore, owing to the confinement of insulin inside DMSNs, the diffraction peaks originating from the semi-crystalline structure of insulin disappeared and were replaced by a typical amorphous ‘halo’ (Figure S5).

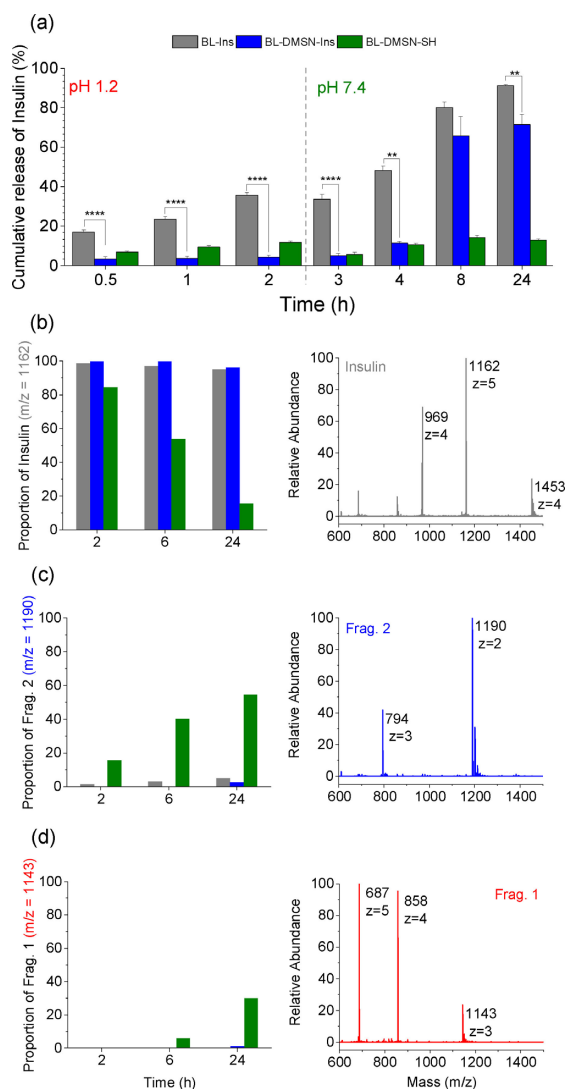
As depicted in the Scheme 1, either pristine insulin or insulin confined into DMSN-Hex or DMSN-SH was further tableted with the succinylated  $\beta$ -lactoglobulin protein in order to obtain different pH-responsive formulations which were evaluated for their ability to protect insulin at the acidic stage and



**Scheme 1.** Scheme representing the loading of insulin inside DMSNs and the formulation of the BL tablets for the release tests (ZP stands for Zeta-potential).

releasing it, undegraded, in near neutral conditions. In addition, release profiles obtained with BL-DMSN-Tol-Ins, i.e., insulin confined in larger pores of DMSN-Tol and mixed homogeneously with BL, and a layer-by-layer formulation approach are reported as well and discussed in Figure S6 of the SI. Already at the acidic stage, significant variation in the mean comparison could be observed between BL-Ins and BL-DMSN-Ins, as illustrated in Figure 2 (a different representation of the release profiles is available in SI, Figure S6a). While almost 40% of insulin is eluted from the BL-Ins tablets after 2 h, only 5% was released from BL-DMSN-Ins (\*\*\*\*  $p < 0.0001$ ) and less than 10% from BL-DMSN-SH-Ins. In addition to the pH-responsiveness of BL, confining insulin into DMSNs has permitted to keep it in the pores, undegraded. Since after the acidic stage, the intestinal tract is normally reached, the same tablets were transferred to pH 7.4. In the case of BL-Ins, a period of 4 h was required for insulin to dissolve completely. Interestingly, for BL-DMSN-Ins, the release profile can be divided into two sequences: a slow sustained release in the first two hours, followed by a faster one for the next two hours until  $\approx 80\%$  release is ob-



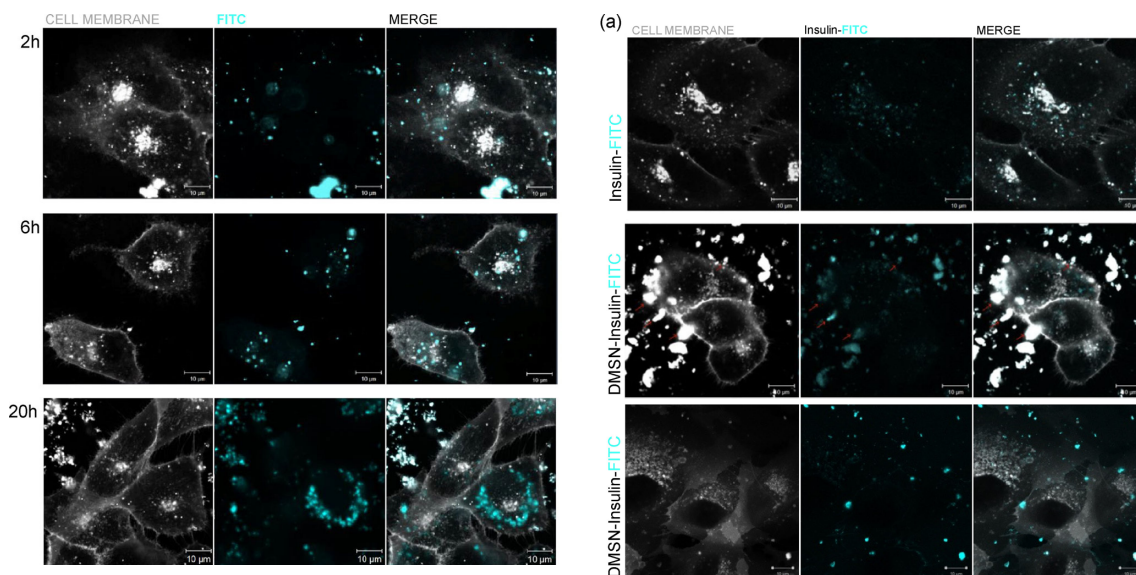


**Figure 2.** (a) Cumulative release of insulin from the different tablets immersed 2 h at pH 1.2 and subsequently at pH 7.4. Data shown as mean  $\pm$  SE ( $n=3$ ). Significant difference express  $**p < 0.01$ ,  $****p < 0.0001$ , One-way ANOVA and Fisher Test; (b–d) MS characterization of the released insulin or the fragments of insulin at different time periods in correlation with their respective proportion.

served after 24 h. The slow release observed within the first 2 h at pH 7.4 can therefore offer a window for the DMSNs to transport, within their pores, the loaded insulin through the epithelial barrier. A different release profile was obtained with the thiolated-DMSNs tablets. Here, thiol groups were anchored through post-synthesis grafting on the surface of DMSNs, as they are believed to enhance the permeability of the nanocarriers.<sup>[7]</sup> However, in addition to a poor release as compared to BL-Ins and BL-DMSN-Ins (Figure 2a), the fragmentation of insulin in its chain A, named Frag. 2 with a molecular weight of

2377 Da and chain B, named Frag. 1 with a molecular weight of 3431 Da, was witnessed and is supported by mass spectrometry (MS) data (Figure 2c–d).<sup>[9]</sup> Once at pH 7.4, the tablets started to erode and thiol groups present at the surface of DMSN-SH deprotonate, and  $R-S^-$  species should predominate under these conditions. Thereafter, the disulfide bond holding the two chains of insulin together is likely to be reduced releasing the two distinct chains. Although, thiol groups have been investigated as permeation enhancer, according to our results, their use would be at the cost of potential protein unfolding which could lead to the loss of the pharmacological activity.<sup>[10]</sup> Thus far, this undesired reductive activity of thiolated-nanocarriers has not been reported in the literature. Nevertheless, such an issue might be avoided through the replacement of the original disulfide bond with a diselenide bridge which was shown to be resistant against reduction.<sup>[11]</sup>

Once they have reached the intestinal lumen, DMSNs would have to carry insulin across the epithelium. Various pathways can be followed by the nanoparticles to reach the systemic circulation, however the transcellular transport remains the most likely path considering the surface area of the epithelial membrane.<sup>[12]</sup> Apart from the transport mechanism, nanocarriers with smaller particle size ( $\approx 100$  nm) and negative surface charge are assumed to increase the permeation across the intestinal membrane while reducing their hepatic and splenic accumulation; although, depending on the surface chemistry, some positively charged nanoparticles have also shown enhanced cellular interactions.<sup>[13]</sup> As supported by our characterization, pure DMSNs and DMSN-SH materials have both a hydrodynamic diameter in water of around 150 nm and a negative surface charge above pH 3 which match well the above-mentioned criteria. Therefore, the ability of pure DMSNs, DMSN-SH, and insulin to be efficiently internalized by intestinal cells was tested using HCEC cells through live cell imaging. The resulting confocal microscopy images are presented in Figures 3, 4, S7 and S8. Prior to the experiment, DMSNs and insulin were coupled with Rhodamine (Rhod) or FITC fluorescent probes (see SI for more details). As it can be observed in the Figure S7, Ins-FITC was insufficiently taken up by the cells until at least 3 h. This supports the interpretation that insulin requires a performant shuttle to be transported through the intestinal epithelium and to help overcome oral bioavailability issues which were previously described *in vivo*.<sup>[7b]</sup> On the other hand, DMSNs penetrated efficiently the cytoplasm, as illustrated in Figure 3. Indeed, the presence of DMSN-FITC was monitored through time-dependent kinetic experiments. After already 2 h of incubation, DMSN-FITC were present in the cytoplasm and the density of internalized DMSNs increased progressively up to 20 h of incubation. In order to prove that the cellular uptake of the DMSNs was not probe-dependent, a second fluorescent label, i.e., Rhod, was coupled to DMSNs. The ability of DMSN-Rhod and DMSN-SH-Rhod to penetrate the cells was also confirmed, as shown in Figure S8. It makes no doubt that DMSNs are good candidates to enhance protein permeation. Therefore, Ins-FITC was loaded in non-labeled DMSN-Hex and the resulting DMSN-Ins-FITC assembly was incubated with the cells for 2 h. The signal intensity from Ins-



**Figure 3.** Live cell fluorescence images of the uptake of FITC-labeled DMSNs by HCEC cells after 2 h, 6 h or 20 h. FITC is represented in light blue and the plasma membrane in white.

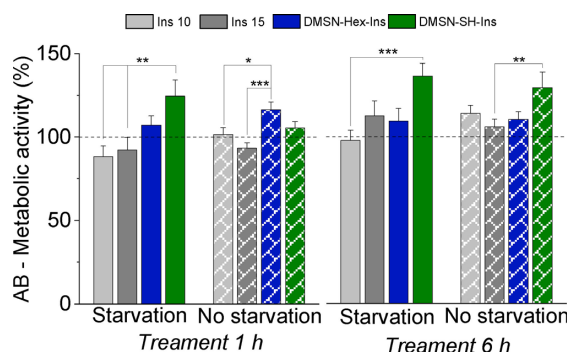
FITC confined in DMSNs was compared to Ins-FITC in its free form, similarly incubated. The resulting images, presented in Figure 4a, clearly show a higher concentration of Ins-FITC inside the cells when transported in DMSNs (red arrows). Moreover, from the cross section of the z stack presented in Figure 4b, we could confirm that within the 2 h period, the DMSN-Ins-FITC were reaching the cell membrane of HCEC cells.

As insulin confined into DMSNs appeared to interact with the membrane of intestinal cells, we performed additional experiments in order to verify if our observation could be accompanied also by a functional readout. The effects of unconfined insulin and insulin confined in both pure and thiol-modified DMSNs on the metabolic activity of HCEC cells have thus been compared and the results are presented in Figure 5. To verify the efficacy of the transport, HCEC cells were deprived of insulin supplement ( $10 \mu\text{g mL}^{-1}$ ) which is originally present in the culture media, thus generating a starvation condition mimicking pathological lack of the protein (see SI for the experimental details). Because of its pivotal role in many metabolic cascade reactions, such as glucose metabolism, lipogenesis, glycogen synthesis, insulin deprivation is supposed to considerably reduce the metabolic activity of the cells.<sup>[14]</sup> In turn, this enabled us to test whether the DMSN-based systems could maintain viable cell activity under these conditions. In “starvation” condition, i.e., in absence of insulin in the medium, the incubation with DMSN-Ins and DMSN-SH-Ins triggered a significant increase of the metabolism of the Alamar Blue (AB) reagent in comparison to the incubation with the same insulin but in non-confined form. This difference was reduced by the incubation in complete medium, implying that the metabolic need of the cells enhances the response of the test system. Along that

**Figure 4.** Live cell fluorescence imaging of HCEC cells incubated with Ins-FITC or DMSN-Ins-FITC for 2 h; (a) 2D images and (b) Zoom in the vertical cross-section of the 3D cut stack. The plasma membrane is represented in white and, the fluorescence coming from Ins-FITC in light blue.

line, longer incubation time (6 h) allowed to observe similar increase in dye metabolism when insulin was applied with the DMSNs both in presence or absence of the supplement, suggesting that insulin starvation might contribute to improve the kinetics of the observed effect.

Altogether, our results described a robust and versatile functional solid dosage for the oral delivery of insulin. We have demonstrated that, already in vitro, the acidic release of insulin from BL-Ins, that is, DMSN-free tablets, was above the recommended limit and the cellular permeation of unformulated insulin was clearly insufficient. When confined in the pores of DMSNs, the release of insulin in gastric fluid was lowered



**Figure 5.** In vitro assay based on the presence (no starvation) or absence (starvation) of insulin in the culture media of HCEC cells prior to the incubation of different treatments: commercial human insulin at the concentration 10 or 15  $\mu\text{g mL}^{-1}$ , insulin confined in pure DMSNs or thiol-functionalized DMSN-SH at the concentration equivalent to 15  $\mu\text{g mL}^{-1}$  of insulin. One-way ANOVA and Fisher Test expressed significant difference by \* $p < 0.05$ , \*\* $p < 0.01$ , \*\*\* $p < 0.001$ .

down to acceptable threshold (less than 10%) and the enhanced permeation of labeled insulin (Ins-FITC) was evidenced by confocal fluorescence microscopy. Despite the mucoadhesive properties of thiol groups, proteolysis of insulin was witnessed, and it might therefore not be the most appropriate formulation strategy. In contrast, pure DMSNs provided all the ideal benefits for insulin nanocarriers. Small particle size and tunable large pores along with a negatively charged surface allowed a simultaneous high protein loading and efficient epithelial cell uptake, while incorporation of the nanocarriers in a smart pH-sensitive protein formulation prevented the premature gastric release and degradation of insulin.

### Acknowledgements

The authors would like to thank the University of Vienna (Austria) for the financial support as well as the Mass Spectrometry Centre (MSC) and the Core Facility Multimodal Imaging of the Faculty of Chemistry (members of the VLSI). The authors thank especially Ms. Anna Fabisikova, Ms. Eva Attakpah and Mr. Manuel Felkl for their valuable technical help. The authors are grateful to Prof. Dr. C. Gerner (Department of Analytical Chemistry, Faculty of Chemistry, University of Vienna) for precious suggestions and stimulating discussion.

### Conflict of interest

The authors declare no conflict of interest.

**Keywords:** beta-lactoglobulin tablets · cellular insulin starvation · dendritic mesoporous silica nanoparticles · oral insulin dosage · transcellular epithelial transport

- [1] International Diabetes Atlas, 9th ed., 2019.
- [2] C. Y. Wong, J. Martinez, C. R. Dass, *J. Pharm. Pharmacol.* **2016**, *68*, 1093–1108.
- [3] A. Abramson, E. Caffarel-Salvador, M. Khang, D. Dellal, D. Silverstein, Y. Gao, M. R. Frederiksen, A. Vegge, F. Hubálek, J. J. Water, A. V. Friderichsen, J. Fels, R. K. Kirk, C. Cleveland, J. Collins, S. Tamang, A. Hayward, T. Landh, S. T. Buckley, N. Roxhed, U. Rahbek, R. Langer, G. Traverso, *Science* **2019**, *363*, 611–615.
- [4] a) Y. Zhao, B. G. Trewyn, I. I. Slowing, V. S.-Y. Lin, *J. Am. Chem. Soc.* **2009**, *131*, 8398–8400; b) L. Sun, X. Zhang, Z. Wu, C. Zheng, C. Li, *Polym. Chem.* **2014**, *5*, 1999–2009; c) D. Desai, N. Prabhakar, V. Mamaeva, D. Sen Karaman, I. A. K. Lähdeniemi, C. Sahlgren, J. M. Rosenholm, D. Toivola, R. C. Gaudreault, M. A. Fortin, F. Kleitz, *Chem. Mater.* **2016**, *28*, 4243–4258; e) C. T. Nguyen, R. I. Webb, L. K. Lambert, E. Strounina, E. C. Lee, M. O. Parat, M. A. McGuckin, A. Popat, P. J. Cabot, B. P. Ross, *ACS Appl. Mater. Interfaces* **2017**, *9*, 9470–9483; f) J. Florek, R. Caillard, F. Kleitz, *Nanoscale* **2017**, *9*, 15252–15277; g) E. Juère, J. Florek, M. Bouchoucha, S. Jambhrunkar, K. Y. Wong, A. Popat, F. Kleitz, *Mol. Pharm.* **2017**, *14*, 4431–4441.
- [5] a) Y. Wang, Y. A. Nor, H. Song, Y. Yang, C. Xu, M. Yu, C. Yu, *J. Mater. Chem. B* **2016**, *4*, 2646–2653; b) C. Lei, C. Xu, A. Nouwens, C. Yu, *J. Mater. Chem. B* **2016**, *4*, 4975–4979; c) D. Shen, J. Yang, X. Li, L. Zhou, R. Zhang, W. Li, L. Chen, R. Wang, F. Zhang, D. Zhao, *Nano Lett.* **2014**, *14*, 923–932; d) X. Du, L. Xiong, S. Dai, F. Kleitz, S. Z. Qiao, *Adv. Funct. Mater.* **2014**, *24*, 7627–7637; e) A. K. Meka, P. L. Abbaraju, H. Song, C. Xu, J. Zhang, H. Zhang, M. Yu, C. Yu, *Small* **2016**, *12*, 5169–5177; f) K. Möller, T. Bein, *Chem. Mater.* **2017**, *29*, 371–388; g) M. M. Abeer, A. K. Meka, N. Pujara, T. Kumeria, E. Strounina, R. Nunes, A. Costa, B. Sarmento, S. Z. Hasnain, B. P. Ross, A. Popat, *Pharmaceutics* **2019**, *11*, 418.
- [6] R. Guillet-Nicolas, A. Popat, J. L. Bridot, G. Monteith, S. Z. Qiao, F. Kleitz, *Angew. Chem. Int. Ed.* **2013**, *52*, 2318–2322; *Angew. Chem.* **2013**, *125*, 2374–2378.
- [7] a) S. Maher, R. J. Mrsny, D. J. Brayden, *Adv. Drug Delivery Rev.* **2016**, *106*, 277–319; b) N. Shrestha, F. Araújo, M.-A. Shahbazi, E. Mäkilä, M. J. Gomes, B. Herranz-Blanco, R. Lindgren, S. Granroth, E. Kukk, J. Salonen, J. Hirvonen, B. Sarmento, H. A. Santos, *Adv. Funct. Mater.* **2016**, *26*, 3405–3416.
- [8] X. Zhao, C. Shan, Y. Zu, Y. Zhang, W. Wang, K. Wang, X. Sui, R. Li, *Int. J. Pharm.* **2013**, *454*, 278–284.
- [9] Z. Chen, M. P. Caulfield, M. J. McPhaul, R. E. Reitz, S. W. Taylor, N. J. Clarke, *Clin. Chem.* **2013**, *59*, 1349–1356.
- [10] A. Gori, P. Gagni, S. Rinaldi, *Chem. Eur. J.* **2017**, *23*, 14987–14995.
- [11] K. Arai, T. Takei, M. Okumara, S. Watanabe, Y. Amagai, Y. Asahina, L. Moroder, H. Hojo, K. Inaba, M. Iwaoka, *Angew. Chem. Int. Ed.* **2017**, *56*, 5522–5526; *Angew. Chem.* **2017**, *129*, 5614–5618.
- [12] K. Netsomboon, A. Bernkop-Schnürch, *Eur. J. Pharm. Biopharm.* **2016**, *98*, 76–89.
- [13] a) K. Maisel, L. Ensign, M. Reddy, R. Cone, J. Hanes, *J. Controlled Release* **2015**, *197*, 48–57; b) P. Dogra, N. L. Adolphi, Z. Wang, Y. S. Lin, K. S. Butler, P. N. Durfee, J. G. Croissant, A. Noureddine, E. N. Coker, E. L. Bearer, V. Cristini, C. J. Brinker, *Nat. Commun.* **2018**, *9*, 4551–4564; c) N. Shrestha, M. A. Shahbazi, F. Araújo, H. Zhang, E. M. Mäkilä, J. Kauppila, B. Sarmento, J. J. Salonen, J. T. Hirvonen, H. A. Santos, *Biomaterials* **2014**, *35*, 7172–7179; d) T. Andreani, L. Miziara, E. N. Lorenzón, A. L. R. de Souza, C. P. Kiill, J. F. Fanguero, M. L. Garcia, P. D. Gremião, A. M. Silva, E. B. Souto, *Eur. J. Pharm. Biopharm.* **2015**, *93*, 118–126.
- [14] G. N. Rueggsegger, A. L. Creo, T. M. Cortes, S. Dasari, K. Sreekumaran Nair, *J. Clin. Invest.* **2018**, *128*, 3671–3681.

Manuscript received: February 12, 2020

Accepted manuscript online: February 14, 2020

Version of record online: ■■■■■, 0000

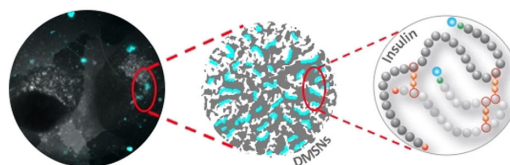
## COMMUNICATION

### Medicinal Chemistry

E. Juère, R. Caillard, D. Marko,  
G. Del Favero, F. Kleitz\*



### Smart Protein-Based Formulation of Dendritic Mesoporous Silica Nanoparticles: Toward Oral Delivery of Insulin



**Insulin delivery:** A pH-responsive protein combined with the key attributes of dendrimer-like mesoporous silica nanoparticles act synergistically as a smart oral drug-delivery platform to reduce substantially the premature release and degradation of gastro-sensi-

tive insulin. As evidenced by confocal microscopy, the designed nanocarriers mediated significant cellular permeation of the nanopore-confined fluorescent-labeled insulin across human intestinal cells (see figure).

# **Chemistry–A European Journal**

Supporting Information

## **Smart Protein-Based Formulation of Dendritic Mesoporous Silica Nanoparticles: Toward Oral Delivery of Insulin**

Estelle Juère,<sup>[a]</sup> Romain Caillard,<sup>[b]</sup> Doris Marko,<sup>[c]</sup> Giorgia Del Favero,<sup>[c]</sup> and Freddy Kleitz\*<sup>[a]</sup>

## SUPPORTING INFORMATION

## Table of Contents

TABLE OF CONTENTS.....	2
EXPERIMENTAL PROCEDURES .....	2
MATERIALS .....	2
METHODS .....	2
RESULTS AND DISCUSSION.....	5
CHARACTERIZATION OF THE DMSNs .....	5
INSULIN LOADING STRATEGY .....	7
INSULIN LOADING RESULTS .....	8
RELEASE OF INSULIN .....	11
CELLULAR UPTAKE EXPERIMENTS .....	12
REFERENCES .....	14

## Experimental Procedures

## Materials

Cetyltrimethylammonium chloride (CTAC, 25 wt% H<sub>2</sub>O), Tetraethylorthosilicate (TEOS, 99%), Insulin (human recombinant, 5800 Da), (3-mercaptopropyl)triethoxysilane (MPTS, 95 %), (3-aminopropyl)triethoxysilane (APTS), Fluorescein isothiocyanate (FITC, > 90%), Rhodamine isothiocyanate (Rhod) were obtained from Sigma Aldrich (Austria). Triethanolamine (TEA, 98 %) was purchased from Alfa Aesar (USA). 50 % succinylated  $\beta$ -lactoglobulin (BL) was provided by Aventus Innovations (Levis, QC, Canada). Materials for cell culture and cytotoxicity experiments were purchased from GIBCO Invitrogen (Karlsruhe, Germany), Lonza Group Ltd (Basel, Switzerland), Sigma-Aldrich Chemie GmbH (Munich, Germany) and Sarstedt AG&Co (Nuembrecht, Germany).

## Methods

*Synthesis of Dendritic Mesoporous Silica Nanoparticles (DMSNs).* DMSNs with various pore sizes were synthesized by adapting the procedure previously reported.[1] First, the aqueous solution was prepared: 8 ml of CTAC, 360 mg of TEA and 72 ml of H<sub>2</sub>O were mixed together for 1h at 60 °C (stirring plate Heidolph, stirring rate 150 rpm). Then, the organic solution was prepared: 32 ml of organic solvent (hexane, cyclohexane or toluene) and 8 ml TEOS were mixed and subsequently added to the first solution. The solution was kept at 60 °C under the same stirring rate overnight. Prior to the centrifugation at 10000 rpm for 20 min, the organic phase was removed. After drying at 100 °C overnight, the as-made nanoparticles were extracted for 2h with 100 ml of EtOH and 1 drop of HCl (37%). After drying the extracted nanoparticles at 100 °C overnight, they were calcined under air at 550 °C for 5h. The resulting calcined nanoparticles are named DMSN-Hex, DMSN-Cyclo or DMSN-Tol.

*Functionalization of DMSN-Hex.* DMSN-Hex were functionalized with MPTS. Typically, 500 mg of calcined DMSN-Hex were dispersed in 50 ml of anhydrous toluene under stirring and N<sub>2</sub> atmosphere at 115 °C for 2h. Then, 0.5 ml of MPTS was added and the mixture was allowed to proceed overnight. The functionalized DMSN-Hex were recovered by centrifugation at 9000 rpm for 20 min, washed twice with toluene and once with ethanol and dried at 80 °C overnight. The resulting functionalized DMSN-Hex are named DMSN-SH.

*Labeling of DMSNs.* DMSN-Hex and DMSN-SH were labeled with Rhodamine isothiocyanate based on previously reported method.[2] For DMSN-Hex labeling, first Rho-APTS silane was prepared. Rhod was reacted with APTS: 10 mg of Rhod was dissolved in 0.5 ml of anhydrous DMSO and 0.1 ml of APTS was added at RT, under stirring and N<sub>2</sub> atmosphere. The reaction was left 24h in the dark. Then, 100 mg of DMSN-Hex was dispersed in 10 ml anhydrous toluene for 2h at 110 °C. A volume of 0.5 ml of Rho-APTS was added to the dispersion of DMSN-Hex and the grafting was further carried out overnight. For DMSN-SH labeling, 8.2 mg of Rhod was added to a suspension of 100 mg of DMSN-SH in EtOH (25 ml) and the reaction between thiol and isothiocyanate further proceeded in the dark under stirring for 24h. DMSN-Hex was also labeled with FITC as follows: DMSN-Hex was first grafted with APTS and 50 mg of the resulting amino-modified DMSN-Hex was reacted with 17.6 mg of FITC in 20 ml EtOH in the dark for 24h. The samples were recovered

## SUPPORTING INFORMATION

by centrifugation at 9000 rpm for 20 min, washed several times with EtOH and dried at 80 °C overnight. The resulting labeled materials are named DMSN-Rhod, DMSN-SH-Rhod and DMSN-FITC.

**Labeling of Insulin.** Insulin was coupled with FITC according to standard protocol.[3] Briefly, 10 mg of insulin was first dissolved in 1 ml of Na<sub>2</sub>CO<sub>3</sub> 0.1 M. In parallel, 5 mg of FITC was dissolved in 0.5 ml of DMSO. The FITC solution was added to insulin by increment of 50 µl and the mixture was stirred at RT for 1h and protected from light exposure. After semi-preparative HPLC purification, the coupling was confirmed by mass spectrometry. The resulting labeled insulin is named Ins-FITC.

**Loading of Insulin.** Insulin, human recombinant, was introduced into the pores of DMSNs through an electrostatic attraction technique. First, 40 mg of Insulin was dispersed in V = 20 ml of nanopure H<sub>2</sub>O and the pH was brought to 3 with HCl 0.01 M until complete dissolution is observed. Then, the pH was increased to 4 using NaOH 0.2 M. In the meantime, a suspension of 100 mg of either DMSN-Hex, DMSN-Tol or DMSN-SH is prepared using V = 5 ml of a solution at pH 4. The solution of insulin was added to the different suspensions of DMSN-Hex, DMSN-Tol and DMSN-SH and the mixtures were placed in a mechanical rocker for 1.5h. The resulting DMSNs loaded with insulin were recovered by centrifugation (9000 rpm, 10 min), frozen overnight and lyophilized for 2 days. The obtained DMSNs are named DMSN-Hex-Ins, DMSN-Tol-Ins and DMSN-SH-Ins.

**Characterization of the materials.** N<sub>2</sub> physisorption isotherms were measured at -196 °C (77 K) using an Autosorb-iQ3 sorption analyzer (Anton Paar, Boynton Beach, USA). Prior to the analysis, calcined DMSNs, functionalized DMSN-SH and insulin loaded DMSNs were outgassed 10h at 150 °C, 12h at 80 °C and 20h at 35 °C, respectively. The specific surface area (S<sub>BET</sub>) was determined using the Brunauer-Emmet-Teller (BET) equation in the relative pressure range 0.05 - 0.2. The total pore volume was determined at P/P<sub>0</sub> = 0.95. The pore size distributions were calculated using the non-local density functional theory (NLDFT) method considering a model of silica with cylindrical pores. Transmission Electron Microscopy (TEM) images were recorded with a Philips CM200 microscope at an accelerating voltage of 200 keV using suspensions of DMSNs in EtOH (4 µl) deposited on a carbon-coated copper grid. Dynamic light scattering (DLS) analyses were performed on a Malvern DTS Nano Zetasizer 173 ° (equilibrium time set at 3 min, 3 measurements for each sample). The samples were dispersed in H<sub>2</sub>O with a concentration of 0.7 mg ml<sup>-1</sup>, shaken and sonicated prior to the analysis. The Zeta Potential measurements of the DMSNs and insulin over the pH range 2 – 6 were obtained using a titrator coupled to the Malvern DTS Nano Zetasizer. Thermogravimetric (TG) and Differential Scanning Calorimetry (DSC) analyses were performed on a Netzsch STA-449 F3 Jupiter instrument under airflow of 20 ml min<sup>-1</sup> with a heating rate of 10 °C min<sup>-1</sup>, from 40 to 700 °C. The percentage of mass loss was assessed in the temperature range 120 – 700 °C. Wide angle powder X-ray diffraction (WXR) measurements were performed using a Panalytical Empyrean diffractometer (Malvern Panalytical, UK) in reflection geometry (Bragg-Brentano HD) using Cu Kα<sub>1+2</sub> radiation operated at a voltage of 45 kV, a tube current of 40 mA, with a fixed divergence slit of 0.05 mm. The measurements were performed in a continuous mode with a step size 2θ of 0.013° and a time per step of 200 s. The quantification of insulin was performed using a Vanquish ultra-high-performance liquid chromatography (UHPLC) system (Thermo Fisher Scientific, Bremen, Germany) coupled with a LTQ Orbitrap Velos mass spectrometer equipped with an electrospray ion source with the voltage 2.1 kV and the ion transfer capillary temperature was 300 °C. The retention of insulin was carried out on a C-18 analytical column Acclaim 120™ (Thermo Scientific, 2.1 x 150 mm, 3 µm, 10 nm) at a flow rate of 0.4 ml min<sup>-1</sup> and a temperature of 40 °C. The injection volume was 5 µl. The mobile phases were A: 100 % H<sub>2</sub>O, 0.1 % FA and B: 100 % ACN, 0.1 % FA. A gradient method was applied as follow: 0.0 – 8.0 min 5 - 53 % B, 8.0 - 8.5 min 53 - 95 % B, 12.5 - 13.0 min 95 - 5 % B and re-equilibration was made until 17 min. The full MS scans were acquired in positive ion mode at 400 – 2000 m/z range at a resolution of 60000 (FWHM at 400 m/z).

**Tablet formulations.** Tablets of BL combined with either insulin (BL-Ins) or insulin loaded in the different DMSNs (BL-DMSN-Hex-Ins, BL-DMSN-Tol-Ins, BL-DMSN-SH-Ins) were prepared using a single punch press (PerkinElmer, UK). Prior to the compression, the powders were mixed together in a vial with a spatula, this refers to the mixed formulation. For comparison purposes, a layer-by-layer formulation (lbl) was also tested and in this case the tablet of BL-DMSN-Hex-Ins (lbl) was prepared as follows: 100 mg of BL was first placed at the bottom of the compression tool followed by a layer of 30 mg of DMSN-Hex-Ins and finally the second layer of BL was placed at the top. Unless otherwise stated, all the tablets were prepared through the mixed formulation.

**Insulin release experiments.** The solution at pH 1.2 and 7.4 were prepared according to previously reported protocols.[4] For the solution at pH 1.2, 2 g of NaCl, 7 ml of HCl (37 %) and 1 l of nanopure H<sub>2</sub>O were mixed. For the solution at pH 7.4, first 6.8 g of KH<sub>2</sub>PO<sub>4</sub> was dissolved in 250 ml of nanopure H<sub>2</sub>O and then combined to 190 ml of NaOH 0.2 M and 400 ml of nanopure H<sub>2</sub>O. If needed, the pH was adjusted using NaOH 0.2 M and the volume was completed to 1 l with nanopure H<sub>2</sub>O. For each dissolution test, 400 ml of the solutions at pH 1.2 or 7.4 were introduced into a 500 ml erlenmeyer, subsequently placed inside an incubator set at 37 °C and stirring at 150 rpm was allowed prior to the addition of the tablets. The tablets were first soaked 2h at pH 1.2, were then taken out and directly placed in 5 ml of PBS for few minutes to prepare the solution at pH 7.4. Once transferred in pH 7.4, the test continued until 24h. Aliquots of 1 ml were taken out at adequate period of time and replaced by 1 ml of the fresh solution to maintain the same volume. The concentration of insulin released in both solutions was quantified using UHPLC-MS system. Triplicates were only realized for BL-Ins, BL-DMSN-Hex-Ins and BL-DMSN-SH-Ins, experiments made for comparison purposes *i.e.*, BL-Ins (lbl), BL-DMSN-Tol-Ins were performed once. Statistical analysis was performed with OriginPro 9.55 (OriginLab) applying one-way ANOVA with Fisher test for pairwise comparison (threshold value  $p < 0.05$ ).

## SUPPORTING INFORMATION

**Cell culture.** Non-tumorigenic human colonic epithelial cells (HCEC) were cultivated in DMEM supplemented with 2 % medium 199 (10X), 2% cosmic calf serum, HEPES 20 mM, gentamycin ( $50 \mu\text{g ml}^{-1}$ ), insulin-transferrin-selenium-G ( $10 \mu\text{g ml}^{-1}$ ), recombinant human EGF ( $20 \text{ ng ml}^{-1}$ ), hydrocortisone ( $1 \mu\text{g ml}^{-1}$ ). The cells were incubated in a humidified incubator with 5 %  $\text{CO}_2$  at  $37^\circ\text{C}$ . The HCEC cells (HCEC-1CT) were kindly provided by Prof. Jerry W. Shay (UT Southwestern Medical Center, Dallas, TX, USA) and cultivated as previously described.[5,6]

**Fluorescent microscopy experiments.** For the live cell imaging experiment, a confocal LSM microscope Zeiss 710 was equipped with ELYRA PS.1 and a Water Plan Apochromat 63x/1.2 objective. HCEC were seeded in Ibitreat slides, 6000 cells/slide and incubated at  $37^\circ\text{C}$  for 48h before the live cell imaging experiments. Prior to their incubation, the DMSNs, *i.e.*, DMSN-FITC, DMSN-SH-Rhod and DMSN-Rhod were dispersed in DMEM, vortexed for 15 sec and sonicated for 30 min, this procedure was repeated three times and a concentration of  $200 \mu\text{g ml}^{-1}$  was applied to the cells. Ins-FITC was dissolved in the cell culture media at a concentration of  $10 \mu\text{g ml}^{-1}$ , equivalent concentration of insulin was used for DMSN-Ins-FITC. In the case of DMSN-Ins-FITC, the dispersion procedure was only applied once to avoid premature release of Ins-FITC. At the end of the treatments, the cells were washed three times with LCI to remove non-internalized DMSN-FITC, DMSN-SH-Rhod, DMSN-Rhod, Ins-FITC or DMSN-Ins-FITC. Then, the cells were stained with CellMask™ Deep Red Plasma Membrane Stain (1:1000 dilution). [7] Imaging was performed in Live Cell Imaging Solution (Molecular Probes, Life Technologies, Thermo Fisher Scientific, USA).

**Insulin starvation of HCEC.** HCEC are normally cultured with insulin in their media at the concentration of  $10 \mu\text{g ml}^{-1}$ . Thus, the removal of insulin-transferrin-selenium-G from their culture media has permitted to test the metabolic activity of the cells in presence of the different insulin-containing DMSNs and compare with the unformulated insulin purchased. To achieve so, 8000 cells per well were seeded in a 96-wells black sided plate at  $37^\circ\text{C}$  for 48h. Once confluency could be observed, the culture media was removed, replaced by an equivalent volume lacking insulin-transferrin-selenium-G and the cells were further incubated at  $37^\circ\text{C}$  for 1h. Then, the cells were treated with insulin, *i.e.*, the unformulated purchased one, at a concentration of 10 or  $15 \mu\text{g ml}^{-1}$  in DMEM or the insulin-containing DMSNs, *i.e.*, DMSN-Hex-Ins or DMSN-SH-Ins at an equivalent concentration of insulin of  $15 \mu\text{g ml}^{-1}$  in DMEM. The samples were vortexed and sonicated to ensure the dissolution of unformulated insulin or the suspension of DMSN-Hex-Ins and DMSN-SH-Ins. A volume of  $100 \mu\text{l}$  was added to the insulin starved cells; the wells were then completed with  $100 \mu\text{l}$  of culture media lacking insulin. The incubation was continued for a time period of either 1 or 6h. For comparison purposes, the same experiment was conducted in normal culturing conditions, *i.e.*, cells were not insulin-starved and they were incubated with a full media. At the end of the incubation, cells were washed twice with  $100 \mu\text{l}$  of DPBS prior to the Alamar Blue assay.

**Alamar Blue (AB) assay.** AB assay was used following methods previously reported with slight modifications.[8] Briefly, a solution of 10% AB in DMEM (v/v) was prepared and  $100 \mu\text{l}$  of this solution was added to each well and the reaction was allowed for 40 min in the incubator. The fluorescence was measured at 530/560 nm (excitation/emission) using a Cytation 3 Imaging Multi Mode Reader (BioTek, Bad Friedrichshall, Germany). Cells incubated were compared to the respective control cells and the ratio treated over control was calculated in %. The data presented are the mean  $\pm$  standard error of at least three independent cell preparations made in triplicates. Statistical analysis was performed with OriginPro 9.55 (OriginLab) applying one-way ANOVA with Fisher test for pairwise comparison (threshold value  $p < 0.05$ ).



## SUPPORTING INFORMATION

## Results and Discussion

## Characterization of the DMSNs

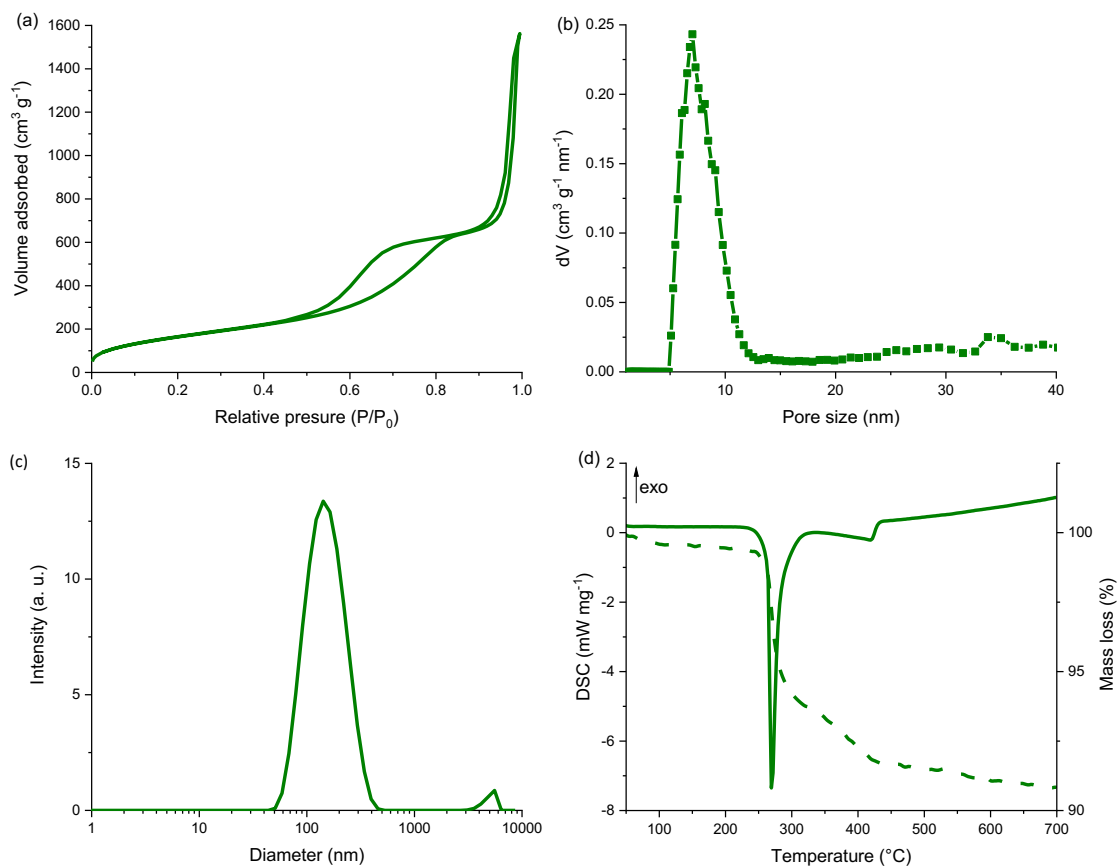
**Table S1.** Physicochemical parameters of the pure DMSNs, the functionalized DMSNs and the insulin-loaded DMSNs.

	$S_{\text{BET}}^{\text{[a]}}$ ( $\text{m}^2 \text{g}^{-1}$ )	Pore volume <sup>[a]</sup> ( $\text{cm}^3 \text{g}^{-1}$ )	Pore size <sup>[a]</sup> (nm)	Particle size <sup>[b]</sup> (nm)	Mass loss <sup>[c]</sup> (%)
DMSN-Hex	823	1.5	7.6	151	-
DMSN-Cyclo	868	1.60	8.4	154	-
DMSN-Tol	949	2.70	11.7	238	-
DMSN-SH	615	1.15	7.0	159	8.6
DMSN-Hex-Ins	600	1.15	7.0		20.4
DMSN-Tol-Ins	589	1.75	11.7		17.8
DMSN-SH-Ins	633	1.15	7.0		20.2

[a] The specific surface area  $S_{\text{BET}}$ , pore volume and pore size were obtained from the  $\text{N}_2$  physisorption analysis. [b] The particle size has been measured using DLS [c] Mass loss values were calculated in the temperature range of 120 - 700 °C from the thermogravimetry analysis.

Whilst the pore sizes of the DMSNs have been tailored upon changing the nature of the organic solvent, the particle sizes of the resulting nanoparticles are only slightly changed. As seen in Table S1, while the DMSNs made with hexane or cyclohexane have very similar particle sizes of approximately 150 nm and comparable porosity characteristics, *i.e.*, pore sizes of 7.6 nm for DMSN-Cyclo and 8.4 nm for DMSN-Hex, the ones made with toluene have bigger particle diameter of almost 240 nm and much larger pores of almost 12 nm.

## SUPPORTING INFORMATION

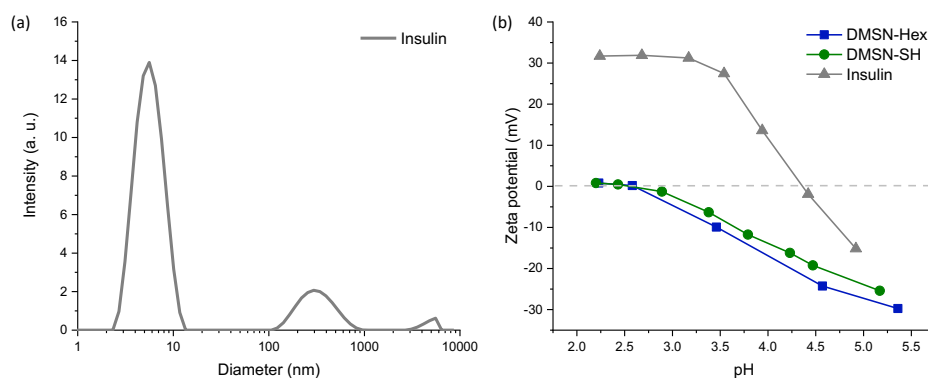


**Figure S1.** Physicochemical characterization of the thiol-functionalized DMSNs; (a)  $N_2$  physisorption isotherm of DMSN-SH measured at  $-196^{\circ}\text{C}$ ; (b) Pore size distribution of DMSN-SH calculated using NLDFT method considering the adsorption of  $N_2$  in silica materials with cylindrical-like pores; (c) Hydrodynamic diameter of the particles in suspension in water measured by DLS; (d) TG-DSC analysis of DMSN-SH.

DMSN-Hex have been further functionalized with thiol groups using (3-mercaptopropyl)triethoxysilane (MPTS) which decreased the pore size from 7.6 to 6.9 nm, the surface area from 823 to 615  $\text{m}^2 \text{g}^{-1}$  and the pore volume from 1.50 to 1.15  $\text{cm}^3 \text{g}^{-1}$ . However, the particle size did not change and stayed centred at 159 nm. As it can be seen from Figure S1d, the combustion of the thiol-silane occurs at approximately 275  $^{\circ}\text{C}$  and around 9 wt% has been anchored on the surface through post-synthesis grafting.

## SUPPORTING INFORMATION

## Insulin loading strategy

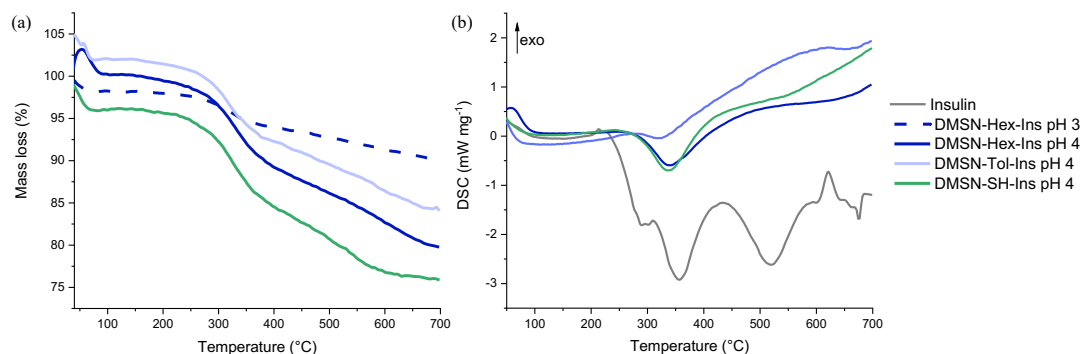


**Figure S2.** (a) Diameter of insulin in pH 7.4 measured by DLS; (b) Zeta potential of insulin, DMSN-Hex and DMSN-SH measured over the pH range 2-6.

As it can be seen in Figure S2a, the size of insulin in an aqueous solution is around 6 nm, therefore, larger pore sizes of DMSNs were used for loading. Then, the effect of the charge of insulin and the DMSNs in solution on the loading efficiency was assessed. To begin with, insulin has a positive charge in the pH range 2 – 3, as determined by the results of the Zeta potential measurements depicted in Figure S2b. On the other hand, both the pure and the thiol-functionalized DMSNs have nearly a neutral charge at this pH. The loading of insulin at pH 3 was first attempted followed by an attempt at pH 4.

## SUPPORTING INFORMATION

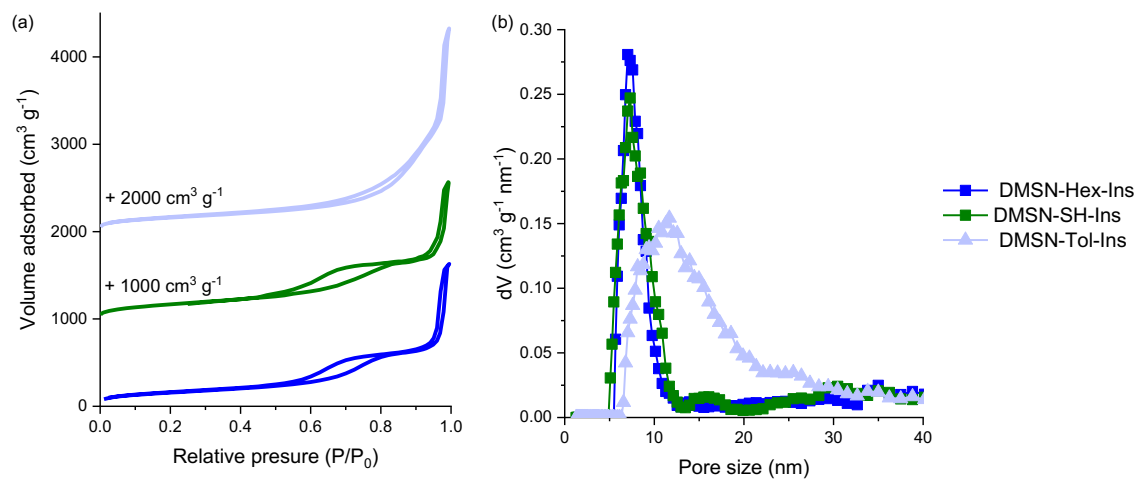
## Insulin loading results



**Figure S3.** (a) Mass loss and (b) DSC profiles of the different materials: insulin, insulin loaded at pH 4 in pure DMSN-Hex and DMSN-Tol or thiol-functionalized DMSN-Hex (DMSN-SH). For comparison purpose, insulin loaded at pH 3 in DMSN-Hex is shown.

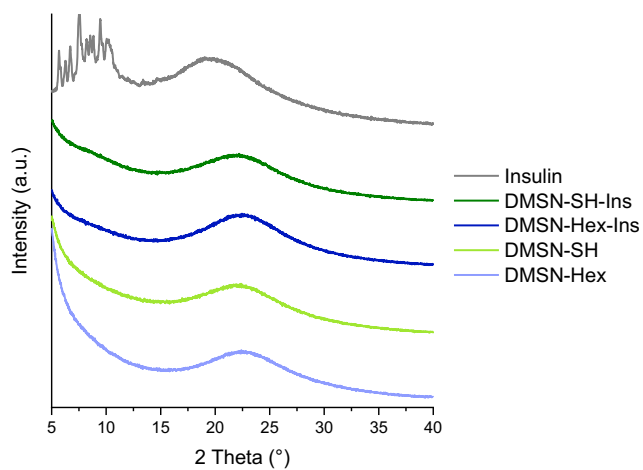
A mass loss of around 10 wt% was calculated for the loading of insulin inside both DMSN-Hex and DMSN-Tol (data not shown for DMSN-Tol) at pH 3. Further optimization has led to the loading of insulin at pH 4 since, at this pH, insulin has a positive charge of around + 10 mV and the pure or thiol-DMSN have a negative charge of around – 20 mV. The important difference in the charges makes the electrostatic attraction between both parts stronger. Indeed, the mass loss increased to 20 wt% (Table S1) for DMSN-Hex-Ins and DMSN-Tol-Ins. Using the same amount of insulin and silica materials, lower loading was detected for the thiol-functionalized DMSNs, *i.e.*, 12 wt% (Figure S3a and Table S1). In this case, the initial amount of insulin was increased to 60 mg while keeping an equal quantity of DMSN-SH. By doing so, the loading of insulin reached also around 20 wt% (data not shown). The structure of insulin was maintained during the loading procedure as confirmed by MS spectrometry. The effect of the confinement of insulin inside the mesopores of the different DMSNs can be appreciated from the Figure S3b. While the combustion of insulin confined in the mesopores occurs during one exothermic event at  $T = 340$  °C, insulin itself is decomposed throughout several exothermic and endothermic processes.

## SUPPORTING INFORMATION



**Figure S4.** (a) Isotherms and (b) pore size distributions obtained from N<sub>2</sub> physisorption analysis (-196 °C) of insulin loaded into DMSN-Hex, DMSN-Tol and DMSN-SH. Physicochemical values are reported in the Table S1.

## SUPPORTING INFORMATION

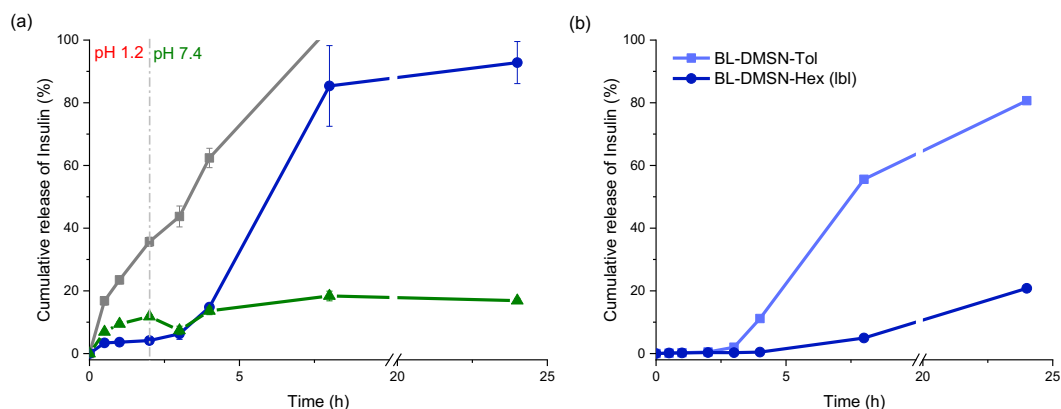


**Figure S5.** Wide-angle powder X-ray diffractograms of the starting DMSN-Hex and DMSN-SH, the insulin-loaded into DMSN-Hex and DMSN-SH and insulin alone.

The wide-angle powder X-ray diffractogram presented in Figure S5 shows that insulin itself can be considered as a semi-crystalline peptide with diffraction peaks in the region  $5 < 2\theta < 15^\circ$ . Differently, when incorporated inside the pores of either DMSN-Hex or the thiol-functionalized version, DMSN-SH, no diffraction peaks can be seen, therefore insulin is confined as an amorphous protein in the pores.

## SUPPORTING INFORMATION

## Release of insulin

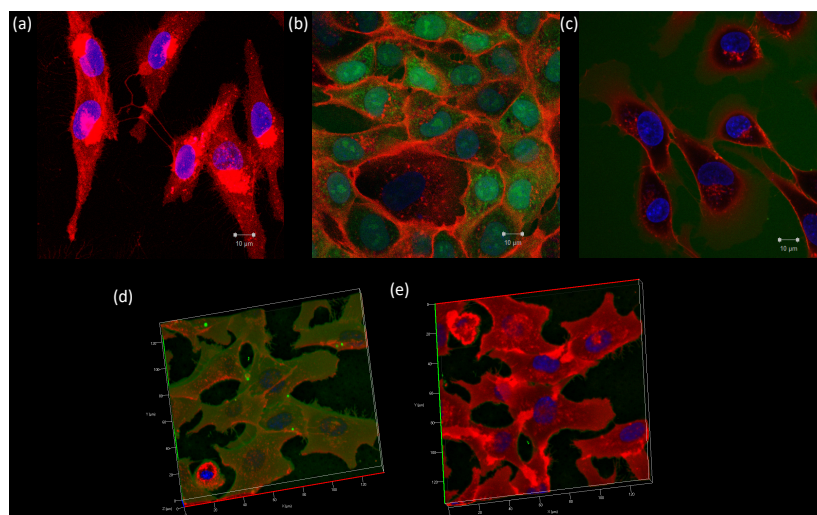


**Figure S6.** (a) Second representation of the cumulative release of insulin over time from the different formulations (BL-Ins in grey, BL-DMSN-Ins in blue and BL-DMSN-SH-Ins in green) immersed 2h at pH 1.2 and subsequently at pH 7.4; (b) Cumulative release of insulin over time from BL-DMSN-Tol, *i.e.*, insulin confined in larger pores (DMSN-Tol) and from BL-DMSN-Hex lbl, *i.e.*, insulin confined in DMSN-Hex and tableted in sandwich with BL (one layer of BL, one layer of DMSN-Hex-Ins, one layer of BL), similar to (a) the tablets were first immersed 2h at pH 1.2 and subsequently transferred at pH 7.4.

As it can be observed, the release of insulin from the pure DMSNs does not seem to depend on the pore sizes as similar performances have been observed for both DMSN-Hex (pore size: 7.6 nm) and DMSN-Tol (pore size: 11.7 nm). However, changing the formulation of the BL tablet resulted in drastically decreasing the elution of insulin at pH 7.4. This might originate from the fact that, in the layer-by-layer formulation, the DMSN-Hex are located in the center of the tablet and therefore more time is needed to navigate from the center to the media. Nevertheless, this gives an interesting insight supporting the assumption that after 1h at pH 7.4, the DMSNs in the mixed formulation start to reach the media and would be ready to be transported through the intestinal barrier.

## SUPPORTING INFORMATION

## Cellular uptake experiments

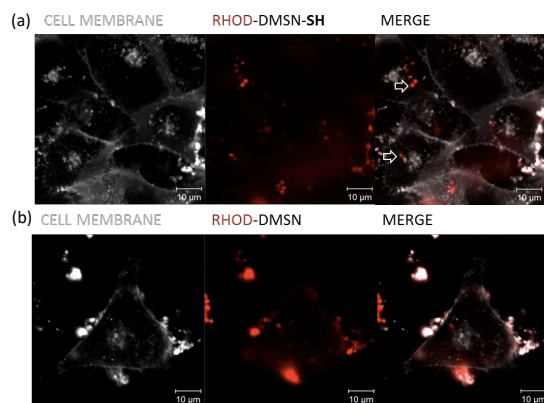


**Figure S7.** Live cell fluorescence images (a) HCEC control cells, (b) FITC control, (c) Ins-FITC incubated for 45 min; 3D stack after 3 h incubation of Ins-FITC (d) upper and (e) bottom view. The plasma membrane is represented in red, the nucleus in blue and Ins-FITC in green.

FITC was solubilized in DMSO and applied to the cells, the images were taken immediately after the incubation. Thus, it can be concluded that FITC alone goes quickly in the cells and reach the nucleus (Figure S7b). Insulin coupled with FITC does not seem to penetrate the cells and this up to 3h. From the upper view, Ins-FITC dispersed in the medium can be observed, however from the bottom view, no Ins-FITC was seen to approach the cells.



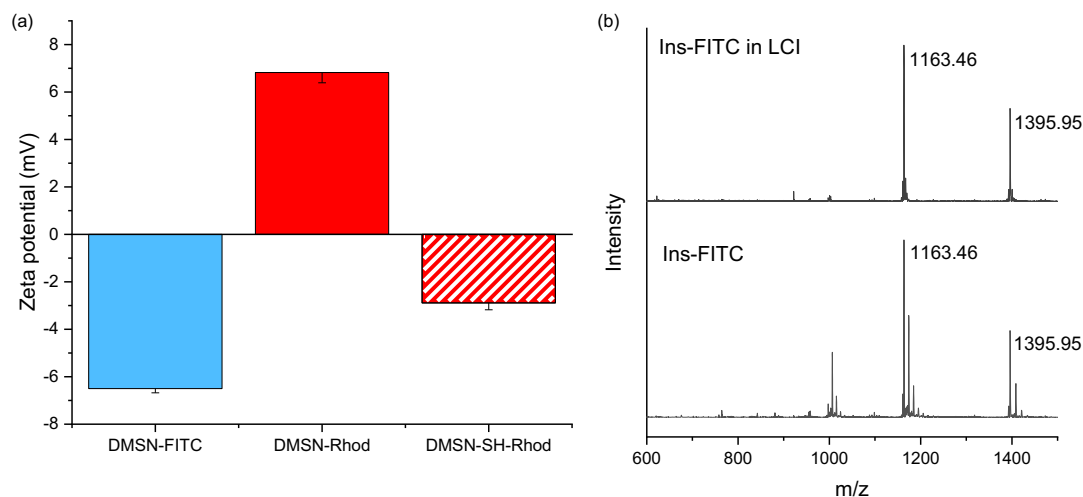
## SUPPORTING INFORMATION



**Figure S8.** Live cell fluorescence images of the uptake of Rhod-labeled DMSNs after 20h of incubation of (a) DMSN-SH-Rhod and (b) DMSN-Rhod with HCEC. The plasma membrane is represented in white and the signal from Rhod in red.

It can be seen that the thiol function seemed to enable a more uniform distribution of the nanoparticles in the cells. Because of the presence of non-reacted amine groups at the particle surface, DMSN-Rhod expressed a positive charge (see Figure S9 for Zeta potential measurements) which led to agglomeration of these particles and decreased cellular uptake. With their negative charges, DMSN-FITC and DMSN-SH-Rhod were equally capable of entering the cells.

## SUPPORTING INFORMATION



**Figure S8.** (a) Zeta potential measurements of the different labelled-DMSNs: DMSN-FITC, DMSN-Rhod, DMSN-SH-Rhod. The positive charge of DMSN-Rhod might originate from remaining non-coupled APTS (b) MS spectrum of Ins-FITC after the synthesis (bottom) and confirmation of the structure of insulin in live cell imaging solution (LCI) added to the cells.

## References

- [1] C. Lei, C. Xu, A. Nouwens, C. Yu, *J. Mater. Chem. B* **2016**, *4*, 4975-4979.
- [2] J. Ciccione, T. Jia, J. L. Coli, K. Parra, M. Amblard, S. Jebors, J. Martinez, A. Mehdi, G. Subra, *Chem. Mater.* **2016**, *28*, 885-889.
- [3] Amine-Reactive Probe Labelling Protocol, ThermoFisher Scientific.
- [4] R. Caillard, M. Subirade, *Int. J. Pharm.* **2012**, *437*, 130-136.
- [5] G. Del Favero, R. Zaharescu, D. Marko, D. *Archives of toxicology* **2018**, *92*, 3535-3547.
- [6] V. Khare, K. Dammann, M. Asboth, A. Krnjic, M. Jambrich, C. Gasche, *Inflammatory bowel diseases* **2015**, *21*, 287-96.
- [7] G. Del Favero, L. Woelflingseder, L. Janker, B. Neuditschko, S. Seriani, P. Gallina, O. Sbaizero, C. Gerner, D. Marko, *Sci. Rep.* **2018**, *8*, 11351-11368.
- [8] L. Woelflingseder, G. Del Favero, T. Blažević, E. H. Heiss, M. Haider, B. Warth, G. Adam, D. Marko, *Toxicol. Letters* **2018**, *299*, 104-117.

## Author Contributions

**E.J.** has performed the experimental work, treated the data and written the original draft. **G.D.F.** has contributed to the cell studies and confocal microscopy data acquisition and treatment. **R.C.** has contributed to the investigation and formal analysis of the pH-gating system based on beta-lactoglobulin. **E.J.**, **R.C.**, **F.K.** have worked together on the materials chemistry experiment design, analysis and interpretation. **E.J.**, **G.D.F.**, **D.M.**, **F.K.** have worked together on the biological studies, acquisition and interpretation. **D. M.** has provided additional supporting supervision for the cell studies. **F.K.** is lead PI and project administrator, and main coordinator and supervisor of the work. All the authors have contributed to the revision of the original draft.





## Chapter 5 – Conclusion

---

### I. Summary of key results

The general aim of this thesis was to develop a versatile system to address the solubility and permeability issues faced in the GIT by most therapeutic agents and in particular, resveratrol, omeprazole and insulin. More specifically, this thesis attempted to (1) demonstrate pore confinement effects on the solubility and permeability of therapeutic agents, (2) develop a pH-responsive formulation that protects gastro-sensitive drugs and (3) design a nanocarrier for oral solid dosage of insulin.

Resveratrol was encapsulated into MCM-48-type MSNs of different particle (90, 150 or 300 nm) and pore (3.5 or 7 nm) sizes using the solvent evaporation technique. We established that the amorphization of resveratrol in the mesopores led to an increased release *in vitro*, enhancing drug transportation across the tight junctions of Caco-2 monolayer, and a certain effect of the particle size of the MSNs on the saturated solubility was extracted from results. Upon anti-inflammatory evaluation, the highest response was obtained with the proposed nanoformulation. The completion of objective (1) ensured that MSNs could improve the physico-chemical and the biological properties of confined resveratrol.

In regard to objective (2), omeprazole-loaded MSNs were combined to a protein excipient, succinylated  $\beta$ -lactoglobulin, to afford pH-responsive tablets. Combined together, succinylated  $\beta$ -lactoglobulin and MSNs permitted to satisfy the United States Pharmacopeia (USP) requirement as less than 10 % of omeprazole was released in SGF; furthermore, owing to nanopore confinement, the release of omeprazole at near neutral pH was higher than MSNs-free tablets. Hydrophobic surfaces were obtained through silanization of the MSNs with methyl-silane (HMDS) but the resulting MSNs systematically mediated higher mortality of HT-29 and Caco-2 cells. Contrastingly, upon progressive release of omeprazole-confined in MSNs, toxicity against Caco-2 and HCEC cells could be avoided.

With the combination of objectives (1) and (2), the development of oral solid dosage for resveratrol-loaded MCM-48-type MSNs followed. We realized that the loss of porosity of

the resulting drug-loaded MSNs depended on the functionality anchored at the surface of the MSNs, *i.e.*, amine, methyl vs pure silica surface. We also revealed stability limitations of the BL tablets: the combined positive charges in presence of amine-functionalized MCM-48-type MSNs caused the premature erosion of the omeprazole tablet in gastric fluid.

Finally, objective (3) was dedicated to the creation of an oral formulation for insulin. Fine control of the pore size of DMSNs was achieved upon increasing the steric hindrance of the organic co-solvent from hexane, cyclohexane to toluene in the synthesis procedure. Through electrostatic attraction between oppositely charged insulin and DMSNs at pH 4, the confinement of 20 wt % of insulin in the 7.6 nm pores was successful and highly reproducible. Following this, the combination of the DMSNs with BL synergistically prevented the premature release and degradation of insulin in gastric fluid. Undesired proteolysis was revealed only in the case of thiolated-DMSNs in intestinal fluid. Thus, the association of insulin and thiol groups would not be recommended for future studies, although thiol groups are known to be mucoadhesion enhancers. With the use of pure DMSNs, fluorescent confocal microscopy images provided evidence of the ability of DMSNs to greatly improve the transport of insulin across intestinal cellular membranes.

## II. Perspectives

This thesis paves the way for new avenues which are listed below as problematic to elucidate. The list comprises the consequences of the accomplished studies and new ideas generated throughout the work.

Topic	Challenges
Encapsulation and release	Dynamics study of the therapeutics agents confined in MSNs followed by Solid-State NMR - Is there a correlation between mobility and release rate of the confined drug?

	Is it possible to modulate the release through complexation of drugs on metals previously grafted on the surface of MSNs?
Insulin – permeability	Coating of MSNs with lipids – Would this formulation enhance the permeation of MSNs across the intestinal membrane?  Would the PEGylation of the DMSNs increase the permeation of the DMSNs without altering the loading and release of insulin?
Insulin – <i>in vitro</i> test	Proteomic analysis of the cells in absence of insulin supplement – How does the treatment with formulated insulin impact on the cellular proteomic?
Insulin – <i>in vivo</i> test	Would the BL tablets help in reaching sufficient <i>in vivo</i> pharmacological effect of oral insulin on diabetic rats?

### III. Concluding remarks

In the future, drug delivery platforms would have to be commercialized by the pharmaceutical industry if they were to have an impact on the life of patients. Only technologies offering an ease of manufacturing and high reproducibility in their performances would be considered adequate for marketability. To get closer to industrial applications and, bearing in mind the translation of MSNs into next generation oral drug delivery nanocarriers, this thesis focused on the development of tablets and correlated the confinement effects provided by adequately designed MSNs with the pH-responsiveness of BL protein. More specifically, the work achieved evidenced how the confinement of therapeutic agents into MSNs can circumvent solubility and permeability issues in the oral delivery route.





## References

---

- <sup>1</sup> A. Abramson, E. Caffarel-Salvador, M. Khang, D. Dellal, D. Silverstein, Y. Gao, M. Revsgaard Frederiksen, A. Vegge, F. Hubálek, J. J. Water, A. V. Friderichsen, J. Fels, R. K. Kirk, C. Cleveland, J. Collins, S. Tamang, A. Hayward, T. Landh, S. T. Buckley, N. Roxhed, U. Rahbek, R. Langer, G. Traverso, An ingestible self-orienting system for oral delivery of macromolecules, *Science* 2019, 363, 611-615.
- <sup>2</sup> D. Eek, M. Krohe, I. Mazar, A. Horsfield, F. Pompilus, R. Friebe, A. L. Shields, Patient-reported preferences for oral versus intravenous administration for the treatment of cancer: a review of the literature, *Patient Pref. Adherence* 2016, 10, 1609-1621.
- <sup>3</sup> M. M. Borner, P. Schöffski, R. de Wit, F. Caponigro, G. Comella, A. Sulkes, G. Greim, G. J. Peters, K. van der Born, J. Wanders, R. F. de Boer, C. Martin, P. Fumoleau, Patient preference and pharmacokinetics of oral modulated UFT versus intravenous fluorouracil and leucovorin: a randomized crossover trial in advanced colorectal cancer, *Eur. J. Cancer* 2002, 38, 349-358.
- <sup>4</sup> S. E. Ward, E. Kaltenthaler, J. Cowan, M. Marples, B. Orr, M. T. Seymour, The clinical and economic benefits of capecitabine and tegafur with uracil in metastatic colorectal cancer, *British J. Cancer* 2006, 95, 27-34.
- <sup>5</sup> S. Mitragotri, P. A. Burke, R. Langer, Overcoming the challenges in administering biopharmaceuticals: formulation and delivery strategies, *Nat. Rev.* 2014, 13, 655-672.
- <sup>6</sup> A. Dahan, A. Beig, D. Lindley, J. M. Miller, The solubility and permeability interplays: two heads are better than one, *Adv. Drug Deliv. Rev.* 2016, 101, 99-107.
- <sup>7</sup> S. K. Bardal, J. E. Waechter, D. S. Martin, Chap. 2 Pharmacokinetics, *Applied Pharmacology*, 1<sup>st</sup> Edition, 2011, Elsevier.
- <sup>8</sup> M. A. Navia, P. R. Chaturvedi, Design principles for orally bioavailable drugs, *Drug Discov. Today* 1996, 1, 179-189.
- <sup>9</sup> C. A. Lipinski, Drug-like properties and the causes of poor solubility and poor permeability, *J. Pharm. Toxicol. Methods* 2000, 44, 235-249.
- <sup>10</sup> D. F. Veber, S. R. Johnson, H. Y. Cheng, B. R. Smith, K. W. Ward, K. D. Kopple, Molecular properties that influence the oral bioavailability of drug candidates, *J. Med. Chem.* 2002, 45, 2615-2623.
- <sup>11</sup> Y. Yang, O. Engkvist, A. Llinàs, H. Chen, Beyond size, ionization state, and lipophilicity: influence of molecular topology on absorption, distribution, metabolism, excretion, and toxicity for druglike compounds, *J. Med. Chem.* 2012, 55, 3667-3677.
- <sup>12</sup> C. A. Lipinski, F. Lombardo, B. W. Dominy, P. J. Feeney, Experimental and computational approaches to estimate solubility and permeability in drug discovery and development settings, *Adv. Drug Deliv. Rev.* 1997, 23, 3-25.
- <sup>13</sup> P. Matsson, B. C. Doak, B. Over, J. Kihlberg, Cell permeability beyond the rule of 5, *Adv. Drug Delivery Rev.* 2016, 101, 42-61.
- <sup>14</sup> N. A. Meanwell, Improving drug candidates by design: a focus on physicochemical properties as a means of improving compound disposition and safety, *Chem. Res. Toxicol.* 2011, 24, 1420-1456.

- <sup>15</sup> R. Ghadi, N. Dand, BCS Class IV drugs: Highly notorious candidates for formulation development, *J. Control. Release* 2017, 248, 71-95.
- <sup>16</sup> K. Thanki, R. P. Gangwal, A. T. Sangamwar, S. Jain, Oral delivery of anticancer drugs: challenges and opportunities, *J. Control. Release* 2013, 170, 15-40.
- <sup>17</sup> A. Wicki, D. Witzigmann, V. Balasubramanian, J. Huwyler, Nanomedicine in cancer therapy: challenges, opportunities, and clinical applications, *J. Control. Release* 2015, 200, 138-157.
- <sup>18</sup> J. Brouwers, M. E. Brewster, P. Augustijns, Supersaturating drug delivery systems: the answer to solubility-limited oral bioavailability ?, *J. Pharm. Sci.* 2009, 98, 2549-2572.
- <sup>19</sup> G. T. Rengarajan, D. Enke, M. Steinhart, M. Beiner, Stabilization of the amorphous state of pharmaceuticals in nanopores, *J. Mater. Chem.* 2008, 18, 2537-2539.
- <sup>20</sup> D. Bobo, K. J. Robinson, J. Islam, K. J. Thurecht, S. R. Corrie, *Pharm. Res.* 2016, 33, 2373-2387.
- <sup>21</sup> C. T. Kresge, M. E. Leonowicz, W. J. Roth, J. C. Vartuli, J. S. Beck, Ordered mesoporous molecular sieves synthesized by a liquid-crystal template mechanism, *Nature* 1992, 359, 710-712.
- <sup>22</sup> T. W. Kim, P. W. Chung, I. I. Slowing, M. Tsunoda, E. S. Yeung, V. S. Y. Lin, Structurally ordered mesoporous carbon nanoparticles as transmembrane delivery vehicle in human cancer cells, *Nano Lett.* 2008, 8, 3724-3727
- <sup>23</sup> T. W. Kim, F. Kleitz, B. Paul, R. Ryoo, MCM-48-like large mesoporous silicas with tailored pore structure: facile synthesis domain in a ternary triblock copolymer-butanol-water system, *J. Am. Chem. Soc.* 2005, 127, 7601-7610.
- <sup>24</sup> D. Shen, J. Yang, X. Li, L. Zhou, R. Zhang, W. Li, L. Chen, R. Wang, F. Zhang, D. Zhao, Biphasic stratification approach to three-dimensional dendritic biodegradable mesoporous silica nanospheres, *Nano Lett.* 2014, 14, 923-932.
- <sup>25</sup> M. Bouchoucha, M. F. Côté, R. C.-Gaudreault, M. A. Fortin, F. Kleitz, Size-controlled functionalized mesoporous silica nanoparticles for tunable drug release and enhanced anti-tumoral activity, *Chem. Mater.* 2016, 28, 4243-4258.
- <sup>26</sup> L. T. Gibson, Mesosilica materials and organic pollutant adsorption: part A removal from air, *Chem. Soc. Rev.* 2014, 43, 5163-5172.
- <sup>27</sup> F. Hoffmann, M. Fröba, Vitalising porous inorganic silica networks with organic functions-PMOs and related hybrid materials, *Chem. Soc. Rev.* 2011, 40, 608-620.
- <sup>28</sup> F. Hoffmann, M. Cornelius, J. Morell, M. Fröba, Silica-based mesoporous organic-inorganic hybrid materials, *Angew. Chem. Int. Ed.* 2006, 45, 3216-3251.
- <sup>29</sup> W. Stöber, A. Fink, E. Bohn, Controlled growth of monodisperse silica spheres in the micron size range, *J. Colloid Interface Sci.* 1968, 26, 62-69.
- <sup>30</sup> M. Grün, I. Lauer, K. K. Unger, The synthesis of micrometer- and submicrometer-size spheres of ordered mesoporous oxide MCM-41, *Adv. Mater.* 1997, 9, 254-257.
- <sup>31</sup> S. H. Wu, C. Y. Mou, H. P. Lin, Synthesis of mesoporous silica nanoparticles, *Chem. Soc. Rev.* 2013, 42, 3862-3875.
- <sup>32</sup> K. Suzuki, K. Ikari, H. Imai, Synthesis of silica nanoparticles having a well-ordered mesostructure using a double surfactant system, *J. Am. Chem. Soc.* 2004, 126, 462-463.

- <sup>33</sup> T. W. Kim, P. W. Chung, V. S. Y. Lin, Synthesis of monodisperse spherical MCM-48 mesoporous silica nanoparticles with controlled particle size, *Chem. Mater.* 2010, 22, 5093-5104.
- <sup>34</sup> K. Möller, J. Kobler, T. Bein, Colloidal suspensions of nanometer-sized mesoporous silica, *Adv. Funct. Mater.* 2007, 17, 605-612.
- <sup>35</sup> X. Du, S. Z. Qiao, Dendritic silica particles with center-radial pore channels: promising platforms for catalysis and biomedical applications, *Small* 2015, 11, 392-413.
- <sup>36</sup> K. Möller, T. Bein, Talented mesoporous silica nanoparticles, *Chem. Mater.* 2017, 29, 371-388.
- <sup>37</sup> M. Dang, W. Li, Y. Zheng, X. Su, X. Ma, Y. Zhang, Q. Ni, J. Tao, J. Zhang, G. Lu, Z. Teng, L. Wang, Mesoporous organosilica nanoparticles with large radial pores via an assembly-reconstruction process in bi-phase, *J. Mater. Chem. B* 2017, 5, 2625-2634.
- <sup>38</sup> Y. Wang, H. Song, Y. Yang, Y. Liu, J. Tang, C. Yu, Kinetically controlled dendritic mesoporous silica nanoparticles: from dahlia- to pomegranate-like structures by micelle filling, *Chem. Mater.* 2018, 30, 5770-5776.
- <sup>39</sup> L. Xiong, X. Du, B. Shi, J. Bi, F. Kleitz, S. Z. Qiao, Tunable stellate mesoporous silica nanoparticles for intracellular drug delivery, *J. Mater. Chem. B*, 2015, 3, 1712.
- <sup>40</sup> A. K. Meka, P. L. Abbaraju, H. Song, C. Xu, J. Zhang, H. Zhang, M. Yu, C. Yu, A vesicle supra-assembly approach to synthesize amine-functionalized hollow dendritic mesoporous silica nanospheres for protein delivery, *Small* 2016, 12, 5169-5177.
- <sup>41</sup> C. von Baeckmann, R. Guillet-Nicolas, D. Renfer, H. Kählig, F. Kleitz, A toolbox for the synthesis of multifunctionalized mesoporous silica nanoparticles for biomedical applications, *ACS Omega* 2018, 3, 17496-17510.
- <sup>42</sup> E. E. Connor, J. Mwamuka, A. Gole, C. J. Murphy, M. D. Wyatt, Gold nanoparticles are taken up by human cells but do not cause acute cytotoxicity, *Small* 2005, 1, 325-327.
- <sup>43</sup> K. E. Sapsford, W. R. Algar, L. Berti, K. B. Gemmil, B. J. Casey, E. Oh, M. H. Stewart, I. L. Medintz, Functionalizing nanoparticles with biological molecules: developing chemistries that facilitate nanotechnology, *Chem. Rev.* 2013, 113, 1904-2074.
- <sup>44</sup> A. Popat, B. P. Ross, J. Liu, S. Jambhrunkar, F. Kleitz, S. Z. Qiao, Enzyme-responsive controlled release of covalently bound prodrug from functional mesoporous silica nanospheres, *Angew. Chem. Int. Ed.* 2012, 51, 12486-12489.
- <sup>45</sup> S. Jambhrunkar, Z. Qu, A. Popat, J. Yang, O. Noonan, L. Acauan, Y. Ahmad Nor, C. Yu, S. Karmakar, Effect of surface functionality of silica nanoparticles on cellular uptake and cytotoxicity, *Mol. Pharm.* 2014, 11, 3642-3655.
- <sup>46</sup> S. Jambhrunkar, Z. Qu, A. Popat, S. Karmakar, C. Xu, C. Yu, Modulating *in vitro* release and solubility of griseofulvin using functionalized mesoporous silica nanoparticles, *J. Colloid Interfaces Sci.* 2014, 434, 218-225.
- <sup>47</sup> H. Meng, M. Xue, T. Xia, Y. L. Zhao, F. Tamanoi, J. F. Stoddart, J. I. Zink, A. E. Nel, Autonomous *in vitro* anticancer drug release from mesoporous silica nanoparticles by pH-sensitive nanovalves, *J. Am. Chem. Soc.* 2010, 132, 12690-12697.
- <sup>48</sup> Q. Zhang, F. Liu, K. T. Nguyen, X. Ma, X. Wang, B. Xing, Y. Zhao, Multifunctional mesoporous silica nanoparticles for cancer-targeted and controlled drug delivery, *Adv. Funct. Mater.* 2012, 22, 5144-5156.

- <sup>49</sup> M. Bouchoucha, R C.-Gaudreault, M. A. Fortin, F. Kleitz, Mesoporous silica nanoparticles: selective surface functionalization for optimal relaxometric and drug loading performances, *Adv. Funct. Mater.* 2014, 24, 5911-5923.
- <sup>50</sup> M. E. M. Braga, M. T. Vaz Pato, H. S. R. Costa Silva, E. I. Ferreira, M. H. Gil, C. M. M. Duarte, H. C. de Sousa, Supercritical solvent impregnation of ophthalmic drugs on chitosan derivatives, *J. Supercrit. Fluids* 2008, 44, 245-257.
- <sup>51</sup> R. Mellaerts, J. A. G. Jammaer, M. Van Speybroeck, H. Chen, J. Van Humbeeck, P. Augustijns, G. Van der Mooter, J. A. Martens, Physical state of poorly water soluble therapeutic molecules loaded into SBA-15 ordered mesoporous silica carriers: a case study with itraconazole and ibuprofen, *Langmuir* 2008, 24, 8651-8659.
- <sup>52</sup> M. Delle Piane, M. Corno, P. Ugliengo, Does dispersion dominate over H-bonds in drug-surface interactions? The case of silica-based materials as excipients and drug-delivery agents, *J. Chem. Theory Comput.* 2013, 9, 2404-2415.
- <sup>53</sup> A. Gignone, M. Delle Piane, M. Corno, P. Ugliengo, B. Onida, Simulation and experiment reveal a complex scenario for the adsorption of an antifungal drug in ordered mesoporous silica, *J. Phys. Chem. C* 2015, 119, 13068-13079.
- <sup>54</sup> E. Mäkilä, H. Kivelä, N. Shrestha, A. Correia, M. Kaasalainen, E. Kukk, J. Hirvonen, H. A. Santos, J. Salonen, Influence of surface chemistry on ibuprofen adsorption and confinement in mesoporous silicon microparticles, *Langmuir* 2016, 32, 13020-13029.
- <sup>55</sup> J. Andersson, J. Rosenholm, S. Areva, M. Lindén, Influences of material characteristics on ibuprofen drug loading and release profiles from ordered micro- and mesoporous silica matrices, *Chem. Mater.* 2004, 16, 4160-4167.
- <sup>56</sup> A. Datt, I. El-Maazawi, S. C. Larsen, Aspirin loading and release from MCM-41 functionalized with aminopropyl groups via co-condensation or postsynthesis modification methods, *J. Phys. Chem. C* 2012, 116, 18358-18366.
- <sup>57</sup> F. Ballas, M. Manzano, P. Horcajaba, M. Vallet-Regí, Confinement and controlled release of bisphosphonates on ordered mesoporous silica-based materials, *J. Am. Chem. Soc.* 2006, 128, 8116-8117.
- <sup>58</sup> G. T. Rengarajan, D. Enke, M. Steinhart, M. Beiner, Stabilization of the amorphous state of pharmaceuticals in nanopores, *J. Mater. Chem.* 2008, 18, 2537-2539.
- <sup>59</sup> K. P. Nartowski, D. Malhotra, L. E. Hawarden, J. Sibik, D. Iuga, J. A. Zeitler, L. Fábíán, Y. Z. Khimyak, <sup>19</sup>F NMR Spectroscopy as a highly sensitive method for the direct monitoring of confined crystallization within nanoporous materials, *Angew. Chem. Int. Ed.* 2016, 55, 8904-8908.
- <sup>60</sup> T. Azaïs, C. Tourné-Péteilh, F. Aussenac, N. Baccile, C. Coelho, J. M. Devoisselle, F. Babonneau, Solid-state NMR study of ibuprofen confined in MCM-41 materials, *Chem. Mater.* 2006, 18, 6382-6390.
- <sup>61</sup> S. R. Vippagunta, H. G. Brittain, D. J. W. Grant, Crystalline solids, *Adv. Drug Deliv. Rev.* 2001, 48, 3-26.
- <sup>62</sup> K.P. Nartowski, J. Tedder, D. E. Braun, L. Fábíán, Y. Z. Khimyak, Building solids inside nano-space: from confined amorphous through confined solvate to confined 'metastable' polymorph, *Phys. Chem. Chem. Phys.* 2015, 17, 24761-24773.

- <sup>63</sup> K. P. Nartowski, D. Malhotra, L. E. Hawarden, L. Fábíán, Y. Z. Khimyak, Nanocrystallization of rare tolbutamide form V in mesoporous MCM-41 silica, *Mol. Pharm.* 2018, 15, 4926-4932.
- <sup>64</sup> Q. Wei, C. M. Keck, R. H. Müller, Oral hesperidin-amorphization and improved dissolution properties by controlled loading onto porous silica, *Int. J. Pharm.* 2017, 518, 253-263.
- <sup>65</sup> J. Knapik, Z. Wojnarowska, K. Grzybowska, K. Jurkiewicz, A. Stankiewicz, M. Paluch, Stabilization of the amorphous ezetimibe drug by confining its dimension, *Mol. Pharm.* 2016, 13, 1308-1316.
- <sup>66</sup> V. Ambrogi, F. Marmottini, C. Pagano, Amorphous carbamazepine stabilization by the mesoporous silicate SBA-15, *Microporous Mesoporous Mater.* 2013, 177, 1-7.
- <sup>67</sup> S. C. Shen, W. K. Ng, L. Chia, J. Hu, R. B. H. Tan, Physical state and dissolution of ibuprofen formulated by co-spray drying with mesoporous silica: effect of pore and particle size, *Int. J. Pharm.* 2011, 410, 188-195.
- <sup>68</sup> S. Jambhrunkar, S. Karmakar, A. Popat, M. Yu, C. Yu, Mesoporous silica nanoparticles enhance the cytotoxicity of curcumin, *RSC Adv.* 2014, 4, 709-712.
- <sup>69</sup> Q. Tang, Y. Xu, D. Wu, Y. Sun, J. Wang, J. Xu, F. Deng, Studies on a new carrier of trimethylsilyl-modified mesoporous material for controlled drug delivery, *J. Control. Release* 2006, 114, 41-46.
- <sup>70</sup> S. Jambhrunkar, Z. Qu, A. Popat, S. Karmakar, C. Xu, C. Yu, Modulating *in vitro* release and solubility of griseofulvin using functionalized mesoporous silica nanoparticles, *J. Colloid Interface Sci.* 2014, 434, 218-225.
- <sup>71</sup> P. Horcajada, A. Rámila, J. Pérez-Pariente, M. Vallet-Regí, Influence of pore size of MCM-41 matrices on drug delivery rate, *Microporous Mesoporous Mater.* 2004, 68, 105-109.
- <sup>72</sup> T. Ukmar, U. Maver, O. Planinšek, V. Kaučič, M. Gaberšček, A. Godec, Understanding controlled drug release from mesoporous silicates: theory and experiment, *J. Control. Release* 2011, 155, 409-417.
- <sup>73</sup> Z. Guo, X. M. Liu, L. Ma, J. Li, H. Zhang, Y. P. Gao, Y. Yuan, Effects of particle morphology, pore size and surface coating of mesoporous silica on naproxen dissolution rate enhancement, *Colloids Surf. B* 2013, 101, 228-235.
- <sup>74</sup> I. Izquierdo-Barba, Á. Martínez, A. L. Doadrio, J. Pérez-Pariente, M. Vallet-Regí, Release evaluation of drugs from ordered three-dimensional silica structures, *Eur. J. Pharm. Sci.* 2005, 26, 365-373.
- <sup>75</sup> P. Lundquist, P. Artursson, Oral absorption of peptides and nanoparticles across the human intestine: opportunities, limitations and studies in human tissues, *Adv. Drug Deliv. Rev.* 2016, 106, 256-276.
- <sup>76</sup> K. Braun, A. Pochert, M. Beck, R. Fiedler, J. Gruber, M. Lindén, Dissolution kinetics of mesoporous silica nanoparticles in different simulated body fluid, *J. Sol-Gel Sci. Technol.* 2016, 79, 319-327.
- <sup>77</sup> K. Netsomboon, A. Bernkop-Schnürch, Mucoadhesive vs. mucopenetrating particulate drug delivery, *Eur. J. Pharm. Biopharm.* 2016, 98, 76-89.
- <sup>78</sup> J. Florek, R. Caillard, F. Kleitz, Evaluation of mesoporous silica nanoparticles for oral drug delivery – current status and perspective of MSNs drug carriers, *Nanoscale* 2017, 9, 15252-15277.

- <sup>79</sup> C. Y. Wong, J. Martinez, C. R. Dass, Oral delivery of insulin for treatment of diabetes: status quo, challenges and opportunities, *J. Pharm. Pharmacol.* 2016, 68, 1093-1108.
- <sup>80</sup> S. D. Conner, S. L. Schmid, Regulated portals of entry into the cell, *Nature* 2003, 422, 37-44.
- <sup>81</sup> A. Beloqui, A. des Rieux, V. Pr eat, Mechanisms of transport of polymeric and lipidic nanoparticles across the intestinal barriers, *Adv. Drug Deliv. Rev.* 2016, 106, 242-255.
- <sup>82</sup> H. Vallhov, S. Gabrielsson, M. Str omme, A. Scheynius, A. E. Garcia-Bennett, Mesoporous silica particles induce size dependant effects on human dendritic cells, *Nano Lett.* 2007, 7, 3576-3582.
- <sup>83</sup> F. Lu, S. H. Wu, Y. Hung, C. Y. Mou, Size effect on cell uptake in well-suspended uniform mesoporous silica nanoparticles, *Small* 2009, 5, 1408-1413.
- <sup>84</sup> Y. Zhang, L. Hu, D. Yu, C. Gao, Influence of silica particle internalization on adhesion and migration of human dermal fibroblasts, *Biomaterials* 2010, 31, 8465-8474.
- <sup>85</sup> C.-C. Chou, W. Chen, Y. Hung, C.-Y. Mou, Molecular elucidation of biological response to mesoporous silica nanoparticles in vitro and in vivo, *ACS Appl. Mater. Interfaces* 2017, 9, 22235-22251.
- <sup>86</sup> K. Braun, C. M. St urzel, J. Biskupek, U. Kaiser, F. Kirchhoff, M. Lind en, Comparison of different cytotoxicity assays for in vitro evaluation of mesoporous silica nanoparticles, *Toxicol. in Vitro*, 2018, 52, 214-221.
- <sup>87</sup> I. Slowing, B. G. Trewyn, V. S. -Y. Lin, Effect of surface functionalization of MCM-41 type mesoporous silica nanoparticles on the endocytosis by human cancer cells, *J. Am. Chem. Soc.* 2006, 128, 14792-14793.
- <sup>88</sup> D. Desai, N. Prabhakar, V. Mamaeva, I. AK L ahdeniemi, C. Sahlgren, J. M. Rosenholm, D. M. Toivola, Targeted modulation of cell differentiation in distinct regions of the gastrointestinal tract via oral administration of differently PEG-PEI functionalized mesoporous silica nanoparticles, *Int. J. Nanomedicine* 2016, 11, 299-313.
- <sup>89</sup> T. Asefa, Z. Tao, Biocompatibility of mesoporous silica nanoparticles, *Chem. Res. Toxicol.* 2012, 25, 2265-2284.
- <sup>90</sup> T. P. Liu, S. H. Wu, Y. P. Chen, C. M. Chou, C. T. Chen, Biosafety evaluations of well-dispersed mesoporous silica nanoparticles: towards in vivo-relevant conditions, *Nanoscale* 2015, 7, 6471-6480.
- <sup>91</sup> M. Beck, T. Mandal, C. Buske, M. Lind en, Serum protein adsorption enhances active leukemia stem cell targeting of mesoporous silica nanoparticles, *ACS Appl. Mater. Interfaces* 2017, 9, 18566-18574.
- <sup>92</sup> C. Y. Lin, C. M. Yang, M. Lind en, Influence of serum concentration and surface functionalization on the protein adsorption to mesoporous silica nanoparticles, *RSC Adv.* 2019, 9, 33912-33921.
- <sup>93</sup> V. Mamaeva, C. Sahlgren, M. Lind en, Mesoporous silica nanoparticles in medicine – recent advances, *Adv. Drug. Deliv. Rev.* 2013, 65, 689-702.
- <sup>94</sup> J. G. Croissant, Y. Fatieiev, N. M. Khashab, Degradability and clearance of silicon, organosilica, silsesquioxane, silica mixed oxide, and mesoporous silica nanoparticles, *Adv. Mater.* 2017, 1604634-1604685.

- <sup>95</sup> P. Dogra, N. L. Adolphi, Z. Wang, Y.-S. Lin, K. S. Butler, P. N. Durfee, J. G. Croissant, A. Nouredine, E. N. Coker, E. L. Bearer, V. Cristini, C. J. Brinker, Establishing the effects of mesoporous silica nanoparticle properties on in vivo disposition using imaging-based pharmacokinetics, *Nat. Commun.* 2018, 9, 4551-4564.
- <sup>96</sup> M. Benezra, O. Penate-Medina, P. B. Zanzonico, D. Schaer, H. Ow, A. Burns, E. DeStanchina, V. Longo, E. Herz, S. Lyer, J. Wolchok, S. M. Larson, U. Wiesner, M. S. Bradbury, Multimodal silica nanoparticles are effective cancer-targeted probes in a model of human melanoma, *J. Clin. Invest.* 2011, 121, 2768-2780.
- <sup>97</sup> R. Caillard, Y. Boutin, M. Subirade, Characterization of succinylated  $\beta$ -lactoglobulin and its application as the excipient in novel delayed release tablets, *Int. J. Dairy* 2011, 21, 27-33.
- <sup>98</sup> R. Guillet-Nicolas, A. Popat, J. L. Bridot, G. Monteith, S. Z. Qiao, F. Kleitz, pH-Responsive nutraceutical-mesoporous silica nanoparticles with enhanced colloidal stability, *Angew. Chem. Int. Ed.* 2013, 52, 2318-2322.
- <sup>99</sup> R. Caillard, A. Petit, M. Subirade, Design and evaluation of succinylated soy protein tablets as delayed drug delivery systems, *Int. J. Biol. Macromol.* 2009, 45, 414-420.
- <sup>100</sup> A. Popat, S. Jambhrunkar, J. Zhang, J. Yang, H. Zhang, A. Meka, C. Yu, Programmable drug release using bioresponsive mesoporous silica nanoparticles for site-specific oral drug delivery, *Chem. Commun.* 2014, 50, 5547-5550.
- <sup>101</sup> C. T. H. Nguyen, R. I. Webb, L. K. Lambert, E. Strounina, E. C. Lee, M. O. Parat, M. A. McGuckin, A. Popat, P. J. Cabot, B. P. Ross, Bifunctional succinylated  $\epsilon$ -polylysine-coated mesoporous silica nanoparticles for pH-responsive and intracellular drug delivery targeting the colon, *ACS Appl. Mater. Interfaces* 2017, 9, 9470-9483.
- <sup>102</sup> R.J. Mudakavi, A.M. Raichur, D. Chakravorty, Lipid coated mesoporous silica nanoparticles as an oral delivery system for targeting and treatment of intravacuolar *Salmonella* infections, *RSC Adv.* 2014, 4, 61160-61166.
- <sup>103</sup> T. Chen, J. Yang, L. Chen, X. Qian, Q. Zheng, T. Fu, H. Qiao, J. Li, L. Di, Use of ordered mesoporous silica-loaded phytophospholipid complex for BCS IV class plant drug to enhance oral bioavailability: a case report of tanshinone II<sub>A</sub>, *RSC Adv.* 2016, 6, 115010-115020.
- <sup>104</sup> L. Sun, Y. Wang, T. Jiang, X. Zheng, J. Zhang, J. Sun, C. Sun, S. Wang, Novel Chitosan-Functionalized Spherical Nanosilica Matrix As an Oral Sustained Drug Delivery System for Poorly Water-Soluble Drug Carvedilol, *ACS Appl. Mater.* 2013, 5, 103-113
- <sup>105</sup> L. Hu, H. Sun, Q. Zhao, N. Han, L. Bai, Y. Wang, T. Jiang, S. Wang, Multilayer encapsulated mesoporous silica nanospheres as an oral sustained drug delivery system for the poorly water-soluble drug felodipine, *Mater. Sci. Eng. C* 2015, 47, 313-324.
- <sup>106</sup> A. Popat, J. Liu, G. Q. Lu, S. Z. Qiao, A pH-responsive drug delivery system based on chitosan coated mesoporous silica nanoparticles, *J. Mater. Chem. B* 2012, 22, 11173.
- <sup>107</sup> L. Sun, X. Zhang, Z. Wu, C. Zheng, C. Li, Oral glucose- and pH-sensitive nanocarriers for simulating insulin release *in vivo*, *Polym. Chem.* 2014, 5, 1999-2009.
- <sup>108</sup> N. Shrestha, F. Araújo, M.-A. Shahbazi, E. Mäkilä, M. J. Gomes, B. Herranz-Blanco, R. Lindgren, S. Granroth, E. Kukk, J. Salonen, J. Hirvonen, B. Sarmiento, H. A. Santos, Thiolation and cell-penetrating peptide surface functionalization of porous silicon nanoparticles for oral delivery of insulin, *Adv. Funct. Mater.* 2016, 26, 3405-3416.

## References

---

- <sup>109</sup> M. Thommes, K. Kaneko, A. V. Neimark, J. P. Olivier, F. Rodriguez-Reinoso, J. Rouquerol, K. S. W. Sing, Physisorption of gases, with special reference to the evaluation of surface area and pore size distribution (IUPAC Technical Report), *Pure Appl. Chem.* 2015, 87, 1051-1069.
- <sup>110</sup> M. Thommes, Physical adsorption characterization of ordered and amorphous mesoporous materials, Nanoporous materials: science and engineering, Imperial College Press, Chapter 11, 2004.
- <sup>111</sup> P. I. Ravikovitch, S. C. Ó Domhnaill, A. V. Neimark, F. Schüth, K. K. Unger, Capillary hysteresis in nanopores: theoretical and experimental studies of nitrogen adsorption on MCM-41, *Langmuir* 1995, 11, 4765-4772.
- <sup>112</sup> Microscopy and Imaging, J. W. Niemantsverdriet, Chap. 7 in Spectroscopy in Catalysis: an introduction, 3rd Ed., 2007, Wiley-VCH, Weinheim.
- <sup>113</sup> An introduction to electron microscopy FEI™, 4<sup>th</sup> edition, booklet made by the FEI Company.
- <sup>114</sup> S. Bhattacharjee, DLS and zeta potential – What they are and what they are not ?, *J. Control. Release* 2016, 235, 337-351.
- <sup>115</sup> F. Kleitz, Ordered microporous and mesoporous materials, Nanoscale Materials in Chemistry, John Wiley & Sons, Inc., Chapter 9, 2009.